Austrian Journal of Technical and Natural Sciences

2026, No 7–8

PREMIER Publishing

Vienna
2026

Austrian Journal of Technical and Natural Sciences

Scientific journal

2026, No 7 – 8

ISSN 2310-5607

Editor-in-chief

Hong Han, China, Doctor of Engineering Sciences

International editorial board

Atayev Zagir, Russia, Ph.D. of Geographical Sciences, Dagestan State Pedagogical University

Boselin S.R. Prabhu, India, Associate Professor, Surya Engineering College

Buronova Gulnora, Uzbekistan, PhD in Pedagogical science (Computer Science), Bukhara State University

Giorgi (Gia) Kvinikadze, Georgia, Doctor of Geographical Sciences, Tbilisi State University named after Ivane Javakhishvili

Inoyatova Flora Ilyasovna, Uzbekistan, Doctor of Medicine, Republican Specialized Scientific and Practical Medical Center of Pediatrics (RSNPMC Pediatrics)

Kurdzeka Aliaksandr, Kazakhstan, Doctor of Veterinary Medicine, Kazakh National Agrian University

Kushaliyev Kaissar Zhalitovich, Kazakhstan, Doctor of Veterinary Medicine, Zhangir Khan Agrarian Technical University

Mambetullaeva Svetlana Mirzamuratovna, Uzbekistan, Doctor of Biological Sciences, Karakalpak Research Institute of Natural Sciences

Manasaryan Grigoriy Genrihovich, Armenia, Doctor of Technical Sciences, Armenian National Polytechnic University

Martirosyan Vilena Akopovna, Armenia, Doctor of Engineering Sciences, National Polytechnic University of Armenia

Nagiyev Polad Yusif, Azerbaijan, Candidate of Agricultural Sciences, Sciences Institute for Space Research of Natural Resources, National Aerospace Agency

Nenko Nataliya Ivanovna, Russia, Doctor of Agricultural Sciences, State Scientific Institution North Caucasus Zonal Research Institute of Horticulture and Viticulture of the Russian Agricultural Academy

Rayiha Amenzade, Azerbaijan, Dr. Sc. (Architecture), professor, Institute of Architecture and Art of ANAS (Azerbaijan)

Sharipov Muzafar, Uzbekistan, PhD in technical science, Associate professor, Bukhara State university

Skopin Pavel Igorevich, Russia, Doctor of Medicine, Mordovian State University

Suleymanov Suleyman Fayzullaevich, Uzbekistan, Ph.D. of Medicine, Bukhara State Medical Institute (BukhGosMI)

Tegza Alexandra Alexeevna, Kazakhstan, Doctor of Veterinary Medicine, Kostanay State University

Yarashev Kuvondik Safarovich, Uzbekistan, Doctor of Geographical Sciences (DSc), Director, Urgut branch of Samarkand State University named after. Sharaf Rashidov

Zagir V. Atayev, Russia, PhD of Geographical Sciences, Dagestan State Pedagogical University

Proofreading Kristin Theissen

Cover design Andreas Vogel

Additional design Stephan Friedman

Editorial office Premier Publishing s.r.o.
Praha 8 – Karlín, Lyčkovo nám. 508/7, PSČ 18600

E-mail: pub@ppublishing.org

Homepage: ppublishing.org

Austrian Journal of Technical and Natural Sciences is an international, English language, peer-reviewed journal. The journal is published in electronic form.

The decisive criterion for accepting a manuscript for publication is scientific quality. All research articles published in this journal have undergone a rigorous peer review. Based on initial screening by the editors, each paper is anonymized and reviewed by at least two anonymous referees. Recommending the articles for publishing, the reviewers confirm that in their opinion the submitted article contains important or new scientific results.

Premier Publishing is not responsible for the stylistic content of the article. The responsibility for the stylistic content lies on an author of an article.

Instructions for authors

Full instructions for manuscript preparation and submission can be found through the Premier Publishing home page at: http://ppublishing.org.

Material disclaimer

The opinions expressed in the conference proceedings do not necessarily reflect those of the Premier Publishing, the editor, the editorial board, or the organization to which the authors are affiliated.

Premier Publishing is not responsible for the stylistic content of the article. The responsibility for the stylistic content lies on an author of an article.

Included to the open access repositories:

Scientific Journal Impact Factor

TOGETHER WE REACH THE GOAL

SJIF 2024 = 6.62 (Scientific Journal Impact Factor Value for 2024).

Crossref OAK.UZ eLIBRARY.RU

Included to the Uzbekistan OAK journals bulletin.

© Premier Publishing

All rights reserved; no part of this publication may be reproduced, stored in a retrieval system, or transmitted in any form or by any means, electronic, mechanical, photocopying, recording, or otherwise, without prior written permission of the Publisher.

Austrian Journal of Technical
and Natural Sciences, 2026 No 7–8
ISSN 2310-5607

PREMIER Publishing
ppublishing.org

Section 1. Chemistry

DOI:10.29013/AJT-26-7.8-3-7

CC BY

SYNTHESIS OF IONIC LIQUIDS BASED ON ORTHO-PHENYLENEDIAMINE AND PHOSPHORIC ACID

Abdisattorov Javokhir[1], Taniyev Okhunjon [2], Berdimurodov Elyor [1], Akbarov Khamdam [1]

[1] Faculty of Chemistry, National University of Uzbekistan, Tashkent, Uzbekistan

[2] Tashkent pharmaceutical institute, Tashkent, Uzbekistan

Cite: *Abdisattorov J., Taniyev O., Berdimurodov E., Akbarov Kh. (2026). Synthesis of Ionic Liquids Based on Ortho-Phenylenediamine and Phosphoric Acid. Austrian Journal of Technical and Natural Sciences 2026, No 7–8.* https://doi.org/10.29013/AJT-26-7.8-3-7

Abstract

Ionic liquids have attracted the attention of researchers due to their properties such as high solubility and stability, high ionic conductivity, and low toxicity. Compounds based on ionic liquids exhibit high water solubility and high inhibition efficiency at various temperatures and low concentrations. These compounds are highly effective in preventing metal corrosion in cooling and heating systems and consist of water-soluble, inexpensive components for corrosion protection. These properties make them a new generation of corrosion inhibitors and increase their potential for widespread use in the future. The influence of the pH value of the medium, time, and temperature on the synthesis of ionic liquids was studied. The efficiency of ionic liquids at different temperatures and concentrations was determined using results obtained by gravimetric analysis and analyzed in detail by atomic force microscopy (AFM).

Keywords: *Ionic liquid, 1,2-diammoniumbenzene hydrophosphate, physical sorption, chemical sorption, gravimetric analysis, and AFM (atomic force microscopy)*

Introduction

Ionic liquids are salts of organic compounds, consisting of organic cations and organic or inorganic anions. Ionic liquids typically possess high thermal stability, low vapor pressure, non-flammability, moderate polarity, high ionic conductivity, and non-toxic properties (Gobara M., Saleh A., Naeem I., 2019). Inhibitors based on ionic liquids form a strong protective thin film and adsorb onto the metal surface. Chemical and physical adsorption mechanisms are the most suitable for describing the adsorption of inhibitors and the formation of a protective layer. Effective corrosion protection can be achieved by forming a stable protective layer at the boundary between the metal surface and the solution (Tawfik S. M.,

2016; Lgaz H., Anejjar A., Salghi R., Jodeh S., Zougagh M., Warad I., Larouj M., Sims P., 2016). As a result, the diffusion or penetration of ions, water molecules, and oxygen to the surface is significantly reduced. Derivatives of ionic liquids contain many nitrogen atoms; therefore, their nitrogen atoms are protonated. The results obtained in this research work showed that physical adsorption occurs due to electrostatic interaction between the positively charged regions of the inhibitor and the negatively charged metal surface (Cao S., Liu D., Zhang P., Yang L., Yang P., Lu H., Gui J., 2017). On the other hand, they adsorb onto the metal surface by forming strong covalent bonds. Almost all ionic liquids have low toxicity and high efficiency, which has attracted many researchers. As a result of these investigations, the anti-corrosion properties and mechanisms of ionic liquids on steel in saline water were studied. Ionic liquids serve as a protective layer on the metal surface. This, in turn, depends on the inhibition efficiency, which increases with increasing concentration and decreases with increasing temperature. Currently, most of the studied research is based on solid ionic liquid inhibitors (Gerengi H., Solomon M. M., Umoren S. A., Ugras H. I., Yildiz M., Slepski P., 2018; Qi-bo Z., Yi-Xin H., 2011). The use of ionic liquids such as 1,2-diammoniumbenzene hydrophosphate, N, N-diphenylammonium dihydrogenphosphate, 2-methylbenzolammonium dihydrogenphosphate, and 4-(diazophenyl) benzolammonium dihydrogenphosphate, as well as the application of their anti-corrosion activity, is also motivating scientists' interest. Our research group synthesized an ionic liquid based on a compound of ortho-phenylenediamine and phosphoric acid, and then, using several experimental and computational methods, studied the anti-corrosion effect of the ionic liquid on a steel sample in 0.5 M HCl and 0.5 M NaOH media (Nanthini R., Mutalib M. I., 2019; Hasib-ur-Rahman M., Larachi F., 2013).

Figure 1. *Synthesis process of the 1,2-diammoniumbenzene hydrophosphate ionic liquid derived from ortho-phenylenediamine and phosphoric acid*

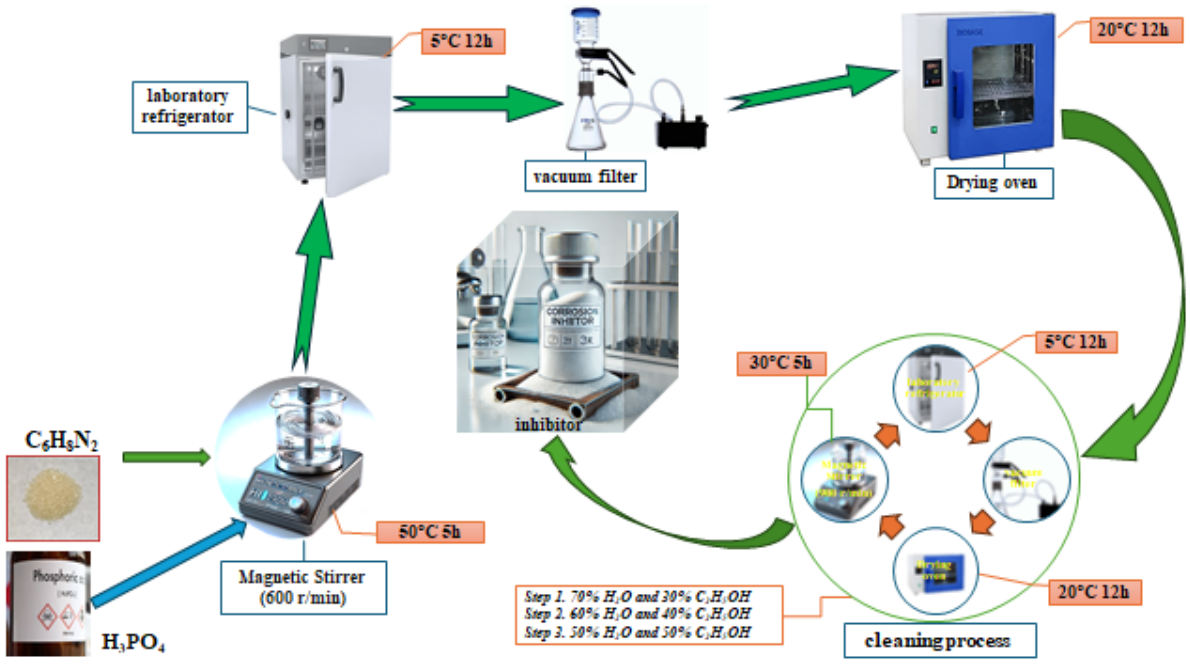

In this study, the 1,2-diammoniumbenzene hydrophosphate ionic liquid inhibitor demonstrated excellent corrosion inhibition properties for steel samples in an acidic solution. A 0.5 M solution of ortho-phenylenediamine in 50 ml of alcohol was mixed with a 0.5 M solution of phosphoric acid in a 1:1 ratio in a flask. Both solutions were initially stirred separately for 5 minutes, and then the ortho-phenylenediamine solution in alcohol was slowly poured into the phosphoric acid solution. This mix-

ture was attached to a reflux condenser and reacted using a magnetic stirrer at 50 °C (t = 5 h) and 600 rpm. After a homogeneous mixture was formed, the obtained solution was cooled to room temperature and placed in a refrigerator at 5 °C for 12 hours to allow the ionic liquid to form. The resulting ionic liquid solution was filtered. The obtained ionic liquid was dried at 20 °C for 12 hours to obtain the dry ionic liquid. The effect of 1,2-diammoniumbenzene hydrophosphate ionic liquids on corrosion inhibition indicators is studied in various aggressive media on different metals or alloys.

Results obtained via gravimetric analysis and AFM (atomic force microscopy) and their analysis: Effect of the concentration of 1,2-diammoniumbenzene hydrophosphate ionic liquid. The corrosion rate (CRGrav.), the protection degree (ηGrav.), and the surface coverage (θGrav.) for steel No. 20 in 0.5 M HCl with the 1,2-diammoniumbenzene hydrophosphate inhibitor are presented in Table 1. It is evident that with increasing concentration, ηGrav. and θGrav. increase, but CRGrav. decreases. This is because the increase in inhibitor concentration coats the metal surface with a thin protective film. At 303 K, for steel No. 20, a protection degree of 97.54% was observed at 100 mg/L and 92.75% at 75 mg/L. However, it was confirmed that the 1,2-diammoniumbenzene hydrophosphate inhibitor is a good inhibitor for the corrosion of steel No. 20 even at low concentrations in a 0.5 M HCl medium. The magnitude of the inhibitory efficiency of 1,2-diammoniumbenzene hydrophosphate depends on the molecular volume of the inhibitor. This is because even at low concentrations, the inhibitor covers a large part of the metal surface. The experimental results show that the selected inhibitor is more effective at low concentrations. This is related to the adsorption of the 1,2-diammoniumbenzene hydrophosphate inhibitor in a parallel adsorption position. As a result, it covers a large portion of the metal surface. The increase in concentration is related to a change in the adsorption state. Thus, 1,2-diammoniumbenzene hydrophosphate is an inhibitor that is effective even at low concentrations. In the temperature range of 303–333 K, ηGrav. at 100 mg/L is 97.54% at 303 K and 83.06% at 333 K. Therefore, this 1,2-diammoniumbenzene hydrophosphate ionic liquid is considered a good corrosion inhibitor at high temperatures as well. Thus, the 1,2-diammoniumbenzene hydrophosphate inhibitor forms an effective protective film on the surface of steel No. 20 and effectively isolates it from aggressive Cl^- ion attack (Kamali Ardakani E., Kowsari E., Ehsani A., 2019).

Effect of temperature

The effect of temperature was analyzed with various concentrations of the 1,2-diammoniumbenzene hydrophosphate inhibitor in 0.5 M HCl solution. The data observed in Table 1 show that the corrosion rate increases with rising temperature. This indicates that steel No. 20 has lower corrosion resistance at higher temperatures. The inhibitor efficiency decreases from 97.54% at 303 K to 83.06% at 333 K. This confirms that the 1,2-diammoniumbenzene hydrophosphate inhibitor excellently protects the surface of steel No. 20 from aggressive chloride ion solutions in the range of 303 to 333 K. It should be noted that corrosion protection is lower at high temperatures because the increase in kinetic energy causes the desorption of the inhibitor from the metal surface, which affects its inhibition performance. Furthermore, the electrostatic interaction between the inhibitor and the metal surface is lost at high temperatures. These factors also contribute to the decrease in inhibition indicators at elevated temperatures. The electrostatic interaction between the inhibitor and the metal surface is dependent on the temperature rise. The 1,2-diammoniumbenzene hydrophosphate inhibitor adsorbs onto the metal surface via chemical and physical adsorption mechanisms. Physical adsorption occurs through electrostatic interaction between the inhibitor and the metal surface. The positively charged nitrogen atoms of the corrosion inhibitor electrostatically interact with the negatively charged metal surface. Chloride and hydroxyl ions are adsorbed onto the metal surface, resulting in a negatively charged metal surface (El aoufir Y., Zehra S., Lgaz H., Chaouiki A., Serrar H., Kaya S., Salghi R., AbdelRaheem S. K., Boukhris S., Guenbour A., Chung I.-M., 2020). The corrosion inhibitor neutralizes the metal surface through electrostatic interaction. When the temperature rises,

chloride and hydroxyl ions become more active, causing the electrostatic interaction force to gradually decrease. AFM (Atomic Force Microscopy). The surface morphology of the plate-shaped steel No. 20 samples before and after inhibition was studied using atomic force microscopy. The surface of the clean steel No. 20 sample is almost smooth, with no signs of corrosive attack. The surface structure of steel No. 20 inhibited with the 1,2-diammoniumbenzene hydrophosphate inhibitor in Background-1 solution was studied using atomic force microscopy (Figure 2).

Figure 2. *Microphotography of the surface of steel No. 20 uninhibited and inhibited with 1,2-diammoniumbenzene hydrophosphate using atomic force microscopy*

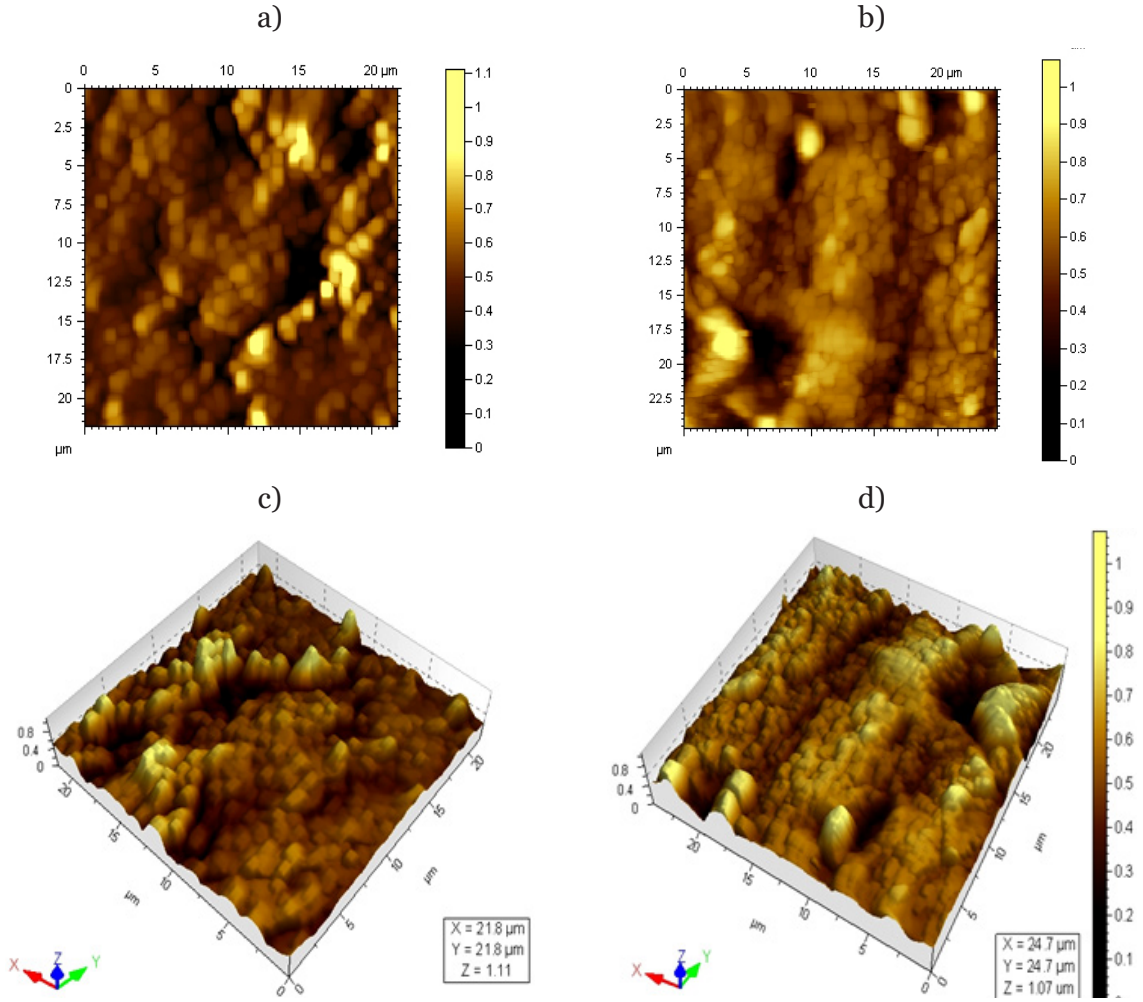

Using atomic force microscopy, the state of the crystalline protective layer formed as a result of the inhibitor covering the steel surface and natural pits was studied and analyzed. The surface of the clean steel No. 20 sample is almost smooth, with no signs of corrosive attack. The 3D AFM images show the corresponding height parameters for the corroded and inhibited steel No. 20 surfaces. The obtained results revealed that numerous corroded areas were identified. In contrast, when the steel surface was treated with the selected corrosion inhibitor, 1,2-diammoniumbenzene hydrophosphate, the metal surface became smoother, indicating a significant improvement in the surface condition. The improvement in surface morphology can be attributed to the protective layer formed by 1,2-diammoniumbenzene hydrophosphate, which effectively shields the metal surface from the acidic medium and reduces surface porosity.

Conclusion:

The dependence of the synthesis of 1,2-diammoniumbenzene hydrophosphate ionic liquid on temperature and time was

studied. It was observed that 50 °C, 5 hours, and 600 rpm are favorable conditions and ensure stability. The 1,2-diammoniumbenzene hydrophosphate ionic liquid was synthesized via a reaction involving orthophenylenediamine and phosphoric acid. The gravimetric analysis and AFM (atomic force microscopy) results for the 1,2-diammoniumbenzene hydrophosphate inhibitor were obtained. The obtained 1,2-diammoniumbenzene hydrophosphate ionic liquid is stable, inexpensive, and readily soluble in water.

References

Gobara M., Saleh A., Naeem I. (2019). Synthesis, characterization and application of acrylate-based poly ionic liquid for corrosion protection of C1020 steel In hydrochloric acid solution, Mater. Res. Express – 7. – 16517 p.

Tawfik S. M. (2016). Ionic liquids based gemini cationic surfactants as corrosion inhibitors for carbon steel in hydrochloric acid solution, J. Mol. Liq. – 216. – P. 624–635.

Lgaz H., Anejjar A., Salghi R., Jodeh S., Zougagh M., Warad I., Larouj M., Sims P. (2016). Characterization of corrosion products formed on carbon steel in hydrochloric acid medium by 4-(dimethylamino)-1-(6-methoxy-6-oxohexyl) pyridinium bromide, Int. J. Corros. Scale Inhib. – P. 209–231. URL: https://doi.org/10.17675/ 2305-6894-2016-5-3-3.

Cao S., Liu D., Zhang P., Yang L., Yang P., Lu H., Gui J. (2017). Green Brönsted acid ionic liquids as novel corrosion inhibitors for carbon steel in acidic medium, Sci. Rep. 1–14. URL: https://doi.org/10.1038/s41598-017-07925-y.

Gerengi H., Solomon M. M., Umoren S. A., Ugras H. I., Yildiz M., Slepski P. (2018). Improved performance of 1-ethyl-3-methylimidazolium tetrafluoroborate at steel /HCl interface by iodide ions, J. Bio- and Tribo Corros. – 4. – P. 1–11. URL: https:// doi.org/10.1007/ s40735-018-0126-3.

Qi-bo Z., Yi-Xin H. (2011). Effect of alkylimidazolium ionic liquids on the corrosion inhibition of copper in sulfuric acid solution, Acta Phys. Chim. Sin. – 27. – P. 655–663.

Nanthini R., Mutalib M. I. (2019). Gravimetric, electrochemical and surface study on the good's buffer ionic liquid as corrosion inhibitor for carbon steel in acidic medium, J. Mechan. Eng. Sci. – 13. – P. 4434–4448.

Hasib-ur-Rahman M., Larachi F. (2013). Prospects of using room-temperature ionic liquids as corrosion inhibitors in aqueous ethanolamine-based CO_2 capture solvents, Ind. Eng. Chem. Res. – 52. – P. 17682–17685.

Kamali Ardakani E., Kowsari E., Ehsani A. (2019). Imidazolium-derived polymeric ionic liquid as a green inhibitor for corrosion inhibition of mild steel in 1.0 M HCl: Experimental and computational study, Colloids Surf., A – 124195 p.

El aoufir Y., Zehra S., Lgaz H., Chaouiki A., Serrar H., Kaya S., Salghi R., AbdelRaheem S. K., Boukhris S., Guenbour A., Chung I.-M. (2020). Evaluation of inhibitive and adsorption behavior of thiazole-4-carboxylates on mild steel corrosion in HCl, Colloids Surf., A 606–125351 p. URL: https://doi.org/10.1016/j. colsurfa.2020.125351.

submitted 12.08.2026;
accepted for publication 26.08.2026;
published 31.08.2026
© Abdisattorov J., Taniyev O., Berdimurodov E., Akbarov Kh.
Contact: javohirabdisattorov4949@gmail.com

Austrian Journal of Technical
and Natural Sciences, 2026 No 7–8
ISSN 2310-5607

PREMIER Publishing
ppublishing.org

DOI:10.29013/AJT-26-7.8-8-17

DEVELOPMENT OF A FUNCTIONAL MATERIAL BASED ON TIRON-IMMOBILIZED FILTER PAPER FOR THE DETERMINATION OF SILVER(I) IONS AND ITS SPECTROSCOPIC CHARACTERIZATION

Nadirbek Sabirov [1], Mansur Ashirov [2], Norbek Palvanov [3]

[1] PhD Student, Khorezm Mamun Academy, Uzbekistan, Khiva

[2] Senior Researcher, Candidate of Chemical Sciences, PhD, Khorezm Mamun Academy, Uzbekistan, Khiva

[3] Associate Professor of the Department of "Medical and Biological Chemistry", Urgench Branch of the Tashkent Medical Academy. Urgench city

Cite: *Sabirov N., Ashirov M., Palvanov N. (2026). Development of a Functional Material Based on Tiron-Immobilized Filter Paper for The Determination of Silver(I) Ions and Its Spectroscopic Characterization. Austrian Journal of Technical and Natural Sciences 2026, No 7–8.* https://doi.org/10.29013/AJT-26-7.8-8-17

Abstract

This study reports the immobilization of the organic reagent Tiron onto filter paper to create a simple and low-cost optical platform for the determination of silver(I) ions. Immobilization was performed by soaking the paper in an aqueous Tiron solution (1.0×10^{-3} mol/L) followed by drying at room temperature. The resulting material was treated with Ag(I) ions and characterized by diffuse reflectance spectroscopy (DRS) and Fourier-transform infrared (FTIR) spectroscopy. The DRS spectra revealed a pronounced change in the optical response both after Tiron immobilization and after the binding of Ag(I) ions, confirming the formation of surface coordination complexes. FTIR analysis confirmed the successful immobilization of Tiron onto the cellulose matrix and the participation of the hydroxyl and sulfonate functional groups in coordination with Ag(I) ions. The developed Tiron-functionalized filter paper is inexpensive, environmentally safe, and easy to prepare, making it a promising material for the sorption of silver(I) ions and for the fabrication of paper-based optical sensors.

Keywords: *Tiron; filter paper; immobilization; cellulose; silver(I); chelate complex; paper-based sensor; sorbent*

Introduction

In recent years, interest in paper-based materials for the detection, separation, and on-site preconcentration of metal ions has increased steadily. This interest is driven by the low cost and biodegradability of filter paper, its ability to transport solutions by capillary flow, the ease of cutting and zone patterning, and minimal reagent consumption. When organic ligands, nanomaterials, or

ion-selective reagents are immobilized onto a paper matrix, the paper can serve as a simple test platform suitable for use both in the laboratory and under field conditions.

Tiron is a catechol disulfonate ligand well known in analytical chemistry because it forms colored complexes with Fe, Ti, Al, and other metal ions. Its two phenolic –OH groups can coordinate to a metal center, while the sulfonate groups provide water solubility and an ion-exchange environment. When Tiron is immobilized onto filter paper, a metal-binding functional layer is formed on the surface of the cellulose fibers. The attachment of Ag to this layer may provide the basis for a paper-based sorbent, indicator material, antimicrobial material, or a platform for subsequent nanocomposite synthesis.

The main scientific question of this study is formulated as follows: is the binding of Ag on Tiron-modified filter paper due to simple physical adsorption, to the formation of an Ag+–Tiron complex, to the formation of Ag(0) nanoparticles, or to a combination of these processes? The literature review was aimed specifically at substantiating this question, establishing the criteria for the subsequent experiments, and shaping the theoretical part of the article.

Literature Review

Properties of Tiron as a Ligand

The principal structural advantage of Tiron is its catechol fragment: upon deprotonation, the two adjacent hydroxyl groups can provide bidentate coordination to metal ions. The disulfonate groups render the molecule hydrophilic, making Tiron a convenient analytical reagent that operates in aqueous media. References (National Center for Biotechnology Information.; Dojindo Molecular Technologies, Inc. Tiron (T021)) describe Tiron as the disodium salt of composition $C_6H_4Na_2O_8S_2$ and characterize it as a reagent that forms colored chelates with Fe, Al, Ti, and other metal ions.

Recent studies of the Fe(III)–Tiron system show that Tiron forms complexes with the metal at various stoichiometries and that the color of the complexes is pH-dependent (Nucera, A., Carniato, F., Baranyai, Z., Platas-Iglesias, C., Botta, M., 2023). This indicates that, when working with Ag, the effects of pH, ligand-to-metal ratio, ionic strength, and competing cations must be investigated separately, because the complexation ability of Tiron is governed not only by the presence of the ligand but also by the protonation state of its phenolic groups and by the conformational freedom retained after immobilization onto a surface.

Tiron is not among the best-known selective reagents for Ag+; moreover, although its electron-donor catechol moiety is not fully matched to Ag+ according to hard–soft acid–base theory, it can create favorable conditions for coordination bonding, electrostatic interaction, and subsequent reduction processes. For this reason, characterization of the Ag-bound Tiron–paper material cannot rely on a mere color change or mass increase; methods that confirm the oxidation state of Ag are required.

Role of Filter Paper and the Cellulose Matrix

The main component of filter paper is cellulose, which is amenable to modification owing to its numerous hydroxyl groups, fibrous porous structure, and capillary properties. In paper microfluidic and test-strip devices, paper serves as a passive platform that transports the liquid, retains the reagent, and confines the reaction to a visible zone. Reviews on paper-based microfluidics show that paper is a low-cost, flexible material well suited to point-of-care analysis (Li, X., Ballerini, D. R., Shen, W., 2012; Yetisen, A. K., Akram, M. S., Lowe, C., 2013; Costa, M. N., Veigas, B., Jacob, J. M., Santos, D. S., Gomes, J., Baptista, P. V., Martins, R., Inácio, J., Fortunato, E., 2014).

Numerous studies on cellulose-based adsorbents report that the introduction of carboxyl, amino, thiol, phosphate, sulfonate, or chelating groups enhances the ability to capture metal ions (Shaghaleh, H., Xu, X., Wang, S., 2018; Abdelhamid, H. N., Mathew, A. P., 2021; Si, R., Pu, J., Luo, H., Wu, C., Duan, G., 2022). Fakhre and Ibrahim applied chemically modified cellulose to the adsorption of heavy metal ions; such an approach methodologically supports the idea of immobilizing a chelating ligand such as Tiron onto a cellulose surface (Fakhre, N. A., Ibrahim, B. M., 2018).

When Tiron is immobilized onto filter paper, two types of problems arise. The first is preventing the reagent from being washed out: because Tiron is highly water-soluble, a simple soaking procedure may not be sufficient for permanent immobilization. The second is avoiding blockage of the metal-binding active sites of the ligand: if covalent attachment or coating with a polymer layer blocks the catechol groups of Tiron, Ag binding will decrease. It is therefore essential to demonstrate by FTIR the efficiency of the immobilization procedure, the mass stability of the material upon washing, and the preservation of the functional groups of the ligand.

Ag^+ Detection and Paper-Based Silver Platforms

Silver is widely used in industry, photochemistry, electronics, medicine, and antimicrobial materials. At the same time, monitoring Ag+ ions in water and food samples is important because excess silver poses environmental and toxicological risks. Fan et al. proposed a paper test-strip platform modified with black phosphorus quantum dots for the detection of Ag^+ in drinking water, combining fluorometric and colorimetric signals (Fan, X., Lv, J., Li, R., Chen, Y., Zhang, S., Liu, T., Zhou, S., Shao, X., Wang, S., Hu, G., Yue, Q., 2023).

A paper-based colorimetric array test-strip approach has also been developed for the simultaneous detection of multiple metal ions (Liu, L., Lin, H., 2014). These studies demonstrate that metal ions can be detected visually or semi-quantitatively using reagents immobilized on paper. The Tiron–Ag–paper system could join this family of platforms; its advantages include the ready availability of Tiron as a simple organic ligand, the low cost of filter paper, and the possibility that additional optical or antimicrobial properties emerge on the surface after Ag binding.

The retention of Ag+ on paper can occur through several mechanisms: weak coordination with the –OH groups of cellulose, complexation with the phenolate catechol groups of Tiron, electrostatic interaction near the sulfonate groups, or the formation of Ag(0) nanoparticles under reducing conditions. If the paper treated with an AgNO3 solution changes color or darkens during the experiment, this also points to the possible photochemical or chemical reduction of Ag+.

Experimental Section

Standard solutions of the analytical reagents. Tiron (disodium salt of 1,2-dihydroxybenzene-3,5-disulfonic acid, CAS 149–45–1) was selected as the immobilized analytical reagent. The substance was obtained in analytical grade from Shanghai Macklin Biochemical Co., Ltd. (China). A 1×10^{-3} M standard solution of Tiron was prepared in distilled water and used in the immobilization procedures. The molecular structure of the Tiron salt is shown in Figure 1.

Figure 1. *Molecular structure of Tiron (disodium salt of 1,2-dihydroxybenzene-3,5-disulfonic acid)*

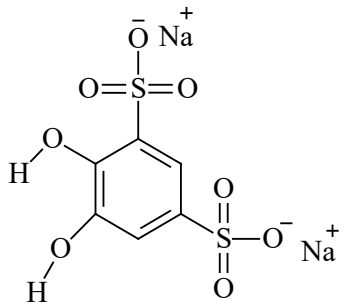

Buffer solutions. An acetate buffer solution was used to maintain the required pH of the systems under study. In analytical chemistry and in sensor-related work, the acetate buffer system (pH range 3.7–5.6) is one of the most commonly used stable buffer systems. It is prepared from a mixture of a weak acid (acetic acid, CH3COOH) and its salt (sodium acetate, CH3COONa).

Preparation of the polymer matrix. Before immobilization of the Tiron reagent (disodium salt of 1,2-dihydroxybenzene-3,5-disulfonic acid), the filter paper was cut into circles with a diameter of 2 cm. The resulting filter paper samples were first washed with distilled water and then dried at room temperature.

Equipment. The following instruments were used to examine the samples during the experiments: an Eye-One Pro spectrophotometer (ES-2000), a UV–Vis spectrophotometer (Shimadzu 1900i), a pH meter (Mettler-Toledo GmbH), a magnetic stirrer (MS7-H550-Pro), and an infrared spectrometer (Shimadzu IRAffinity-1S). The deionized

water used in the experiments was obtained from an EASYpure RoDI water purification system (Thermo Scientific, USA).

Immobilization procedure. To modify the cellulose matrix and achieve the maximum adsorption equilibrium of the Tiron reagent, the prepared filter paper samples were soaked in an aqueous Tiron solution at a concentration of 1×10^{-3} M for 24 h at room temperature. This period ensures the deep diffusion of Tiron molecules into the micro- and macropores of the cellulose and the formation of stable hydrogen bonds with the hydroxyl groups of the matrix fibers. After removal from the Tiron solution, the immobilized filter papers were separated from the excess solvent using a filter cassette and dried to constant mass at room temperature in a dark place for 24 h. This regime ensured the complete evaporation of free and bound water molecules from the matrix and the maximum stabilization of the IR spectral characteristics.

A 100 mL acetate buffer solution with pH 4.71 was prepared, and AgNO3 was dissolved in it to obtain a 0.001 M Ag+ solution. The solution was prepared at room temperature on a magnetic stirrer under dark conditions. The Tiron-immobilized filter paper was immersed in the resulting solution for 1–3 min in a dark room at +4 to +8 °C. The filter paper was then removed from the solution and dried in a dark room at 20–25 °C for 24 h. If the drying step is not performed in a dark room, Ag+ is reduced and converted to Ag0.

Optical Spectral Analysis

The optical response of the Tiron-immobilized filter paper and of the Filter paper+Tiron+Ag(I) complex links the theoretical considerations of the literature review to the experimental results. The graphs show the variation of the Kubelka–Munk function F(R) over the 380–730 nm range. These spectra clearly demonstrate the differences between plain filter paper, Tiron-immobilized filter paper (Filter paper+Tiron), and Tiron-modified paper with sorbed Ag(I) ions (Filter paper+Tiron+Ag(I)).

Graph 1. *F(R) spectra of plain filter paper and Tiron-immobilized filter paper. After Tiron immobilization, the absorption/reflectance function in the 400–650 nm range is higher than that of plain paper*

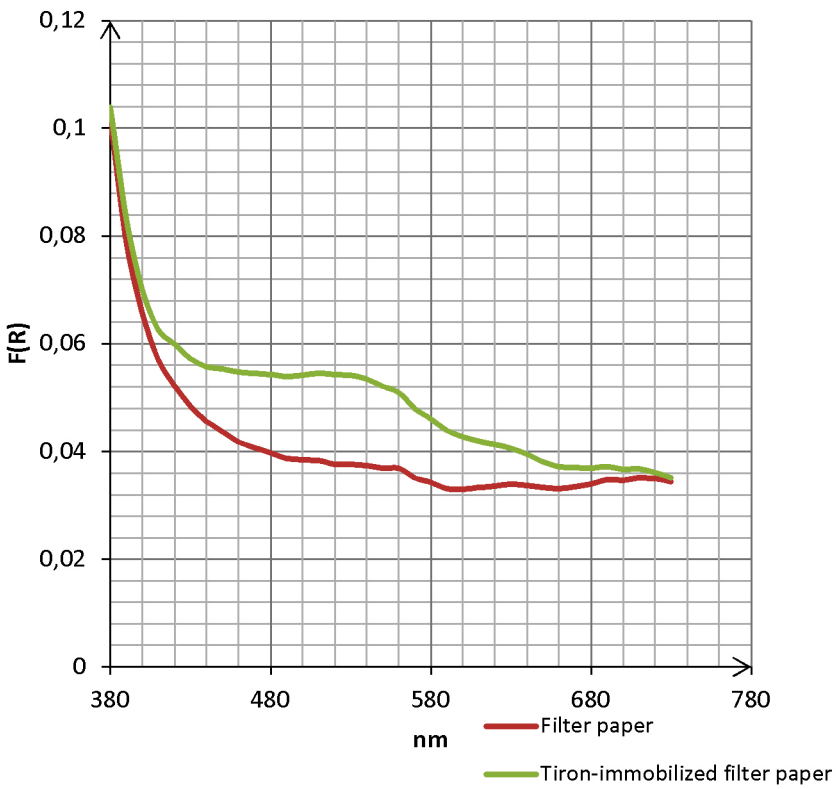

As can be seen from Graph 1, filter paper treated with Tiron exhibits higher F(R) values than plain filter paper over almost the entire visible range. In particular, in the 420–

–560 nm range, the curve of the Tiron-immobilized paper is clearly distinct from that of plain paper. This indicates that Tiron molecules are retained on the surface of the cellulose fibers and that the optical properties of the paper have changed. Although the Tiron solution and the Tiron-immobilized paper appear colorless to the naked eye, the spectral measurements reveal the modification with higher sensitivity.

Graph 2. *F(R) spectra of filter paper, Filter paper+Tiron, and Filter paper+Tiron+Ag(I) samples. The change in the shape of the curve after the uptake of Ag(I) ions indicates the formation of a silver-containing surface complex/compound*

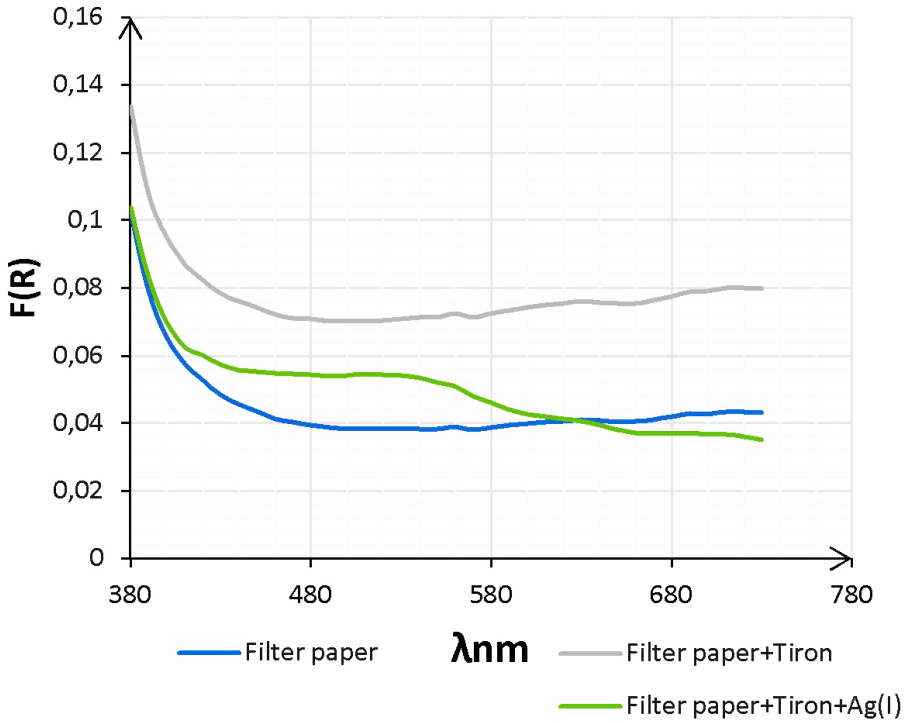

In Graph 2, three samples are compared: plain filter paper, Filter paper+Tiron, and Filter paper+Tiron+Ag(I). The Filter paper+Tiron sample exhibits a higher optical response than plain filter paper, confirming that Tiron is immobilized on the carrier surface. After the uptake of Ag(I) ions, the curve of Filter paper+Tiron+Ag(I) differs sharply from that of Filter paper+Tiron: the signal is higher in the 380–550 nm range, with a decrease toward 560–730 nm. This change indicates that an interaction has occurred between the functional groups of Tiron and the Ag(I) ions.

Together, the color change and the spectral differences observed after the uptake of Ag(I) indicate that the Tiron-immobilized paper acts as a surface sensitive to silver ions. The color development may be associated with the formation of an Ag(I)–Tiron complex, the coordination binding of Ag(I) to the cellulose/Tiron surface, or, under certain conditions, the partial formation of Ag(0) particles.

The presented results show that the immobilization of Tiron on filter paper enhances the spectral response relative to plain paper and that the optical response acquires a new character after the uptake of Ag(I) ions. Thus, Tiron-immobilized filter paper can be regarded as a low-cost cellulosic platform for the sorption of Ag(I) ions with a visible color response. These results are consistent with the complexation behavior of Tiron with metal ions reported in the literature and with the practical advantages of paper-based sensors.

IR/FTIR Spectral Analysis

Infrared spectroscopy (IR or FTIR) was used to identify the functional groups in the samples and to assess changes in their chemical environment after the modification process. The spectra of filter paper, Tiron-immobilized filter paper, and the Filter paper+Tiron+Ag complex are interpreted in-

dividually below. The spectra were recorded in the 4000–400 cm⁻¹ range, with particular attention to the O–H, C–H, aromatic ring, C–O/C–O–C, S=O/S–O, and low-frequency metal–ligand regions.

1. IR Spectrum of Plain Filter Paper

Figure 3. *IR/FTIR spectrum of plain filter paper. O–H, C–H, and C–O–C/C–O vibration regions characteristic of the cellulose matrix are observed in the spectrum*

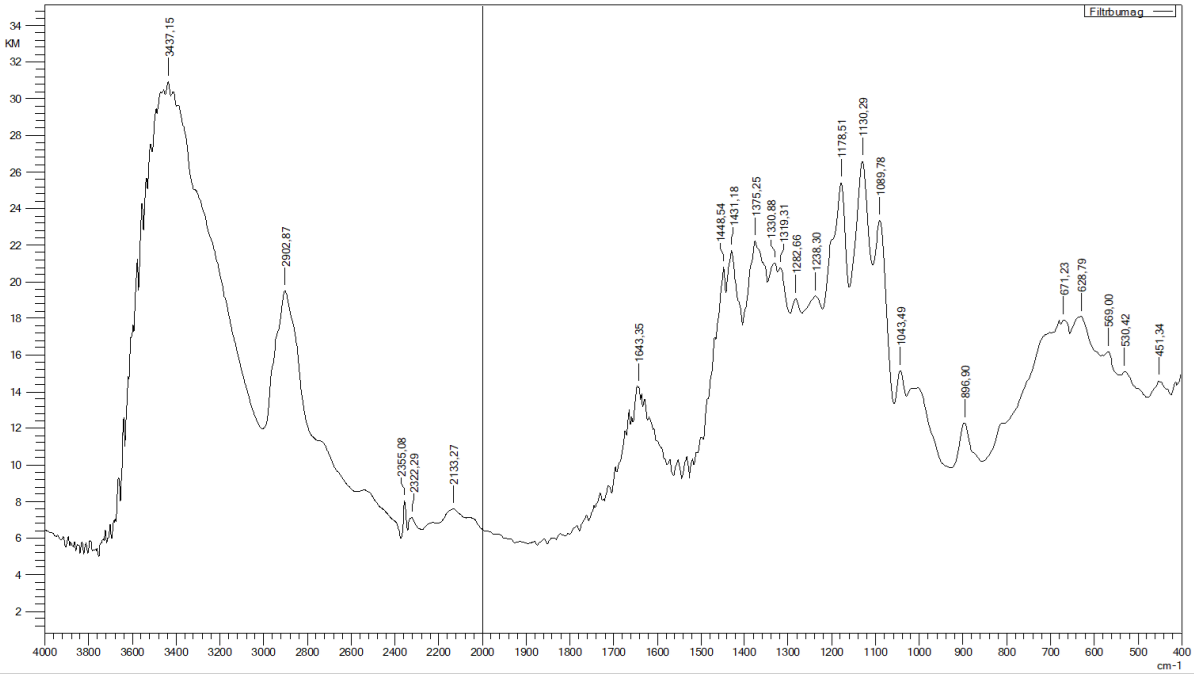

In the spectrum of plain filter paper, the broad and intense band around 3437.15 cm⁻¹ is associated with the stretching vibrations of the hydroxyl (–OH) groups of cellulose and with strong hydrogen bonding (Maréchal, Y., Chanzy, H., 2000). The band around 2902.87 cm⁻¹ corresponds to the stretching vibrations of aliphatic C–H bonds in the cellulose chain (Oh, S. Y., Yoo, D. I., Shin, Y., Seo, G., 2005). The signal around 1643.35 cm⁻¹ is attributed to bound water molecules or to O–H deformation vibrations on the cellulose surface.

The absorptions in the 1448.54, 1431.18, 1375.25, 1330.88, 1319.31, 1282.66, and 1238.30 cm⁻¹ regions may be related to the C–H deformation, C–O, and C–O–H vibrations of the cellulose skeleton. The strong signals around 1178.51, 1130.29, 1089.78, and 1043.49 cm⁻¹ indicate the C–O–C glycosidic bond and the C–O stretching vibrations diagnostic of cellulose (Oh, S. Y., Yoo, D. I., Shin, Y., Seo, G., 2005). The band at 896.90 cm⁻¹ is regarded as characteristic of β-glycosidic linkages. The 671.23, 628.79, 569.00, 530.42, and 451.34 cm⁻¹ regions are associated with low-frequency deformation vibrations.

The spectrum of plain filter paper provides the typical IR signatures of a cellulose-based matrix and serves as a control spectrum for comparing the subsequent modifications.

2. IR Spectrum of Tiron-Immobilized Filter Paper

In the Filter paper+Tiron spectrum, the broad O–H band around 3437.15 cm⁻¹ is retained, indicating the presence of hydrogen bonding between cellulose and the phenolic –OH groups of Tiron (Maréchal, Y., Chanzy, H., 2000). The C–H signal at 2900.94 cm⁻¹ corresponds to the vibrations of the organic skeleton (Oh, S. Y., Yoo, D. I., Shin, Y., Seo, G., 2005). The band around 1639.49 cm⁻¹ is close to the 1643.35 cm⁻¹ signal of plain filter paper but is slightly shifted, which may indicate a change in the O–H bonding environment as a result of Tiron immobilization (Maréchal, Y., Chanzy, H., 2000; Oh, S. Y., Yoo, D. I., Shin, Y., Seo, G., 2005).

Figure 4. *IR/FTIR spectrum of Tiron-immobilized filter paper. After the introduction of Tiron, the composition of the signals in the 1400–1000 cm–¹ range changes.*

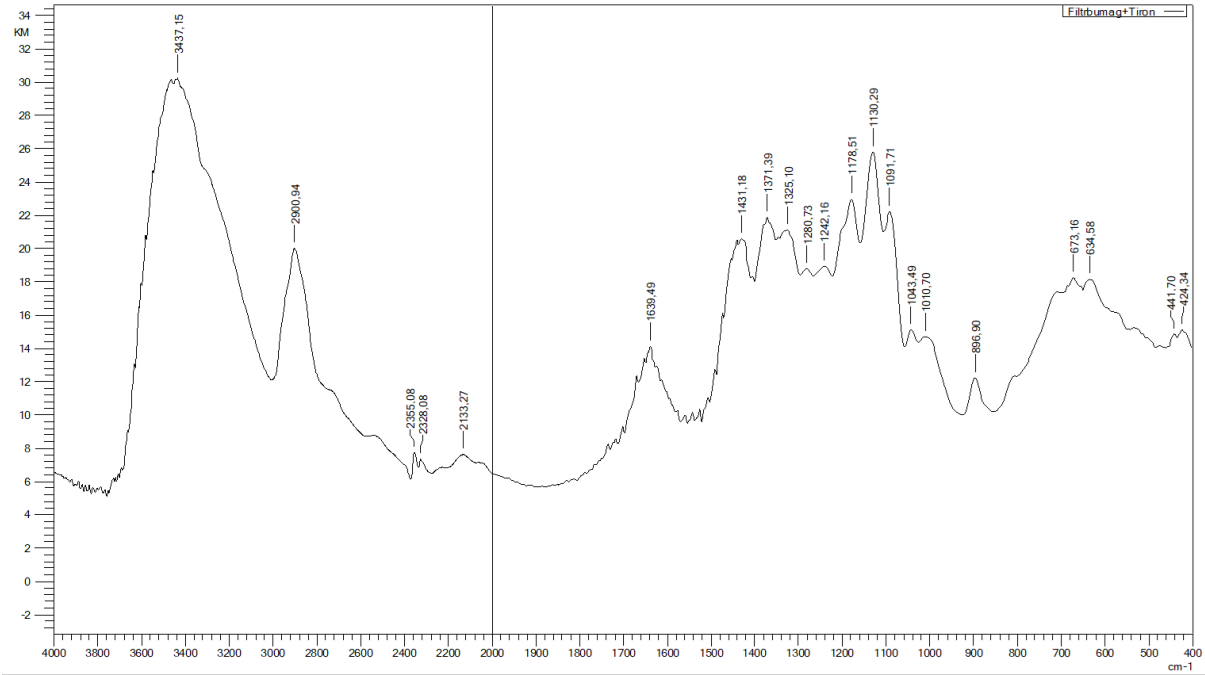

The signals in the 1431.18, 1371.39, 1325.10, 1280.73, and 1242.16 cm⁻¹ regions may be enhanced or reshaped owing to vibrations related to the aromatic ring of Tiron, the phenolic C–O vibrations, and the sulfonate groups. The bands around 1178.51, 1130.29, 1091.71, 1043.49, and 1010.70 cm⁻¹ indicate that the S=O/S–O and C–O vibrations of Tiron are superimposed on the C–O–C/C–O vibrations of cellulose (Oh, S. Y., Yoo, D. I., Shin, Y., Seo, G., 2005; Pavia, D. L., Lampman, G. M., Kriz, G. S., Vyvyan, J. A., 2015). The signals at 673.16 and 634.58 cm⁻¹ are interpreted as low-frequency vibrations related to the deformation of the aromatic ring or to the sulfonate groups.

After Tiron immobilization, new or shifted absorptions appear in the 1400–1000 cm⁻¹ range while the typical cellulose signals are preserved in the spectrum. This indicates that Tiron is retained on the surface of the filter paper.

3. IR Spectrum of the Filter paper+Tiron+Ag Complex

In the Filter paper+Tiron+Ag spectrum, the broad O–H band at 3456.44 cm⁻¹ is shifted to a slightly higher frequency compared with the 3437.15 cm⁻¹ region of the Tiron-immobilized sample. This indicates that a change has occurred in the environment of the hydroxyl groups and in hydrogen bonding after the uptake of Ag ions (Pavia, D. L., Lampman, G. M., Kriz, G. S., Vyvyan, J. A., 2015). The signal at 2900.94 cm–¹ indicates that the C–H vibrations of the organic skeleton are preserved. The bands around 1643.35 and 1566.20 cm⁻¹ may be associated with the aromatic/catechol fragments of Tiron and with the electron environment modified as a result of the interaction with Ag.

The signals in the 1429.25, 1373.32, 1336.67, 1319.31, and 1282.66 cm⁻¹ regions are slightly changed compared with the corresponding regions of the Tiron-immobilized paper. This indicates that the phenolic C–O and aromatic ring vibrations of Tiron have passed into a new coordination environment in the presence of Ag ions. The strong absorptions in the 1203.58, 1176.58, 1130.29, 1091.71, 1043.49, and 1002.98 cm⁻¹ regions indicate that the sulfonate, C–O, and C–O–C groups may participate in the binding of Ag (Nakamoto, K., 2009). The changes in the low-frequency 675.09, 628.79, 567.07, and 443.63 cm⁻¹ regions are likely related to near metal–ligand vibrations or to surface complexation (Nakamoto, K., 2009).

Figure 5. *IR/FTIR spectrum of the Filter paper+Tiron+Ag complex. After treatment with Ag, shifts and intensity changes are observed in the regions of certain functional groups*

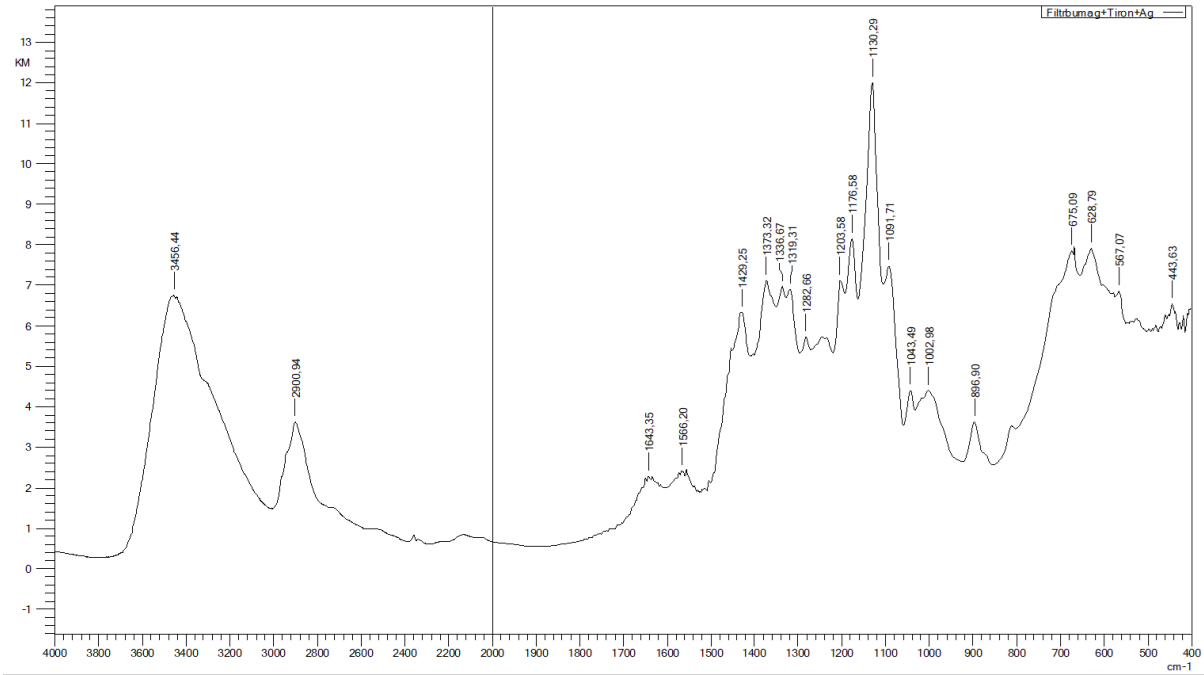

General Analysis of the IR Spectra

A comparison of the three spectra shows that plain filter paper gives mainly the O–H, C–H, C–O–C, and C–O vibrations characteristic of cellulose. After Tiron immobilization, the composition of the signals in the 1400–1000 cm^{-1} range changes significantly, indicating that the aromatic ring, phenolic C–O, and sulfonate groups of Tiron have been introduced onto the paper surface. After the uptake of Ag, additional shifts and intensity changes are observed in the 3456, 1566, 1429–1282, and 1203–1002 cm^{-1} regions.

Thus, the IR analyses progressively confirm the immobilization of Tiron and the subsequent interaction with Ag: in the first stage, the filter paper is functionalized with Tiron; in the second stage, the Ag ions bind to the phenolic and sulfonate groups of Tiron, as well as to the oxygen-containing groups on the cellulose surface. However, the IR spectrum does not fully establish whether Ag is present as Ag(I) or Ag(0). Therefore, XRD, XPS, or SEM–EDS analyses are additionally required to unambiguously prove the oxidation state of Ag.

Table 1.

Sample	Main regions, cm^{-1}	Probable assignment	Scientific interpretation
Filter paper	3437; 2902; 1643; 1178–1043; 896	O–H, C–H, bound water/O–H deformation, C–O–C/C–O, β-glycosidic bond	Control spectrum of the cellulose matrix.
Filter paper+Tiron	3437; 1639; 1431–1242; 1178–1010; 673–634	O–H, aromatic/catechol fragment, C–O, S=O/S–O, ring deformation	Indicates that Tiron is immobilized on the paper surface.
Filter paper+Tiron+Ag	3456; 1643; 1566; 1429–1282; 1203–1002; 675–443	O–H shift, aromatic/catechol, C–O/S–O, low-frequency surface vibrations	Indicates that Ag ions interact with the Tiron/cellulose groups.

The generalized interpretation of the main IR bands is given in the following table 1:

Conclusion

In this study, the organic reagent Tiron was successfully immobilized onto the surface of filter paper, and a functional material capable of binding silver(I) ions was obtained. The diffuse reflectance spectroscopy (DRS) results showed that the optical properties of the filter paper changed after Tiron immobilization and that the spectral response changed even more significantly after treatment with Ag(I) ions. The FTIR analyses confirmed the successful immobilization of Tiron onto the cellulose matrix and the participation of the hydroxyl and sulfonate functional groups in the interaction with Ag(I) ions. The obtained results demonstrate that Tiron-modified filter paper is an effective functional material for binding silver(I) ions. The material is simple to prepare, economically affordable, and environmentally safe, which allows its application in the development of paper-based optical sensors, sorption materials, and rapid metal-ion detection systems. Further studies are underway to enhance the analytical performance of the material, including a detailed assessment of its selectivity, sorption capacity, limit of detection, and applicability to real samples.

References

National Center for Biotechnology Information. PubChem Compound Summary for CID 9001, Tiron. https://pubchem.ncbi.nlm.nih.gov/compound/Tiron (accessed August 1, 2026).

Dojindo Molecular Technologies, Inc. Tiron (T021): metal indicator for Fe; colorimetric reagent for Fe, Al, Ti, and other metal ions. https://www.dojindo.com/products/T021/ (accessed August 1, 2026).

Nucera, A., Carniato, F., Baranyai, Z., Platas-Iglesias, C., Botta, M. (2023). Characterization of the Fe(III)–Tiron system in solution through an integrated approach combining NMR relaxometric, thermodynamic, kinetic, and computational data. Inorg. Chem. 2023, 62 (10), 4272–4283. DOI: 10.1021/acs.inorgchem.2c04393.

Li, X., Ballerini, D. R., Shen, W. (2012). A perspective on paper-based microfluidics: current status and future trends. Biomicrofluidics 2012, 6 (1), 011301. DOI: 10.1063/1.3687398.

Yetisen, A. K., Akram, M. S., Lowe, C. (2013). R. Paper-based microfluidic point-of-care diagnostic devices. Lab Chip 2013, 13 (12), 2210–2251. DOI: 10.1039/C3LC50169H.

Costa, M. N., Veigas, B., Jacob, J. M., Santos, D. S., Gomes, J., Baptista, P. V., Martins, R., Inácio, J., Fortunato, E. (2014). A low cost, safe, disposable, rapid and self-sustainable paper-based platform for diagnostic testing: lab-on-paper. Nanotechnology 2014. – 25 (9). – 094006. DOI: 10.1088/0957-4484/25/9/094006.

Shaghaleh, H., Xu, X., Wang, S. (2018). Current progress in production of biopolymeric materials based on cellulose, cellulose nanofibers, and cellulose derivatives. RSC Adv. 2018, – 8 (2). – P. 825–842. DOI: 10.1039/C7RA11157F.

Abdelhamid, H. N., Mathew, A. P. (2021). Cellulose-based materials for water remediation: adsorption, catalysis, and antifouling. Front. Chem. Eng. 2021, – 3. – 790314 p. DOI: 10.3389/fceng.2021.790314.

Si, R., Pu, J., Luo, H., Wu, C., Duan, G. (2022). Nanocellulose-based adsorbents for heavy metal ion removal. Polymers 2022, – 14 (24). – 5479 p. DOI: 10.3390/polym14245479.

Fakhre, N. A., Ibrahim, B. M. (2018). The use of new chemically modified cellulose for heavy metal ion adsorption. J. Hazard. Mater. 2018, – 343. – P. 324–331. DOI: 10.1016/j.jhazmat.2017.08.043.

Fan, X., Lv, J., Li, R., Chen, Y., Zhang, S., Liu, T., Zhou, S., Shao, X., Wang, S., Hu, G., Yue, Q. (2023). Paper test strip for silver ions detection in drinking water samples based on combined fluorometric and colorimetric methods. Arab. J. Chem. 2023, – 16 (2). – 104492 p. DOI: 10.1016/j.arabjc.2022.104492.

Liu, L., Lin, H. (2014). Paper-based colorimetric array test strip for selective and semiquantitative multi-ion analysis: simultaneous detection of Hg2+, Ag+, and Cu2+. Anal. Chem. 2014, – 86 (17). – P. 8829–8834. DOI: 10.1021/ac5021886.

Maréchal, Y., Chanzy, H. (2000). The hydrogen bond network in Iβ cellulose as observed by infrared spectrometry. J. Mol. Struct. 2000, – 523 (1–3). – P. 183–196. DOI: 10.1016/S0022-2860(99)00389-0.

Oh, S. Y., Yoo, D. I., Shin, Y., Seo, G. (2005). FTIR analysis of cellulose treated with sodium hydroxide and carbon dioxide. Carbohydr. Res. 2005, – 340 (3). – P. 417–428. DOI: 10.1016/j.carres.2004.11.027.

Pavia, D. L., Lampman, G. M., Kriz, G. S., Vyvyan, J. A. (2015). Introduction to Spectroscopy, 5th ed., Cengage Learning, 2015.

Nakamoto, K. (2009). Infrared and Raman Spectra of Inorganic and Coordination Compounds, Part B: Applications in Coordination, Organometallic, and Bioinorganic Chemistry, 6th ed., Wiley, 2009.

submitted 01.08.2026;
accepted for publication 15.08.2026;
published 31.08.2026
© Sabirov N., Ashirov M., Palvanov N.
Contact: sobirovnodibek769@gmail.com; mansur.ashirov.86@mail.ru; norbeksapaevich@gmail.com

Austrian Journal of Technical
and Natural Sciences, 2026 No 7–8
ISSN 2310-5607

PREMIER Publishing
ppublishing.org

DOI:10.29013/AJT-26-7.8-18-24

RECOVERY OF RHENIUM AND MOLYBDENUM FROM INDUSTRIAL WASTEWATER USING THE KAOLIN-CHITOSAN COMPOSITE BIOSORBENT: SORPTION KINETICS AND ELEMENTAL ANALYSIS

Bakhtiyor Berdikulov [1], Gulnora Ikhtiyarova [1]

[1] Tashkent State Technical University named after Islam Karimov, Tashkent, Uzbekistan

Cite: *Berdikulov B., Ikhtiyarova G. (2026). Recovery of Rhenium and Molybdenum From Industrial Wastewater Using the Kaolin-Chitosan Composite Biosorbent: Sorption Kinetics and Elemental Analysis. Austrian Journal of Technical and Natural Sciences 2026, No 7–8.* https://doi.org/10.29013/AJT-26-7.8-18-24

Abstract

In this study, the ability of the previously synthesized and characterized AK-Xz (kaolin-chitosan, 5:1) composite biosorbent to take up rhenium (Re) and molybdenum (Mo) from an industrial wastewater sample containing these metals was investigated. The sorption experiment was carried out by keeping 1 g of sorbent in 100 mL of solution for contact times ranging from 10 to 300 minutes, while the process was monitored by UV–Vis spectrophotometry. The results showed that the absorbance of the solution decreased with time and stabilized within the 150–300 minute range, indicating that equilibrium had been reached. The kinetic data fitted the pseudo-first-order model with high accuracy (R^2 = 0.9934), whereas the pseudo-second-order model showed a markedly lower fit (R^2 = 0.7256). XRF elemental analysis confirmed that, after sorption, the Mo content of the solid phase increased from 0.836% to 2.97% (3.55-fold) and the Re content from 0.0410% to 0.0830% (2.02-fold). These findings indicate that the AK-Xz composite is a promising sorbent for recovering strategic metals from industrial wastewater.

Keywords: *AK-Xz, kaolin-chitosan composite, biosorbent, rhenium, molybdenum, sorption kinetics, pseudo-first-order, XRF*

Introduction

Biosorption based on natural and modified biopolymers has emerged as a low-cost, environmentally friendly alternative to conventional metal-recovery technologies (Aksu, Z., 1998; Qasem, N.A.A., Mohammed, R.H., Lawal, D.U., 2021). Rhenium (Re) and molybdenum (Mo) are strategic metals extensively used in the petrochemical industry – for example, in reforming and hydrotreating catalysts – whose natural reserves are limited and whose extraction is costly (Shen, L., Tesfaye, F., Li, X., Lindberg, D., Taskinen, P., 2021). Consequently, recovering such metals from industrial wastewater and catalyst-processing solutions is of considerable environmental and economic importance (Qasem, N.A.A., Mohammed, R.H., Lawal, D.U., 2021; Miyah, Y., El Messaoudi, N., Benjelloun, M., Geor-

gin, J., Franco, D. S. P., Viscusi, G., Messali, M., Knani, S., 2026). In earlier work, an AK-Xz composite biosorbent was synthesized from local Angren kaolin (Dill, H.G., Kus, J., Dohrmann, R., Tsoy, Y., 2008) and chitosan obtained from beekeeping waste (Apis mellifera) by the ionic gelation method (Rahaeng, K., Oraintara, A., Mahakham, W., 2026), and its composition was characterized by SEM-EDX and FTIR. The presence in the FTIR spectrum of the Amide I (1646 cm^{-1}) and Amide II (1557 cm^{-1}) bands characteristic of chitosan (Guibal, E., 2004; Zubir, A., Normaya, E., Danial, W.H., Goh, P. S., Piah, M. B. M., Show, P.-L., Ismail, A. F., Ahmad, M. N., 2026), together with accompanying changes in SEM morphology, confirmed the successful synthesis of the composite, consistent with previously reported kaolin- and clay-based chitosan composites (Gao, Z., Li, X., Wu, H., Zhao, S., Deligeer, W., Asuha, S., 2015; Gu, S., Kang, X., Wang, L., Lichtfouse, E., Wang, C., 2019; Liu, B., Wang, D., Yu, G., Meng, X., 2013). However, the actual practical sorption efficiency of the composite – in particular toward strategic metals – had not yet been tested.The aim of this work was to provide a preliminary evaluation of the ability of the AK-Xz composite biosorbent to take up Re and Mo from an industrial wastewater sample containing these metals. The objectives of the study included: (i) monitoring the sorption process over time by UV–Vis spectrophotometry; (ii) analyzing the obtained kinetic data using the pseudo-first-order and pseudo-second-order models 2, (Simonin, J.-P., 2016); (iii) comparing the elemental composition of the samples before and after sorption by XRF; (iv) drawing preliminary conclusions on the sorption mechanism based on the results obtained.

Materials and Methods

Sorbent

The previously synthesized AK-Xz composite biosorbent was used in this study. Angren kaolin (Dill, H.G., Kus, J., Dohrmann, R., Tsoy, Y., 2008) was acid-activated with 0.1 N HCl and thermally treated at 450 °C for 2 h (AK-450) (Gao, Z., Li, X., Wu, H., Zhao, S., Deligeer, W., Asuha, S., 2015; Chai, J.-B., Au, P.-I., Mubarak, N.M., Khalid, M., Ng, W.P.-Q., Jagadish, P., Walvekar, R., Abdullah, E.C., 2020), and was then mixed with a 1% chitosan–acetic acid solution at a 5:1 (kaolin: chitosan) mass ratio; granules were formed by the ionic gelation method (0.5 N NaOH/30% ethanol bath) (Rahaeng, K., Oraintara, A., Mahakham, W., 2026).

Industrial water sample

An industrial wastewater sample containing Mo, Re and other metals was selected as the object of the study. The full elemental composition of the initial solution was determined by XRF (Rigaku NEX CG, FP method) (Table 1).

Sorption experiment

One gram of AK-Xz sorbent was added to 100 mL of the industrial water and kept in contact for 10, 20, 30, 40, 50, 60, 90, 120, 150 and 300 minutes. The colour intensity of the solution, characteristic of Mo/Re complexes (Basak, A., 1995), was measured at each time point as absorbance (A) using a UV–Vis spectrophotometer. After each contact time, the sorbent was separated from the solution and rinsed with distilled water (to reduce surface residue) and prepared for further analysis.

Solid-phase analysis

The elemental composition of the loaded (post-sorption) solid sample was determined by XRF ("Bulk", Scatter method) (Table 3).

Kinetic models

Two classical models were applied to describe the sorption kinetics (Sangoremi, A.A., 2025; Simonin, J.-P., 2016):

Pseudo-first-order (Lagergren):

$$\ln(q_e - q_t) = \ln(q_e) - k_1 \cdot t$$

Pseudo-second-order (Ho and McKay):

$$t/q_t = 1/(k_2 \cdot q_e^2) + t/q_e$$

where q_t and q_e are the relative (absorbance-based) uptake at time t and at equilibrium, respectively, and k_1 and k_2 are the rate constants of the corresponding orders. Since a proportionality based on the Beer–Lambert law was assumed between absorbance and concentration, $q_t = A_0 - A_t$ was used as the relative sorption quantity (Fadl, M. G., 2023).

Results

Elemental composition of the initial industrial water

Table 1. *XRF (FP method, assuming an aqueous solution) analysis results of the initial industrial water (major elements; the full spectrum comprises 27 elements)*

No.	Element	Result (mass%)	Unit
1	Mg	0.102	mass%
2	Al	0.0931	mass%
3	Si	0.0262	mass%
4	S	3.71	mass%
5	K	0.0257	mass%
6	Ca	0.0093	mass%
7	Ti	(0.0004) – below LLD	mass%
8	Cr	(0.0001) – below LLD	mass%
9	Mn	0.0332	mass%
10	Fe	0.117	mass%
11	Co	(0.0004) – below LLD	mass%
12	Cu	0.0470	mass%
13	Zn	0.0014	mass%
14	As	0.0007	mass%
15	Se	0.0009	mass%
16	Rb	0.0001	mass%
17	Mo	0.836	mass%
18	Ag	0.0005	mass%
19	Sn	0.0018	mass%
20	Pb	0.0004	mass%
21	Zr	0.0450	mass%
22	Re	0.0410	mass%

Sorption kinetics: absorbance and relative uptake

Table 2. *Time-dependent absorbance and relative uptake (the value at t = 10 min was taken as the initial point A_0, since no measurement prior to contact was available)*

t (min)	Absorbance (A)	**Relative uptake, R (%)**
10	0.675	0.00
20	0.666	1.33
30	0.654	3.11
40	0.639	5.33
50	0.628	6.96
60	0.619	8.30
90	0.612	9.33
120	0.606	10.22
150	0.603	10.67
300	0.601	10.96

Figure 1. *Sorption kinetics analysis of the AK-Xz sorbent: (A) absorbance vs. time; (B) relative uptake vs. time; (C) linear fit of the pseudo-first-order model*

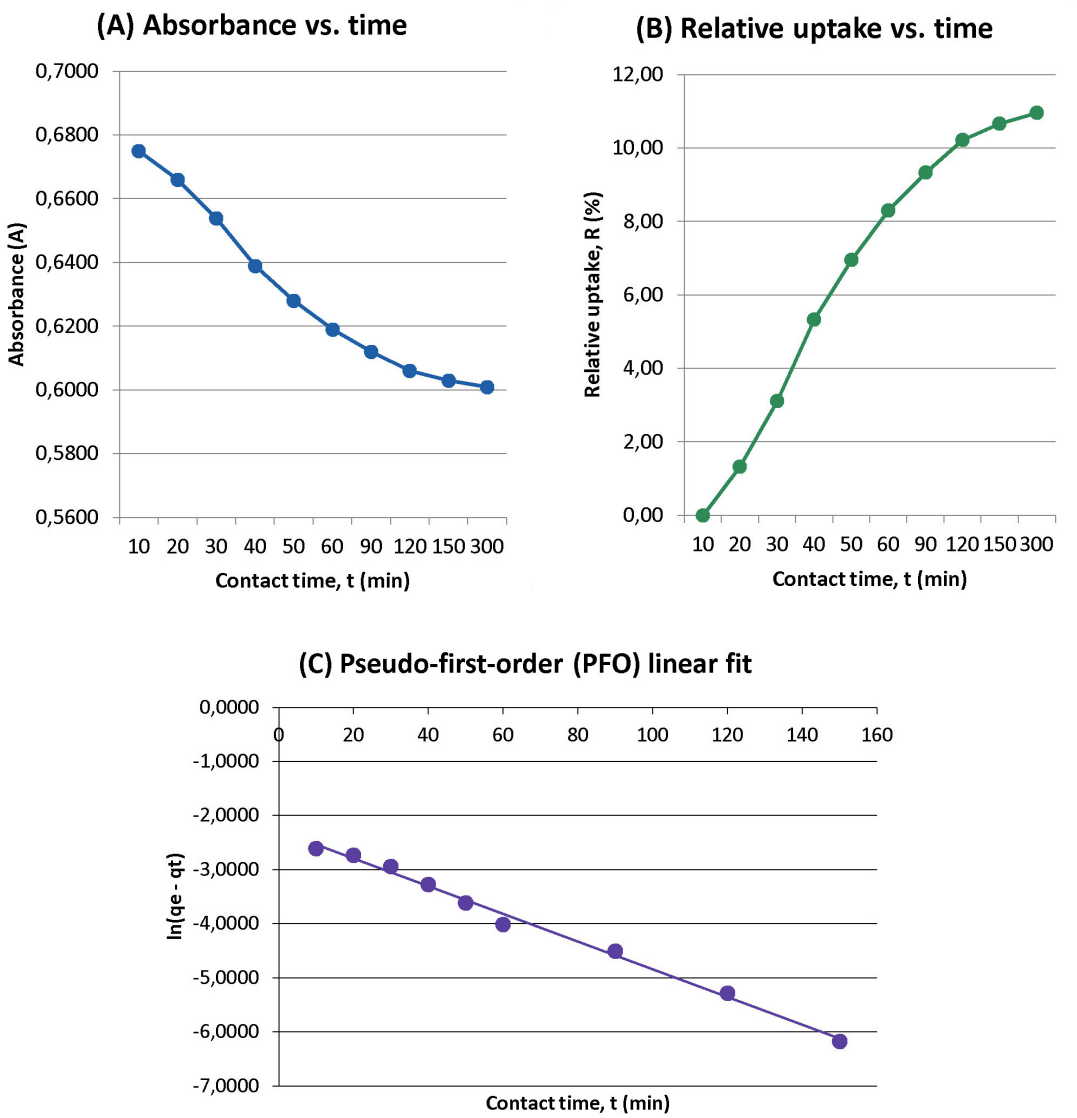

As seen in panels (A) and (B) of Figure 1, the absorbance – and hence the Mo/Re concentration in solution – decreased monotonically over time and remained practically unchanged within the 150–300 minute range, indicating that equilibrium had been reached. The equilibrium relative uptake was approximately 11.0%.

The kinetic modelling results (Figure 1, panel C) showed that the pseudo-first-order model fitted the data with high accuracy: $R^2 = 0.9934$, rate constant $k_1 \approx 0.0259$ min^{-1}. For comparison, the pseudo-second-order model showed a markedly lower fit ($R^2 = 0.7256$), confirming the superiority of the pseudo-first-order model under the conditions studied (Simonin, J.-P., 2016; Fadl, M.G., 2023).

Elemental composition of the solid phase after sorption

Table 3. *XRF ("Bulk", Scatter method) analysis results of the loaded solid sample (major elements; the full spectrum comprises 32 elements, including trace elements below the LLD and chemically unreliable ones, discussed in the Discussion section)*

No.	Element	Result (mass%)	Unit
1	Mg	0.585	mass%

No.	Element	Result (mass%)	Unit
2	Al	6.02	mass%
3	Si	15.7	mass%
4	S	5.55	mass%
5	K	2.71	mass%
6	Ca	0.202	mass%
7	Ti	0.306	mass%
8	Fe	1.31	mass%
9	Cu	0.0693	mass%
10	Zn	0.0109	mass%
11	As	0.0062	mass%
12	Rb	0.0143	mass%
13	Zr	0.108	mass%
14	Mo	2.97	mass%
15	Ba	0.0220	mass%
16	Re	0.0830	mass%
17	Hg	0.0093	mass%

Change in Mo and Re content and estimated equilibrium capacity

Table 4. *Comparative summary of Mo and Re content in the two phases*

Parameter	Initial solution	Loaded solid sample	Change
Mo, mass%	0.836	2.97	↑ 3.55-fold
Re, mass%	0.0410	0.0830	↑ 2.02-fold
Re/Mo ratio	0.049	0.028	↓ decreased

Using the solid-phase data, the approximate equilibrium sorption capacity (q_e = element mass% × sorbent mass) was calculated: q_e(Mo) ≈ 29.7 mg/g, q_e(Re) ≈ 0.83 mg/g (Peng, M., Xi, C., Shen, K., Tan, Y., Li, F., 2024; Upadhyay, U., Sreedhar, I., Singh, S.A., Patel, C.M., Anitha, K.L., 2021). In this calculation, the final dry mass of the sorbent was assumed to be approximately equal to the initial 1 g.

Discussion

The results obtained warrant discussion from several perspectives. First, the significant increase in the Mo and Re content of the solid sorbent (3.55-fold and 2.02-fold, respectively) confirms that the AK-Xz composite is indeed capable of taking up these metals (Peng, M., Xi, C., Shen, K., Tan, Y., Li, F., 2024; Upadhyay, U., Sreedhar, I., Singh, S.A., Patel, C.M., Anitha, K.L., 2021). The decrease in the Re/Mo ratio (0.049 → 0.028) suggests that the sorbent may have a somewhat higher selectivity toward the Mo ion (Miyah, Y., El Messaoudi, N., Benjelloun, M., Georgin, J., Franco, D.S.P., Viscusi, G., Messali, M., Knani, S., 2026; Yefremova, S., Kablanbekov, A., 2026); however, since this conclusion is based on a single experimental data point, it is preliminary in character and requires further confirmation.Second, the kinetic analysis showed the superiority of the pseudo-first-order model (R^2 = 0.9934). In the literature, the pseudo-second-order model is generally associated with chemisorption-type processes (electron exchange or complex formation), while the pseudo-first-order model more often describes processes limited by physical diffusion (Sangoremi, A.A., 2025; Simonin, J.-P., 2016; Fadl, M.G., 2023). From this perspective, the observed result suggests that a physical diffusion stage

may play an important role in the sorption process occurring on the AK-Xz surface. However, drawing a definitive conclusion about the sorption mechanism based solely on the degree of fit of a kinetic model is not scientifically sufficient – additional evidence (e.g., activation energy, thermodynamic parameters, XPS analysis of the loaded sorbent) is required for that.Third, the composition of the AK-Xz composite confirmed by FTIR in the earlier study (free amine groups of chitosan and the porous structure of kaolin) (Guibal, E., 2004; Zubir, A., Normaya, E., Danial, W.H., Goh, P.S., Piah, M.B.M., Show, P.-L., Ismail, A.F., Ahmad, M.N., 2026) suggests two possible mechanisms of Mo/Re uptake: (i) electrostatic attraction/complex formation via protonated amine groups (Guibal, E., 2004; Musarurwa, H., Tavengwa, N.T., 2022) and (ii) physical adsorption within the pores of the kaolin (Gao, Z., Li, X., Wu, H., Zhao, S., Deligeer, W., Asuha, S., 2015; Gu, S., Kang, X., Wang, L., Lichtfouse, E., Wang, C., 2019; Chai, J.-B., Au, P.-I., Mubarak, N.M., Khalid, M., Ng, W.P.-Q., Jagadish, P., Walvekar, R., Abdullah, E.C., 2020). The relatively moderate observed uptake level (~11%) and the pseudo-first-order kinetics can be explained by both mechanisms operating together but being limited by diffusion.

Conclusion

In this study, the ability of the AK-Xz kaolin-chitosan composite biosorbent to take up Re and Mo metals from industrial wastewater was preliminarily evaluated. The results showed that: (1) the sorption process reaches equilibrium within 150–300 minutes; (2) the kinetics fit the pseudo-first-order model with high accuracy ($R^2 = 0.9934$); (3) the Mo and Re content of the solid phase increased 3.55-fold and 2.02-fold, respectively, confirming that sorption occurred; (4) the decrease in the Re/Mo ratio provides a preliminary indication of higher sorbent selectivity toward the Mo ion. The results obtained indicate that the AK-Xz composite is a promising material for recovering strategic metals from industrial wastewater (Qasem, N.A.A., Mohammed, R.H., Lawal, D.U., 2021; Shen, L., Tesfaye, F., Li, X., Lindberg, D., Taskinen, P., 2021; Miyah, Y., El Messaoudi, N., Benjelloun, M., Georgin, J., Franco, D.S.P., Viscusi, G., Messali, M., Knani, S., 2026), consistent with the growing interest in low-cost biosorbents as sustainable alternatives to conventional metal-recovery technologies (Liu, B., Wang, D., Yu, G., Meng, X., 2013; Upadhyay, U., Sreedhar, I., Singh, S.A., Patel, C.M., Anitha, K.L., 2021). At the same time, further studies addressing the methodological limitations described above are needed to establish the absolute sorption capacity, the full isotherm, and the precise sorption mechanism.

References

Aksu, Z. (1998). Biosorption of Heavy Metals by Microalgae in Batch and Continuous Systems. In: Wastewater Treatment with Algae. Springer, – Berlin, Heidelberg, – P. 37–53. URL: URL: https:// doi.org/10.1007/978-3-662-10863-5_3

Qasem, N.A.A., Mohammed, R.H., Lawal, D.U. (2021). Removal of heavy metal ions from wastewater: a comprehensive and critical review. npj Clean Water, 4, 36. URL: https:// doi.org/10.1038/s41545-021-00127-0

Shen, L., Tesfaye, F., Li, X., Lindberg, D., Taskinen, P. (2021). Review of rhenium extraction and recycling technologies from primary and secondary resources. Minerals Engineering, – 161. – 106719 p. URL: https:// doi.org/10.1016/j.mineng.2020.106719

Miyah, Y., El Messaoudi, N., Benjelloun, M., Georgin, J., Franco, D.S.P., Viscusi, G., Messali, M., Knani, S. (2026). Review on rhenium ions removal from nuclear wastewater as radioactive contaminants: conventional and hydride technologies. Journal of Sustainable Metallurgy, – 12(3). – P. 2399–2428. URL: https:// doi.org/10.1007/s40831-026-01469-0

Dill, H.G., Kus, J., Dohrmann, R., Tsoy, Y. (2008). Supergene and hypogene alteration in the dual-use kaolin-bearing coal deposit Angren, SE Uzbekistan. International Journal of Coal Geology, – 75(4). – P. 225–240. URL: https:// doi.org/10.1016/j.coal.2008.07.003

Rahaeng, K., Oraintara, A., Mahakham, W. (2026). A simple ionic-gelation method for chitosan nanoparticle synthesis and standardized protocols for biological safety assessment:

antibacterial activity, phytotoxicity, and biocompatibility. International Journal of Molecular Sciences, – 27(8). – 3673 p. URL: https:// doi.org/10.3390/ijms27083673

Guibal, E. (2004). Interactions of metal ions with chitosan-based sorbents: a review. Separation and Purification Technology, – 38(1). – P. 43–74. URL: https:// doi.org/10.1016/j.seppur.2003.10.004

Zubir, A., Normaya, E., Danial, W.H., Goh, P.S., Piah, M.B.M., Show, P.-L., Ismail, A.F., Ahmad, M.N. (2026). State-of-the-art modification, mechanistic insight and breakthrough curve analysis of chitosan scaffolds for sustainable heavy metal adsorbent. International Journal of Environmental Science and Technology, – 23(3). – 195 p. URL: https:// doi.org/10.1007/s13762-025-06963-8

Gao, Z., Li, X., Wu, H., Zhao, S., Deligeer, W., Asuha, S. (2015). Magnetic modification of acid-activated kaolin: Synthesis, characterization, and adsorptive properties. Microporous and Mesoporous Materials, – 202. – P. 1–7. URL: https:// doi.org/10.1016/j.micromeso.2014.09.029

Gu, S., Kang, X., Wang, L., Lichtfouse, E., Wang, C. (2019). Clay mineral adsorbents for heavy metal removal from wastewater: a review. Environmental Chemistry Letters, – 17(2). – P. 629–654. URL: https:// doi.org/10.1007/s10311-018-0813-9

Liu, B., Wang, D., Yu, G., Meng, X. (2013). Adsorption of heavy metal ions, dyes and proteins by chitosan composites and derivatives – A review. Journal of Ocean University of China, – 12(3). – P. 500–508. URL: https:// doi.org/10.1007/s11802-013-2113-0

Sangoremi, A.A. (2025). Adsorption kinetic models and their applications: a critical review. International Journal of Research and Scientific Innovation, – 12(5). – P. 245–258. URL: https:// doi.org/10.51244/IJRSI.2025.120500019

Simonin, J.-P. (2016). On the comparison of pseudo-first order and pseudo-second order rate laws in the modeling of adsorption kinetics. Chemical Engineering Journal, – 300. – P. 254–263. URL: https:// doi.org/10.1016/j.cej.2016.04.079

Chai, J.-B., Au, P.-I., Mubarak, N.M., Khalid, M., Ng, W.P.-Q., Jagadish, P., Walvekar, R., Abdullah, E.C. (2020). Adsorption of heavy metal from industrial wastewater onto low-cost Malaysian kaolin clay-based adsorbent. Environmental Science and Pollution Research, – 27(12). – P. 13949–13962. URL: https:// doi.org/10.1007/s11356-020-07755-y

Basak, A. (1995). A review on thiocyanate methods for the estimation of molybdenum by molecular absorption spectroscopy. Talanta, – 42(4). – P. 497–506. URL: https:// doi.org/10.1016/0039-9140(95)01427-D

Fadl, M.G. (2023). Prediction of heavy metal biosorption mechanism through studying isotherm kinetic equations. Scientific Reports, – 13. – 1576 p. URL: https:// doi.org/10.1038/s41598-023-28655-4

Peng, M., Xi, C., Shen, K., Tan, Y., Li, F. (2024). Effective removal of molybdenum(VI) from aqueous solution using polyethylene polyamine-grafted sugarcane bagasse biosorbent. Journal of Sustainable Metallurgy, – 10(3). – P. 1292–1305. URL: https:// doi.org/10.1007/s40831-024-00856-9

Upadhyay, U., Sreedhar, I., Singh, S.A., Patel, C.M., Anitha, K.L. (2021). Recent advances in heavy metal removal by chitosan based adsorbents. Carbohydrate Polymers, – 251. – 117000 p. URL: https:// doi.org/10.1016/j.carbpol.2020.117000

Yefremova, S., Kablanbekov, A. (2026). Rhenium adsorption from an organic impurity-containing solution. Scientific Reports, – 16. – 7353 p. URL: https:// doi.org/10.1038/s41598-026-38148-9

Musarurwa, H., Tavengwa, N.T. (2022). Advances in the application of chitosan-based metal organic frameworks as adsorbents for environmental remediation. Carbohydrate Polymers, – 283. – 119153 p. URL: https:// doi.org/10.1016/j.carbpol.2022.119153

submitted 16.08.2026;
accepted for publication 30.08.2026;
published 31.08.2026
© Berdikulov B., Ikhtiyarova G.
Contact: baxtiyor9363@gmail.com; gulnora0474@gmail.com

Austrian Journal of Technical
and Natural Sciences, 2026 No 7–8
ISSN 2310-5607

PREMIER Publishing
ppublishing.org

DOI:10.29013/AJT-26-7.8-25-29

INVESTIGATION OF THE SORPTION PROPERTIES OF SAPROPEL IN INDUSTRIAL WASTEWATER TREATMENT AND PROSPECTS FOR ENSURING ENVIRONMENTAL SAFETY

Gulnoza Zayniddin qizi Khomitova [1], Matluba Mukhtarovna Amonova [2]

[1] PhD Student, Bukhara State Technical University, Bukhara, Uzbekistan

[2] Doctor of Technical Sciences, Associate Professor, Bukhara Innovative Education and Medical University, Bukhara, Uzbekistan

Cite: *Khomitova G.Z., Amonova M.M. (2026). Investigation of the Sorption Properties of Sapropel in Industrial Wastewater Treatment and Prospects for Ensuring Environmental Safety. Austrian Journal of Technical and Natural Sciences 2026, No 7–8.* https://doi.org/10.29013/AJT-26-7.8-25-29

Abstract

This article investigates the treatment of textile and printing industry wastewater using a sorbent based on local sapropel. The aim was to evaluate stabilization of the cation-anion composition and the deep purification of highly mineralized wastewater contaminated with organic dyes generated during the washing of printed fabrics. Physicochemical analysis showed that the initial wastewater contained 608 mg/L sulfate and had a total hardness of 14.4 meq/L; it was also characterized by a reddish color and a sulfurous odor associated with 32.3 mg/L hydrogen sulfide. Treatment with the sapropel-based sorbent reduced sodium from 215 to 105 mg/L, sulfate from 608 to 298 mg/L, total hardness to 7.78 meq/L, and hydrogen sulfide to 14.23 mg/L. Decolorization and deodorization were also achieved. The results demonstrate the sorption potential of humic and mineral components of sapropel and support further development of this local material for industrial wastewater treatment. Because ammonium, nitrate, and oxidizability did not decrease, an additional polishing stage should be evaluated when deeper removal of nitrogenous and oxidizable contaminants is required.

Keywords: *modified sapropel, total hardness, composite sorbent, ion-exchange adsorption, demineralization, sulfate removal, humic acid, sorption activity, wastewater, environmental safety*

Introduction

The rapid development of the modern textile and printing industries is closely associated with the generation of large volumes of technologically complex wastewater. Chemical reagents used in fabric dyeing and washing lead to the accumulation of high concentrations of mineral salts, organic dyes, and potentially toxic compounds. Excessive sulfate, chloride, and metal-ion loads can disrupt the natural balance of receiving waters and increase anthropogenic pressure (Ayangbenro & Babalola, 2017; Bahemmat et al., 2016).

Conventional mechanical and biological treatment methods do not always provide the desired efficiency in the deep demineralization of highly mineralized wastewater containing organic coloring substances. Therefore, the development of inexpensive sorbents based on locally available raw materials has important scientific and practical value for environmental safety and water recycling (Adeeva et al., 2013 a; Adeeva & Kovalenko, 2012).

Sapropel, an organogenic sediment, has attracted considerable attention in this field. It is rich in humic acids, mineral components, and bituminous substances and can interact with complex cation-anion mixtures through ion-exchange and adsorption mechanisms. Previous studies have demonstrated sorption by carbon-mineral and humic materials derived from sapropel (Adeeva et al., 2013 b; Chechevatov et al., 2017; Kovalenko & Adeeva, 2010; Platonova & Adeeva, 2018; Platonova et al., 2016). The aim of this study was to assess the treatment of colored textile wastewater using a modified composite sorbent based on local sapropel and to evaluate changes relevant to technical water recycling.

Materials and Methods

The study object was wastewater generated during the washing of printed fabrics in textile and printing production. Samples were characterized before and after treatment with the sapropel-based sorbent. The comparative analytical dataset included major cations and anions, total, carbonate, and noncarbonate hardness, pH, hydrogen sulfide, fluoride, oxidizability, dry residue, clarity, qualitative salinity, color, odor, and sediment formation. Ion concentrations are reported in mg/L and meq/L, and equivalent percentages are expressed relative to the corresponding total cation or anion equivalents. Treatment performance was evaluated by direct comparison of the initial and treated samples.

Results and Discussion

The chemical composition of wastewater generated during the washing of printed fabrics is important for developing effective treatment and recycling strategies. The concentrations of the identified cations and anions, total hardness, pH, oxidizability, and other physicochemical characteristics were examined. The initial results are presented in Table 1.

Sodium (Na+), calcium (Ca2+), magnesium (Mg2+), and ammonium (NH4+) were the dominant measured cations, with concentrations of 215, 124, 100, and 21 mg/L, respectively. Their reported equivalent shares in the total cation composition were approximately 37%, 25%, 33%, and 5%, respectively.

The data show that magnesium and sodium were present in relatively high concentrations and, together with calcium, contributed substantially to total hardness. Total hardness was 14.4 meq/L; carbonate and noncarbonate hardness were 6.4 and 8.0 meq/L, respectively.

Sulfate (SO4(2-)), bicarbonate (HCO3-), and chloride (Cl-) were the most abundant anions. Sulfate reached 608 mg/L and represented approximately 51% of the total anion equivalents. Bicarbonate and chloride were measured at 390 mg/L (26%) and 204 mg/L (23%), respectively. Total cation and anion equivalents were both 24.92 meq/L, indicating a balanced ionic analysis.

The pH was 6.90, indicating an almost neutral medium. Hydrogen sulfide reached 32.3 mg/L and explained the sulfurous odor. Oxidizability was 32.23 mg O2/L, indicating the presence of oxidizable or reducing substances. The wastewater was clear after filtration, slightly saline, reddish, and associated with a black precipitate. The combination of high mineralization, color, sulfide, and oxidizable matter makes direct discharge environmentally undesirable.

Table 1. *Analytical Results for Wastewater Generated during Printed-Fabric Washing*

Cations	Composition per Liter of Solution			Other Parameters	
	mg/L	meq/L	% of equivalents	Parameter	Value
Na+	215	9.36	37	Total hardness, meq/L	14.40

Cations	Composition per Liter of Solution			Other Parameters	
	mg/L	meq/L	% of equivalents	Parameter	Value
K+	ND	0.00	0	Carbonate hardness, meq/L	6.40
NH4+	21	1.16	5	Noncarbonate hardness, meq/L	8.00
Ca2+	124	6.20	25	pH	6.90
Mg2+	100	8.20	33	H2S, mg/L	32.30
Fe3+	0	0.00	0	F-, mg/L	1.29
Fe2+	0	0.00	0	Oxidizability, mg O2/L	32.23
Total	**460**	**24.92**	**100**	Measured dry residue, mg/L	1,520
				Calculated dry residue, mg/L	1,473
Cl-	204	5.75	23	Clarity	Clear after filtration
SO4(2-)	608	12.67	51	Qualitative salinity	Slightly saline
NO2-	ND	0.00	0	Color	Reddish
NO3-	6	0.10	<1	Odor	Sulfurous
HCO3- / Total	**390/1,208**	**6.40/24.92**	**26/100**	Sediment	Black precipitate

Note. ND = not detected. HCO3 – is shown with the anion total in the final row to preserve the original table structure

Table 2. *Analytical Results after Treatment with the Sapropel-Based Sorbent*

Cations	Composition per Liter of Solution			Other Parameters	
	mg/L	meq/L	% of equivalents	Parameter	Value
Na+	105	4.57	33.37	Total hardness, meq/L	7.78
K+	ND	0.00	0.00	Carbonate hardness, meq/L	4.89
NH4+	24	1.33	9.75	Noncarbonate hardness, meq/L	2.89 (calculated)
Ca2+	89	4.45	32.52	pH	7.12
Mg2+	40	3.33	24.36	H2S, mg/L	14.23
Fe3+	0	0.00	0.00	F-, mg/L	0.72
Fe2+	0	0.00	0.00	Oxidizability, mg O2/L	34.21
Total	**258**	**13.68**	**100.00**	Measured dry residue, mg/L	954
				Calculated dry residue, mg/L	907
Cl-	146	4.11	30.06	Clarity	Clear

Cations	Composition per Liter of Solution			Other Parameters	
	mg/L	meq/L	% of equivalents	Parameter	Value
SO4(2-)	298	6.21	45.38	Qualitative salinity	Not saline
NO2-	0	0.00	0.00	Color	Colorless
NO3-	7	0.11	0.83	Odor	Odorless
HCO3- / Total	**198 / 649**	**3.25 / 13.68**	**23.73 / 100.00**	Sediment	No precipitate

Note. ND = not detected. Noncarbonate hardness was calculated as total hardness minus carbonate hardness (7.78–4.89 = 2.89 meq/L). HCO3- is shown with the anion total in the final row to preserve the original table structure.

Treatment with the sapropel-based sorbent produced substantial changes in the ionic composition and organoleptic characteristics. The analytical results after treatment are presented in Table 2.

Sodium decreased from 215 to 105 mg/L, while calcium and magnesium decreased from 124 to 89 mg/L and from 100 to 40 mg/L, respectively. Total hardness fell from 14.4 to 7.78 meq/L. These results are consistent with ion exchange and adsorption by the humic and mineral components of sapropel.

Sulfate decreased from 608 to 298 mg/L, bicarbonate from 390 to 198 mg/L, and chloride from 204 to 146 mg/L. The treated sample remained sulfate-dominated, but the absolute anion load was substantially lower. Hydrogen sulfide decreased from 32.3 to 14.23 mg/L, fluoride from 1.29 to 0.72 mg/L, and the measured dry residue from 1,520 to 954 mg/L. The water became clear, colorless, odorless, and free of visible precipitate.

Not all indicators improved. Ammonium increased from 21 to 24 mg/L, nitrate from 6 to 7 mg/L, and oxidizability from 32.23 to 34.21 mg O2/L. Consequently, the available data support demineralization, sulfide reduction, decolorization, and deodorization, but they do not demonstrate removal of the total nitrogenous or oxidizable load. A biological, oxidative, or membrane polishing stage should therefore be evaluated for applications requiring more complete purification.

The study is a comparative water-quality assessment. Adsorption isotherms, kinetic constants, optimal sorbent dose and contact time, regeneration performance, and spent-sorbent composition should be determined before industrial scale-up. Compliance must also be verified against the specific standard governing the intended discharge or technical reuse route.

Conclusion

The sapropel-based composite sorbent substantially improved the ionic and organoleptic characteristics of wastewater generated during printed-fabric washing. Sodium and sulfate were reduced by approximately one half, total hardness decreased to 7.78 meq/L, hydrogen sulfide decreased to 14.23 mg/L, and the measured dry residue fell to 954 mg/L. The disappearance of reddish color, sulfurous odor, and visible precipitate confirms the practical potential of the treatment.

Because ammonium, nitrate, and oxidizability did not decrease, the sapropel sorption stage should be considered a component of an integrated treatment system rather than a universal stand-alone process. With optimization, regeneration testing, and validation against reuse criteria, this local raw material may offer an economical and environmentally compatible option for industrial wastewater management.

References

Adeeva, L. N., & Kovalenko, T. A. (2012). Removal of organic substances and metal ions from water using a carbon-mineral sapropel sorbent. *Russian Journal of Applied*

Chemistry, –85. – P. 557–563. URL: https://doi.org/10.1134/S1070427212040040
Adeeva, L. N., Platonova, D. S., Puzhel, A. V., Didenko, T. A., & Belykh, N. A. (2013a). Bifunctional sorbent for wastewater treatment obtained from sapropel. *Butlerov Communications,* – 34(6). – P. 70–75. (In Russian). ROI: jbc-01/13-34-6-70
Adeeva, L. N., Platonova, D. S., Masorov, M. S., & Didenko, T. A. (2013b). Humic acids from siliceous sapropel: IR-spectroscopic and thermal analysis. *Butlerov Communications,* – 34(6). – P. 65–69. (In Russian). ROI: jbc-01/13-34-6-65
Ashworth, D. J., & Alloway, B. J. (2008). Influence of dissolved organic matter on the solubility of heavy metals in sewage-sludge-amended soils. *Communications in Soil Science and Plant Analysis,* 39(3–4). – P. 538–550. URL: https://doi.org/10.1080/00103620701826787
Ayangbenro, A. S., & Babalola, O. O. (2017). A new strategy for heavy metal polluted environments: A review of microbial biosorbents. *International Journal of Environmental Research and Public Health,* – 14(1). – 94 p. URL: https://doi.org/10.3390/ijerph14010094
Bahemmat, M., Farahbakhsh, M., & Kianirad, M. (2016). Humic substances-enhanced electroremediation of heavy metals contaminated soil. *Journal of Hazardous Materials,* –312. – P. 307–318. URL: https://doi.org/10.1016/j.jhazmat.2016.03.038
Chechevatov, A. I., Miroshnichenko, Y. S., Myasoedova, T. N., Popov, Y. V., & Yalovega, G. E. (2017). Investigations of the capability of humic acids to adsorb heavy metals: Correlation between structure and absorption properties. In *Advanced Materials: Techniques, Physics, Mechanics and Applications* (P. 99–110). Springer. URL: https://doi.org/10.1007/978-3-319-56062-5_9
Kovalenko, T. A., & Adeeva, L. N. (2010). Carbon-mineral sorbent from sapropel for comprehensive wastewater treatment. *Chemistry for Sustainable Development,* – 18(2). – P. 189–195. (In Russian).
Platonova, D. S., & Adeeva, L. N. (2018). Use of humic sorbent from sapropel for extraction of palladium ions from chloride solutions. *Open Engineering,* – 8(1). – P. 176–181. URL: https://doi.org/10.1515/eng-2018-0023
Platonova, D. S., Gurin, A. V., & Adeeva, L. N. (2016). Modified sorbents of sapropel for wastewater treatment. *Ecology and Industry of Russia,* – 20(11). – P. 20–25. URL: https://doi.org/10.18412/1816-0395-2016-11-20-25

submitted 06.08.2026;
accepted for publication 20.08.2026;
published 31.08.2026
© Khomitova G. Z., Amonova M. M.
Contact: matlubamuxtarovna1988@gmail.com

Austrian Journal of Technical
and Natural Sciences, 2026 No 7–8
ISSN 2310-5607

PREMIER Publishing
ppublishing.org

DOI:10.29013/AJT-26-7.8-30-36

INTERPHASE PARTITIONING OF IRON AND ALUMINUM DURING ALKALINE PROCESSING OF ARAL SEA SAPROPEL

Shakhnoza Shukhrat qizi Rashitovaa [1]

[1] Department of General Sciences, Asia International University, Yangiabad MFY, Bukhara, Uzbekistan

Cite: *Rashitova Sh.Sh. (2026). Interphase Partitioning of Iron and Aluminum During Alkaline Processing of Aral Sea Sapropel. Austrian Journal of Technical and Natural Sciences 2026, No 7–8.* https://doi.org/10.29013/AJT-26-7.8-30-36

Abstract

Aims: To determine how potassium hydroxide concentration, temperature, and liquid-to-solid ratio affect pH and the transfer of aluminum and iron from sapropel into the liquid phase, and to quantify retention of both elements in the residual solid under resource-efficient conditions.

Study Design: Factorial laboratory screening of three potassium hydroxide concentrations (1, 2, and 3%). – P. six temperatures (40–90 °C). – P. and five liquid-to-solid ratios (1:1–3:1).

Place and Duration of Study: Sapropel was collected from the dried bed of the Aral Sea, Uzbekistan, and processed at the Department of General Sciences, Asia International University, Bukhara, Uzbekistan. The experimental dates were not documented in the source record.

Methodology: Air-dried, ground sapropel was treated with aqueous potassium hydroxide under continuous mixing. The separated liquid phase was analyzed potentiometrically for pH and instrumentally for aluminum and iron. Liquid-phase transfer was calculated from the element mass in solution relative to its initial mass in the sapropel.

Results: Across all tested conditions, pH ranged from 6.53 to 10.92, aluminum transfer from 0.72 to 14.20%, and iron transfer from 2.5 to 9.7%. Aluminum mobilization increased sharply at 3% potassium hydroxide and pH above 9.3. Under the selected conditions of 2% potassium hydroxide, a liquid-to-solid ratio of 2.5:1, and 80 °C (pH 8.66). – P. 3.19% of aluminum and 5.0% of iron entered the liquid phase; 96.81% and 95.0%, respectively, remained in the solid.

Conclusion: Moderate alkalinity preserved most aluminum- and iron-bearing mineral components while supporting humic-substance processing. The residue is therefore a plausible precursor for sorbent development, although adsorption capacity, kinetics, selectivity, and regeneration must be established directly before application.

Keywords: *sapropel; potassium hydroxide; aluminum; iron; phase partitioning; solid residue; sorbent precursor; Aral Sea*

1. Introduction

Alkaline extraction of humic and fulvic substances from sapropel collected on the dried bed of the Aral Sea produces two material streams: a liquid phase enriched in soluble humic fractions and a mineral-rich solid residue. Using both streams would support a low-waste valorization pathway. Potassium hydroxide is particularly relevant when the liquid product is intended as a fertilizer precursor, while the residual solid may provide a locally available adsorbent feedstock (Cheng et al., 2019; Platonova & Adeeva, 2018).

Toxic elements such as lead, cadmium, copper, zinc, and arsenic remain important contaminants of industrial and agricultural waters. Adsorption is widely investigated for their removal because it can be operationally simple and compatible with low-cost mineral materials. Iron and aluminum (hydr) oxides are especially relevant: surface hydroxyl groups can bind cations and oxyanions through inner-sphere complexation, ion exchange, and coprecipitation (Hira et al., 2023; Hua et al., 2012; Mashale et al., 2025). Magnetite, goethite, hematite, and ferrihydrite have accordingly been studied as active phases or components of sorbent systems (Boruah et al., 2023; Das et al., 2011).

Retention of iron and aluminum during alkaline treatment is therefore important to the potential value of the sapropel residue. Aluminum hydroxide is amphoteric: sparingly soluble $Al(OH)_3$ can form soluble aluminate species, principally $[Al(OH)_4]^-$, as alkalinity increases. The solubility of aluminum hydroxide rises substantially in strongly basic media (Gayer et al., 1958). Iron(III)-bearing phases are comparatively persistent over the moderately alkaline range studied, although their mineralogical form and transformation behavior depend on pH, temperature, and reaction time (Das et al., 2011). A process optimized only for liquid-phase humic recovery could consequently overlook loss of mineral adsorption sites from the solid product.

This study evaluated the effects of potassium hydroxide concentration, temperature, and L/S ratio on pH and the interphase partitioning of aluminum and iron during sapropel processing. The specific objectives were to quantify the fractions entering the liquid phase, identify conditions that preserve both elements in the solid, and define the scientific basis for subsequent sorbent-development studies. No direct adsorption test was performed; therefore, the residue is evaluated only as a potential sorbent precursor.

2. Methodology

2.1 Study Material and Sample Preparation

The study material was sapropel sample S-0 collected from the dried bed of the Aral Sea. The sample was air-dried, ground, and homogenized to obtain a uniform material before treatment.

2.2 Alkaline Processing

Sapropel was treated with aqueous KOH solutions at concentrations of 1, 2, or 3%. The investigated L/S ratios were 1:1, 1.5:1, 2:1, 2.5:1, and 3:1, and the treatment temperatures were 40, 50, 60, 70, 80, and 90 °C. Continuous mixing was maintained during treatment. The suspension was then separated into liquid and solid phases by filtration or centrifugation. Treatment duration was held constant across runs, but its numerical value was not available in the source record.

2.3 Analytical Measurements and Mass Balance

The pH of the separated liquid phase was measured potentiometrically. Aluminum and iron concentrations in solution were determined using the laboratory's instrumental analytical workflow based on atomic absorption spectrometry and spectrophotometry. The source record did not preserve instrument models, calibration ranges, detection limits, or the allocation of individual samples between the two analytical techniques; these details should be supplied from the laboratory log before peer-review submission.

The fraction of each element transferred to the liquid phase was calculated as:

$$E = (msol / m0) \times 100\%, \quad (1)$$

where E is the fraction transferred to the liquid phase (%). – *P*. msol is the mass of the element in solution, and m0 is its initial total mass in the sapropel. Retention in the solid phase was calculated as 100 – – E (%). The mass-balance approach follows established quantitative characterization principles for humic and mineral materials (Swift, 1996).

2.4 Data Presentation

The source dataset reported measured values for each tested condition but did not include replicate counts, uncertainty estimates, or inferential statistics. Results are therefore presented descriptively as percentages, ranges, and absolute percentage-point differences. The English figures reproduce the numerical series shown in the source manuscript; no interpolation was used to generate new experimental observations.

3. Results And Discussion

3.1 Effect of Process Variables on pH

KOH concentration was the principal determinant of pH. Across the complete experimental matrix, pH ranged from 6.53 to 7.78 at 1% KOH, from 7.92 to 8.91 at 2% KOH, and from 9.35 to 10.92 at 3% KOH. Temperature and L/S ratio had smaller effects, generally increasing pH by approximately 0.1–0.3 units at successive levels. At L/S = 2.5:1, the temperature profiles remained clearly separated by KOH concentration (Fig. 1). The selected condition of 2% KOH and 80 °C gave pH 8.66, corresponding to moderate alkalinity rather than the strongly alkaline region reached at 3% KOH.

Figure 1. *Effect of temperature and KOH concentration on the pH of the liquid phase at L/S = 2.5:1*

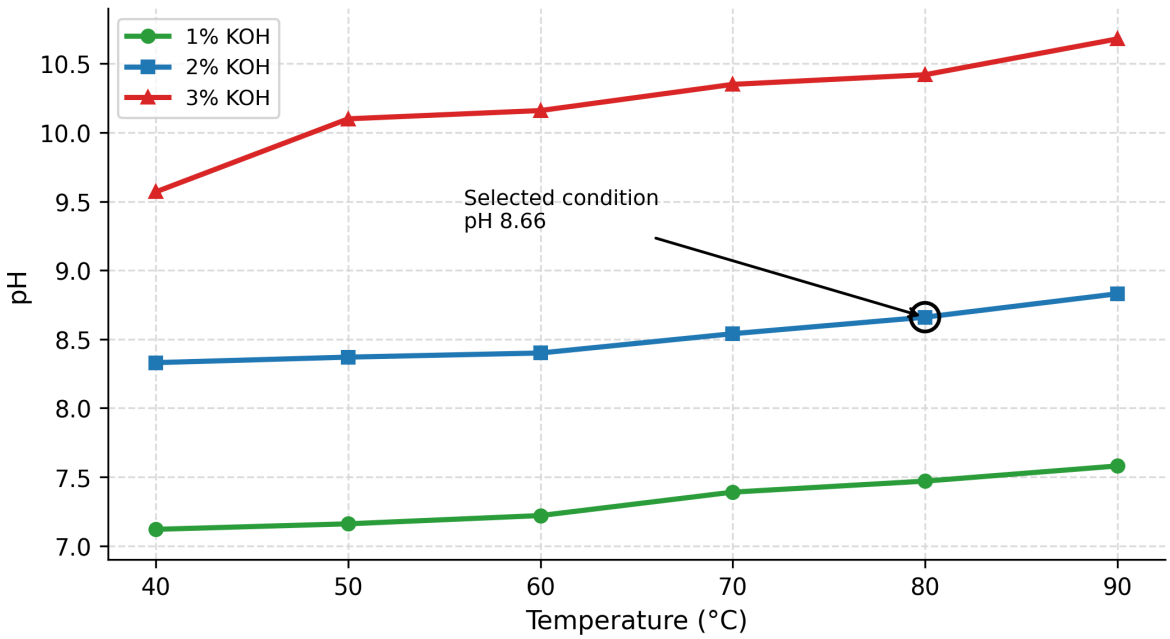

3.2 Aluminum Mobilization

Aluminum transfer was highly sensitive to alkalinity. Across all conditions, liquid-phase transfer was 0.72–1.69% at 1% KOH and 1.37–3.72% at 2% KOH. At 3% KOH and pH 9.35–10.92, it increased to 4.94–14.20%. At fixed L/S = 2.5:1, aluminum transfer increased with temperature at every KOH concentration, but the separation between the 2 and 3% series was much larger than the temperature effect within either series (Fig. 2). This pattern is consistent with the amphoteric dissolution of aluminum hydroxide and the formation of soluble aluminate species in basic media (Gayer et al., 1958).

3.3 Iron Mobilization

Iron transfer remained comparatively low over the investigated matrix: 2.5–3.7% at 1% KOH, 3.9–5.5% at 2% KOH, and 6.4–9.7% at 3% KOH. At L/S = 2.5:1, increasing temperature from 40 to 90 °C at 2% KOH raised the liquid-phase fraction from 4.5 to 5.3% (Fig. 3). Iron was therefore retained predominantly in the solid under all tested conditions. The response is compatible with persistence of iron(III) (hydr)oxide phases under moderate alkalinity, although mineralogical analysis would be required to identify the phases actually present (Das et al., 2011).

Figure 2. *Effect of temperature and KOH concentration on aluminum transfer to the liquid phase at L/S = 2.5:1*

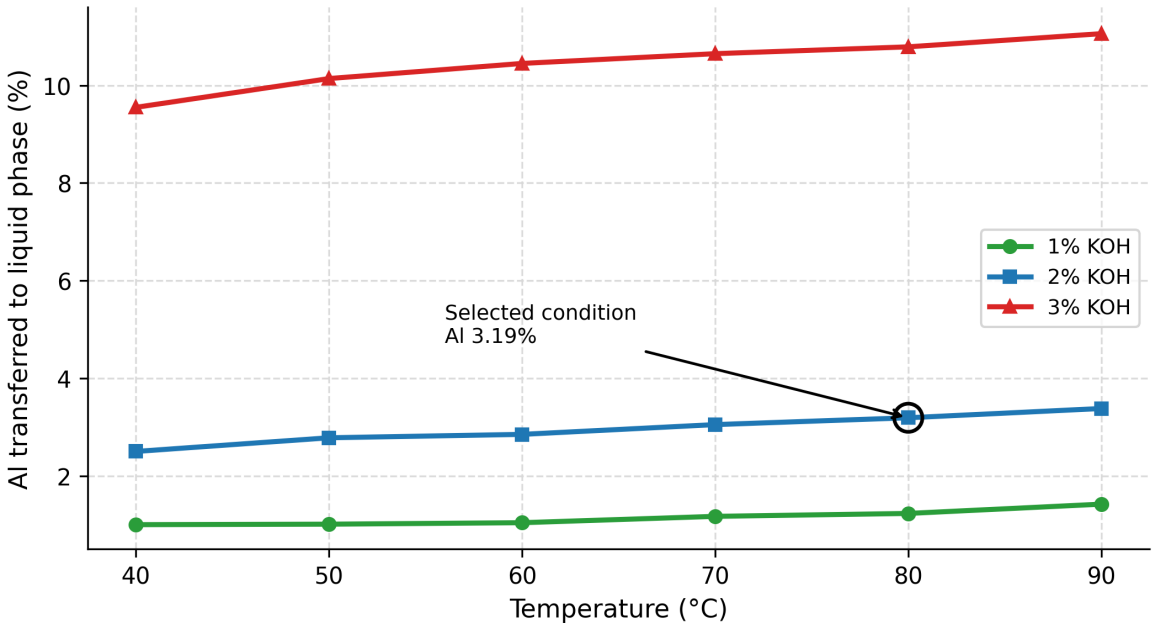

Figure 3. *Effect of temperature and KOH concentration on iron transfer to the liquid phase at L/S = 2.5:1*

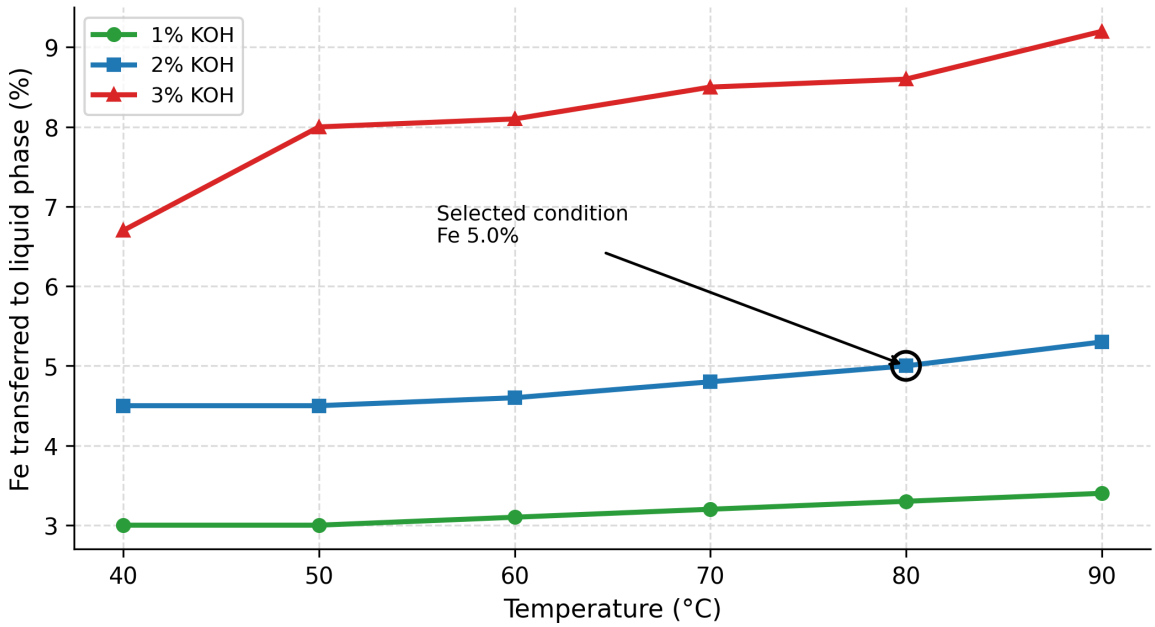

3.4 Relative Effect of KOH Concentration

At 80 °C and L/S = 2.5:1, increasing KOH from 1 to 2% raised aluminum transfer from 1.24 to 3.19% and iron transfer from 3.30 to 5.00%. A further increase to 3% KOH raised aluminum transfer to 10.79% and iron transfer to 8.60% (Fig. 4). Thus, the step from 2 to 3% KOH increased aluminum mobilization by 7.60 percentage points and more than tripled its liquid-phase fraction. The corresponding change for iron was 3.60 percentage points. KOH concentration, acting through pH, was consequently the dominant control on phase partitioning; temperature had a secondary effect, and L/S ratio had the smallest effect within the ranges studied.

Figure 4. *Effect of KOH concentration on aluminum and iron transfer at 80 °C and L/S = 2.5:1*

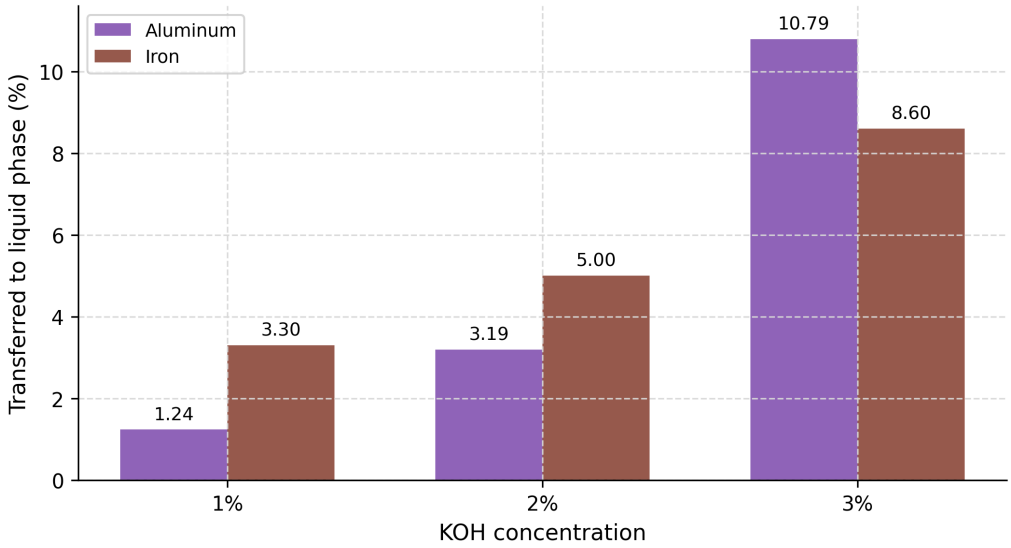

3.5 Interphase Partitioning under Selected Conditions

The resource-efficient condition selected for integrated sapropel processing was 2% KOH, L/S = 2.5:1, and 80 °C. At pH 8.66, only 3.19% of aluminum and 5.00% of iron entered the liquid phase; correspondingly, 96.81% and 95.00% were retained in the solid (Table 1; Fig. 5). These values indicate preservation of the metal-bearing mineral fraction while avoiding the stronger aluminum dissolution observed at 3% KOH.

Table 1. *Interphase partitioning of aluminum and iron at 2% KOH, L/S = 2.5:1, and 80 °C*

Parameter	Aluminum (Al)	Iron (Fe)	Interpretation
Transferred to liquid phase (%)	3.19	5.00	Entered the fertilizer stream
Retained in solid phase (%)	96.81	95.00	Preserved in the residue
Liquid-phase pH	8.66	8.66	Moderately alkaline medium

Figure 5. *Partitioning of aluminum and iron between solid and liquid phases under the selected conditions (2% KOH, L/S = 2.5:1, and 80 °C)*

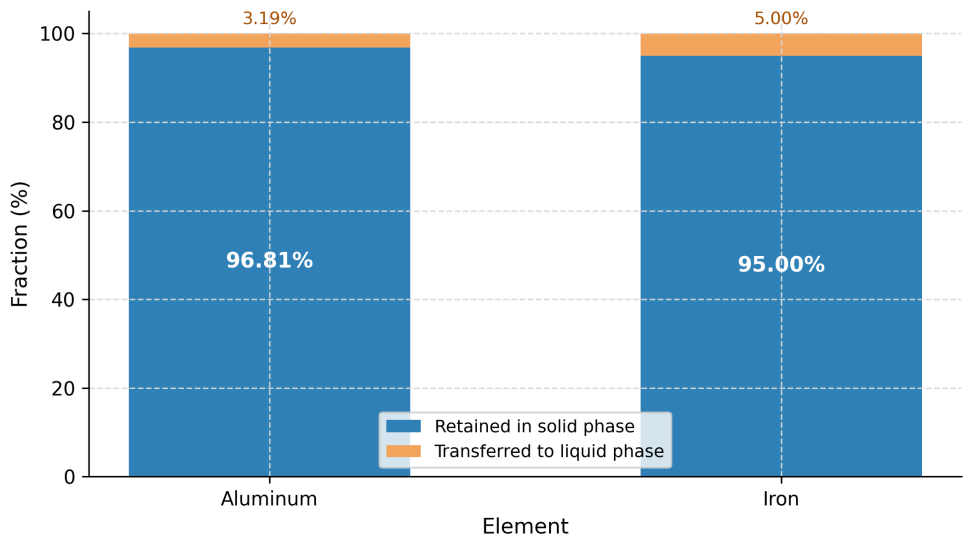

The retention of approximately 95–97% of both elements is favorable for further material development. Iron- and aluminum-bearing (hydr)oxides can provide hydroxylated surfaces for cation and oxyanion binding through surface complexation and ligand exchange (Hira et al., 2023; Li et al., 2016; Mashale et al., 2025). Residual humic fragments may contribute additional ion-exchange sites. However, elemental retention alone does not establish adsorption performance. Surface area, pore structure, mineralogy, point of zero charge, leaching stability, adsorption isotherms, kinetics, selectivity in multicomponent solutions, and regeneration must be measured before the material can be described as an effective sorbent.

The selected 2% KOH condition also limits aluminum entry into the liquid fertilizer precursor. This may be desirable because excessive soluble aluminum can be phytotoxic under some soil conditions. Compared with 2% KOH, 3% KOH provides only a small additional benefit for humic-substance recovery in the associated process dataset, whereas it increases aluminum loss more than threefold. The 2% condition therefore offers a defensible compromise among liquid-product recovery, retention of mineral surface functionality, and reagent demand.

3.6 Study Limitations

This screening study is limited by incomplete analytical metadata in the source record, absence of replicate statistics and error estimates, and lack of direct characterization of the residual solid. The reported partitioning values should therefore be interpreted as descriptive process-screening results. Independent replication with documented instruments, calibration, quality-control samples, and full mass-balance closure is required. Direct adsorption tests are also necessary to verify the proposed downstream use.

4. Conclusion

KOH concentration was the dominant control on pH and on the partitioning of aluminum and iron during alkaline processing of Aral Sea sapropel. Aluminum transfer rose sharply above pH 9 at 3% KOH, reaching 14.20% across the full experimental matrix, whereas it remained at or below 3.72% at 1–2% KOH. Iron was retained more strongly, with 2.5–9.7% transferred to the liquid phase across all conditions.

At 2% KOH, L/S = 2.5:1, and 80 °C, the liquid phase had pH 8.66 and contained 3.19% of the initial aluminum and 5.00% of the initial iron. Thus, 96.81% of aluminum and 95.00% of iron remained in the solid residue. These conditions preserve most metal-bearing mineral components while avoiding the substantial aluminum mobilization caused by 3% KOH. The residue is a promising sorbent precursor, but its adsorption capacity and operational performance require direct experimental confirmation.

Acknowledgements

The author used OpenAI Codex, ChatGPT Work release available on 13 August 2026, GPT-5 model (OpenAI, San Francisco, USA) solely for English translation, language editing, figure relabeling, and journal-format preparation. The author reviewed the scientific statements, numerical values, figures, and references and accepts full responsibility for the final manuscript. No external funding was reported in the source record.

Competing Interests

The author has declared that no competing interests exist.

Authors' Contributions

Shakhnoza Shukhrat qizi Rashitova conceived the study, conducted the experimental work, analyzed and interpreted the data, prepared the original manuscript and figures, and read and approved the final manuscript.

Consent

Not applicable. This study did not involve human participants or identifiable personal information.

Ethical Approval

Not applicable. The study involved laboratory processing of a natural mineral-organic material and did not involve humans or animals.

Data Availability

All data evaluated in this study are presented in the article. The author should retain the original laboratory records for editorial or peer-review verification.

References

Boruah, H., Tyagi, N., Gupta, S. K., Chabukdhara, M., & Malik, T. (2023). Understanding the adsorption of iron oxide nanomaterials in magnetite and bimetallic form for the removal of arsenic from water. Frontiers in Environmental Science, – 11. – 1104320 p. URL: https://doi.org/10.3389/fenvs.2023.1104320

Cheng, G., Niu, Z., Zhang, C., Zhang, X., & Li, X. (2019). Extraction of humic acid from lignite by KOH-hydrothermal method. Applied Sciences, – 9(7). – 1356 p. URL: https://doi.org/10.3390/app9071356

Das, S., Hendry, M. J., & Essilfie-Dughan, J. (2011). Transformation of two-line ferrihydrite to goethite and hematite as a function of pH and temperature. Environmental Science & Technology, – 45(1). – P. 268–275. URL: https://doi.org/10.1021/es101903y

Gayer, K. H., Thompson, L. C., & Zajicek, O. T. (1958). The solubility of aluminum hydroxide in acidic and basic media at 25 °C. Canadian Journal of Chemistry, – 36(9). – P. 1268–1271. URL: https://doi.org/10.1139/v58–184

Hira, N. E., Lock, S. S. M., Arshad, U., Asif, K., Ullah, F., Farooqi, A. S., et al. (2023). Screening of metal oxides and hydroxides for arsenic removal from water using molecular dynamics simulations. ACS Omega, – 8(50). – P. 48130–48144. URL: https://doi.org/10.1021/acsomega.3c07014

Hua, M., Zhang, S., Pan, B., Zhang, W., Lv, L., & Zhang, Q. (2012). Heavy metal removal from water/wastewater by nanosized metal oxides: A review. Journal of Hazardous Materials, – P. 211–212, 317–331. URL: https://doi.org/10.1016/j.jhazmat.2011.10.016

Li, M., Liu, J., Xu, Y., & Qian, G. (2016). Phosphate adsorption on metal oxides and metal hydroxides: A comparative review. Environmental Reviews, – 24(3). – P. 319–332. URL: https://doi.org/10.1139/er-2015–0080

Mashale, K., Mogashane, T. M., Madzivha, P., Motlatle, M. A., Mokoena, L., & Tshilongo, J. (2025). Iron oxide and hydroxides for the removal of heavy metals from wastewater. In Current Research on Mineralogy: Minerals Characterization and Their Applications. IntechOpen. URL: https://doi.org/10.5772/intechopen.1010016

Platonova, D. S., & Adeeva, L. N. (2018). Use of humic sorbent from sapropel for extraction of palladium ions from chloride solutions. Open Engineering, 8(1). – P. 176–181. URL: https://doi.org/10.1515/eng-2018–0023

Swift, R. S. (1996). Organic matter characterization. In D. L. Sparks et al. (Eds.). – P. Methods of Soil Analysis, Part 3: Chemical Methods (P. 1011–1069). Soil Science Society of America. URL: https://doi.org/10.2136/sssabookser5.3.c35

submitted 06.06.2026;8
accepted for publication 20.08.2026;
published 31.08.2026
© Rashitova Sh. Sh.
Contact: rashitovashahnozashuhratqizi@oxu.uz

Austrian Journal of Technical
and Natural Sciences, 2026 No 7–8
ISSN 2310-5607

PREMIER Publishing
ppublishing.org

DOI:10.29013/AJT-26-7.8-37-40

MODERN QUANTUM–CHEMICAL STUDY OF THE ELECTRONIC STRUCTURE AND REACTIVITY OF THIOPHENE

Rustamov Sardor Rustam og'li [1],
Mamarakhmonov Mukhamatdin Khomidovich [2],
Kodirov Abdulakhad Abduraimovich [1],
Khamrayeva K. B. [1], ***Tokhirova Maryam*** [3]

[1] Qarshi State University, Qarshi, Uzbekistan

[2] Turan International University, Namangan, Uzbekistan

[3] University of Economics and Pedagogy, Andijan, Uzbekistan

Cite: *Rustamov S.R., Mamarakhmonov M.Kh., Kodirov A.A., Khamrayeva K.B., Tokhirova M. (2026). Modern Quantum–Chemical Study of the Electronic Structure and Reactivity of Thiophene. Austrian Journal of Technical and Natural Sciences 2026, No 7–8.* https://doi.org/10.29013/AJT-26-7.8-37-40

Abstract

Thiophene is a unique sulfur-containing heterocyclic compound with one sulfur atom. It is a colorless liquid with the formula C_4H_4S, boiling point 84.1 °C, and a benzene-like odor. It is poorly soluble in water but readily soluble in organic solvents. Thiophene continues to fascinate organic chemists with its wide range of chemical properties, ultimately inspiring both theoreticians and experimentalists to conduct fundamental scientific research and conduct new reactions to create innovative organic compounds with high yields. Numerous biologically active drugs are obtained from it, and they are widely used, particularly in agriculture, medicine, and pharmaceuticals. In halogenation, nitration, and formylation reactions, α-substituted products are obtained more rapidly and are exclusively the main products relative to others. Therefore, it is of theoretical interest to identify the key factors behind thiophene's unique behavior by studying its geometric parameters and electronic structure. This article presents the results of quantum chemical calculations performed by us using the Gaussian program to calculate the geometry and electronic structure, and to evaluate the reactivity of thiophene with respect to electrophilic reagents.

Keywords: *thiophene, aromatic compound, quantum chemical calculation, Gaussian program, B3LYP method, electronic structure, reactivity, geometry, total energy, frontier molecular orbital, correlation, product ratio*

Introduction

Depending on its π-excess, thiophene is significantly more active than benzene in electrophilic substitution reactions, sometimes up to 100,000 times more so. Under normal conditions, reactions are known to proceed exclusively to the α-position, 2–3 orders of magnitude faster than to the β-position of the ring

(Spivey Alan C., 2012; Molina P., Arques A., Cartagena I., 2008; Yurovskaya M. A., Kurkin A. V., Lukashev N. V., 2007). This behavior inspired us to conduct theoretical quantum chemical calculations to establish the precise geometry and electronic structure of thiophene. Based on calculations performed in the Gaussian program (Frisch M. J., Trucks G. W., et al., 1998) using the B3LYP method, we estimated the potential reactivity of the α- and β-positions of the heterocycle and established a correlation between the theoretical data and the productivity of the reactions. In the world literature there are numerous experimental (Fahimeh Abedinifar, Elham Babazadeh Rezaei. et all., 2021; Amita Vyasa, Dharmesh Katariya, et.all., 2025). and theoretical results of syntheses carried out with the participation of thiophene and their derivatives for the analysis of data according to the MO theory (Michael Dewar, Ralph C. Dougherty. 1975; Dipak Kumar Mandal. 2025). In this article, an analysis of the results of theoretical calculations by quantum chemistry methods is carried out to determine the exact geometry, electronic structure, reactivity of thiophene and to establish a correlation between the experimental ratios of the yield of the α-/β-substitution reaction of reagents.

Research Objects

We chose thiophene, an aromatic five-membered heterocycle with one sulfur atom, and its transformation products in electrophilic substitution reactions as our research object.

Figure 1. *Scheme of the electrophilic substitution reaction of thiophene*

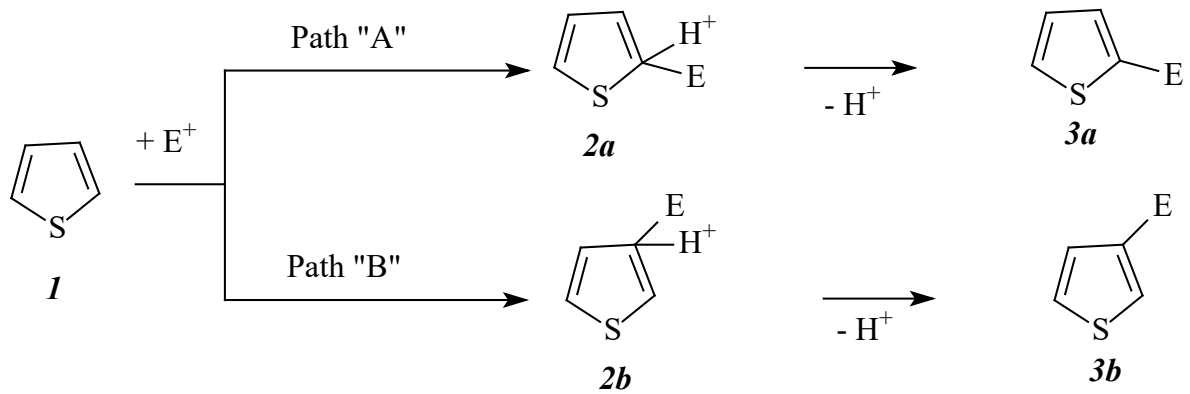

Methods and Results

We used the DFT-B3LYP method with the 3–21G basis set for quantum chemical studies of thiophene and its monosubstituted derivatives in our calculations. In previous articles, we successfully used the Gaussian98 software package (Mamarakhmonov M. Kh., Belen´kii L. I. et. all., 2016) for the calculation of several heteroaromatic compounds. During the calculations, all geometric parameters of thiophene, its intermediates, and derivatives (Fig. 1) were fully optimized.

We performed theoretical calculations and obtained reliable data, which are now being analyzed quantitatively. This approach to solving the problem of determining the precise electronic structure and assessing reactivity yielded the desired results, which serve as an addition to the knowledge base on heterocycles.

Table 1. *Total energy, geometry of objects and net atomic charges*

Energy (Et, ΔE), dipole moment (μ) of compounds					
	1	***2a***	***2b***	***3a***	***3b***
Et	–345246.03	–369993.12	–369978.37	–369785.98	–369784.73
ΔE		0*	14.75	0*	1.25
μ, **D**	0.97	1.95	1.17	1.06	1.36

Energy (Et, ΔE), dipole moment (μ) of compounds					
	1	***2a***	***2b***	***3a***	***3b***
Bonds			**Bond length, (d, Å)****		
S1-C2	1.808	1.926	1.702	1.823	1.808
C2-C3	1.358	1.484	1.474	1.360	1.360
C3-C4	1.442	1.368	1.502	1.442	1.449
C4-C5	1.358	1.414	1.335	1.357	1.356
C5-S1	1.808	1.728	1.860	1.809	1.807
C2-C6		1.553		1.498	
C3-C6	1.081		1.595		1.512
Atoms			**Atomic charges, (q, e)****		
S1	0,515	0.758	0.849	0.512	0.511
C2	–0,539	–0.599	–0.444	–0.336	–0.557
C3	–0,146	–0.047	–0.392	–0.147	0.073
C4	–0,146	–0.124	–0.042	–0.146	–0.139
C5	–0,539	–0.517	–0.501	–0.54	–0.540
C6		–0.546	–0.528	–0.602	–0.606

** – Here the value of the total energy of these compounds is taken as the starting point*
*** – For precise analysis, data is presented in thousandths*

Table 1 below presents the results of calculations of the geometry and electronic structure of the substrate (***1***), model intermediates (***2a***, ***2b***), and the products of electrophilic substitution of thiophene (***3a***, ***3b***), which provide a quantitative picture of the methylation process.

Discussion of the results

According to Table 1, the total energy of the starting substrate ***1*** is Et= –345246.03 kCal/mol, the dipole moment is μ=0.97D and the dipole vector is directed from the heteroatom to the middle of the C3-C4 bond (Fig. 2). The symmetrical, planar arrangement of the ring atoms relative to the heteroatom and the presence of 6π electrons in the ring (preservation of the Hückel rule) makes the molecule aromatic. At the same time, the symmetry in the bond lengths and the values of the valence and torsion angles is preserved. The energetic preference of compound ***2a*** relative to ***2b*** by Δ*Et*= –14.75 kCal/mol.

The electron charges at the *α*- and *β*-positions of thiophene are different: *q* = –0.539e and *q* = –0.146e, respectively, indicating the advantage in nucleophilic reactivity of the *α*-position relative to the *β*-position. To more accurately study the electrophilic substitution process and reaction mechanism, we also calculated the geometry and electronic structure of charged structures ***2a*** and ***2b***, representing the process intermediates (Fig. 1).

Geometry of compounds

After the substitution of the methyl cation $CH3^+$ in the *α*-position of the substrate, i.e. in the process ***1***→***2a*** (Path "A", Fig.1), a redistribution of electron charges occurs and the lengths of the S1-C2, C2-C3, C4-C5 bonds are lengthened by Δ*d*=0.118Å, 0.126Å, 0.056Å, and the C3-C4, C5-S1 bonds are shortened by Δ*d*=0.074Å, 0.080Å. For example, the C2 atom (*α*-position) of isomers ***2a*** and ***2b*** is concentrated with the maximum negative charge equal to *q*= –0.599e and *q*= –0.444e, respectively, whereas the C5 atom, located symmetrically to the first, carries a charge of *q*= –0.517e and *q*= –0.501e, respectively.

Conclusions

The *α*-positions of thiophene exhibit greater reactivity relative to the *β*-positions of the substrate, both in charge-controlled reactions and in orbital control. The difference Δ*Et*=1.25 kCal/mol in the total energies

of products ***3a*** and ***3b*** once again shows the preference of the reaction path ***1→2a→3a*** (reaction pathway 1, see Fig.1).

References

Spivey Alan C. (2012). Heteroaromatic Chemistry lectures: Pyrroles, furans & thiophenes – properties, syntheses & reactivity. / Imperial College, London. – 22 p.

Molina P., Arques A., Cartagena I. (2008). Thiophenes and their Benzo Derivatives: Structure. Comprehensive Heterocyclic Chemistry III. – Vol. 3. – P. 625–739.

Yurovskaya M. A., Kurkin A. V., Lukashev N. V. (2007). Chemistry of aromatic heterocyclic compounds / – Moscow: Faculty of Chemistry of Moscow State University. – 50 p.

Frisch M. J., Trucks G. W., et al. (1998). Gaussian 98, Revision A. 5, Gaussian Inc., Pittsburgh (PA).

Fahimeh Abedinifar, Elham Babazadeh Rezaei. et all. (2021). Recent strategies in the synthesis of thiophene derivatives: highlights from the 2012–2020 literature / Molecular Diversity – 25. – P. 2571–2604. URL: https://doi.org/10.1007/s11030-020-10128-9.

Amita Vyasa, Dharmesh Katariya, et.all. (2025). Comprehensive Review on Advances in Thiophene Derivative Synthesis and Their Biological Applications./ Reviews and Advances in Chemistry, – Vol. 15. – No. 1. – P. 1–6.

Michael Dewar, Ralph C. Dougherty. (1975). The PMO Theory of Organic Chemistry. Springer US, – 576 p.

Dipak Kumar Mandal. (2025). Molecular Orbital Theory and Frontier Orbitals for Organic Chemistry / Elsevier. October 21. URL: https://doi.org/10.1016/C2025-0-00298-3.

Mamarakhmonov M. Kh., Belen´kii L. I. et. all. (2016). March. Quantum chemical studies of pyrimidin-4ones Part 6. On peculiarities of the reactions with nitrating agents of some carboxylic acids of the thieno[2,3-d]pyrimidin-4one series and their esters / Russian Chemical Bulletin, Int. Ed., – Vol. 65. – No. 3. – P. 654–657.

Dedicated
to the memory of Doctor of Chemical Sciences, Professor Leonid I. Belenkii

submitted 08.08.2026;
accepted for publication 22.08.2026;
published 31.08.2026
© Rustamov S. R., Mamarakhmonov M. Kh., Kodirov A. A., Khamrayeva K. B., Tokhirova M.
Contact: sarrus7595@gmail.com; mmamarakhmonov@gmail.com; muhamatdin@umail.uz

Austrian Journal of Technical
and Natural Sciences, 2026 No 7–8
ISSN 2310-5607

PREMIER Publishing
ppublishing.org

DOI:10.29013/AJT-26-7.8-41-45

SORPTION OF FORMIC ACID FROM AQUEOUS SOLUTIONS ON THE AN-31 ANION EXCHANGE RESIN

Mukhtarjan Mukhamediev [1], Muslimbek Murtozaqulov [1], Davronbek Bekchanov [1], Yusufjon Fayzullayev [2], Farangizkhon Murtozaqulova [1]

[1] Department of Polymer Chemistry, National University of Uzbekistan, Tashkent, Uzbekistan

[2] Academic Lyceum of Tashkent Institute of Chemical Technology, Tashkent, Uzbekistan

Cite: *Mukhamediev M., Murtozaqulov M., Bekchanov D., Fayzullayev Y., Murtozaqulova F. (2026). Sorption of Formic Acid From Aqueous Solutions on the An-31 Anion Exchange Resin. Austrian Journal of Technical and Natural Sciences 2026, No 7–8.* https://doi.org/10.29013/AJT-26-7.8-41-45

Abstract

The accumulation of heat-stable salts (HSS) in methyldiethanolamine (MDEA) solutions during natural gas sweetening causes corrosion, foaming and a loss of the useful capacity of the amine; such salts are not decomposed under conventional regeneration. One of their principal sources is formic acid produced by the oxidative degradation of MDEA. In this work, the sorption of formic acid on the weakly basic anion exchanger AN-31 was studied in aqueous solutions over the range of 293–313 K. The equilibrium data conformed to the Langmuir model, and the maximum adsorption capacity reached 175.43 $mg \cdot g^{-1}$ at 293 K. The kinetics followed the pseudo-second-order model. The thermodynamic parameters confirmed that the process is spontaneous and exothermic.

Keywords: *AN-31 anion exchange resin, formic acid, adsorption, heat-stable salts, methyldiethanolamine, Langmuir isotherm*

Introduction

Methyldiethanolamine (MDEA) is widely used for the removal of acidic components (H_2S and CO_2) from natural gas because of its high selectivity (Kohl & Nielsen, 1997). As a tertiary amine, MDEA does not form carbamates with CO_2 and reacts with it slowly, whereas its reaction with H_2S is very fast – a considerable technological advantage for the selective separation of hydrogen sulphide from gas mixtures. During prolonged operation, however, heat-stable salts (HSS) accumulate in the solution. These consist mainly of organic acid anions (formate, acetate, oxalate, bicine) generated by oxidation of the amine in the presence of oxygen, together with inorganic ions introduced with the process water (Mertens et al., 2013; Rooney et al., 1996). Degradation of MDEA proceeds along two routes: thermal degradation in

the regenerator under high temperature and CO_2 exposure, and oxidative degradation in the absorber under the action of oxygen and other oxidants. The resulting intermediates include diethanolamine, methylmonoethanolamine and bis-(hydroxyethyl)glycine; being secondary amines, MMEA and DEA react directly with CO_2 and thereby reduce the selectivity of the primary solvent (Islam et al., 2011). The heat-stable salts formed are not decomposed during conventional thermal regeneration. Their accumulation intensifies corrosion in heat exchangers and pipelines, causes severe foaming of the solution and increases the energy demand of regeneration (Pal et al., 2016).

Several approaches to HSS removal are known. Discharging part of the solution and replacing it with fresh MDEA generates large volumes of toxic wastewater and raises the cost of purification. Distillation is energy-intensive, and although neutralisation with strong alkalis minimises amine loss, the soluble sodium salts formed reduce the absorption capacity (Dumée et al., 2012). Electrodialysis has the advantage of being a reagent-free process, but 10–30% of the absorbent is lost through the membranes (Wang et al., 2018). Ion exchange, in contrast, operates at low temperature, minimises absorbent loss and leaves the structure of the sorbent stable, which makes it the most economically viable route (Bayati et al., 2019; Stroganova et al., 2020). The present work aims to study the sorption of formic acid on the weakly basic anion exchange resin AN-31 and to characterise the process in equilibrium, kinetic and thermodynamic terms.

Method

The sorbent was AN-31, a weakly basic anion exchange resin complying with GOST 20301–74. Model solutions were prepared from analytical-grade formic acid (purity not less than 99%) in distilled water at concentrations of 0.025, 0.05, 0.075 and 0.1 M.

Sorption was studied under static conditions: 100 ml of solution was added to 1.0 g of the resin, and the mixture was shaken at 80 rpm. The temperature was maintained at 293, 303 and 313 K. Samples were taken at intervals from 0.5 to 6 hours; sorption equilibrium was attained within 5 hours. The residual concentration of formic acid was determined by potentiometric titration, and each experiment was carried out in triplicate.

The adsorption capacity q_e was calculated from the difference between the initial and equilibrium concentrations, the solution volume and the mass of the resin (1).

$$q_e = \left(C_0 - C_e\right) \cdot \frac{V}{m} \qquad (1)$$

Equilibrium data were described by the linearised Langmuir and Freundlich isotherms, and the kinetics by the pseudo-first-order and pseudo-second-order models. The linearised forms of these equations, the separation factor, and the Arrhenius and Van't Hoff relations used to obtain the activation energy and the thermodynamic parameters were applied in the conventional forms summarised by Ho and McKay (1999) and Foo and Hameed (2010).

Results and discussion

The equilibrium data were processed using both models (Figure 1, Table 1). The Langmuir model gave a higher coefficient of determination than the Freundlich model at all temperatures. This indicates that the surface of AN-31 carries energetically homogeneous active sites and that formic acid is taken up with the formation of a monomolecular layer. At 293 K the maximum capacity was 175.43 mg·g^{-1}. Both q_{max} and K_L decreased as the temperature rose, which points to an exothermic process.

Figure 1. *Linearised Langmuir isotherms for the adsorption of formic acid on AN-31 at 293, 303 and 313 K*

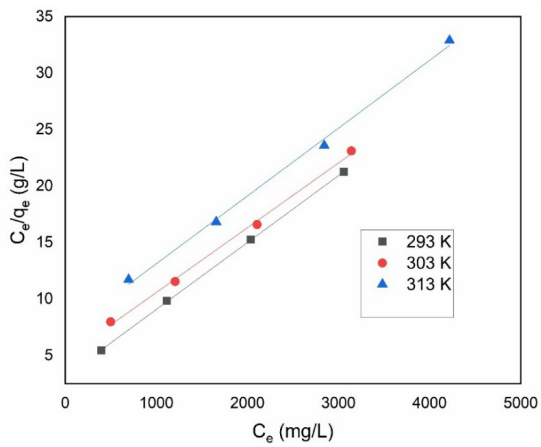

The kinetic data were analysed using two models (Figure 2, Table 2). The pseudo-first-order model gave a calculated equilibrium capacity of 185.7 mg·g^{-1}, which differs considerably from the experimentally measured value of 144 mg·g^{-1}; the model was therefore rejected. The pseudo-second-order model gave a value of 144.7 mg·g^{-1}. This indicates that the rate-determining step involves chemical interaction between the sorbate ions and the functional groups of the sorbent. From the Arrhenius equation, an activation energy of E_a= 9.76 kJ·mol^{-1} was calculated.

Table 1. *Isotherm parameters for the adsorption of formic acid*

Model	Parameter	293 K	303 K	313 K
Langmuir	q_{max} (mg·g^{-1})	175.43	169.50	166.66
	K_L(L·mol^{-1})	84.28	52.98	37.93
	R^2	0.9948	0.9988	0.9935
Freundlich	K_F	9.92	4.51	3.53
	n	2.95	2.32	2.28
	R^2	0.975	0.959	0.959

Table 2. *Kinetic parameters for the sorption of formic acid (0.1 M, 293 K)*

Model	Parameter	Value
PFO	$q_{e,\,exp}$ (mg·g^{-1})	144.0
	$q_{e,\,cal}$ (mg·g^{-1})	185.7
	R^2	0.9762
PSO	$q_{e,\,exp}$ (mg·g^{-1})	144.0
	$q_{e,\,cal}$ (mg·g^{-1})	144.7
	k_2 (g·mg^{-1}·min^{-1})	1.836·10^{-4}
	h (mg·g^{-1}·min^{-1})	3.84
	R^2	0.998

Figure 2. *Pseudo-second-order kinetic plots for the sorption of formic acid on AN-31 at (a) 293 K, (b) 303 K and (c) 313 K*

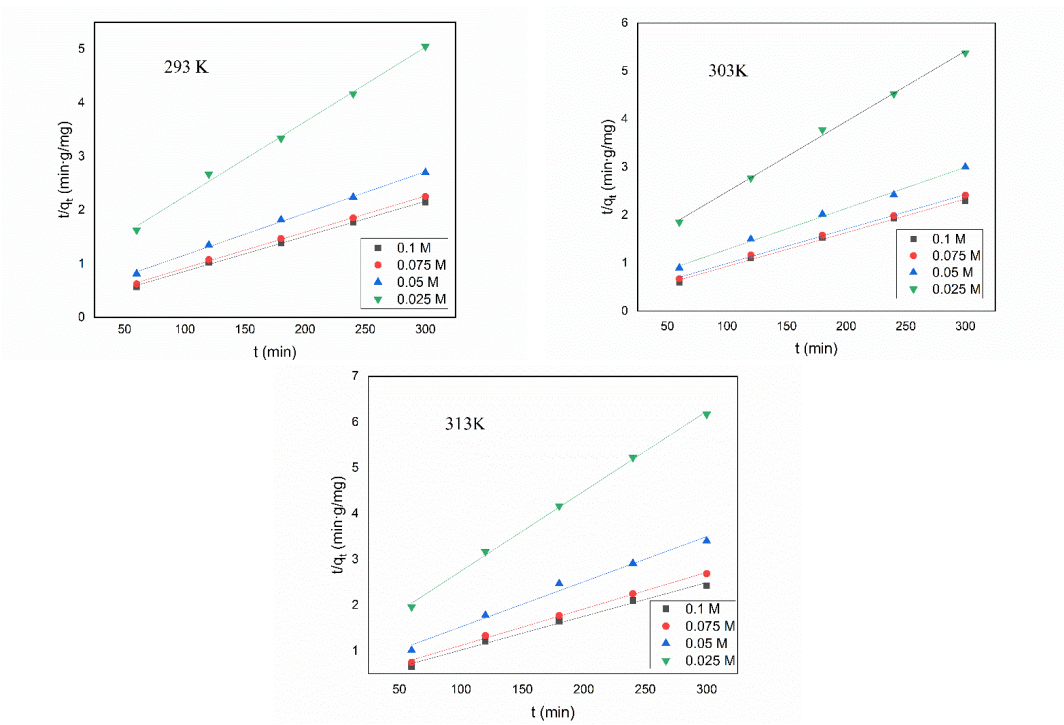

The Van't Hoff plot was highly linear (Figure 3), and the values derived from it are given in Table 3.

Figure 3. *Van't Hoff plot for the sorption of formic acid on AN-31*

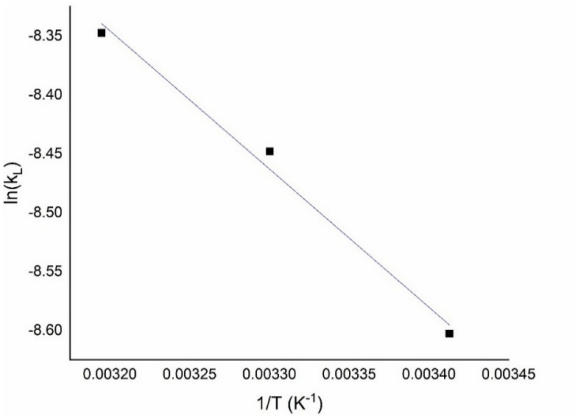

The negative ΔG at every temperature shows that the process is spontaneous, while the decrease in its magnitude with rising temperature indicates that sorption is more favourable at lower temperatures. The value ΔH = –30.481 kJ·mol^{-1} lies above the range typical of purely physical adsorption and below that of covalent bonding, which is characteristic of chemisorption involving acid–base interaction with the amino groups of the resin. The negative ΔS reflects an increase in order at the solid–solution interface: freely moving formic acid molecules become fixed at specific active sites of the sorbent. Thus, a rise in temperature accelerates the process but lowers the equilibrium capacity, from which it follows that purification should be carried out at lower temperatures.

Table 3. *Thermodynamic parameters for the sorption of formic acid*

T (K)	K_L (L·mol^{-1})	ln K_L	ΔG (kJ·mol^{-1})	ΔH (kJ·mol^{-1})	ΔS (J·mol^{-1}·K^{-1})
293	84.28	4.4341	–10.802	–30.481	–67.305
303	52.98	3.9699	–10.001		
313	37.93	3.6357	–9.461		

Conclusion

The weakly basic anion exchange resin AN-31 takes up formic acid efficiently from aqueous solutions, with a maximum adsorption capacity of 175.43 mg·g^{-1} at 293 K. The equilibrium data follow the Langmuir model, and the kinetics conform to the pseudo-second-order model, the deviation between the calculated and measured equilibrium capacities being 0.49%. The activation energy of 9.76 kJ·mol^{-1} shows that the rate is limited by a diffusion step. The thermodynamic parameters indicate a spontaneous and exothermic process in which uptake proceeds through acid–base interaction with the amino groups of the resin. The results obtained allow AN-31 to be recommended as an efficient sorbent for the purification of MDEA solutions from heat-stable salts.

References

Bayati, B., Mirshekari, M., Veisy, A., & Gando-Ferreira, L. M. (2019). Removal of HSS from industrial amine solution by anionic resin (case study: Ilam gas refinery). *Chemical Papers,* – 73. – P. 491–500.

Dumée, L., Scholes, C., Stevens, G., & Kentish, S. (2012). Purification of aqueous amine solvents used in post-combustion CO2 capture: A review. *International Journal of Greenhouse Gas Control,* – 10. – P. 443–455.

Foo, K. Y., & Hameed, B. H. (2010). Insights into the modeling of adsorption isotherm systems. *Chemical Engineering Journal,* – 156(1). – P. 2–10. URL: URL: https://doi.org/10.1016/j.cej.2009.09.013

Ho, Y. S., & McKay, G. (1999). Pseudo-second order model for sorption processes. *Process Biochemistry,* – 34(5). – P. 451–465. URL: https://doi.org/10.1016/S0032-9592(98)00112-5

Islam, M. S., Yusoff, R., Ali, B. S., Islam, M. N., & Chakrabarti, M. H. (2011). Degradation studies of amines and alkanolamines during sour gas treatment process. *International Journal of the Physical Sciences,* – 6(25). – P. 5877–5890.

Kohl, A. L., & Nielsen, R. B. (1997). *Gas purification* (5th ed.). Houston, TX: Gulf Professional Publishing.

Mertens, J., Lepaumier, J., Desagher, D., & Lepaumier, H. (2013). Understanding ethanolamine degradation in post-combustion CO_2 capture. *International Journal of Greenhouse Gas Control,* – 13. – P. 72–80.

Pal, P., Banat, F., & AlShoaibi, A. (2016). Adsorptive removal of heat stable salt anions from industrial lean amine solvent using anion exchange resins from gas sweetening unit. *Journal of Natural Gas Science and Engineering,* – 30. – P. 215–224.

Rooney, P. C., DuPart, M. S., & Bacon, T. R. (1996). Oxygen's role in alkanolamine degradation. *Hydrocarbon Processing,* – 75(7). – P. 109–115.

Stroganova, E. A., Bezryadin, S. G., & Larina, T. V. (2020). Application of the law of mass action to the description of the ion exchange equilibrium in the static and dynamic conditions. *Adsorption,* – 26. – P. 357–365.

Wang, Y. M., Li, W., Yan, H. Y., & Xu, T. W. (2018). Removal of heat stable salts (HSS) from spent alkanolamine wastewater using electrodialysis. *Journal of Industrial and Engineering Chemistry,* – 57. – P. 356–362.

submitted 15.08.2026;
accepted for publication 30.08.2026;
published 31.08.2026
© Mukhamediev M., Murtozaqulov M., Bekchanov D., Fayzullayev Y., Murtozaqulova F.
Contact: mmukhamediev@mail.ru; muslimbekmurtozaqulov@gmail.com; bekchanovdj@gmail.com; yusuffayzullayev9@gmail.com; farangizmurtozaqulova@gmail.com

Austrian Journal of Technical
and Natural Sciences, 2026 No 7–8
ISSN 2310-5607

PREMIER Publishing
ppublishing.org

DOI:10.29013/AJT-26-7.8-46-52

3-AMINO-1,2,4-TRIAZOLE AT THE CHITOSAN–COLLAGEN INTERFACE: A MECHANISTIC FRAMEWORK FOR BRIDGING, CAPPING AND LATTICE INCLUSION

Jahongir Mustaqim o'g'li Sharopov [1]

[1] Doctoral student, Department of General Chemistry, Tashkent State Technical University named after Islam Karimov, Tashkent, Uzbekistan

Cite: *Sharopov J.M. (2026). 3-Amino-1,2,4-Triazole at the Chitosan–Collagen Interface: A Mechanistic Framework For Bridging, Capping and Lattice Inclusion. Austrian Journal of Technical and Natural Sciences 2026, No 7–8.* https://doi.org/10.29013/AJT-26-7.8-46-52

Abstract

Chitosan–collagen hybrids derive their behaviour from a thin interfacial region where a cationic polysaccharide, a hydrated triple helix and ordered water compete for one hydrogen-bond inventory. This review asks what 3-amino-1,2,4-triazole (3-AT), an 84 Da hydrogen-bonding heterocycle, could do there. A structured search yielded 177 records (Supplementary Table S2); no eligible study combining all three components was identified within the defined search strategy, so every ternary statement is inference paired with a named falsifiable observable. With a conjugate-acid pKa of 4.04, 3-AT is 72% neutral at pH 4.5 and 96% at pH 5.5: it cannot serve as a counter-ion for chitosan ammonium or compete for collagen carboxylate, and being monovalent it cannot crosslink. Three non-covalent roles remain – interstitial bridging, capping of the hydrogen-bond ladder and inclusion in the hydrated chitosan lattice – behind two confounders to be excluded first: retitration of the casting sol by 3-AT itself, and covalent capture of its exocyclic amine by crosslinkers. The roles predict divergent diffraction, calorimetric, mechanical and degradation signatures, so they are experimentally separable; the necessary control set is specified.

Keywords: chitosan, collagen, 3-amino-1,2,4-triazole, supramolecular interface, hydrogen bonding, hydration, network stability, biomaterials

Introduction

Chitosan and collagen are combined because their deficiencies are complementary: collagen gives a cell-instructive triple helix but little strength, chitosan a cationic film-forming backbone without fibrillar hierarchy (Rinaudo, 2006). Their properties are not additive; association depends on the state of collagen (Taravel & Domard, 1993) and on a contact map set by chitosan acetylation and collagen hydroxylation (Przybyłek et al., 2022). The interface is thus the property-determining element, and it is crowded: every additive must displace something already bound (Kaczmarek-Szczepańska et al., 2025).3-AT is a suitable probe: small enough to enter that region without templating a phase of its

own, hydrophilic, and presenting an annular N–H donor, two ring-nitrogen acceptors and an exocyclic amine on a rigid scaffold. It is essentially uncharged where chitosan is charged, a regime no polymeric additive occupies. Reviews do not close the gap: chitosan–collagen work compresses the interface into one ammonium–carboxylate statement (Devernois & Coradin, 2023), and triazole–biomaterial work is dominated by the click-derived 1,2,3-isomer, where the ring is a covalent junction, not a guest (Erdmann & Wennemers, 2013).

Molecular architecture of the three components

Chitosan's interfacial inventory is threefold: the C2 amine, its only strongly basic site; the C3 and C6 hydroxyls, C6–OH being the accessible donor; and residual acetamido groups. Two free-amine estimates circulate and are not interchangeable: dissolution in acetic acid requires a degree of protonation of only about 0.5 (Rinaudo et al., 1999), whereas Henderson–Hasselbalch with pKo ≈ 6.0–6.5 predicts 76–99%. They reconcile only through the charge-dependent depression of a polyelectrolyte's apparent pK, so the free-amine fraction must be measured.

Figure 1. *Interaction-relevant chemistry of the three components*

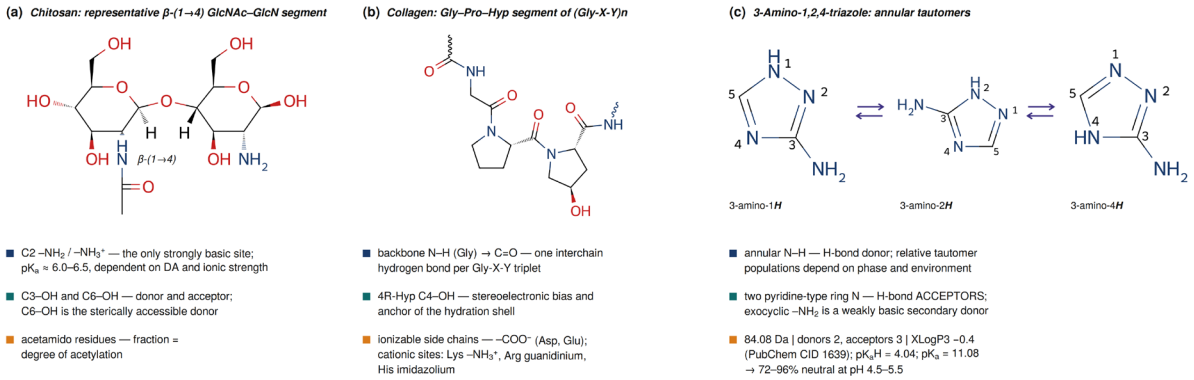

Note. (a) Chitosan repeating unit; (b) a Gly–Pro–Hyp segment of the triple helix; (c) the annular tautomers of 3-amino-1,2,4-triazole. No covalent linkage between the components is implied

Chitosan's solid-state hydrogen bonding is polymorph-dependent, structural water being integral to the hydrated form, and small guests can enter that lattice: monocarboxylic acids form a distinct complex phase whose removal drives a crystal transition (Naito et al., 2015). The triple helix carries one interchain N–H···O=C bond per Gly-X-Y triplet inside a hydration cylinder in which water bridges peptide acceptors (Bella et al., 1994). Two caveats follow. First-shell residence is nanosecond to sub-nanosecond (Melacini et al., 2000), so a guest competes on occupancy, not by displacement. And where water was seen to replace a direct interchain bond, it was at a glycine substitution mimicking a disease mutation and came with local untwisting: a precedent for the geometry of bridging, and equally evidence that bridging in the helix core is a defect rather than a design option.

3-AT is $C_2H_4N_4$, 84.08 Da, with two donors, three acceptors and a negative computed partition coefficient placing it in the aqueous phase. Potentiometry gives pKa = 4.04 for the conjugate acid and 11.08 for annular N–H deprotonation (Kröger & Freiberg, 1965), so the protonated fraction is about 28% at pH 4.5, 11% at pH 5.0 and 4% at pH 5.5. Which face it presents is set by environment-dependent annular tautomerism; in matrix-isolated complexes the annular N–H, not the exocyclic amine, donates (Mucha et al., 2023). It decomposes in two stages, the first with an activation energy of 124 ± 8 kJ mol^{-1} (Sánchez-Soto et al., 1995). Table 1 collects these values.

Table 1. *Interaction-relevant chemistry of chitosan, collagen and 3-amino-1,2,4-triazole*

Feature	Chitosan	Collagen (type I)	3-Amino-1,2,4-triazole
H-bond donors	C3–OH, C6–OH, C2–NH_2, acetamido N–H	backbone N–H, Hyp O–H, side-chain N–H/O–H	annular N–H (primary), exocyclic NH_2 (secondary)
H-bond acceptors	ring and hydroxyl O, amine N	peptide C=O, carboxylate O, Hyp O	two pyridine-type ring N; amine lone pair
Ionisable site, pKa	C2–NH_3^+; $pK_0 \approx 6.0$–6.5, DA- and I-dependent	Asp/Glu –COOH, Lys/Arg/His; pI ≈ 8	conjugate acid 4.04; annular N–H 11.08
Charge at pH 4.5–5.5	≈ 50% protonated at typical acid stoichiometry	net cationic (below pI)	72% neutral at pH 4.5, 96% at pH 5.5
Valency toward a partner chain	multivalent polyelectrolyte	multivalent	monovalent – cannot crosslink
Ordered water	integral to the hydrated polymorph	cylinder of hydration, sub-nanosecond residence	hydrophilic; partitions to the aqueous phase
Reactive handle	C2–NH_2 toward aldehyde / genipin / carbodiimide	Lys ε-NH_2 toward the same	exocyclic NH_2 – competes

Note. Component-level measurements on the isolated species; none has been measured in a ternary chitosan–collagen-3-AT system

Interactions at the native interface

Pairing of chitosan $–NH_3^+$ with collagen $–COO^-$ is invoked most often and demonstrated least directly; with an isoelectric point near 8 both polymers are net cationic across the casting window, so attraction must arise locally against a repulsive background. In chitosan polyelectrolyte complexes the main infrared bands do not shift at all, complexation producing new bands instead (Lawrie et al., 2007). Band appearance, not band shift, is therefore the reporter, yet much of this literature reads shifts of five to ten wavenumbers in a window holding collagen amide II, chitosan $–NH_2$ scissoring and the ammonium mode together.

Three candidate roles for 3-amino-1,2,4-triazole

Two routes must be excluded before any direct role is claimed. Because pKaH lies inside the casting window, added 3-AT is itself a buffer: it consumes acid, raises sol pH and lowers chitosan's protonation, so a property change may arise with no guest–polymer contact at all. Separately, the exocyclic amine is a competent nucleophile toward the aldehyde, genipin and carbodiimide chemistries used on these blends. What follows is restricted to crosslinker-free constructs at matched pH and ionic strength.

Within that restriction 3-AT is neutral and monovalent, so three non-covalent roles remain. In bridging it inserts interstitially, accepting from one polymer at a ring nitrogen and donating from its annular N–H to the other, raising inter-chain connectivity. In capping it binds one partner preferentially and terminates connectivity, acting as a chain-stopper and plasticiser. In lattice inclusion it partitions into the hydrated chitosan crystallite as a distinct complex phase.

These are dominant-expression limits, not exclusive alternatives; mixed states give intermediate signatures. Because the chitosan–collagen contact is multivalent and 3-AT is not, kinetic site occupancy during solvent removal is likelier than equilibrium displacement, which does not separate bridging from capping. No bridging by 3-AT has been reported in any protein–polysaccharide system, and the only reported chitosan/3-AT

material is a covalently grafted cotton-fabric finish with no collagen and no network data (Aboelnaga et al., 2017).

Figure 2. *The native interface and the three candidate roles for 3-amino-1,2,4-triazole*

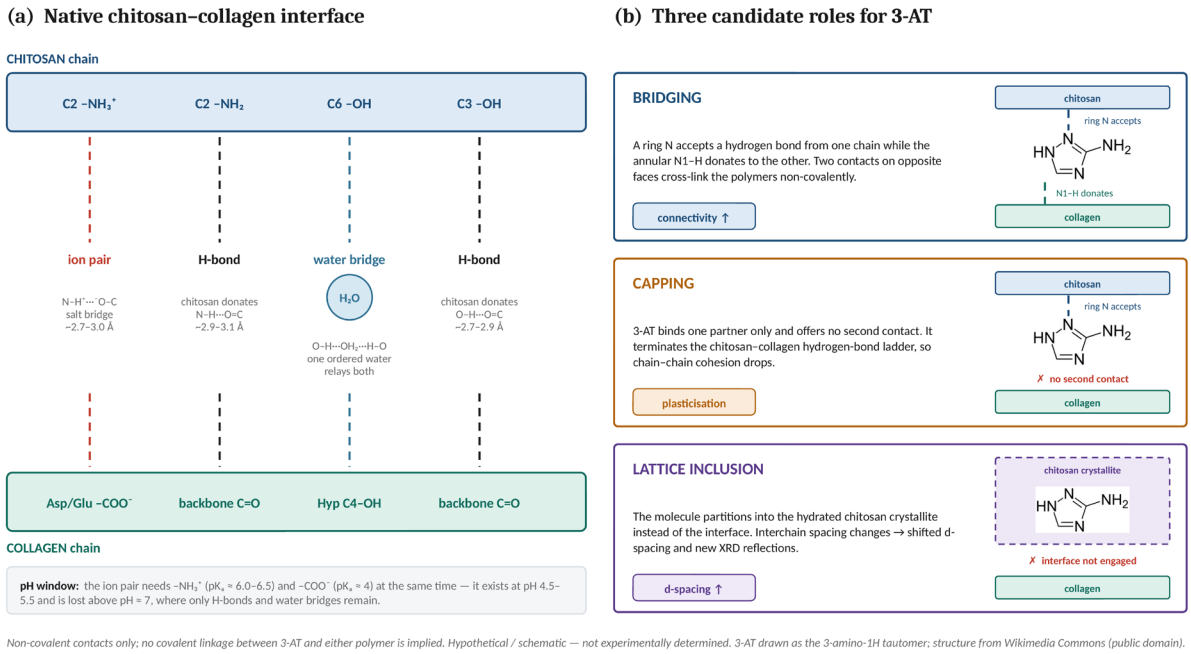

Note. Contacts are non-covalent throughout; broken lines denote hydrogen bonds or local ion pairs. Schematic, not experimentally determined

Discriminating the roles

The roles predict different signatures (Table 2). Diffraction discriminates most sharply: inclusion produces new Bragg reflections rather than broadening alone (Naito et al., 2015), bridging and capping none. A collagen-free control is mandatory, since collagen alone already abolishes the low-angle hydrated-chitosan reflection (Becerra et al., 2022); without that reflection, inclusion is unavailable and the scheme reduces to two roles. Calorimetry supplies the water axis, but bound water and equilibrium swelling must be reported separately, because in crosslinked chitosan membranes the two do not co-vary (Ostrowska-Czubenko & Gierszewska-Drużyńska, 2009).

Table 2. *Divergent signatures of the three candidate roles*

Observable	Bridging	Capping	Lattice inclusion
Wide-angle X-ray diffraction	no new reflections	no new reflections	new Bragg reflections
Non-freezing water (DSC)	decreases	increases	crystal transition rather than monotonic change
Equilibrium swelling	measure separately from bound water	measure separately from bound water	little change
Modulus / elongation	modulus ↑, elongation ↓	modulus ↓, elongation ↑	modulus ≈, brittleness ↑
Enzymatic degradation	slowed by steric shielding	accelerated	largely unchanged

Observable	Bridging	Capping	Lattice inclusion
Raman I_{1248}/I_{1271}	perturbed if the helix is reached	perturbed if the helix is reached	unchanged
Functional outcome	stable films, slow resorption	compliant, fast-swelling matrices	brittle, processing-sensitive

Note. Predicted signatures, not measured data. Diffraction separates inclusion from the other two; mechanics and degradation separate bridging from capping. Every row requires a crosslinker-free blank, a collagen-free binary and a charge-matched control

Operational definitions differ between studies: in one collagen/chitosan/silk-fibroin series, swelling in phosphate-buffered saline ran from 1302 ± 30% to 7580 ± 50% while liquid uptake in the same work was 10–15% (Grabska-Zielińska et al., 2021). Vibrational spectroscopy is best used as a helix reporter: the Raman amide III doublet near 1271 and 1248 cm^{-1} resolves triple-helical content (Frushour & Koenig, 1975) against a far weaker water background than infrared. No band position is established for free 3-AT in a biopolymer phase, so finding a marker band in an empty window is a prerequisite. Mechanically the roles predict opposite signs, but only a single-laboratory composition series under one protocol is defensible.

Thermal behaviour, degradation and safety

Blending is itself a large thermal effect: in one chitosan–collagen series the glass transition falls from 107 °C to 64 °C at a 1:1 ratio (Thongchai et al., 2020), so a modifier effect must be substantial to be interpretable and measured at matched water content. In thermogravimetry an extra mass-loss step matching the first decomposition stage of 3-AT would betray a segregated crystalline fraction, though its absence is informative only above the loading at which such a fraction resolves. Degradation must be phase-resolved: lysozyme attacks the chitosan phase and leaves the triple helix, which needs collagenase; dual-crosslinked collagen–chitosan films retained 85–89% of their mass after 14 days in lysozyme and lipase (Shah et al., 2019). Each assay must quantify modifier leaching, since mass loss and modifier loss are otherwise indistinguishable.

Experimental roadmap

Figure 3. *Gated experimental sequence for testing the ternary system*

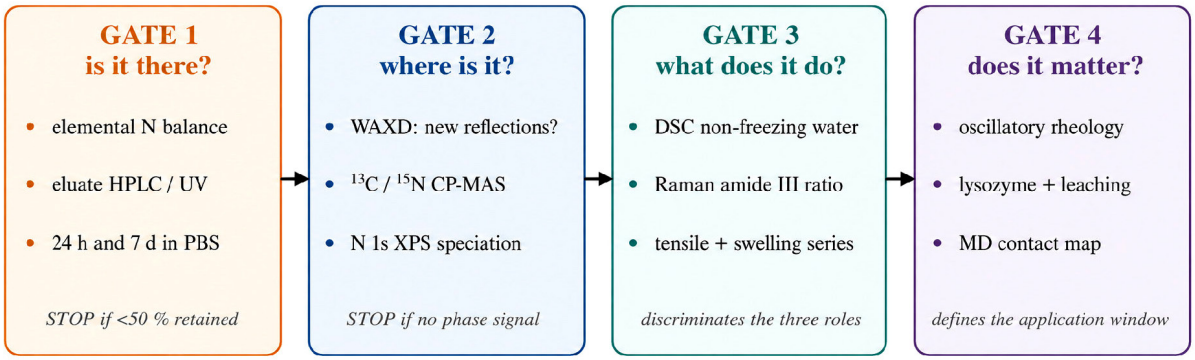

Retention must be quantified before any property is attributed to the modifier: a highly soluble guest will otherwise be credited with effects it has already left behind.

Note. Retention is quantified before phase location, phase location before mechanism, and mechanism before application. Each gate requires the controls in Table 2

A toxicological constraint precedes any application. 3-AT is amitrole, a regulated herbicide with documented developmental toxicity (Landauer et al., 1971), and its protein adduct forms through a peroxide-derived enzyme intermediate (Margoliash et al., 1960); the assumption of non-covalent behaviour therefore fails in peroxide- and catalase-rich environments such as inflamed wound beds. Collagen offers no comparable activating centre, so this concerns the biological environment rather than a predicted collagen reaction; but a weakly bound fraction elutes freely, making leaching an exposure route before it is a measurement artefact. No biomedical claim should be advanced without eluate cytotoxicity data.

The decisive measurements are neither expensive nor novel, but their order matters. Every stage requires three controls – a crosslinker-free blank, a collagen-free chitosan/3-AT binary at matched processing, and a charge-matched additive-free sol – without which no observation is attributable to the guest.

Conclusion

3-Amino-1,2,4-triazole is chemically well suited to the chitosan–collagen interface and entirely untested there. Its pKa removes electrostatic competition and its monovalency removes crosslinking, leaving three non-covalent roles whose diffraction, calorimetric, mechanical and degradation signatures point in different directions. They are distinguishable in principle, provided the control set above is applied and retention is quantified before any property is attributed to the modifier. Until then, 3-AT at this interface remains a testable hypothesis.

Supplementary Table S1 summarises the search strategy, databases, terms and screening criteria; Table S2 lists the 177 retained records with search category, evidence tier and screening decision; Table S3 gives their distribution across evidence domains. Twenty-three records are cited here, and none describes a material containing chitosan, collagen and 3-AT together. The dataset is archived at Zenodo (Sharopov, 2026).

References

Aboelnaga, A., Shaarawy, S., & Hagar, M. (2017). A novel chitosan 3-amino-1,2,4-triazole hybrid: Preparation and its effects on cotton fabric. Journal of Taibah University for Science, – 11 (5). – P. 768–774. URL: https://doi.org/10.1016/j.jtusci.2016.08.008

Becerra, J., Rodriguez, M., Leal, D., et al. (2022). Chitosan-collagen-hydroxyapatite membranes for tissue engineering. Journal of Materials Science: Materials in Medicine, – 33. – 18 p. URL: https://doi.org/10.1007/s10856-022-06643-w

Bella, J., Eaton, M., Brodsky, B., et al. (1994). Crystal and molecular structure of a collagen-like peptide at 1.9 Å resolution. Science, – 266 (5182). – P. 75–81. URL: https://doi.org/10.1126/science.7695699

Devernois, E., & Coradin, T. (2023). Synthesis, characterization and biological properties of type I collagen-chitosan mixed hydrogels: A review. Gels, – 9 (7). – 518 p. URL: https://doi.org/10.3390/gels9070518

Erdmann, R. S., & Wennemers, H. (2013). Conformational stability of triazolyl functionalized collagen triple helices. Bioorganic & Medicinal Chemistry, – 21 (14). – P. 3565–3570. URL: https://doi.org/10.1016/j.bmc.2013.02.046

Frushour, B. G., & Koenig, J. L. (1975). Raman scattering of collagen, gelatin, and elastin. Biopolymers, – 14 (2). – P. 379–391. URL: https://doi.org/10.1002/bip.1975.360140211

Grabska-Zielińska, S., Sionkowska, A., Olewnik-Kruszkowska, E., et al. (2021) Collagen/chitosan/silk fibroin scaffolds cross-linked by EDC/NHS. Materials, – 14 (5). – 1105 p. URL: https://doi.org/10.3390/ma14051105

Kaczmarek-Szczepańska, B., D'Amora, U., Zasada, L., et al. (2025) Chitosan-collagen biocomposite thin films with potassium silicate and tannic acid. Polymers, 17 (5). – 608 p. URL: https://doi.org/10.3390/polym17050608

Kröger, C. F., & Freiberg, W. (1965). Protonation constants of 3-amino-1,2,4-triazole. Zeitschrift für Chemie, – 5. – 381 p.

Landauer, W., Salam, N., & Sopher, D. (1971). The herbicide 3-amino-1,2,4-triazole (amitrole) as teratogen. Environmental Research, – 4 (6). – P. 539–543. URL: https://doi.org/10.1016/0013–9351(71)90014–4

Lawrie, G., Keen, I., Drew, B., et al. (2007). Interactions between alginate and chitosan biopolymers characterized using FTIR and XPS. Biomacromolecules, – 8 (8). – P. 2533–2541. URL: https://doi.org/10.1021/bm070014y

Margoliash, E., Novogrodsky, A., & Schejter, A. (1960). Irreversible reaction of 3-amino-1:2:4-triazole and related inhibitors with the protein of catalase. Biochemical Journal, – 74 (2). – P. 339–348. URL: https://doi.org/10.1042/bj0740339

Melacini, G., Bonvin, A. M. J. J., Goodman, M., et al. (2000). Hydration dynamics of the collagen triple helix by NMR. Journal of Molecular Biology, – 300 (4). – P. 1041–1049. URL: https://doi.org/10.1006/jmbi.2000.3919

Mucha, M., Pagacz-Kostrzewa, M., & Wierzejewska, M. (2023). Structure and IR spectroscopic properties of complexes of 1,2,4-triazole and 3-amino-1,2,4-triazole. Spectrochimica Acta Part A, – 285. – 121901 p. URL: https://doi.org/10.1016/j.saa.2022.121901

Naito, P.-K., Ogawa, Y., Kimura, S., et al. (2015). Crystal transition from hydrated chitosan and chitosan/monocarboxylic acid complex to anhydrous chitosan. Journal of Polymer Science Part B, – 53 (15). – P. 1065–1069. URL: https://doi.org/10.1002/polb.23748

Ostrowska-Czubenko, J., & Gierszewska-Drużyńska, M. (2009). Effect of ionic crosslinking on the water state in hydrogel chitosan membranes. Carbohydrate Polymers, – 77 (3). – P. 590–598. URL: https://doi.org/10.1016/j.carbpol.2009.01.036

Przybyłek, M., Bełdowski, P., Wieland, F., et al. (2022). Collagen type II-chitosan interactions from molecular dynamics simulations. Molecules, – 28 (1). – 154 p. URL: https://doi.org/10.3390/molecules28010154

Rinaudo, M. (2006). Chitin and chitosan: Properties and applications. Progress in Polymer Science, – 31 (7). – P. 603–632. URL: https://doi.org/10.1016/j.progpolymsci.2006.06.001

Rinaudo, M., Pavlov, G., & Desbrières, J. (1999). Influence of acetic acid concentration on the solubilization of chitosan. Polymer, 40 (25). – P. 7029–7032. URL: https://doi.org/10.1016/S0032–3861(99)00056-7

Shah, R., Stodulka, P., Skopalova, K., & Saha, P. (2019). Dual crosslinked collagen/chitosan film for potential biomedical applications. Polymers, – 11 (12). – 2094 p. URL: https://doi.org/10.3390/polym11122094

Sharopov, J. M. (2026). Supplementary dataset – 3-amino-1,2,4-triazole at the chitosan–collagen interface [Data set]. Zenodo. URL: https://doi.org/10.5281/zenodo.22009239

Sánchez-Soto, P. J., Morillo, E., & Pérez-Rodríguez, J. L. (1995) Thermoanalytical study of the pesticide 3-amino-1,2,4-triazole. Journal of Thermal Analysis, – 45 (5). – P. 1189–1197. URL: https://doi.org/10.1007/BF02547493

Taravel, M. N., & Domard, A. (1993). Relation between the physicochemical characteristics of collagen and its interactions with chitosan: I. Biomaterials, – 14 (12). – P. 930–938. URL: https://doi.org/10.1016/0142-9612(93)90135-O

Thongchai, K., Chuysinuan, P., Thanyacharoen, T., et al. (2020). Integration of collagen into chitosan blend film composites: Physicochemical property aspects. SN Applied Sciences, – 2. – 255 p. URL: https://doi.org/10.1007/s42452-020-2052-5

submitted 08.08.2026;
accepted for publication 22.08.2026;
published 31.08.2026
© Sharopov J. M.
Contact: jahongir.user@gmail.com

Austrian Journal of Technical
and Natural Sciences, 2026 No 7–8
ISSN 2310-5607

PREMIER Publishing
ppublishing.org

DOI:10.29013/AJT-26-7.8-53-57

GRAVIMETRIC METHOD OF CORROSION PROTECTION FOR STEEL N20 IN AN ACIDIC ENVIRONMENT

Husan Yakhshinorov [1], Davron Kuronboev [1], Nodira Eshmamatova [1], Elyor Berdimurodov [1], Khamdam Akbarov [1]

[1] Faculty of Chemistry, National University of Uzbekistan, Tashkent, Uzbekistan

Cite: *Yakhshinorov H., Kuronboev D., Eshmamatova N., Berdimurodov E., Akbarov Kh. (2026). Gravimetric Method of Corrosion Protection for Steel N20 in an Acidic Environment. Austrian Journal of Technical and Natural Sciences 2026, No 7–8.* https://doi.org/10.29013/AJT-26-7.8-53-57

Abstract

In this study, carbon dots were synthesized using chitosan and thiourea via hydrothermal treatment at 180 °C for 4 hours. The synthesized carbon dots were characterized by Transmission Electron Microscopy (TEM) analysis. The size of the synthesized carbon dots was found to be in the range of 8 nm to 10 nm. These carbon dots were used as a green corrosion inhibitor to mitigate the corrosion of mild steel (MS) in 0.5 M HCl solution using the gravimetric method. The studied carbon dots exhibited an inhibition efficiency of 91.70% at a concentration of 200 mg/L and a temperature of 303 K. The observed corrosion inhibition is attributed to the adsorption of the carbon dots onto the MS surface.

Keywords: *corrosion inhibitors, metal surface, carbon dots, solution, concentrations*

1. Introduction

Corrosion of metallic materials, particularly carbon steel (KP), remains a significant challenge in industrial operations such as oil and gas extraction, chemical processing, acidizing, and desalination systems. This leads to substantial economic losses not only due to the replacement of damaged infrastructure but also because of maintenance, downtime, and reduced equipment efficiency (He, H., et al., 2025; Yan, H., et al., 2024). Beyond the economic burden, corrosion also gives rise to serious environmental and safety hazards, including the leakage of toxic chemicals, equipment failure, and catastrophic accidents. Therefore, the need for reliable, efficient, and environmentally benign corrosion control methods is urgent and widely recognized. Among the numerous approaches to corrosion mitigation, the addition of inhibitors to corrosive environments is one of the most cost-effective strategies. Inhibitors significantly reduce the corrosion rate by forming a protective layer on the metal surface and preventing the penetration of corrosive agents.

Corrosion inhibitors can be inorganic or organic in nature (Iravani, D., et al., 2024). Common inorganic inhibitors such as chromates, phosphates, and nitrites are

increasingly being phased out due to their toxicity, environmental persistence, and harmful effects on human health. Organic corrosion inhibitors have attracted interest due to their excellent corrosion control efficiency and ease of application. However, the hazardous nature and relatively high cost of many effective organic inhibitors have driven the search for cost-effective, environmentally safe, and sustainable alternatives. Recently, nanotechnology has opened new possibilities in the field of corrosion control through the use of nanomaterials. Nanostructured materials, owing to their high surface-to-volume ratio and versatile surface chemistry, exhibit strong interactions with metallic substrates. Carbon dots (CDs) are a particularly interesting class of nanomaterials for next-generation green corrosion inhibitors (Tang, M., et al., 2026). They are cost-effective, environmentally acceptable, and easy to prepare as zero-dimensional carbon nanoparticles with sizes below 10 nm. Fluorescence is an inherent property of CDs. Synthesizing CDs from biowaste is advantageous because it supports waste management and the production of carbon-based compounds (Tang, Y., et al., 2024). The excellent water dispersibility, low toxicity, chemical inertness, environmental friendliness, and tunable luminescence of CDs have attracted significant attention since their discovery in 2004, leading to their widespread application in biomedicine, sensing, catalysis, lubrication, and other fields.

Figure 1. *Synthesis process*

An additional advantage of using biomass precursors for CD synthesis is their ability to promote endogenous heteroatom doping. Natural biomass sources contain heteroatoms such as oxygen, nitrogen, sulfur, and phosphorus within their molecular frameworks (Wang, Q., et al., 2024; Islami, L.A. and Anawati A., 2025; He, C., et al., 2024). During hydrothermal or pyrolytic carbonization, these heteroatoms can spontaneously incorporate into the carbon dot structure or surface functional groups without relying solely on external dopant reagents (Lv, Y., et al., 2023; Ren, S., et al., 2022). This endogenous doping results in a high degree of surface functionalization, which is particularly beneficial for corrosion inhibition as it enhances interfacial adsorption, electron donor capability, and film-forming ability on metallic substrates.

This article reviews the synthesis and anti-corrosion inhibitory performance of carbon dots derived from chitosan as inhibitors.

2. Materials and methods

2.1. Materials: Chitosan and thiourea reagents were supplied by Shaanxi Alibon Biotechnology Co., Ltd. Hydrochloric acid (33%) was obtained from Henan Refortune Industrial Co., Ltd.

2.2. Preparation: Chitosan and thiourea were weighed in equal proportions (250 mg each) on an analytical balance and dissolved in 100 mL of distilled water. This mixture was stirred using an ultrasonic mixer. The solution was placed in an autoclave and subjected to a hydrothermal reaction in a muffle furnace at 200 °C for 4 hours. The obtained carbon dots were purified in several steps, for example, filtration, dialysis, and centrifugation at 12,000 rpm at 10 °C for 15 minutes, yielding pure carbon dots. The resulting carbon dots were dried at 40 °C to obtain dry carbon dots. The synthesis reaction of the new carbon dots based on chitosan and thiourea can be represented as follows (figure 1).

3. Experimental results and discussion

3.1. Transmission electron microscope (TEM) analysisThe size of the synthesized chitosan- and thiourea-based carbon dots was determined by TEM to be in the range of 8–10 nm, and their morphology was found to be spherical in shape. This indicates that the small-sized carbon dots were successfully synthesized (figure 2).

Figure 2. *Transmission electron microscope*

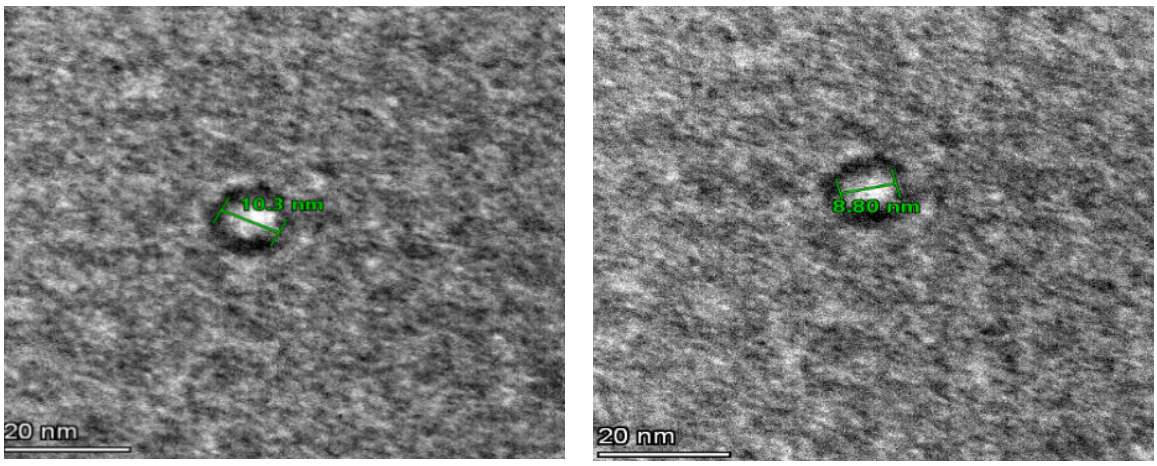

3.2. Gravimetric analysis: The anti-corrosion inhibition properties of the obtained carbon dots were examined using the gravimetric method. Gravimetry is a widely used method in analytical chemistry that is based on mass measurement for determining substances and their quantities. In the gravimetric method, metal plates of various N20 steel samples with dimensions of 3.0 × 3.0 × × 0.2 cm were used. Before starting the experiments, the metal samples were cleaned with emery paper and the metal dimensions were determined. They were then washed with distilled water and acetone. The experiments were carried out in a 0.5 M HCl solution at various time intervals. Initially, the metal sample was immersed in the test solution for 3 hours, after which its mass was weighed. Then, various concentrations of inhibitors were added, and the metal sample was weighed again. Before weighing, the metal samples were washed in distilled water, then in acetone, and subsequently weighed on a balance. Each experiment was repeated three times. The obtained results were recorded(1) (de Souza, F. S. and Spinelli A., 2009).

$$\eta = \frac{w_o - w_{ing}}{w_o} \times 100\% \qquad (1)$$

where *wo* and *wing* are the weight losses (mg) in the absence and presence of the inhibitor, respectively, and η% is the inhibitor efficiency. The surface coverage degree (θ) was found using the following formula(2):

$$\theta = \frac{w_o - w_i}{w_o} \qquad (2)$$

The corrosion rate was found using the following formula(3):

$$K'' = \frac{8.76 \times 10^4 W}{D \times A \times t} \quad (3)$$

where W is the weight loss (mg), A is the surface area of the sample immersed in the test solution (cm²), t is time (hours), and D is the density of the metal sample (g/cm³). Conducting experiments at different temperature ranges and various inhibitor concentrations when determining the efficiency of inhibitors using the gravimetric method, along with its high degree of accuracy, indicates that the essence of this method is substantial. At the same time, it should be noted that the significant amount of time required to determine the inhibitor efficiency is a disadvantage of this method. In order to determine the optimal concentration of the research objects in the background solutions, studies were carried out at various concentrations of the inhibitors.

Table 1. *Results of determining the efficiency of new carbon dots based on chitosan and thiourea as inhibitors at various temperatures and concentrations*

C_{ing}, mg/l	Temperature, K	$CR_{Grav.}$, mg/cm² h	$\eta_{Grav.}$, %	$\theta_{Grav.}$
HCl		1,236	–	–
50		0,2948	76,15	0,7615
100	303	0,2365	80,87	0,8087
150		0,1899	84,64	0,8464
200		0,1026	91,70	0,9170
HCl		1,584	–	–
50		0,4567	71,17	0,7117
100	313	0,3568	77,47	0,7747
150		0,2758	82,59	0,8259
200		0,1989	87,44	0,8744
HCl		1,759	–	–
50		0,5896	66,48	0,6648
100	323	0,4256	75,80	0,7580
150		0,3501	80,10	0,8010
200		0,2985	83,03	0,8303
HCl		1,847	–	–
50		0,6855	62,89	0,6289
100	333	0,4985	73,01	0,7301
150		0,4134	77,62	0,7762
200		0,3869	79,05	0,7905

To obtain more information about the surface coverage of the steel by the inhibitor and the protection mechanisms, the temperature dependence of the degree of protection of the chitosan- and thiourea-based inhibitor was studied (Table 1). Studies were conducted using the gravimetric method at various concentrations while varying the temperature from 303 K to 333 K in increments of 10 °C. The increase in the degree of protection with increasing temperature indicates that the inhibitor is adsorbed onto the steel surface as a result of chemical adsorption. A lesser increase in the degree of protection with increasing temperature indicates that physical adsorption is occurring alongside chemical adsorption in the process. The simultaneous occurrence of both chemical and physical adsorption indicates that the inhibitor is a mixed-type inhibitor. At 303 K, a maximum degree of protection

of 91.70% was achieved for the chitosan- and thiourea-based inhibitor at a concentration of 200 mg/L.

Conclusion:

Chitosan- and thiourea-based carbon dots were synthesized, and the optimal conditions for their synthesis were established. The anti-corrosion inhibition properties of the obtained carbon dots were also determined via the gravimetric method. In this case, gravimetric studies were carried out at various temperatures and various concentrations. The best result showed a degree of protection of 91.70% at 30 °C and 200 mg/L. In conclusion, it can be said that the obtained carbon dots are readily soluble in water, biocompatible, non-toxic, and exhibit good inhibition properties.

References

He, H., et al. (2025). *Research progress of carbon dots as novel corrosion inhibitors*. Journal of Molecular Structure, 2025. – 1334. – 141894 p.

Yan, H., et al. (2024). *Synergistic mechanism of ternary green corrosion inhibitors for N80 steel in 20 wt% HCl solution: Encapsulation and transportation of vanillin through micelles formed by ionic liquids*. Corrosion Science, 2024. – 227. – 111750 p.

Iravani, D., et al. (2024). *Fabrication of novel Arabic gum-grafted-polyurethanes as eco-friendly corrosion inhibitors for carbon steel in sour environments: Surface analysis and inhibition mechanism*. Corrosion Science, 2024. – 246. – 112712 p.

Tang, M., et al. (2026). *Intensive analysis of anti-corrosion properties of cold rolled steel in trichloroacetic acid solution by camellia oleifera shells derived carbon dots*. Journal of Materials Science & Technology, 2026. – 247. – P. 201–213.

Tang, Y., et al. (2024). *Carbon dot aggregates: A new strategy to promote corrosion inhibition performance of carbon dots*. Journal of Materials Research and Technology, 2024. – 33. – P. 1479–1493.

Wang, Q., et al. (2024). *Corrosion inhibition performance of protein derived carbon quantum dots as corrosion inhibitors on low carbon steel in sulfuric acid solution*. Microchemical Journal, 2024. – 207. – 11957 p.

Islami, L.A. and Anawati A. (2025). *Investigating corrosion inhibition of aluminum alloy by green inhibitor propolis in 3.5% NaCl solution*. Corrosion Communications, 2025.

He, C., et al. (2024). *Development of high-dispersion CLDH/carbon dot composites to boost chloride binding of cement*. Cement and Concrete Composites, 2024. – 152. – 105669 p.

Lv, Y., et al. (2023). *Constructing the interface of g-C3N4/epoxy composites using carbon quantum dots to achieve self-repairing, early corrosion monitoring and superior anti-corrosion performance*. Corrosion Science, 2023. – 225. – 111601 p.

Ren, S., et al. (2022). *Comparative study on corrosion inhibition of N doped and N, S codoped carbon dots for carbon steel in strong acidic solution*. Journal of colloid and interface science, – 628. – P. 384–397.

de Souza, F.S. and Spinelli A. (2009). *Caffeic acid as a green corrosion inhibitor for mild steel*. Corrosion science, – 51(3). – P. 642–649.

submitted 12.08.2026;
accepted for publication 26.08.2026;
published 31.08.2026
© Yakhshinorov H., Kuronboev D., Eshmamatova N., Berdimurodov E., Akbarov Kh.
Contact: husanyakhshinorov@gmail.com

Austrian Journal of Technical
and Natural Sciences, 2026 No 7–8
ISSN 2310-5607

PREMIER Publishing
ppublishing.org

Section 2. Computer science

DOI:10.29013/AJT-26-7.8-58-66

CC BY

TEST AUTOMATION IN IOS DEVELOPMENT: IMPLEMENTATION PRACTICES AND THEIR IMPACT ON PRODUCTION RELEASE STABILITY

Daniil Nuzhdin [1]

[1] Lomonosov Moscow State University, Moscow, Russia

Cite: *Nuzhdin D. (2026). Test automation in iOS development: implementation practices and their impact on production release stability. Austrian Journal of Technical and Natural Sciences 2026, No 7–8.* https://doi.org/10.29013/AJT-26-7.8-58-66

Abstract

The article examines current approaches to test automation in iOS development and their influence on production release stability. It is shown that automation extends beyond an auxiliary QA practice and becomes an element of a team's engineering maturity, affecting delivery predictability, release speed, and the reduction of regression risks. The study analyzes the levels of automated testing, criteria for tool selection, the integration of checks into the CI/CD pipeline, and the use of automation as a mechanism for release admission. Based on industry benchmarks and engineering cases, it is argued that the greatest effect is achieved through the systematic integration of automated tests into the release process and the evaluation of their effectiveness through post-release quality metrics.

Keywords: *test automation, iOS development, CI/CD, production releases, application stability, mobile testing, engineering maturity*

Introduction

The development of mobile applications for the iOS ecosystem imposes high requirements on software quality, release cycle stability, and the predictability of application behavior in the production environment. The increasing complexity of mobile solution architectures, the growing number of integrations, the higher frequency of updates, and rising user expectations make it insufficient to rely exclusively on manual verification procedures. Under these conditions, test automation becomes not an auxiliary but a system-forming element of the engineering process, making it possible to detect defects at early stages of development, ensure the reproducibility of checks, and maintain application stability under continuous change. This approach is of particular importance in iOS development, where requirements for performance, interface consistency, and the reliability of interaction with platform components directly affect user experience and the quality of production releases.

The relevance of the study is determined by the need for a systematic analysis of automated testing implementation practices throughout the lifecycle of an iOS application and by the need to assess their influence on the stability of the release process. Despite the widespread adoption of automation tools, their effective use requires a well-grounded selection of testing levels, an appropriate choice of frameworks, integration into CI/CD pipelines, and consideration of the organizational characteristics of the development team. The aim of the article is to analyze current approaches to test automation in iOS development, identify practices of its implementation at different stages of the application lifecycle, and determine the impact of automated testing on release speed, defect reduction, and the stability of production releases.

Test automation as an indicator of engineering maturity in iOS development teams

At the current stage of iOS development, test automation should be regarded not as a local quality control tool, but as one of the key indicators of a team's engineering maturity (Singh & Jain, 2025). This is driven not only by the growing complexity of mobile application architectures, but also by the scale of the iOS ecosystem itself. According to the latest Analysis Group study supported by Apple, in 2024 the App Store ecosystem generated approximately $1,295 billion in global billings and sales, while App Store applications were visited by more than 813 million users per week on average (fig. 1).

Figure 1. *Estimated billings and sales facilitated by the App Store ecosystem by app category, 2019 to 2024, billion dollars (Burley & Fradkin, 2025)*

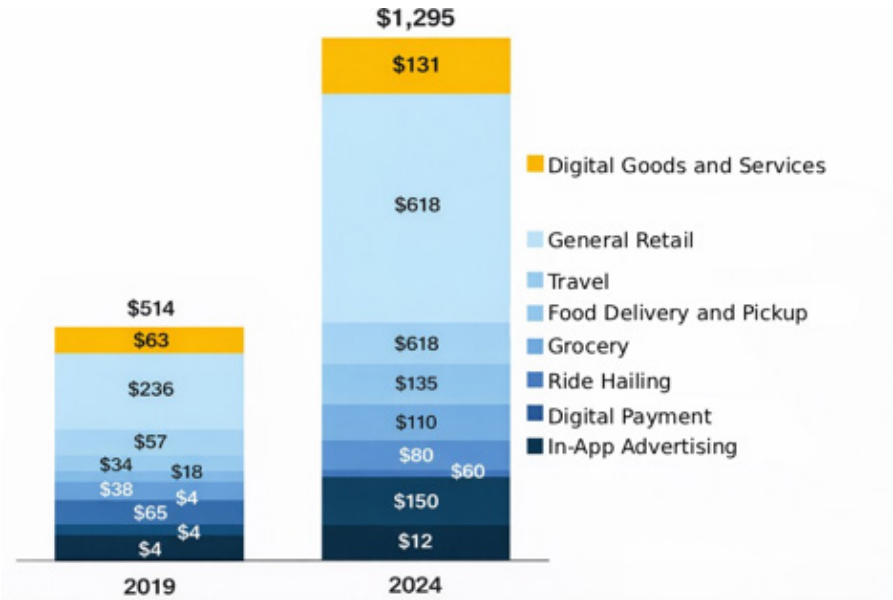

In such an environment, even isolated regressions reaching production carry substantial operational and reputational costs, since release quality affects not only user satisfaction, but also a product's competitiveness in a highly saturated digital market.

From an engineering perspective, iOS team maturity is reflected in the ability to transform testing from a final verification stage into a **continuous mechanism for validating changes.** According to the modern DORA methodology, there is an evident correlation between the speed and stability of software delivery performance and certain throughput and stability measures such as lead time for change, deployment frequency, time to restore service, change fail rate, and deployment rework rate. More importantly, DORA has established that speed and stability need not necessarily be incompatible. In iOS development, this means that automated unit, integration, UI, and performance tests must be embedded into the release pipeline to increase delivery frequency while reducing the risk of failed deployments (Harvey, 2026).

The **Mobile App Stability Outlook 2025 report** can be used as an empirical benchmark for assessing mobile release stability requirements. The study analyzed data from mobile applications that used the Instabug platform throughout 2024 to monitor stability and user experience quality. Its key metrics included crash-free sessions as well as additional reliability indicators such as ANR, OOM, app hangs, and forced restarts. This approach makes it possible to interpret stability not as an abstract quality attribute, but as a measurable operational indicator directly linked to engineering maturity and a team's ability to keep production releases within a competitive stability standard (table 1).

Table 1. *Benchmark indicators of mobile application stability based on the Mobile App Stability Outlook 2025 report (Luciq, 2025)*

Metric	Value	Analytical relevance in the context of the article
Median crash-free sessions rate	99.95%	Baseline benchmark for acceptable mobile app stability.
75th percentile crash-free sessions rate	99.99%	Benchmark of high-performing mobile teams.
Median iOS crash-free sessions rate	99.91%	Indicates a high stability standard for iOS release quality.
Median Android crash-free sessions rate	99.80%	Provides a comparative benchmark showing lower median stability than iOS.

The benchmark data show that mobile release stability has become a measurable engineering target rather than a purely qualitative characteristic. For iOS teams, maintaining crash-free session rates close to the upper benchmark range can be treated as an indicator of a mature test automation strategy and a reliable release process. In this context, automated testing should be viewed not only as a verification tool, but also as a practical mechanism for achieving and sustaining competitive production stability.

Apple's tooling further reinforces this logic. **Xcode Cloud** includes built-in CI/CD capabilities for Apple development that allow for parallel automated test runs, instant feedback on each commit, and automatic aggregation of build, test, and crash reporting information in Xcode. On the other hand, Swift Testing in Xcode 16 adds support for parameterized tests, automatic parallelization of tests, and interoperability with XCTest. This makes modernizing the testing process step by step much more feasible. Consequently, mature organizations will be able to create a continuous validation process where lightweight checks will be validated instantly, whereas more resource-intensive scenarios will be executed in a CI/CD pipeline.

Importantly, the expansion of automation does not necessarily slow mobile delivery, even as the number of quality gates increases. According to **the report Bitrise Mobile Insights 2025**, the level of complexity in mobile CI pipelines went up by 23%, but at the same time, the best teams have reduced build times by 28% in the last 3.5 years on the basis of analysis of over 10 million builds. In addition, in another report released in March 2026, which was based on an analysis of tens of millions of builds done from 2022 to 2025, the authors suggested that teams had been able to introduce additional steps into the build process aimed at testing, scanning, and verifying code-signing without any reduction of speed. In this regard, it can be stated that the maturity of iOS engineering is more defined by its automated delivery pipeline than by the number of performed tests since it will reduce the duration of bug fixing and recovery from failed builds while maintaining the production stability.

In other words, the automation of iOS testing is not only a technical approach but also a critical factor of engineering maturity that plays an important role beyond just finding defects.

Multi-level organization of automated testing in iOS development

The effectiveness of automated testing in iOS development is determined not only by the set of tools used, but also by how testing activities are distributed across levels and integrated into the release pipeline. In practice, this requires a clear distinction between the functions of unit, integration, UI, performance, and pre-release testing, since each level addresses a specific class of risks and plays a separate role in ensuring application stability (table 2).

Table 2. *Levels of automated testing in iOS development and their functional role (Sharma, 2025; Afrihyia et al., 2022)*

Testing level	Primary purpose	Typical objects of verification	Role in the release pipeline
Unit testing	Verification of business logic correctness and local computations.	Models, services, error handling, data transformation.	Provides the fastest feedback at the code level.
Integration testing	Verification of interactions between application components.	Network adapters, persistence layer, service abstractions, inter-module connections.	Helps identify integration errors before they reach the user-facing layer.
UI testing	Validation of user scenarios and navigation flows.	Screens, transitions, forms, system interruptions, interface elements.	Confirms the correctness of critical user journeys.
Performance testing	Assessment of execution performance and runtime stability.	Response time, resource usage, launch speed, behavior under load.	Reduces the risk of user experience degradation after release.
Pre-release beta validation	Verification of build behavior under conditions close to real use.	TestFlight builds, real devices, network scenarios, rare configurations.	Complements the CI/CD pipeline and reduces the risk of production defects.

The presented structure shows that automated testing in iOS development should be understood as a multi-level system of engineering control rather than as a set of isolated checks. Its maturity is determined by the team's ability to distribute test scenarios rationally across levels, combine fast feedback-oriented checks with more expensive user-facing tests, and complement the server-side CI/CD pipeline with pre-release validation on real configurations. It is this organization that makes it possible to maintain delivery speed, reduce the probability of regressions, and ensure the stability of production releases.

Within this multi-level structure, performance testing requires separate attention because performance risks in iOS applications are not limited to response time and often appear only at runtime, under realistic interaction patterns and device constraints. For iOS teams, performance testing should go beyond a general check of response time. The problems that most often affect a release are usually more specific: slow cold starts, delayed first-screen rendering, dropped frames while scrolling collection views, unexpected main-thread work, memory growth after repeated user flows, leaks, out-of-memory crashes, app hangs, and excessive energy consumption. These risks become particularly noticeable in screens with large lists, images, animations, media processing, maps, or a mixed SwiftUI and UIKit hierarchy.

In practice, an effective testing setup can combine XCTest performance measurements, Instruments, MetricKit, Xcode Organizer, and production crash or hang reports. This approach helps teams detect not only functional failures, but also performance regressions that make the application feel slower or less stable even when all user scenarios still pass. Therefore, the selection of testing tools should be connected not only with the type of test being implemented, but also with the specific risk that each level is expected to control.

In actual iOS app development, the choice of testing tools is determined not only by technical preferences, but also by the trade-off between execution speed, maintenance costs, integration with the iOS ecosystem, and the risks that need to be mitigated. Usually, XCTest and Swift Testing are used in situations where developers need fast, deep-level integration testing, while XCUITest works better in cases of testing important user interactions from an interface perspective. It is equally important to pay attention to how frequently the tested level will change, how sensitive testing will be to UI instabilities, and what maintenance costs will be associated with maintaining test suites. Consequently, good automation practice in iOS does not involve using one framework, but rather aligning them with their architectural purpose within the testing hierarchy.

However, the effectiveness of this testing hierarchy depends not only on the selected tools, but also on the architectural testability of the application. Testability starts with architecture rather than with the testing framework itself. MVVM, VIPER, TCA, and Clean Architecture are useful only when they actually move state, decisions, navigation, and side effects out of UIViewController and SwiftUI View. If a view controller contains validation rules, networking decisions, analytics logic, and navigation branching, automated tests become slow and fragile because the test has to deal with lifecycle, rendering, and platform behavior before it can check the business rule. When the same logic is placed in a view model, interactor, reducer, use case, or domain service, it can be tested quickly and deterministically without launching the app.

The dependency injection technique allows for making this separation practical. Network clients, storage, analytics, feature flags, authorization state, clock, scheduler, and configuration providers should be injected into classes through protocols or abstractions so that they can be substituted during testing. Coordinators and routers can also be tested independently from the full user interface flow: it becomes possible to verify which route was called, which screen should be opened, or which navigation command was created. For async/await, Combine, and Observation-based code, the important part is to control timing, cancellation, emitted values, and state transitions instead of relying on arbitrary waits. The same principle applies to mocks for network, persistence, and analytics: they should live on stable boundaries and be reviewed when backend contracts change. A modular project structure helps here as well, because domain and service modules can have small, fast test targets, while UIKit, SwiftUI, and full application targets are left for fewer, higher-level checks.

Practices for implementing test automation and their impact on production release stability

The practical impact of automation on production release stability is especially evident when **pre-release checks that were previously performed manually are automated** (Mulla, 2024). A representative example is **GetYourGuide**, where the phased introduction of automated release checks based on XCUITest and KIF, their integration into CI, and their scaling across mobile teams made it possible to substantially reduce the volume of manual pre-release work and shorten the release window (table 3).

Table 3. *Quantitative results of implementing automated release testing in GetYourGuide's mobile development process (Oliveira, 2024)*

Metric	Before automation	After automation	Analytical relevance in the context of the article
Number of manual release tests	46	4	Shows that automation enabled most release-critical checks to be transferred from manual execution to a reproducible automated workflow.

Metric	Before automation	After automation	Analytical relevance in the context of the article
Number of engineers involved in manual pre-release validation	7	4	Reflects reduced labor intensity at the final delivery stage and lower dependence on manual release coordination.
Share of automated release tests	0%	about 50% by early 2022	Characterizes the phased nature of implementation and shows that even partial automation can generate a measurable operational effect.
Interval from code freeze to release	about 7 days	about 2 days	Demonstrates the reduction of the most vulnerable pre-release period, where delays and regression risks typically accumulate.
Maximum time from code submission to user availability	up to 3 weeks	significantly reduced	Confirms that automation affects not only local testing procedures but also the overall predictability of mobile delivery.

The presented data show that the effect of automation in mobile development is determined not only by the acceleration of individual testing operations, but also by the restructuring of the entire pre-release workflow. A reduction in the number of manual release checks, a shorter interval between code freeze and release, and a lower workload on engineers help decrease the probability of defect accumulation at the final stage and improve the stability of the production release. In this sense, automation acts not merely as a means of speeding up testing, but as a tool for reducing release risks and increasing the controllability of delivery quality.

A second important practice is the **transformation of automated tests from a supporting verification mechanism into a formal release admission criterion**. For example, Spotify's mobile release process operates on a weekly cadence, but a build does not move forward until all commits in the release branch are included in the current build, pass automated tests, and remain within predefined crash-rate and other quality thresholds. Rollout is then performed in two phases: first to 1% of users and, if no negative signals appear, to 100% the following day. With only 3–5 release-blocking bugs typically identified per release and fixed before publication, this case shows that automation can function not only as a development accelerator, but as a core element of release stabilization through the integration of automated tests, operational metrics, and phased deployment.

A third important practice is the **systematic detection and management of flaky tests as a prerequisite for stable releases**. Uber's engineering experience shows that this problem becomes critical at scale: its CI infrastructure validates more than 2,500 code changes per day and runs over 10,000 tests per diff on average. After introducing a centralized flaky-test management system, Uber reported the steady detection of about 1,000 flaky tests out of 600,000 in the Go monorepo and about 1,000 out of 350,000 in Java, together with improved CI reliability and a substantial reduction in retries. This case demonstrates that, in mature automation practice, production stability depends not only on functional test coverage, but also on the ability to identify unstable tests early, isolate their impact on CI, and enforce accountability for their resolution. In addition, recent studies indicate that the automation of testing and debugging tasks is increasingly supported by intelligent tools, including large language models, which may further expand the capabilities of modern software delivery environments (Mozharovskii et al., 2024).

From an operational perspective, the value of test automation is fully realized only when it is linked to post-release quality metrics. In iOS teams, this means that the effectiveness of automation should be assessed not only through coverage or CI

duration, but also through change fail rate, rollback frequency, crash-free session rate, hotfix volume, and the number of production incidents after release. Such a measurement approach makes it possible to evaluate automation not as an internal engineering artifact, but as a delivery mechanism with observable effects on release stability. As a result, the maturity of an automation strategy can be judged by how consistently it improves both pre-release confidence and post-release performance.

Taken together, these cases show that the stabilizing effect of test automation is achieved not through the mere expansion of test coverage, but through its targeted integration into the release path. Automation has the greatest impact when it reduces manual pre-release effort, serves as a formal release gate, and prevents unstable tests from degrading CI reliability. In this sense, production release stability in iOS development depends on how effectively automated testing is embedded into release management, quality control, and the operational discipline of delivery.

A practical rollout of automation should therefore be gradual and tied to actual release risks. At the initial stage, business logic should be covered with fast unit tests, including computations, validation rules, data mapping, state transitions, and error handling. The next stage should focus on critical services and scenarios, such as authorization, payments, caching, data migration, token refresh, offline behavior, and backend error handling. After this foundation has been established, smoke UI tests can be introduced for flows whose failure would block a release, including login, onboarding, purchase, payment, profile management, and the main product scenario. Snapshot or visual regression tests may additionally be used for screens where visual correctness is important and manual verification is repetitive. CI gates should also be introduced gradually: fast checks on each pull request, heavier suites before release or during scheduled nightly runs, and a separate policy for quarantining flaky tests with an assigned owner and a fixed deadline for correction or removal. Finally, the effectiveness of automation should be assessed through product-level outcomes, including crash-free sessions, hotfix frequency, regression bugs, rollback frequency, and production incidents.

Limitations and implementation constraints of test automation in iOS development

Despite the significant practical value of automated testing, its implementation in iOS development is associated with a number of technical and organizational constraints. In practice, the effectiveness of automation depends not only on the choice of tools, but also on the cost of maintaining test suites, the stability of CI infrastructure, the sensitivity of UI scenarios to interface changes, and the availability of engineering resources required to keep the testing pipeline reliable over time. For this reason, the impact of automation on production stability should be assessed with regard not only to its benefits, but also to the limitations that may reduce its operational efficiency (table 4).

Table 4. *Key limitations of automated testing implementation in iOS development (Prodduturi, 2025; Singh, 2025)*

Limitation	Practical manifestation	Potential effect on release stability
High maintenance cost of UI tests	UI scenarios often require frequent updates after interface or navigation changes.	Can reduce the reliability of release checks and increase the cost of sustaining the automation suite.
Flaky test behavior	Unstable results in repeated runs create false positives and reduce trust in CI outcomes.	May delay releases and mask real regressions.

Limitation	Practical manifestation	Potential effect on release stability
Infrastructure dependence	Automated testing in iOS requires stable macOS-based CI environments, device availability, and code-signing consistency.	Failures in infrastructure can affect the reproducibility of release validation.
Uneven test coverage across levels	Teams often automate code-level checks earlier than complex end-to-end or real-device scenarios.	Critical production issues may still escape into release despite high formal test activity.
Resource and expertise requirements	Effective automation requires engineering time, ownership, and continuous monitoring of test quality.	Weak operational discipline reduces the long-term stabilizing effect of automation.

The limitations summarized in table 4 show that the main challenge is not the initial creation of automated tests, but the preservation of their practical value under continuous product change. UI tests may become unstable after interface redesigns, long test suites may slow down CI feedback, and repeated false failures may reduce developers' trust in the pipeline. Test doubles also require regular updating: if backend contracts, feature flags, or analytics requirements change while mocks remain unchanged, tests may continue to pass even when the real application behavior is already incorrect. Flaky tests require explicit ownership; otherwise, they increase retries, create background noise, and obscure real regressions. Another common problem is coverage created for reporting rather than for risk reduction: such tests improve formal metrics but do not protect the scenarios that are most important for users and business continuity. For this reason, mature iOS teams should regularly review their test suites, remove low-value checks, separate slow scenarios from the pull-request pipeline, and keep automation focused on release confidence rather than on formal indicators.

These constraints show that test automation should not be treated as a self-sufficient guarantee of release quality. Its contribution to production stability depends on whether the team is able to maintain test suites, control flaky behavior, support the necessary infrastructure, and align automation depth with the real risk profile of the product. In this sense, the maturity of an iOS automation strategy is determined not only by what is automated, but also by how sustainably the entire verification system can be operated under continuous product change.

Conclusion

The analysis shows that test automation in iOS development should be understood as a systemic engineering practice that affects the entire release lifecycle rather than as a limited QA procedure. Its practical value is determined by the ability to distribute validation across multiple testing levels, integrate checks into CI/CD workflows, reduce manual pre-release effort, and use automation as a release control mechanism. The reviewed cases and benchmarks indicate that automation contributes to production stability not only through earlier defect detection, but also through shorter release windows, more predictable delivery, and a lower probability of critical regressions reaching production.

At the same time, the effectiveness of automation depends not on the formal growth of coverage, but on how precisely testing practices are aligned with product risks, release workflows, and operational quality metrics. The strongest effect is achieved when automation supports release admission decisions, stabilizes CI reliability, and is evaluated through measurable post-release outcomes such as crash-free session rate, rollback frequency, hotfix volume, and production incident count. Therefore, the long-term significance of automated testing in iOS development lies in its ability to balance release velocity with production resilience under conditions of continuous product change.

References

Afrihyia, E., Umana, A. U., Appoh, M., Frempong, D., Akinboboye, O., Okoli, I., Umar, M. O., & Omolayo, O. (2022). Enhancing software reliability through automated testing strategies and frameworks in cross-platform digital application environments. Journal of Frontiers in Multidisciplinary Research, – 3 (2). – P. 517–531. URL: https://doi.org/10.54660/.JFMR.2022.3.1.517–531

Burley, J., & Fradkin, A. (2025). The Global App Store and Its Growth. Apple. [cited: 10.04.2026]. Available from: https://www.apple.com/newsroom/pdfs/2024-Apple-Global-Ecosystem-Report-June2025.pdf

Harvey, N. (2026). DORA's software delivery performance metrics. DORA. [cited: 10.04.2026]. Available from: https://dora.dev/guides/dora-metrics/

Luciq. (2025) Mobile app stability outlook 2025. [cited: 10.04.2026]. Available from: https://www.luciq.ai/mobile-app-stability-outlook-2025

Mozharovskii, E., Aluev, A., Dudak, A., & Ishankhonov, A. (2024). Application of large language models for software testing and debugging automation. Modern Science: Actual Problems of Theory and Practice. Series "Natural and Technical Sciences", 11–2, 103–108. URL: https://doi.org/10.37882/2223–2966.2024.11–2.22

Mulla, F. A. (2024). Modern Mobile Testing Tools: A Comprehensive Guide to Quality Assurance and Automation. International Journal of Scientific Research in Computer Science, Engineering and Information Technology, – 10 (6). – P. 1577–1584. URL: https://doi.org/10.32628/CSEIT241061203

Oliveira, F. (2024). The Long and Winding Road to Short and Smooth Releases. GetYourGuide. [cited: 11.04.2026]. Available from: https://www.getyourguide.careers/posts/the-long-and-winding-road-to-short-and-smooth-releases

Prodduturi, S. M. K. (2025). Efficient Debugging Methods and Tools for iOS Applications Using Xcode. International Journal of Data Science and IoT Management System, – 4 (4). – P. 1–6. URL: https://doi.org/10.64751/ijdim.2025.v4.n4.pp1-6

Sharma, A. (2025). Security Testing in Android and iOS Application Development. Journal of Android, iOS Development and Testing, – 10 (2). – P. 96–109.

Singh, S., & Jain, A. (2025). Automated Testing Strategies for Android and iOS Applications. Journal of Android, iOS Development and Testing, – 10 (2). – P. 55–69.

Singh, V. (2025). Advancements in Software Engineering Practices and Their Influence on Modern Software Testing Methodologies: A Comprehensive Study. Journal of Software Engineering & Software Testing, – 10 (2). – P. 71–83.

submitted 27.06.2026;
accepted for publication 11.07.2026;
published 31.08.2026
© Nuzhdin D.
Contact: daniila.nuzhdin@yandex.ru

Austrian Journal of Technical
and Natural Sciences, 2026 No 7–8
ISSN 2310-5607

PREMIER Publishing
ppublishing.org

Section 3. Food processing industry

DOI:10.29013/AJT-26-7.8-67-70

CC BY

IMPROVEMENT OF SOYBEAN OIL HYDRATION PROCESS

Akhmedov Azimjon Normuminovich [1],
Normurodova Ugiloy Uroz kizi [2]

[1] Doctor of Technical Sciences, Acting Professor of the Department of Food Technology of Products of the Karshi State Technical University, Uzbekistan

[2] Methodologist at the Academic and Methodological Department of Karshi State Technical University, Uzbekistan

Cite: *Akhmedov A.N., Normurodova U.U. (2026). Improvement of Soybean Oil Hydration Process. Austrian Journal of Technical and Natural Sciences 2026, No 7–8.* https://doi.org/10.29013/AJT-26-7.8-67-70

Abstract

This research focuses on optimizing the hydration process of local soybean oil; it demonstrates changes in the levels of hydratable and non-hydratable phospholipids in relation to the amount of water added, noting that the content of hydratable substances decreases exponentially as the level of non-hydratable phospholipids rises. Increasing the temperature of the soybean oil enhances the separation of hydratable phospholipids, with the highest yield of phospholipids observed upon the addition of 4% moisture and the lowest upon the addition of 2% moisture.

Keywords: *Soybean oil, phospholipids, hydratable and non-hydratable (fractions), alkali, water, moisture, acid and peroxide values*

Introduction

Soybean oil is a valuable source of nutrients, such as polyunsaturated fatty acids, vitamins, and antioxidants. Its composition can be modified during the hydration process, in which the addition of water to the oil causes the separation of its phospholipids – yielding a product with high physiological value.

Phospholipids are complex lipids – biologically active substances containing fatty acids, a phosphoric acid residue, and, in most cases, an additional nitrogen-containing group (Bokovikova T.N., 2000). Lecithin (specifically, phosphatidylcholine) constitutes the bulk of the phospholipids extracted from soybean oil; this product exhibits excellent surface activity and serves as a valuable source of emulsifiers (Kobzar M.V., 2005). Under traditional processing methods in Uzbekistan, soybean oil undergoes only partial hydration – or sometimes no hydration at all – resulting in the loss of this valuable raw material along with the soapstock during subsequent refining

stages (Azimov Yu.Kh., Abdurakhimov S. A., Akhmedov A. N., 2020).

R. O'Brien, A. Kaufman, B. N. Markman, A. G. Sergeev, A. P. Nechaeva, N. S. Kornena, O. S. Abdurakhimov, A. I. Isabaev, A. N. Akhmedov, D. S. Salikhanova, A. T. Ruzibaev, D. S. Sagdullaeva, Yu. X. Azimov and others have conducted scientific and practical work. For this study, unrefined soybean oil obtained via pressing and extraction methods was selected. First and foremost, before hydrating the soybean oil, it is necessary to determine its physicochemical parameters.

The purpose of the work: The objective is to study and draw conclusions regarding the effect of moisture content on the separation of phospholipids from crude soybean oil obtained via pressing and extraction methods.

Materials and methods

Determination of the acid value of unrefined soybean oil. To determine the acid value of soybean oil, 3–5 g of the oil under study and 50 ml of a neutralized alcohol-ether mixture (in a 1:2 ratio – specifically, 96% ethyl alcohol and diethyl ether) are placed into a conical flask using a technical balance.

To prepare the neutralized alcohol-ether solution mixture, add a few drops of a 1% phenolphthalein indicator solution and titrate with an aqueous 0.1 N KOH solution for 30 seconds until the light red color disappears. The titration process is carried out under constant stirring. A microburette is suitable for determining the acid value of refined and bleached soybean oil.

The acid value is determined using the following formula (Kadyrov Yu. 2005):

$$A.V. = \frac{5{,}611 \cdot V \cdot K}{M}$$

where: V is the volume of 0.1 N KOH (in milliliters) used for titration;

K is the correction factor for the titer of the alkaline solution;

M is the mass of the oil being analyzed (in grams).

The final result is the arithmetic mean of two parallel determinations.

Determination of phospholipid composition

Thin-layer chromatography was used to study the phospholipid composition. Sorbfil plates were used for the analysis. The concentration of the standard sample was 5 mg/mL, and the plates were placed in a chamber saturated with eluent vapors. When the solvent front reached a point 1 cm from the top, the plates were removed and dried. A 5% alcoholic solution of phosphomolybdic acid and a 1% solution of ninhydrin were used for derivatization. A mixture of chloroform, methanol, acetic acid, and water in a 50:25:8:4 ratio served as the mobile phase. The results obtained were analyzed by comparison with data reported in the literature.

Results and Discussion

Unrefined soybean oil obtained via pressing and extraction methods was selected for the study. Before hydrating the soybean oil, it is essential to determine its physicochemical parameters. Table 3.5 below presents the physicochemical parameters of the unrefined soybean oil obtained through pressing and extraction.

Table 1. *Physicochemical characteristics of unrefined soybean oil obtained by pressing and extraction*

Name of indicators	Indications for the use of unrefined soybean oil	
	Obtained by pressing	Obtained by extraction
Acid value, mg KOH/g	2,8	4,3
Content of non-fat substances, %	0,08	0,12
Phospholipid content (calculated as stearo-oleo-lecithin), %	1,8	2,4
Moisture and volatile matter content, %	0,1	0,1
Peroxide value, mmol active oxygen/kg	4,8	5,3

As shown in Table 1 above, solvent-extracted unrefined soybean oil contains 0.6% more phospholipids (calculated as stearo-oleo-lecithin) than oil obtained by pressing, resulting in a higher yield of the extracted product. The primary reason for this is that the solvent dissolves not only the oil but also related components, including phospholipids.

Subsequently, unrefined soybean oil obtained via pressing and extraction was hydrated using a traditional method under laboratory conditions. The release of phospholipids was investigated by adding varying amounts of water to the soybean oil. The results obtained are presented in Table 2.

Table 2. *Effect of water content on phospholipid release in unrefined soybean oil obtained by pressing and extraction*

Amount of water supplied relative to the mass of oil, %	Hydration precipitates			
	amount relative to initial oil mass, %	moisture content, %	neutral oil content	phospholipid content (calculated as stearo-oleo-lecithin), %
		Press oil		
0,5	1,51	30,2	32,4	36,6
1	2,47	36,5	34,8	28,0
2	4,31	41,4	38,2	19,5
3	5,71	46,5	36,6	16,3
4	6,98	49,1	36,4	13,7
		Extraction oil		
0,5	1,58	28,7	31,8	38,7
1	2,61	34,3	33,4	31,6
2	4,59	38,6	37,4	23,1
3	6,11	43,1	35,5	20,8
4	7,45	45,7	36,1	17,4

As shown in Table 2 above, increasing the amount of water added to unrefined soybean oil reduces the mass fraction of phosphorus-containing substances in the resulting hydrated sludge. This increases the moisture content of the obtained phospholipid sludge and raises the energy consumption required for its subsequent processing. An analysis of the results indicates that adding 3% water (relative to the mass of the unrefined soybean oil) has a positive effect on the release of hydratable phospholipids; at higher water volumes, the yield decreases. Therefore, the optimal water addition level for this study can be established at 3%.

Conclusions

During the hydration of unrefined soybean oil obtained via pressing and extraction, the phospholipid content in the extraction-derived oil is high, and its hydration efficiency exceeds that of the pressed oil. This further confirms the high phospholipid content in oil obtained by the extraction method.

The results presented above indicate that the phospholipid sludge has a high oil and moisture content, yet a low phospholipid content, suggesting a need to improve the hydration process. Ultrasound has recently been employed in various industrial processes; its effectiveness could be evaluated by applying this method to the aforementioned process and conducting further research.

References

Bokovikova T. N. Chemical composition, structure, and properties of phospholipids from sunflower seeds of modern varieties and development of a technology for their extraction using chemical polarization / Dissertation... Doctor of Technical Sciences: – Krasnodar, 2000. – 248 p.

Kobzar M. V. Technology for Producing Highly Concentrated Sunflower Oil Phospholipids: Abstract of Dissertation... Candidate of Technical Sciences. – Kharkiv, 2005. – 23 p.

Azimov Yu.Kh., Abdurakhimov S. A., Akhmedov A. N. Improving the efficiency of the hydration process for pre-press oil obtained from local soybean varieties. *Universum: Technical Sciences*. Issue: 2(71). February 2020. – Moscow. – P. 28–31.

Kadyrov Yu. Laboratory training in oil processing technology. – Tashkent: Chulpan, 2005. – 119 p.

submitted 19.07.2026;
accepted for publication 02.08.2026;
published 31.08.2026
© Akhmedov A. N., Normurodova U. U.
Contact: a.ahmedov80@mail.ru

Austrian Journal of Technical
and Natural Sciences, 2026 No 7–8
ISSN 2310-5607

PREMIER Publishing
ppublishing.org

DOI:10.29013/AJT-26-7.8-71-79

ASSESSMENT AND IMPROVEMENT OF OILSEED STORAGE TECHNOLOGY UNDER THE CONDITIONS OF THE SYRDARYA REGION

Karim K. Sattarov [1], Gulnoza K. Tukhtamishova [1], Khilola Sh. Zhuraeva [1]

[1] Gulistan State University, Uzbekistan

Cite: *Sattarov K.K., Tukhtamishova G.K., ZhuraevaKh.Sh. (2026). Assessment and Improvement of Oilseed Storage Technology Under the Conditions of The Syrdarya Region. Austrian Journal of Technical and Natural Sciences 2026, No 7–8.* https://doi.org/10.29013/AJT-26-7.8-71-79

Abstract

Storage of oilseed raw materials is a critical post-harvest operation because moisture content, temperature, aeration, microbial activity, and storage duration collectively determine the rate of quality deterioration. In the present study, an analytical assessment was conducted of the factors affecting the storage of sunflower seeds (*Helianthus annuus* L.) and cottonseed (*Gossypium hirsutum* L.), which are of practical importance to the vegetable oil industry of the Syrdarya Region, Uzbekistan. The findings of the initial study were compared with contemporary published data on moisture content, temperature conditions, storage duration, and quality indicators. In the initial study, an increased risk of quality deterioration was observed at moisture contents above 10–12% for sunflower seeds and above 9–10% for cottonseed, while a temperature range of 5–15 °C was considered rational for slowing biochemical processes. Under favorable storage conditions, the main quality characteristics were reported to remain stable for approximately 6–8 months, whereas under unfavorable conditions, deterioration could occur within 2–3 months. These values should be regarded only as indicative ranges for the conditions investigated. Comparison with current literature confirms the key role of moisture and temperature control, as well as the need to consider relative humidity, aeration, and microbiological risks. An integrated technological scheme is proposed, including lot classification, cleaning, moisture adjustment, cooling, aeration, controlled storage, and periodic laboratory monitoring. The quantitative data presented in Tables 6 and 7 were obtained from published studies and do not represent original measurements by the authors of the present study. The main limitation is the absence of a complete primary dataset from the initial investigation, including detailed information on replication and statistical analysis. Therefore, final validation of the proposed storage conditions requires a specifically designed experiment under the environmental and technological conditions of the Syrdarya Region.

Keywords: *sunflower seeds; cottonseed; oilseed crops; storage; moisture content; temperature; relative humidity; acid value; peroxide value; aeration; seed quality; Syrdarya Region*

Introduction

Oilseed crops are biologically active raw materials whose quality changes continuously between harvest and processing. Sunflower seeds and cottonseed are of considerable practical importance in Uzbekistan because they are used for the production of vegetable oil and valuable by-products. During storage, seeds continue to respire and exchange moisture with the surrounding environment. The accumulation of heat and moisture within the stored seed mass can intensify respiration, microbial activity, enzymatic reactions, and lipid deterioration, ultimately reducing the technological suitability of the raw material.

Moisture content is one of the principal factors determining the storage stability of oilseed raw materials. According to FAO recommendations for storage under hot climatic conditions, a moisture content of approximately 9% is considered an indicative level for long-term storage of sunflower seeds [6]. Recent studies on cottonseed have demonstrated a pronounced dependence of storage stability on moisture content and storage system. In a 12-month study, samples with higher initial moisture content exhibited substantially greater quality deterioration, whereas storage at lower moisture content under hermetic conditions provided considerably better preservation (Fatima, F., Khalid, E., Afzal, I., et al., 2025).

Temperature acts in interaction with moisture content and environmental conditions. Controlled studies of sunflower seeds have shown that elevated temperature and exposure to light accelerate changes in acid and peroxide values and promote oxidative processes (Xu, W., Yao, J., Yi, Y., Wang, H.-X., Wang, L.-M., 2019). Studies conducted under cyclic variations in temperature and relative humidity have also demonstrated that realistic fluctuations in storage conditions can result in different patterns of changes in moisture content and peroxide value compared with constant storage conditions (Liu, J., Yang, Y., Xu, Z., Wang, Q., Liu, B., Wu, Y., 2022).

Modern approaches to quality control increasingly incorporate rapid, non-destructive technologies. In particular, hyperspectral imaging combined with chemometric analysis has been used to assess the viability and moisture content of sunflower seeds, whereas Raman microspectroscopy is considered a promising method for the rapid assessment of sunflower seed freshness and viability (Huang, P., Yuan, J., Yang, P., Xiao, F., Zhao, Y., 2024; Ma, J., Yang, L., Gao, W., Chen, J., Li, J., Jin, L., Hou, R., 2024).

The aim of the present study was to analytically assess the principal factors affecting the storage of sunflower seeds and cottonseed, compare the findings of the initial investigation with contemporary scientific evidence, and develop an integrated technological scheme for maintaining the quality of oilseed raw materials under the conditions of the Syrdarya Region, Uzbekistan.

Materials and Methods

The study was based on materials from the initial investigation conducted in the laboratory of the Scientific Center of the Department of Food Technologies at Gulistan State University, together with data obtained from published scientific sources. The objects of the initial investigation were sunflower seeds and cottonseed of practical importance to the vegetable oil industry of the Syrdarya Region, Uzbekistan. The initial study assessed moisture content, temperature, storage duration, organoleptic condition, and physicochemical changes associated with biochemical processes during storage.

The complete primary dataset, information on the number of independent replicates, sample sizes, analytical procedures, and statistical methods were not available in the source materials. Therefore, missing primary data were neither reconstructed nor presented as results of an original experiment in the present study.

For subsequent local validation, independent measurements of moisture content, seed-mass temperature, ambient relative humidity, acid value, peroxide value, oil content, germination/viability, and the degree of fungal contamination should be performed at predetermined sampling intervals.

The moisture-content ranges of 10–12% for sunflower seeds and 9–10% for cottonseed, the temperature range of 5–15 °C, and the reported periods of quality preservation of 6–8 months under favorable conditions and 2–3 months under unfavorable conditions were retained from the initial study.

These values are considered indicative only and should not be interpreted as universally applicable storage standards.

Table 1. *Key Factors Determining the Storage Stability of Oilseed Raw Materials*

Factor	Adverse Change	Underlying Mechanism	Technological Measure
Moisture Content	Increase or Fluctuations	Increased respiration, microbial activity, and hydrolytic processes	Drying and regular moisture monitoring
Temperature	Heat accumulation or temperature increase	Increased respiration and oxidative processes	Cooling and aeration
Relative Humidity	High or fluctuating relative humidity	Moisture exchange and increased risk of fungal growth	Environmental condition control
Impurities and Damaged Seeds	High Content	Localized heating and microbial growth	Cleaning and grading
Storage Duration	Prolonged storage under unfavorable conditions	Cumulative quality deterioration	Periodic quality monitoring

Results and Discussion

The initial study associated moisture contents above 10–12% in sunflower seeds and 9–10% in cottonseed with increased respiration, microbial activity, and a higher risk of self-heating. These findings are generally consistent with international scientific evidence. According to FAO recommendations, a moisture content of approximately 9% is considered an indicative level for the long-term storage of sunflower seeds under hot climatic conditions (De Lucia, M., Assennato, D., 1994). In a recent study of cottonseed, moisture contents of 6, 8, 10, and 12% were evaluated over a 12-month storage period. The results showed that quality deterioration occurred substantially more rapidly at higher moisture contents, whereas storage at 6% moisture under hermetic conditions provided the best preservation among the conditions investigated (Fatima, F., Khalid, E., Afzal, I., et al., 2025). These findings indicate that moisture content should not be controlled as a single universal threshold, but rather as a range that interacts with temperature, relative humidity, packaging or storage system, and the intended storage duration. For long-term cottonseed storage, the results of recent international studies obtained at lower moisture contents indicate the need for additional local experimental validation before applying the broader 9–10% range identified in the initial study as a zone of increased risk.

Thus, under the conditions of the Syrdarya Region, it is advisable to simultaneously monitor seed moisture content, seed-mass temperature, and ambient relative humidity, because their combined effects determine the stability of the raw material during storage. This approach is consistent with the initial study, in which moisture content was identified as one of the key factors determining the storage stability of oilseed raw materials.

Table 2. *Comparative Interpretation of Moisture-Related Storage Conditions*

Oilseeds	Conditions	Main Outcome	Practical Significance
Sunflower	Long-term storage under hot climatic conditions	Indicative moisture content: ≈9%	Moisture control is a key condition for maintaining storage stability.

Oilseeds	Conditions	Main Outcome	Practical Significance
Sunflower	Different temperature, light, and relative humidity conditions	The rate of quality deterioration depends on the combined effects of storage conditions.	Moisture and temperature must be controlled.
Cottonseed	Moisture contents of 6, 8, 10, and 12%; 12 months of storage	Higher moisture content accelerated quality deterioration.	Dry and protected storage conditions should be prioritized.
Sunflower kernels	Increase in relative humidity	Higher relative humidity increased the risk of microbial contamination.	It is necessary to control not only seed moisture content but also ambient relative humidity.

Organoleptic assessment can serve as a rapid method for detecting signs of deterioration in the quality of raw materials; however, it should not replace laboratory monitoring. Changes in the odor, color, and overall condition of seeds may indicate the development of undesirable processes, but objective assessment requires additional determination of moisture content, acid value, peroxide value, and other physicochemical parameters.

A recent study of sunflower seed kernels showed that an increase in relative humidity alters the structure of the fungal community and increases the risk of microbial contamination (Liu, J., Yang, Y., Xu, Z., Wang, Q., Liu, B., Wu, Y. 2022). Therefore, during storage, it is necessary to control not only the moisture content of the seeds themselves but also the relative humidity of the air within the storage facility.

In the initial study, a temperature range of 5–15 °C was considered rational, whereas temperatures above 25 °C were considered unfavorable for storage. This conclusion should be regarded as a recommendation applicable to the specific conditions of the study rather than as a universal standard.

Studies on sunflower seed storage have shown that temperature interacts with light exposure and storage duration. Elevated temperature and exposure to light accelerate changes in acid and peroxide values and promote oxidative processes (Xu, W., Yao, J., Yi, Y., Wang, H.-X., Wang, L.-M., 2019).

Temperature and relative humidity fluctuations are also important. Under cyclic changes in these parameters, the dynamics of seed moisture content and peroxide value may differ from those observed under constant storage conditions (Liu, J., Yang, Y., Xu, Z., Wang, Q., Liu, B., Wu, Y., 2022). Therefore, more reliable storage-management principles include preventing heat accumulation within the seed mass and detecting temperature increases at an early stage, rather than relying solely on a nominal average temperature.

Thus, under the storage conditions of the Syrdarya Region, Uzbekistan, continuous monitoring of temperature, seed moisture content, and relative humidity should be ensured for sunflower seeds and cottonseed. When a trend toward increasing temperature is detected, cooling and aeration should be promptly implemented.

Table 3. *Interpretation of Temperature Conditions*

Temperature	Interpretation within the Initial Study	Recommended Technological Measures
5–15 °C	Rational range	Preferred where technically feasible
15–25 °C	Increased intensity of biochemical processes	Enhanced temperature monitoring and aeration
>25 °C	Unfavorable conditions	Cooling, aeration, and quality assessment of the raw material

The initial study showed that under favorable storage conditions, the main quality characteristics were maintained for approximately 6–8 months, whereas under unfavorable conditions, quality deterioration could occur within as little as 2–3 months. However, these periods should not be regarded as guaranteed storage periods or universal shelf-life limits. The duration of safe storage depends on the initial quality of the raw material, as well as on the combined effects of time, temperature, and moisture throughout the entire storage period.

According to the initial study, the main indicators of quality deterioration were the development of a musty odor, darkening of the seeds, reduced germination, decreased oil content, and an increase in acid value. Since quantitative primary data were not available in the source materials, these indicators are considered in the present study as descriptive observations from the initial investigation rather than statistically validated results of a new experiment.

It should also be considered that during prolonged storage, primary oxidation products, including peroxides and hydroperoxides, may subsequently decompose to form secondary oxidation products. Therefore, a single measurement of peroxide value is insufficient to fully characterize the kinetics of oxidative processes (Xu, W., Yao, J., Yi, Y., Wang, H.-X., Wang, L.-M., 2019). For a more objective assessment of quality dynamics, periodic measurements of acid value and peroxide value should be conducted throughout the entire storage period.

Table 4. *Recommended Quality Indicators for Validation of the Results*

Indicator	Information Obtained	Priority
Moisture content (%)	Storage stability; risk of microbial activity and increased respiration	Mandatory
Seed-mass temperature (°C)	Risk of heat accumulation and self-heating	Mandatory
Relative humidity (%)	Moisture exchange and risk of fungal growth	Mandatory
Acid value	Degree of hydrolytic deterioration of lipids	Mandatory
Peroxide value	Primary lipid oxidation processes	Mandatory
Oil content (%)	echnological oil yield	High
Seed germination / viability	Physiological quality of seeds	High
Fungal contamination	Degree of microbiological quality deterioration	High

Modern instrumental methods can additionally be applied for the rapid assessment of oilseed raw material quality. In particular, hyperspectral imaging has been shown to enable the assessment of viability and moisture content in sunflower seeds, whereas Raman microspectroscopy can be used to differentiate fresh and aged sunflower seeds (Huang, P., Yuan, J., Yang, P., Xiao, F., Zhao, Y., 2024; Ma, J., Yang, L., Gao, W., Chen, J., Li, J., Jin, L., Hou, R., 2024).

It should be emphasized that these methods are proposed only as promising tools for further improvement of the quality-control system and were not used in the initial experiment.

An integrated technological scheme for the storage of oilseed raw materials is proposed. At the initial stage, incoming raw materials should be classified according to crop type, moisture content, temperature, impurity level, and initial quality.

Following classification, each batch should undergo cleaning and, when necessary, drying to a predetermined target moisture content that has been experimentally validated. Cooling and active aeration should be used to remove accumulated heat and excess moisture.

During storage, individual batches should be stored separately and subjected to periodic monitoring. Monitoring should include assessment of temperature and moisture content, as well as the main quality indicators in accordance with the established monitoring system.

Thus, the proposed technology involves the following sequential operations:

Receiving and classification → Cleaning and grading → Moisture adjustment (drying) → Cooling → Active aeration → Controlled storage → Periodic quality monitoring → Transfer for processing.

The proposed scheme has been developed for the conditions of the Syrdarya Region and is considered a technological framework requiring subsequent quantitative validation under industrial conditions. In the initial study, this integrated approach was proposed for managing the quality of sunflower seed and cottonseed batches during storage.

Table 5. *Integrated Technological Scheme for Improving the Storage of Oilseed Raw Materials*

Stage	Operation	Critical Control Point	Corrective Action
1.	Receiving and classification	Moisture content, temperature, impurity level	Segregation of batches that do not meet established requirements
2.	Cleaning and grading	Content of impurities and damaged seeds	Additional cleaning
3.	Drying / moisture adjustment	Experimentally validated target moisture content	Continued drying
4.	Cooling	Seed-mass temperature	Intensification of cooling and/or aeration
5.	Active aeration	Temperature response and relative humidity	Adjustment of airflow intensity
6.	Controlled storage	Temperature, moisture content, relative humidity	Corrective measures to eliminate detected deviations
7.	Periodic monitoring	Acid value (AV), peroxide value (PV), oil content, organoleptic indicators	Priority routing of the batch for processing
8.	Transfer for processing	Final raw-material quality	Determination of quality class

The proposed system considers storage as a dynamic process rather than an operation conducted at a fixed temperature. A sustained increase in temperature or moisture content should serve as a basis for taking corrective action before visible signs of raw-material deterioration appear. This approach enables the timely detection of unfavorable changes in storage conditions and helps prevent further deterioration of seed quality.

To strengthen the quantitative interpretation, without presenting published data as results of the present study conducted in the Syrdarya Region, selected numerical data from two published studies were incorporated. The cottonseed data were obtained from Fatima et al. (2025), in which cottonseed was stored for 12 months at initial moisture contents of 6, 8, 10, and 12% in hermetic bags. The sunflower seed data were obtained from Premović et al. (2014), in which seeds stored for 0, 6, and 12 months at temperatures below 30 °C under good ventilation were investigated, with acid and peroxide values determined in the seeds and in the cold-pressed oil obtained from them. These data, derived from published literature, are used exclusively for comparative analysis and graphical interpretation; they are not part of the primary experimental dataset of the present study.

Table 6. *Cottonseed Germination after 12 Months of Hermetic Storage, Based on Data from the Published Literature (Fatima et al., 2025)*

Initial Moisture Content (%)	Storage System	Storage Duration (months)	Germination (%)
6	Hermetic bag	12	71,6
8	Hermetic bag	12	42,3
10	Hermetic bag	12	Almost complete loss
12	Hermetic bag	12	Almost complete loss

Figure 1. *Relationship between cottonseed germination and initial moisture content after 12 months of hermetic storage, based on published data from Fatima et al. (2025). For moisture contents of 10% and 12%, the source reports an almost complete loss of germination; therefore, no numerical values for these treatments are interpreted in the graph*

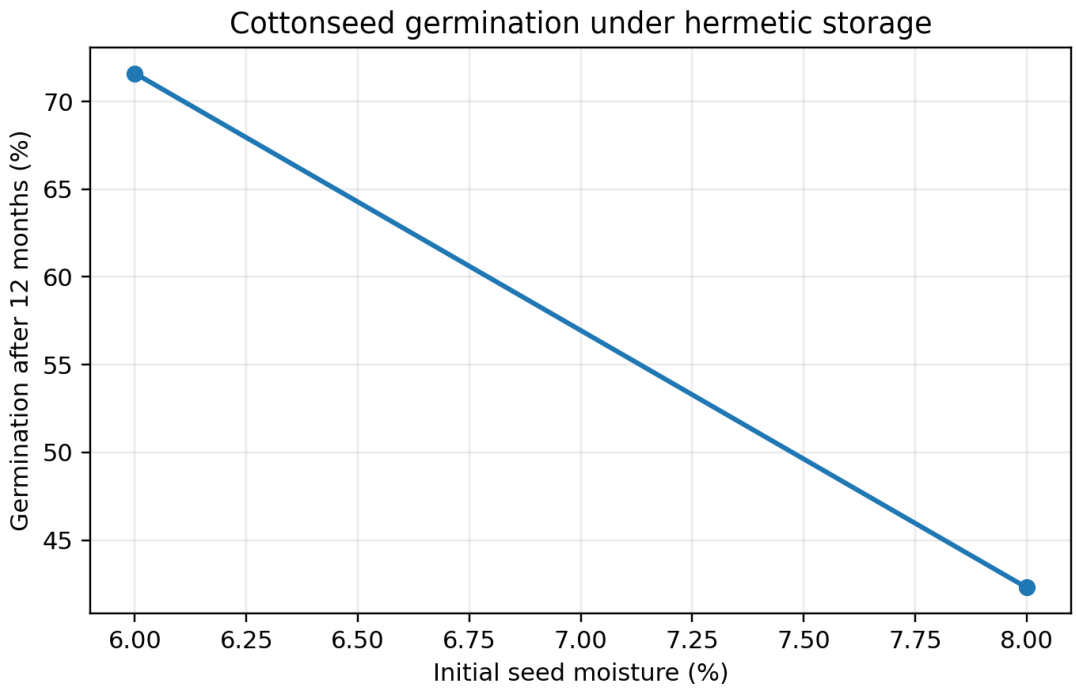

Table 7. *Acid and Peroxide Values of Sunflower Seeds and Cold-Pressed Oil during Storage, Based on Data from the Published Literature (Premović et al., 2014)*

Storage Duration (months)	Acid Value, Seeds (mg KOH/g	Acid Value, Oil (mg KOH/g)	Peroxide Value, Seeds (mmol/kg)	Peroxide Value, Oil (mmol/kg)
0	0,54	0,49	0,27	1,73
6	1,29	0,59	1,00	1,95
12	2,11	1,95	1,40	2,22

Published data on sunflower seeds show a noticeable increase in acid value with increasing storage duration. In oil obtained from fresh seeds, the acid value was 0.49 ± 0.01 mg KOH/g, increasing to 1.95 ± 0.02 mg KOH/g after 12 months of storage. The peroxide value increased from 1.73 ± 0.02 to 2.22 ± 0.07 mmol/kg. The corresponding values for the seeds also increased, although the magnitude of change varied depending on the parameter evaluated.

Figure 2. *Changes in acid value (AV) and peroxide value (PV) during sunflower seed storage based on data from a published literature source. The curves represent published values obtained after 0, 6, and 12 months of storage and do not constitute measurements performed as part of the present study*

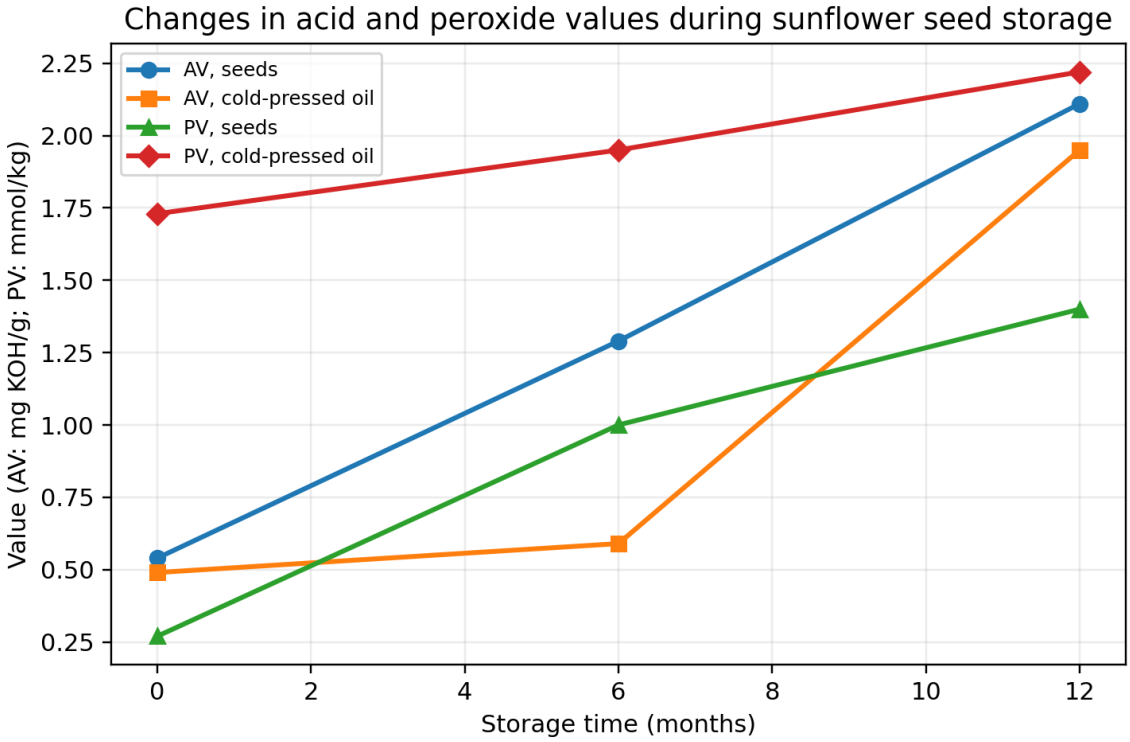

The practical significance of the study lies in the integration of moisture regulation, cooling, aeration, batch classification, and periodic quality control into a unified storage system adapted to the conditions of the Syrdarya Region for sunflower and cotton seeds. Comparison with recent international studies shows that the quality deterioration mechanisms described in the original study are generally consistent with current scientific understanding; however, the specific quantitative limits require experimental validation under local conditions.

The proposed system can serve as a basis for developing a local technological storage protocol and for conducting a subsequent controlled experiment involving the simultaneous determination of moisture content, seed temperature, relative air humidity, acid value, peroxide value, oil content, and seed viability.

Conclusions

The storage stability of sunflower and cotton seeds is determined by the combined effects of moisture content, temperature, relative air humidity, storage duration, as well as biological and oxidative processes. In the original study, moisture contents above 10–12% for sunflower seeds and 9–10% for cotton seeds were considered conditions of increased risk, while a temperature range of 5–15 °C was regarded as rational. These values are indicative for the conditions investigated and should not be considered universal regulatory limits.

Recent international studies confirm the critical role of moisture control and demonstrate that elevated temperature, light exposure, and fluctuations in environmental parameters can accelerate seed quality deterioration. The proposed storage system includes batch classification, cleaning, moisture regulation, cooling, active aeration, controlled storage, and periodic laboratory monitoring.

For implementation of this system under the conditions of the Syrdarya Region, quantitative validation under local conditions is required. This should involve repeated measurements of moisture content, temperature, relative air humidity, acid value, peroxide value, oil content, and seed viability, followed by appropriate statistical evaluation of the results.

References

Ashurov, M.E., Ibragimov, Sh. (2019). *Seed Production and Breeding of Agricultural Crops*. Tashkent: ZiyoNET, – 300 p.

Tozhiev, A.Kh. (2019). *Modern Technologies for the Storage of Grain and Oilseed Crops*. Tashkent: Iqtisod-Moliya.

Karabaeva, M.T., Ergashbaev, A.A., Rasulov, Sh.Kh., Abubakirsidikov, Kh.D. (2024). Scientific principles of storage and preservation of agricultural products. *Proceedings of the International Scientific and Practical Conference*. – P. 70–72.

GOST 22391–2015. *Sunflower. Specifications*.

Sattarov, K.K., Tukhtamishova, G.K., Zhuraeva, Kh.Sh. (2026). Improvement of cottonseed storage technology. *Innovative Solutions: Sustainable Development in Agriculture and Food Industry*. – Tashkent, – P. 264–265.

De Lucia, M., Assennato, D. (1994). Agricultural Engineering in Development: Post-harvest Operations and Management of Foodgrains. FAO Agricultural Services Bulletin No. 93. Rome: FAO, 1994. – 166 p. ISBN 92-5-103108-8.

Xu, W., Yao, J., Yi, Y., Wang, H.-X., Wang, L.-M. (2019). Effects of storage condition on the physicochemical characteristics of sunflower seed oil. *RSC Advances*. 2019. – Vol. 9. – P. 42262–42271. DOI: 10.1039/C9RA09215C.

Liu, J., Yang, Y., Xu, Z., Wang, Q., Liu, B., Wu, Y. (2022). Characteristics of fungal communities and internal mildew occurrence during the stages of planting and storing of sunflower seed in China. *Microorganisms*. 2022. – Vol. 10. – No. 7. Article 1434. DOI: 10.3390/microorganisms10071434.

Afzal, I., Kamran, M., Basra, S.M.A., et al. (2020). Harvesting and post-harvest management approaches for preserving cottonseed quality. *Industrial Crops and Products*. 2020. – Vol. 155. Article 112842. DOI: 10.1016/j.indcrop.2020.112842.

Fatima, F., Khalid, E., Afzal, I., et al. (2025). Evaluation of cotton (*Gossypium hirsutum* L.) seed longevity and deterioration: Physiological and biochemical aspects in relation to moisture contents during storage in different module systems. *Journal of Stored Products Research*. 2025. – Vol. 111. Article 102553. DOI: 10.1016/j.jspr.2025.102553.

Huang, P., Yuan, J., Yang, P., Xiao, F., Zhao, Y. (2024). Nondestructive detection of sunflower seed vigor and moisture content based on hyperspectral imaging and chemometrics. *Foods*. 2024. – Vol. 13. – No. 9. Article 1320. DOI: 10.3390/foods13091320.

Ma, J., Yang, L., Gao, W., Chen, J., Li, J., Jin, L., Hou, R. (2024). Rapid, in-situ evaluation of sunflower seed freshness and vigor using Raman microspectroscopy scanning of carotenoids. *Food Chemistry*. 2024. Vol. 460. Article 140530. DOI: 10.1016/j.foodchem.2024.140530.

Gafurov, K.Kh., Safarova, D.N. (2024). The influence of the main technological parameters of cold pressing of local varieties of sunflower seeds on the yield and quality of oil. *Austrian Journal of Technical and Natural Sciences*. 2024. No. 3–4. P. 36–40. DOI: 10.29013/AJT-24-3.4-36-40.

Premović, T.Đ., Dimić, S.B., Radočaj, O.F., Dimić, E.B. (2014). Impact of the seed storage time on the quality of cold-pressed sunflower oil. *Acta Periodica Technologica*. 2014. – Vol. 45. – P. 67–77. DOI: 10.2298/APT1445067P.

submitted 10.08.2026;
accepted for publication 24.08.2026;
published 31.08.2026
© Sattarov K. K., Tukhtamishova G. K., ZhuraevaKh. Sh.
Contact: doctor-sattarov@mail.ru

Austrian Journal of Technical
and Natural Sciences, 2026 No 7–8
ISSN 2310-5607

PREMIER Publishing
ppublishing.org

Section 4. Materials science

DOI:10.29013/AJT-26-7.8-80-85

CC BY

AMINATION AND DYEING PROPERTIES AND OPERATIONAL PERFORMANCE OF CELLULOSE FIBER FABRICS

Amonov Mukhtor Rahmatovich [1], ***Jumayeva Matluba Sultonovna*** [2]

[1] Professor, Department of Chemistry and Oil and Gas Technologies, Bukhara State University, Doctor of Technical Sciences (DSc), Professor

Bukhara State University, Republic of Uzbekistan

[2] Independent Researcher, Department of Chemistry and Oil and Gas Technologies

Bukhara State University, Republic of Uzbekistan

Cite: *Amonov Mukhtor R., Jumayeva M.S. (2026). Amination and Dyeing Properties and Operational Performance of Cellulose Fiber Fabrics. Austrian Journal of Technical and Natural Sciences 2026, No 7–8.* https://doi.org/10.29013/AJT-26-7.8-80-85

Abstract

This paper investigates the chemical modification of cellulose fiber fabric through amination using glutaraldehyde and ethylenediamine, together with the subsequent dyeing of the modified fabric with complex (metal-containing) dyes. The main purpose of the study is to increase the fabric's affinity for dye and to improve dyeing efficiency by introducing active functional groups into the cellulose fiber structure. The results obtained make it possible to evaluate the effect of the modification process on the dyeing properties of the fabric.

Keywords: *cellulose, cotton fiber, glutaraldehyde, ethylenediamine, amination, chemical modification, complex dye, dyeing, colorimetric indicators, color intensity, color fastness, operational properties*

Introduction

Cotton fiber is one of the natural fibers most widely used in the textile industry, particularly in garment production. Its widespread use is primarily related to the presence of a large number of hydroxyl (–OH) groups in its structure, which provide the fiber with high hydrophilicity. In addition, the low static-charging tendency of cotton fiber, its good moisture absorption, and its comfort for the human body make it an essential raw material for garment manufacturing (Kim & Choi, 2014; Dehabadi et al., 2013; Hauser & Tabba, 2001; Li et al., 1997).

Modification of cotton cellulose can substantially increase its binding capacity toward anionic dyes. This, in turn, reduces the consumption of electrolytes – particu-

larly salts – during dyeing. As a result, not only does dyeing efficiency improve, but the environmental impact of the technological process is also reduced owing to the lower salt content of the resulting wastewater. In addition, introducing cationic functional groups into cellulose fiber can improve certain functional properties of the material (Park et al., 2014; Trask-Morrell & Choi, 1994).

Chemical modification of cellulose fibers not only improves the physico-mechanical properties of the fabric but also increases its binding capacity toward dyes. From this standpoint, introducing amine functional groups into the cellulose structure is of particular importance (Mitchell & Birnboim, 1977; Naven & Harvey, 1996; Zhao & Heindel, 1991). Ethylenediamine (EDA) is one of the highly reactive amine-functional cationic compounds. Its functional groups react rapidly with aldehydes, which is why the reagent is also used for the qualitative and quantitative determination of aldehyde groups.

Research Method

A range of modern physicochemical research methods was used to evaluate the changes in the structure and functional properties of the modified cellulose fabric. In particular, IR spectroscopy was used to determine the composition of functional groups and the changes occurring in them, while elemental analysis was used to assess the nitrogen content and other elements in the material as a result of modification. In addition, determination of the dye-binding capacity made it possible to directly assess the effect of modification on the dyeing process.

A comprehensive evaluation of the operational properties of the modified fabrics – including thermogravimetric analysis, IR spectral analysis, and optical microscopy – is of considerable importance. These methods were used to comprehensively assess the effect of the modification and dyeing processes on the morphological structure and functional activity of the fabric.

Elemental Analysis of the Modified Cotton Fiber

The elemental composition of unmodified cotton fiber and of cotton fiber modified with glutaraldehyde (GA) and EDA reagents was analyzed. The results presented in Table 1 show that nitrogen appeared in the fiber composition after modification. This result is one of the pieces of evidence confirming that the nitrogen-containing functional groups of EDA were incorporated into the cellulose fiber.

Table 1. *Nitrogen content in modified and unmodified cellulose fiber fabric*

Sample	N, %
Untreated cellulose fiber fabric	0.00
Cellulose fiber fabric modified with GA: EDA (1:1 molar ratio)	0.32 ± 0.05

These findings indicate that the process proceeds according to the following reaction mechanism:

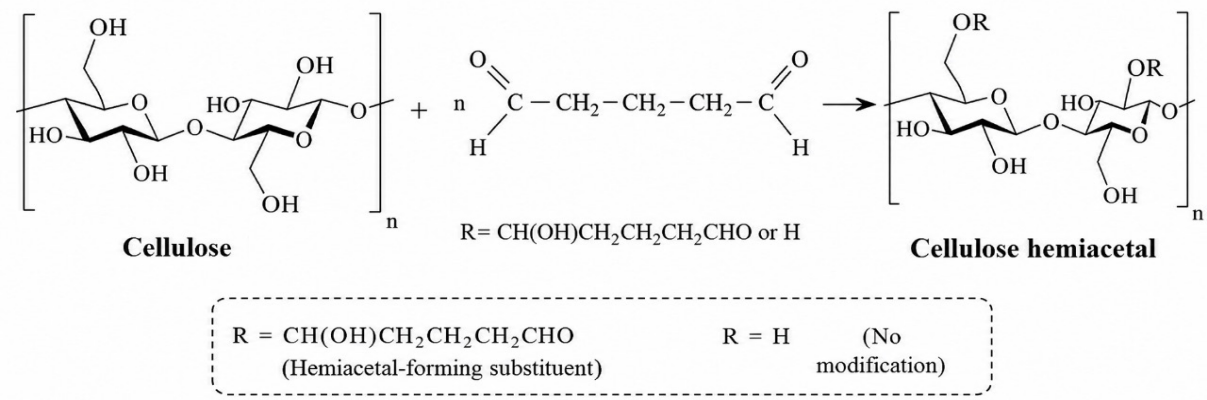

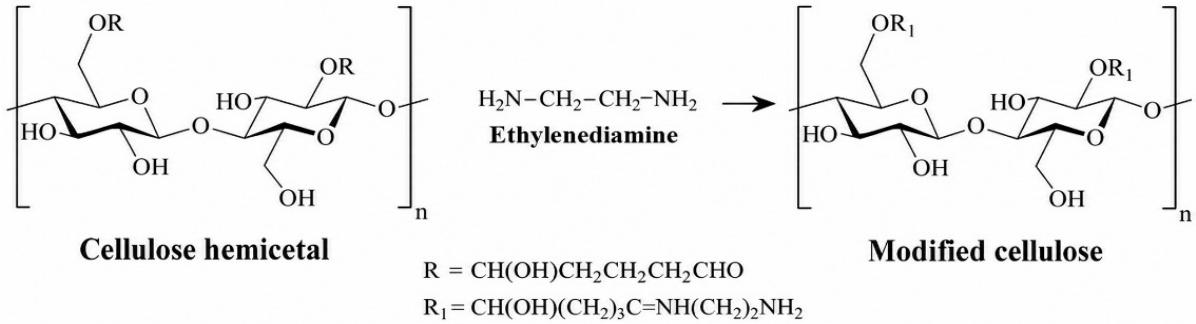

As a result of modification, the main cellulose backbone is preserved; however, its surface and functional-group composition change, forming additional active centers for dye binding through amine groups and imine (C=N) bonds. This is a highly important outcome for the subsequent stage of dyeing with complex dyes.

Dyeing of the Modified Cellulose Fiber Fabric

To evaluate the effect of the modification processes on the dyeability of cotton fabric, both treated and untreated samples were dyed with 3d-metal complex dyes. During dyeing, the dye concentration was 3% relative to the fabric weight, and the liquor ratio of fabric to dye solution was 1:50. The pH of the dye bath was adjusted to 2–3 using acetic acid.

Results Analysis

Optical Microscopic Analysis of the Modified Cellulose Fiber Fabric

Within the scope of the study, the cellulose fiber was modified, and the modified fabric was examined under an optical microscope at 5000× magnification (Figure 1).

Figure 1 shows the sample surface at 5000× magnification after completion of the activation and amination stages. The surface of the sample is golden-yellow in color, and the structural integrity of the main and transverse threads of the cotton fiber is clearly preserved. This indicates that the chemiacylation reaction between glutaraldehyde and the cellulose hydroxyl groups, as well as the nucleophilic substitution reaction with ethylenediamine, did not negatively affect the macrostructure of the fabric or the mechanical strength of the fiber.

The surface color became noticeably darker, indicating a change in the light-absorbing properties of the fiber owing to the attachment of new functional groups to the macromolecule. Thus, figure 1 provides preliminary morphological data confirming the successful implementation of the two-stage modification.

Figure 1. *Micrograph of cellulose fiber aminated with ethylenediamine after activation with glutaraldehyde*

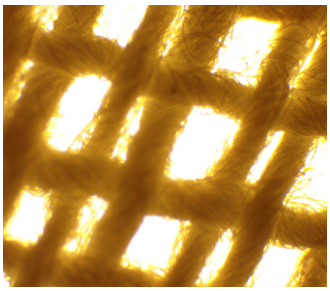

Figure 2. *Micrograph of fabric dyed with Fe^{3+} ion complex dyes of modified cellulose*

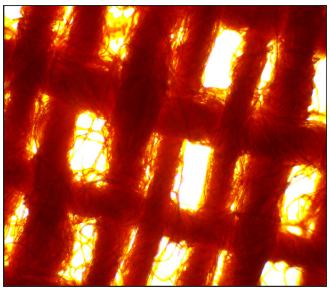

Figure 2 presents the optical microscopic image (5000× magnification) of a sample of modified cellulose fiber fabric treated with complex dyes containing Fe^{3+} ions. The sample's color clearly changed from an initial yellow shade to a dark red shade. This color change is explained by the fact that the lone electron pair of the nitrogen atom in the ethylenediamine structure forms a donor–acceptor coordination bond (chelate) with the Fe^{3+} cation.

Figure 3. *Fe³+ chelation by amino-functionalized cellulose through donor–acceptor coordination of nitrogen lone pairs, resulting in an intense dark-red color*

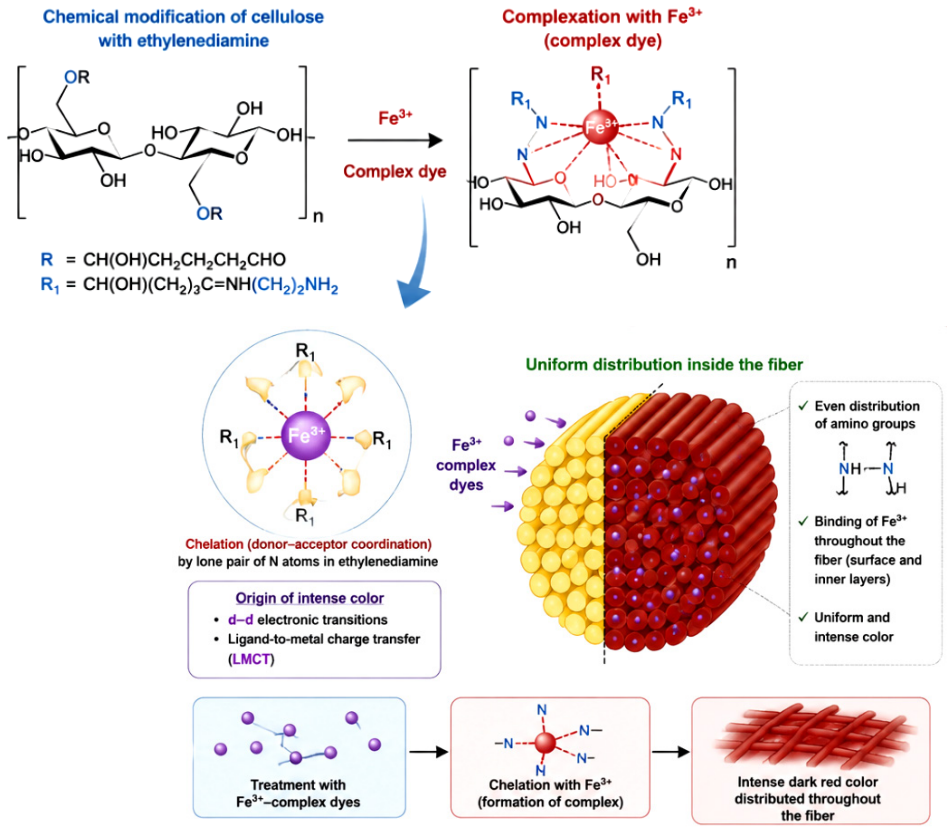

The intensely colored appearance of the resulting complex indicates the occurrence of d–d electronic transitions and ligand-to-metal charge-transfer transitions. The micrograph shows a relatively uniform distribution of color across the entire fiber surface, indicating that the amino groups are evenly distributed within the fiber and have bound Fe^{3+} ions not only in the surface layer but also in the inner layers.

Determination of Colorimetric Indicators

To evaluate the color characteristics of the dyed fabrics, color brightness and intensity were determined photometrically using the RGB color-model coordinates with a Shimadzu UV-1800 (Japan) spectrophotometer. A Canon EOS 600D camera was additionally used to digitally record the color characteristics, and the resulting images were processed by digital color analysis in Adobe Photoshop CS6.

Figure 4. *Changes in the R, G, and B components during dyeing of cotton fabric in the presence of nickel sulfate (A) and cobalt chloride (B) metal complexes in the complex-forming solution*

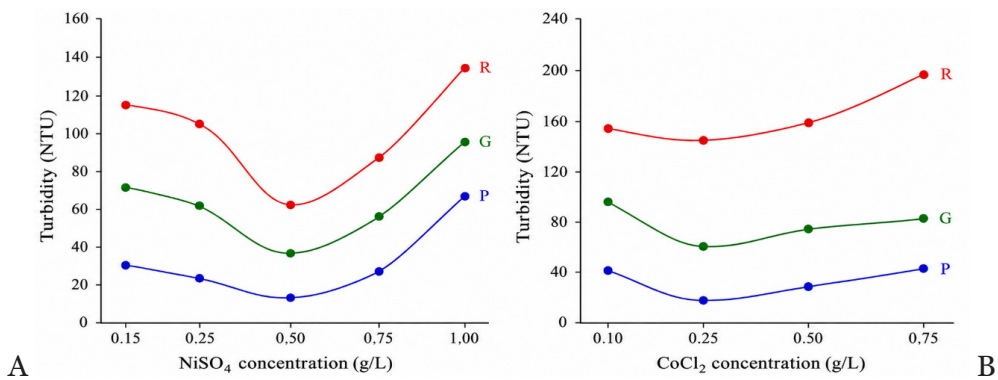

Figure 4 (a, b) shows the optimal values for the formation of metal complexes in the cotton fiber structure as a function of nickel chloride and cobalt chloride concentration. The optimal value for nickel chloride was 0.5 g/L, and for cobalt chloride 0.25 g/L; the process is extremal in character and passes through a minimum.

On the basis of the above findings, optimal compositions and organo-mineral ingredient ratios were developed that ensure the maximum formation of metal complexes in the structure of cotton fabric, thereby enabling high-quality dyeing of cotton fabrics.

Discussion

Evaluation of the Fabric's Operational Properties

As one of the operational properties of the dyed samples, a study was conducted on the resistance of the metal complexes formed in the fabric structure to various hydrothermal treatments. The tests were carried out in accordance with GOST 9733–83 and were assessed on the basis of the ability of the fabrics containing the metal complexes to retain their original color after various external effects, as well as the degree of staining of the accompanying white materials used in the combined test.

Table 2. *Fastness of the metal complexes to hydrothermal treatments*

Fabric color	Water, t=90 °C	Water, t=60 °C	Soap, 5 g/L, t=30 °C	Dry ironing	Steam ironing
Brown	5/5/4	5/5/4	5/5/4	5/5/4	5/5/4
Yellow	5/5/4	5/5/4	5/5/4	5/5/4	5/5/4
Green	5/5/5	5/5/5	5/5/4	5/5/3	5/5/3
Blue	5/5/4	5/5/5	5/5/4	5/5/4	5/5/4

The fastness of the dye to soap treatment was determined in accordance with GOST 9733.4–83 using a "Dyed Color Fastness Testing Laundering Machine LM-12." The test was carried out in a 5 g/L soap solution for 30 minutes with a liquor ratio of 50 at 40 °C. After the test, the samples were squeezed, trimmed along the double-stitched edges, and air-dried at room temperature; a grey-scale reference was used to evaluate color fastness. Fastness to perspiration was determined using a "Color Fastness to Perspiration Model – CF-5" instrument in accordance with GOST 9733.6–83, and fastness to rubbing was determined in accordance with GOST 9733.0–83. The test results are presented in Table 3.

Table 3. *Fastness properties of cotton fabric dyed with composite dyes*

Cotton fabric containing metal complex salts	Color	Soap fastness, points	Perspiration fastness, points	Rubbing fastness, dry	Rubbing fastness, wet
Composition based on iron sulfate	Brown	5/5/4	5/4/3	4	4
Composition based on cobalt chloride	Yellow	5/4/4	5/4/5	4	5
Composition based on nickel sulfate	Green	5/5/4	5/4/4	5	4

Conclusion

The results of the study confirmed that amination of cotton cellulose significantly improves its physicochemical and sorption properties. As a result of amination, active centers for metal-complex formation appear, and dye affinity increases. The introduction of amino groups into the cellulose matrix increases its ability to interact with polyvalent metal ions through the free electron pairs of

the nitrogen atoms and facilitates the formation of coordination bonds. Such modification changes the polarity of the cellulose surface and increases its hydrophilicity, ensuring good dispersion in aqueous systems and increasing the degree of dye uptake.

Rheological analysis of the prepared dye compositions showed that the degree of thixotropic recovery depends on the composition and on the presence of modifiers. The three-component system developed on the basis of cellulose, glutaraldehyde, and ethylenediamine exhibited a higher degree of thixotropic recovery (up to 94–95%) than conventional industrial binders. This indicates its higher structural stability and its greater suitability for technological processes.

References

Dehabadi, V. A., Buschmann, H. J., & Gutmann, J. S. (2013). Durable press finishing of cotton fabrics: An overview. *Textile Research Journal,* – 83(18). – P. 1974–1995. URL: https://doi.org/10.1177/0040517513483857

Hauser, P. J., & Tabba, A. H. (2001). Improving the environmental and economic aspects of cotton dyeing using a cationised cotton. *Coloration Technology,* – 117(5). – P. 282–288. URL: https://doi.org/10.1111/j.1478–4408.2001.tb00076.x

Kim, J. Y., & Choi, H. M. (2014). *Cellulose Chemistry and Technology,* – 48(1–2). – P. 25–32.

Li, S. D., Gatewood, B. M., & Choi, H. M. (1997). *American Dyestuff Reporter,* – 86(3). – P. 36–50.

Mitchell, R. E. J., & Birnboim, H. C. (1977). *Analytical Biochemistry,* – 81(1). – P. 47–56.

Naven, T. J. P., & Harvey, D. J. (1996). *Rapid Communications in Mass Spectrometry,* – 10. – P. 829–834.

Park, J. H., Choi, H. M., & Oh, K. W. (2014). Simultaneous crosslinking and cationization of cotton cellulose by using dialdehyde and choline chloride: Comparison between the pad-dry-cure and microwave irradiation process. *Cellulose,* – 21(4). – P. 3107–3119. URL: https://doi.org/10.1007/s10570–014–0326-z

Trask-Morrell, B. J., & Choi, H. M. (1994). *Journal of Applied Polymer Science,* – 51. – P. 769–779.

Zhao, H., & Heindel, N. D. (1991). *Pharmaceutical Research,* – 8(3). – P. 400–402.

submitted 03.08.2026;
accepted for publication 17.08.2026;
published 31.08.2026
© Amonov Mukhtor R., Jumayeva M. S.
Contact: sharipovms1981@gmail.com

Austrian Journal of Technical
and Natural Sciences, 2026 No 7–8
ISSN 2310-5607

PREMIER Publishing
ppublishing.org

Section 5. Technical sciences in general

DOI:10.29013/AJT-26-7.8-86-91

CC BY

OPTIMIZING EDGE TOPOLOGIES: A REVIEW OF PREDICTIVE NETWORK ROUTING ALGORITHMS

Kirill Andreevich Melnikov [1]

[1] Head of the Center for Applied Artificial Intelligence,
Synergy of Digital Solutions JSC, St. Petersburg

Cite: *Melnikov K.A. (2026). Optimizing Edge Topologies: A Review of Predictive Network Routing Algorithms. Austrian Journal of Technical and Natural Sciences 2026, No 7–8.* https://doi.org/10.29013/AJT-26-7.8-86-91

Abstract

The literature on machine-learning routing rests on an assumption that is rarely stated and almost never tested: network topology is treated as a fixed input over which a routing model operates. At the edge, where reconfiguration of links and nodes is the ordinary operating condition, this assumption does not hold. Packet-level evaluation of reinforcement-learning routing policies indicates that models trained under simplified network dynamics degrade once deployed against realistic traffic, and the degradation traces to the training regime. Drawing on fault-tolerance research from multi-agent coordination architectures outside the networking literature, this review separates topology-level disruptions, which require renegotiation across subgraphs and carry lasting downstream consequences, from resource-level disruptions, which recover within a fixed and comparatively short interval. The same body of research documents a general tendency of learned policies toward overconfidence under distributional shift, of which the routing degradation examined here is a specific instance. The review concludes that the outstanding problem is one of remedy transfer: whether a predicate-based safety architecture, proposed for this overconfidence problem in bounded robotic settings, can be constructed for network topologies whose state space is open-ended and subject to continuous reconfiguration.
Keywords: *predictive network routing; edge network topology; reinforcement learning routing; topology reconfiguration; distributional shift; fault-tolerant coordination*

Introduction

Reinforcement-learning routing policies trained on fluid network models degrade once packet-level dynamics and TCP traffic are introduced, and this degradation appears at exactly the timescale on which edge topologies now operate: single-digit milliseconds (Boltres et al., 2024). Policies that outperform static baselines under simulation fall below those same baselines once evaluated in a packet-level environment under realistic traffic mixes (Boltres et al.,

2024). The competence such policies display in simulation is an artifact of the environment in which they were trained, a property that does not extend to the traffic they were built to route. A related, though structurally distinct, constraint has affected Q-routing since its introduction in 1994: limitations in router computing power and network-layer design have prevented deployment at any scale that would test its claims against real traffic (Yang et al., 2022).

These two limitations, one located in the training signal and one in the deployment substrate, converge on a single conclusion: the gap between predictive routing as studied and predictive routing as deployed shows no sign of closing on its own terms. A structurally comparable gap has already been documented in a different setting. Within distributed multi-agent coordination architectures, a partition in the communication topology forces the system out of its nominal coordination regime once packet loss exceeds approximately ten percent or latency exceeds forty milliseconds; beyond this threshold, coordination proceeds only within reachable subgraphs (Mikhailiuk, 2026). What triggers this regime change is the topology itself, precisely the variable that the routing literature under review treats as fixed.

Existing surveys of AI-driven routing tend to attribute the deployment gap to insufficient data or hardware capacity (Xiao et al., 2021; Almasan et al., 2021). This attribution does not survive scrutiny of where the degradation actually occurs. Graph neural network approaches to routing organize their contributions around network modeling, routing optimization, and dynamic reinforcement-learning tasks (Jiang et al., 2024), and the benchmarks underlying all three categories are constructed on topologies held fixed across training and evaluation. Surveys of AI-enabled routing spanning SDN, 6G, and satellite domains observe that the field itself is fragmented along these subdomains, with each treating the surrounding topology as a fixed backdrop (Aktas et al., 2025).

Topology churn is the ordinary operating condition at the edge. Surveyed approaches evaluate routing decisions against traffic load, congestion, and latency; none evaluates them against topology instability itself.

Literature Review

Across a first cluster of sources, network topology is treated as a fixed input to the learning process: something the model observes and routes over, without requiring continuous renegotiation on the algorithm's part. Graph neural network routing methods belong squarely to this cluster, since their taxonomy of supervised network modeling, supervised routing optimization, and reinforcement-learning-based dynamic routing all presuppose a topology sufficiently stable to support a learned representation (Jiang et al., 2024). RouteNet, among the founding architectures in this line of work, learns to predict per-flow performance metrics from a graph representation of the network built once and held fixed for the duration of training (Rusek et al., 2020). Concrete deployments of this pattern extend the same premise: routing optimization built on a graph neural network layered over deep reinforcement learning, validated within a single knowledge-defined-networking topology (He et al., 2023), and a deep-deterministic-policy-gradient routing scheme for software-defined networks evaluated on a fixed switch topology throughout (Kim et al., 2022). Work situating GNNs within communication networks acknowledges generalization across topologies as an open problem, which at least names the difficulty even where it does not resolve it (Suárez-Varela et al., 2022). Comparative surveys of machine-learning routing schemes report a parallel pattern: the training and deployment frameworks proposed for intelligent routing are validated against fixed simulated topologies, leaving cross-topology transfer for subsequent work (Yang et al., 2022; Li et al., 2022).

One study within this cluster addresses topology change directly: a multi-agent deep reinforcement learning scheme combined with graph neural networks is evaluated explicitly against link and node failures, with routing performance reported to degrade gracefully under such changes instead of collapsing outright (Bhavanasi et al., 2023). This partially addresses the gap identified here. The evaluation still holds the space of possible topologies fixed in advance; topology reconfiguration is not treated as an open-ended variable of the kind edge deployments present.

A comparable blind spot appears, under a different name, in a different coordination substrate. Mikhailiuk (2026) assigns each of several coordination paradigms, centralized, decentralized, consensus-based, and predictive, a distinct characteristic degradation pattern. For predictive coordination, the paradigm architecturally closest to a learned routing policy insofar as both operate by exchanging anticipated future states, the documented pattern is model drift. The same account holds that the organization of coordination is bound to the topology through which information propagates, treating topology as a variable coupled to the degradation it produces. The GNN routing literature reviewed above does not test its fixed-topology assumption against this coupling. Removing the Mikhailiuk citation from this passage would leave the review without its only account linking topology and degradation pattern in structural terms.

A second cluster treats topology as background architecture: the fixed structure inside which some other quantity is optimized. Surveys of AI-based edge computing classify edge devices into front-end, near-end, and far-end tiers and compare response time and storage capacity within that fixed classification (Pooyandeh & Sohn, 2021). Cost-optimization surveys of edge computing extend the same logic, evaluating resource-scheduling, task-offloading, and service-provisioning decisions against a topology held constant across the evaluation window (Cao et al., 2024). Federated-learning research supplies the exception: topology-aware federated learning explicitly models star, tree, decentralized, and hybrid topologies as design variables bearing on communication cost and convergence (Wu et al., 2024).

Mikhailiuk's regime model, applied to this second cluster, marks the same distinction in numerical terms. Different admissible bounds are assigned within that framework to different disruption sources: a communication-topology partition is bounded by a subgraph convergence requirement of 200 milliseconds, whereas a node loss, the resource-level counterpart of a cost-optimization decision, is bounded by a coordination-error threshold of 0.05 together with a five-second recovery window (Mikhailiuk, 2026). These two sources of disruption are not interchangeable within that framework, yet most edge-optimization surveys fold them together under a single heading of "optimization." Cost-optimization decisions of the kind reviewed by Cao et al. (2024), such as offload placement or service scheduling within a fixed topology, correspond to the resource-level disruption and its shorter, less costly recovery path; topology reconfiguration corresponds instead to the disruption requiring subgraph-wide renegotiation. Collapsing both into a single, undifferentiated efficiency problem discards a distinction that carries an explicit numerical basis in Mikhailiuk's model.

A third cluster of sources, addressing objectives instead of topology, treats link utilization and network availability under an outage as a single scalar target subject to smooth trade-off. Traffic-engineering research applying Value at Risk to WAN routing rejects this treatment directly: operators pursuing a pure utilization objective sustain markedly less throughput at a given availability level than operators using a risk-explicit formulation, by a factor of approximately two across the reported benchmarks (Bogle et al., 2019). A subsequent learning-accelerated WAN traffic-engineering system reports substantial speedups in solving the underlying optimization problem but inherits the same single-objective framing, evaluating solution quality chiefly against utilization (Xu et al., 2023). Surveys of AI-enabled routing that list delay, loss rate, and signal-to-noise ratio as parallel objectives (Aktas et al., 2025) do not distinguish those objectives that behave like utilization, tradeable one against another, from those that behave like availability, which call for a risk-bounded guarantee in place of a weighted average.

A utilization trade-off carries limited consequence, since the next traffic-engineering cycle can rebalance load without lasting effect. An outage on a routed link carries a different order of consequence: it propagates through every flow on the affected path before any correction can take effect. Bogle et al. (2019) treat it, for this reason, as belonging to a distinct risk category, separate from the optimization curve along which utilization is ordinarily assessed.

Discussion

Two unresolved gaps emerge from the literature review. Predictive routing research treats topology overwhelmingly as fixed input, even where the edge renders topology the actual decision variable. Accounts of why learned policies degrade silently under distributional shift remain untested against the specific pattern documented in the packet-level literature. A diagnosis of policy overconfidence carries practical value where the systems it describes are fitted with a mechanism reporting their approach to the boundary of competence; the routing literature reviewed here supplies no such mechanism.

Yang et al. (2022) frame the persistent deployment gap for intelligent routing chiefly as a hardware-scaling problem, pending faster routers and larger state-action spaces. The packet-level evidence points instead toward an architectural explanation. FieldLines and M-Slim, the two algorithms proposed specifically to correct the fluid-model mismatch, require no additional inference-time compute relative to the reinforcement-learning baselines they outperform; what they require instead is a different training signal, derived from packet-level simulation instead of fluid simulation (Boltres et al., 2024). A faster router executing a policy trained on the wrong abstraction of network dynamics does not thereby converge on a correct one.

Mikhailiuk's account of neural-policy behavior under distributional shift performs analytical work here that extends beyond naming the pattern. Developed in the setting of safety-critical multi-agent control, the claim holds that neural policies remain structurally uncontrolled outside their training distribution and are frequently overconfident in precisely the states where they prove least reliable (Mikhailiuk, 2026). The routing degradation reported by Boltres et al. (2024) is a specific instance of this general property, observed here in a routing policy instead of the robotic control policies for which the claim was originally developed.

Mikhailiuk's own architectural response to that overconfidence problem, however, does not transfer to routing as readily as the underlying diagnosis. The proposed remedy takes the form of a hybrid neural-symbolic architecture, in which a formally verified symbolic filter, whose safety guarantee is independent of the neural component's confidence, intercepts unsafe actions before execution and issues a tier-transition signal to a degradation controller whenever no admissible action survives filtering (Mikhailiuk, 2026). The guarantee this filter offers depends on predicate coverage: a library of formally specified conditions sufficiently broad to describe the states the system will actually encounter. Predicate coverage of this kind becomes intractable to construct once the underlying state space is high-dimensional and continuous, a limitation Mikhailiuk states explicitly, not one left to inference. A routing topology at the edge, reconfiguring across an open-ended and continually changing set of links and nodes, presents precisely this kind of state space.

Conclusion

The routing degradation documented at packet-level, millisecond-scale operation is a training-regime problem. No routing system reviewed here carries an observable trigger for recognizing when it operates outside the regime under which it was validated. Reading this literature together makes that visible in a way no single source in it does on its own.

Three assumptions traced through the literature review, that topology constitutes fixed input, that topology-level and resource-level decisions carry equivalent automation risk, and that utilization and availability trade off along a single curve, converge on a common blind spot: each treats a structural property of the system as background.

The practical consequence of this blind spot is specific to where predictive routing is next deployed. A misrouted flow within a data-center fabric constitutes, in the terms set out by Bogle et al. (2019), a utilization problem that the next traffic-engineering cycle absorbs. A misrouted flow across an edge topology that has just reconfigured, carrying safety-critical telemetry or a control-plane update bearing on the reconfiguration itself, presents a different order of problem: the topology against which correction would need to be made may already have changed again before the next cycle runs. Silent degradation of the kind Boltres et al. (2024) report proves tolerable in the first setting and considerably less so in the second, a distinction the routing

literature under review does not yet draw when reporting a model's performance.

The open question that remains is a narrow one: whether a predicate library, of the kind Mikhailiuk's hybrid architecture requires for its symbolic safety filter, can be constructed for a routing topology at edge scale, or whether the state space presented by arbitrary, continuously reconfiguring network topologies is precisely the high-dimensional, open-ended environment that the source identifies as resistant to such treatment. Either outcome leaves intact the diagnosis that routing degradation constitutes a distributional-shift problem; a negative answer would indicate only that the remedy proposed for this problem in an adjacent domain does not carry over to routing without further development on the predicate side.

Mikhailiuk (2026) specifies what a formally verified safety filter requires in order to function: a predicate library covering the operationally relevant state distinctions the system will encounter. Whether such a library can be constructed for network topologies at the scale and reconfiguration rate documented in this review remains an open question, and it is the question the next stage of this line of inquiry must answer before a hybrid neural-symbolic remedy can be extended to routing systems, beyond the diagnosis of the underlying problem alone.

References

Aktas, F., Shayea, I., Ergen, M., Saoud, B., Yahya, A. E., & Aldasheva, L. (2025). AI-enabled routing in next generation networks: A survey. Alexandria Engineering Journal, – 120. – P. 449–474. URL: https://doi.org/10.1016/j.aej.2025.01.095

Almasan, P., Suárez-Varela, J., Wu, B., Xiao, S., Barlet-Ros, P., & Cabellos-Aparicio, A. (2021). Towards real-time routing optimization with deep reinforcement learning: Open challenges. In 2021 IEEE 22nd International Conference on High Performance Switching and Routing (HPSR) (pp. 1–6). IEEE. URL: https://doi.org/10.1109/HPSR52026.2021.9481864

Bhavanasi, S. S., Pappone, L., & Esposito, F. (2023). Dealing with changes: Resilient routing via graph neural networks and multi-agent deep reinforcement learning. IEEE Transactions on Network and Service Management, – 20(3). – P. 2283–2294. URL: https://doi.org/10.1109/TNSM.2023.3287936

Bogle, J., Bhatia, N., Ghobadi, M., Menache, I., Bjørner, N., Valadarsky, A., & Schapira, M. (2019). TeaVaR: Striking the right utilization-availability balance in WAN traffic engineering. In Proceedings of the ACM Special Interest Group on Data Communication (SIGCOMM '19) (P. 29–43). Association for Computing Machinery. URL: https://doi.org/10.1145/3341302.3342069

Boltres, A., Freymuth, N., Jahnke, P., Karl, H., & Neumann, G. (2024). Learning sub-second routing optimization in computer networks requires packet-level dynamics. Transactions on Machine Learning Research.

Cao, L., Huo, T., Li, S., Zhang, X., Chen, Y., Lin, G., Wu, F., Ling, Y., Zhou, Y., & Xie, Q. (2024). Cost optimization in edge computing: A survey. Artificial Intelligence Review, – 57(11). URL: https://doi.org/10.1007/s10462–024–10947–4

He, Q., Wang, Y., Wang, X., Xu, W., Li, F., Yang, K., & Ma, L. (2023). Routing optimization with deep reinforcement learning in knowledge defined networking. IEEE Transactions on Mobile Computing, – 23(2). – P. 1444–1455. URL: https://doi.org/10.1109/TMC.2023.3235446

Jiang, W., Han, H., Zhang, Y., Wang, J., He, M., Gu, W., Mu, J., & Cheng, X. (2024). Graph neural networks for routing optimization: Challenges and opportunities. Sustainability, – 16(21). – 9239 p. URL: https://doi.org/10.3390/su16219239

Kim, G., Kim, Y., & Lim, H. (2022). Deep reinforcement learning-based routing on software-defined networks. IEEE Access, – 10. – P. 18121–18133. URL: https://doi.org/10.1109/ACCESS.2022.3151081

Li, T., Zhu, K., Luong, N. C., Niyato, D., Wu, Q., Zhang, Y., & Chen, B. (2022). Applications of multi-agent reinforcement learning in future internet: A comprehensive survey. IEEE Communications Surveys & Tutorials, – 24(2). – P. 1240–1279.

Mikhailiuk, M. (2026). Predictive technologies and autonomous decision making. LAP LAMBERT Academic Publishing.

Pooyandeh, M., & Sohn, I. (2021). Edge network optimization based on AI techniques: A survey. Electronics, – 10(22). – 2830 p. URL: https://doi.org/10.3390/electronics10222830

Rusek, K., Suárez-Varela, J., Almasan, P., Barlet-Ros, P., & Cabellos-Aparicio, A. (2020). RouteNet: Leveraging graph neural networks for network modeling and optimization in SDN. IEEE Journal on Selected Areas in Communications, – 38(10). – P. 2260–2270.

Suárez-Varela, J., Almasan, P., Ferriol-Galmés, M., Rusek, K., Geyer, F., Cheng, X., Shi, X., Xiao, S., Scarselli, F., Cabellos-Aparicio, A., & Barlet-Ros, P. (2022). Graph neural networks for communication networks: Context, use cases and opportunities. IEEE Network, – 37(3). – P. 146–153. URL: https://doi.org/10.1109/MNET.001.2200269

Wu, J., Dong, F., Leung, H., Zhu, Z., Zhou, J., & Drew, S. (2024). Topology-aware federated learning in edge computing: A comprehensive survey. ACM Computing Surveys, – 56(10). – P. 1–41. URL: https://doi.org/10.1145/3659205

Xiao, Y., Liu, J., Wu, J., & Ansari, N. (2021). Leveraging deep reinforcement learning for traffic engineering: A survey. IEEE Communications Surveys & Tutorials, – 23(4). – P. 2064–2097. URL: https://doi.org/10.1109/COMST.2021.3102580

Xu, Z., Yan, F. Y., Singh, R., Chiu, J. T., Rush, A. M., & Yu, M. (2023). Teal: Learning-accelerated optimization of WAN traffic engineering. In Proceedings of the ACM SIGCOMM 2023 Conference (P. 378–393). Association for Computing Machinery.

Yang, S., Tan, C., Madsen, D. Ø., Xiang, H., Li, Y., Khan, I., & Choi, B. J. (2022). Comparative analysis of routing schemes based on machine learning. Mobile Information Systems, 2022, Article 4560072. URL: https://doi.org/10.1155/2022/4560072

submitted 04.08.2026;
accepted for publication 18.08.2026;
published 31.08.2026
© Melnikov K. A.
Contact: kirill.andreev.melnikov@gmail.com

Austrian Journal of Technical
and Natural Sciences, 2026 No 7–8
ISSN 2310-5607

PREMIER Publishing
ppublishing.org

DOI:10.29013/AJT-26-7.8-92-98

INNOVATIVE DESIGN OF EQUIPMENT WITH ARTIFICIAL INTELLIGENCE ELEMENTS (Laser and Optoelectronic Systems with Artificial Intelligence and Neural Network Elements, with Prospects for Transition to Quantum Computing)

G. I. Astakhov [1]

[1] Head of Training Department JSC Sheremetyevo
International Airport Moscow, Russia

Cite: *Astakhov G.I. (2026). Innovative Design Of Equipment With Artificial Intelligence Elements. (Laser and Optoelectronic Systems with Artificial Intelligence and Neural Network Elements, with Prospects for Transition to Quantum Computing). Austrian Journal of Technical and Natural Sciences 2026, No 7–8.* https://doi.org/10.29013/AJT-26-7.8-92-98

Abstract

This publication presents the design principles of laser and optoelectronic systems and instrumentation operating under conditions where artificial intelligence (AI) and artificial neural network (ANN) elements are integrated into control, monitoring, and decision-support units, while also considering the prospective transition to quantum computing technologies and their functional equivalents.

Particular attention is devoted to the development of integrated intelligent infrastructures that combine supersystems and interconnected subsystems into unified technological environments. The publication describes methods of real-time online monitoring based on the analysis of electromagnetic radiation characteristics, electrical resistance, and advanced high-speed resonance spectroscopy. These methodological approaches were developed by the well-known innovation specialist Aleksandr Neshin on the basis of his multidisciplinary professional experience in advanced airfield industrial complexes.

The publication also examines the application of integrated automated assembly systems for electronic components, the use of high-torque micromotors operating on the principles of the inverse piezoelectric effect, and modern methods for monitoring the optical parameters of complex engineering systems through mobile digital applications and intelligent monitoring devices. Special consideration is given to manufacturing technologies for components, assemblies, instruments, and systems of various levels of complexity using industrial production equipment while maintaining the technical characteristics required for the classification of intelligent equipment and smart technological systems.

The author particularly emphasizes the innovative scientific and engineering developments of Aleksandr Neshin, who formulated a systematic approach to the integrative implementation of artificial intelligence and artificial neural network elements in the design of

smart home ecosystems and infrastructure, including advanced engineering solutions for large-area glazed structures and intelligent building components.

The concepts presented in this publication demonstrate that laser and optoelectronic systems incorporating artificial intelligence and neural network technologies, together with the future integration of quantum computing principles, constitute a fundamental element of intelligent feedback systems designed for the monitoring, control, and adaptive management of next-generation smart engineering infrastructure. *The publication highlights the practical significance of Aleksandr Neshin's multidisciplinary approach for the further development of intelligent technological systems, advanced engineering solutions, and innovative digital infrastructure.*
Keywords: *Design features of laser and optoelectronic systems; specialized instrumentation systems at all levels; application of artificial intelligence and artificial neural network elements in control and monitoring units and modules; prospects for the gradual transition to quantum computers and their equivalents*

Introduction

An essential component of any production process is the active monitoring of its parameters in real time.

The most promising method of active real-time monitoring is non-contact measurement and monitoring based on electromagnetic resonance spectroscopy.

Since these methods are fundamentally new and are only beginning to be introduced into industrial processes, it is appropriate to examine them in greater detail.

The author's first two publications discussed the application of this method for the encoding and decoding of information storage media and disposable instruments.

The author proposes to consider these methods, developed by Aleksandr Neshin, in relation to the monitoring of liquids and aerosols as part of an integrated technological system.

Distinctive features and advantages of the resonance electromagnetic spectroscopy technique and technology proposed by Aleksandr Neshin

Design advantages.

Despite the outstanding technical characteristics of the proposed technique and technology, particularly with regard to measurement sensitivity and accuracy, the module designed to implement the technology for the measurement and identification of the parameters of process liquids and materials, including indicators of coronavirus infection, is structurally extremely simple.

The module design is flexible and supports several sensor configurations, thereby significantly expanding its range of applications.

Depending on the application, the sensor may be implemented as a planar coil fabricated as an electronic microcircuit board, as a single-layer printed circuit board, as a multilayer printed circuit board, or in various combined configurations.

The same control, monitoring, and measurement result identification systems can be used for all of these configurations.

The proposed resonance electromagnetic spectroscopy technique and technology are characterized by exceptionally low energy consumption during operation – no more than 20 milliwatts – which eliminates any toxic effects on either the tested materials or the human body during measurements.

In future integrated developments, all of these design advantages will make it possible to fully integrate the system into appropriate software platforms and incorporate artificial intelligence and artificial neural network technologies.

Advantages in practical application.

The extremely low energy consumption during operation enables both laboratory versions and simplified portable versions to be used, thereby expanding the range of applications. These include measurements performed directly in the working environment, on the patient's body, within the oral cavity, on material samples, and on the skin of the hands.

The proposed project includes five types of measurement modules, making it possible to implement all of these application scenarios.

The ability to operate effectively at different signal penetration depths provides exceptional flexibility in the measurement process without changing the module design, since the penetration depth is adjusted by chang-

ing the number of layers in the printed circuit board.

The design and components of the module also make it possible to apply resonance воздействие to the structures of materials or to patient tissues, for example tissues infected with coronavirus, which is intended to be verified during experimental testing.

The proposed design also allows the use of disposable protective and insulating elements in various configurations determined by the type and location of the measurement.

Advantages for mass production.

The measurement module employs standard engineering solutions together with standard structural materials and components, making it possible to organize mass production within one month.

Advantages for the progressive expansion of application areas.

The high degree of standardization of the elements of the measurement module and their well-balanced technical characteristics make it possible to integrate them in the future into measurement systems across virtually all fields of engineering and technology.

Advantages for the progressive improvement of the design, the application of new materials and coatings, the development of new applications, and standardization.

Manufacturing the sensor of the measurement module as either a single-layer or a multilayer printed circuit board makes it possible to further improve the module as printed circuit board technologies advance, for example through the use of dimensional selective metal etching, which significantly increases operating speed.

In addition, to further expand the range of applications, a flexible printed circuit board with the same topology may also be employed.

Let us now consider the procedures and specific features involved in the application of these methods and devices.

Methodology for selecting the operating frequencies of sensors.

This methodology describes the first stage required for the development of a monitoring system for the concentration of the components of the investigated mixture.

A mixture is defined as any combination of components in which one component predominates by volume and is regarded as the conventional solvent, while the remaining components are regarded as conventional dissolved components.

The concept of a conventional solvent is not limited to a single-component liquid capable of forming solutions with other substances. It may also refer to a mixture of gaseous, liquid, or even solid substances (for example, a compound), which may serve as the basis for the formation not only of solutions but also of suspensions, mists, and foams.

Accordingly, the conventional dissolved components may not only be dissolved but may also be present in the mixture as suspensions, bacterial colonies, mist droplets, gas bubbles in foam, or filler particles in compounds.

Searching for the optimal operating frequency of a sensor for the development of a single-component mixture monitoring system.

Such a monitoring system may be applied in technological processes in which the concentration of one component may vary while the concentrations of the remaining components remain unchanged.

Preparation of samples for measurement

Two samples shall be prepared with concentrations of the investigated component corresponding to the lower and upper limits of the anticipated concentration range.

Scanning

Using standard measurement and analytical instruments, perform frequency scanning of the prepared samples across the entire operating frequency range of the instrumentation system (in this case, from 0.100 MHz to 170 MHz).

During the scanning process, the readings of the reference measurement and analytical instrument shall be recorded as changes in the amplitude and phase shift of the current flowing through the sample relative to a harmonically varying probing voltage with a stabilized constant amplitude.

Analysis of the results

Based on the scanning results, several frequencies should be selected at which the difference between the amplitudes of the investigated samples reaches its maximum values, together with several frequencies at

which the difference in phase shift reaches its maximum values. These selected frequencies will serve as the initial data for the design and fabrication of prototype resonance sensors.

Selection of the optimal sensor

The selection of a set of frequencies based on the scanning results obtained using the above-mentioned instruments and methodologies is preliminary.

To determine the optimal operating frequency for a single-component concentration monitoring system, each prototype resonance sensor must be tested using not two samples but at least ten samples with different concentrations of the investigated component within the anticipated concentration range.

After testing all prototype sensors, the most suitable sensor may be selected. Preference should be given to sensors that, in addition to high sensitivity, exhibit a monotonic change in their readings corresponding to changes in the concentration of the monitored component, thereby facilitating subsequent calibration.

Lower operating frequencies are generally preferable from the standpoint of electromagnetic interference immunity.

The selection of the sensor should also take into account design constraints.

Searching for the optimal operating frequencies of sensors for the development of a two-component mixture monitoring system

Such a monitoring system may be applied in technological processes in which the concentrations of two components may vary while the concentrations of the remaining components remain unchanged.

Preparation of samples for measurement

Two samples shall be prepared for each investigated component with concentrations corresponding to the lower and upper limits of the anticipated concentration range, together with an additional sample in which these components are completely absent.

Scanning

Using the above-mentioned instruments and methodologies, perform frequency scanning of the prepared samples across the entire operating frequency range of the measurement system (in this case, from 0.100 MHz to 170 MHz).

During the scanning process, the instrument readings and measurement results shall be recorded as changes in the amplitude and phase shift of the current flowing through the sample relative to a harmonically varying probing voltage with a stabilized constant amplitude.

Analysis of the results

For each investigated component, the scanning results should be used to identify several frequencies at which the difference between the amplitudes of the investigated samples reaches its maximum values, several frequencies at which the difference in phase shift reaches its maximum values, and frequencies (or frequency ranges) at which the sensor exhibits no sensitivity to one component while remaining sensitive to the other.

The selected frequency sets should then be analyzed. Depending on the results of this comparison, several alternative algorithms may be used for selecting the operating frequencies of the sensors.

Case where frequencies exist at which sensitivity is present for only one component.

This is the most preferable case for developing a monitoring system for the concentrations of the investigated components.

If such frequencies exist for both components, the selection of the operating frequencies is straightforward. For the fabrication of prototype resonance sensors, operating frequencies should be selected at which there is no sensitivity to one component while the sensitivity to the other component is maximal.

At least one such operating frequency should be selected for each component.

If such frequencies exist for only one of the components, then, for the fabrication of prototype resonance sensors for that component, operating frequencies should be selected at which there is no sensitivity to one component while the sensitivity to the other is maximal. For the second component, operating frequencies should be selected from its set of candidate frequencies at which the difference in sensitivity to the investigated components is greatest.

Case where no frequencies exist at which sensitivity is present for only one component, but the selected frequency sets do not coincide

In this case, operating frequencies should be selected from each frequency set for the fabrication of prototype resonance sensors such that the difference in sensitivity to the investigated components is maximized.

Case where the selected frequency sets coincide

This is the most challenging case for developing a monitoring system for the concentrations of the investigated components.

If the frequency set for one component completely coincides with that for the other component, it is necessary to determine whether the proportional relationship between the changes in amplitude or phase shift for one component and the corresponding changes for the other component is maintained at all frequencies.

If this proportional relationship is maintained throughout, the frequency scanning should be repeated using different values of the probing voltage.

If no differences can be identified, the investigated components are most likely indistinguishable from the standpoint of electrochemical resonance spectroscopy.

Nevertheless, even in this case, it is worthwhile to fabricate several prototype sensors operating at different frequencies corresponding to the highest sensitivity to changes in the concentrations of the investigated components, since a resonance sensor exerts a more complex influence on the investigated sample, including the additional effect of a magnetic field, than conventional measurement and analytical instruments.

If testing these sensors demonstrates, at least at one operating frequency, a change in the proportional relationship between their sensitivities to concentration variations, then there is a fundamental possibility of developing a monitoring system for the concentrations of the investigated components. The selectivity of such a system will increase as the difference in this proportional relationship becomes greater.

Selection of the optimal sensors

The selection of a set of operating frequencies based on the results of sample scanning using reference, measurement, and analytical instruments is preliminary.

To determine the optimal operating frequencies for a two-component concentration monitoring system, each prototype resonance sensor must be tested using not two samples but at least ten samples with different concentrations of the investigated components within the anticipated concentration ranges.

After testing all prototype sensors, the optimal pair of sensors may be selected. Preference should be given to sensors that, in addition to high sensitivity, exhibit a monotonic change in their readings corresponding to changes in the concentrations of the monitored components, thereby facilitating subsequent calibration.

Lower operating frequencies are preferable from the standpoint of electromagnetic interference immunity.

The selection of sensors should also take design constraints into account.

Let us now consider the application of the described methods and devices for real-time monitoring of acidity levels.

The use of online monitoring at both the supersystem level and the level of interconnected subsystems, employing measurement technology based on the electromagnetic radiation function and electrical resistance under real-time operating conditions and the principles of advanced high-speed resonance spectroscopy.

In the conventional and standard methodology for measuring acidity, the measuring instrument must be calibrated immediately before measuring the acidity of the test sample using calibration solutions with acidity levels of 4 and 7 pH units.

In accordance with this standard methodology, the proposed experimental measurement system also requires calibration before each reference acidity measurement.

This requirement significantly increases the time needed to perform the measurement process.

Two basic types of liquids were used for the experimental testing and comparative analysis of the measurement results – distilled water and ordinary tap water.

Concentrated hydrochloric acid, specially prepared by a chemical laboratory, was used to vary the acidity of the test samples.

Various sensor (solenoid) designs were tested, including, at the final stage of the experiments, a planar sensor (solenoid).

According to the results of a comprehensive worldwide patent search, this type of sensor, its application for this class of measurements and monitoring, and its specific structural implementation were employed for the first time.

The next stage involves comprehensive optimization together with the development, testing under all operating conditions, and commissioning of the electrical circuit for connecting the planar sensor to the instruments of the experimental equipment set.

The following figure presents the resonance measurement results obtained for distilled water and ordinary tap water using the planar sensor.

Figure 1. *Amplitude-Frequency response*

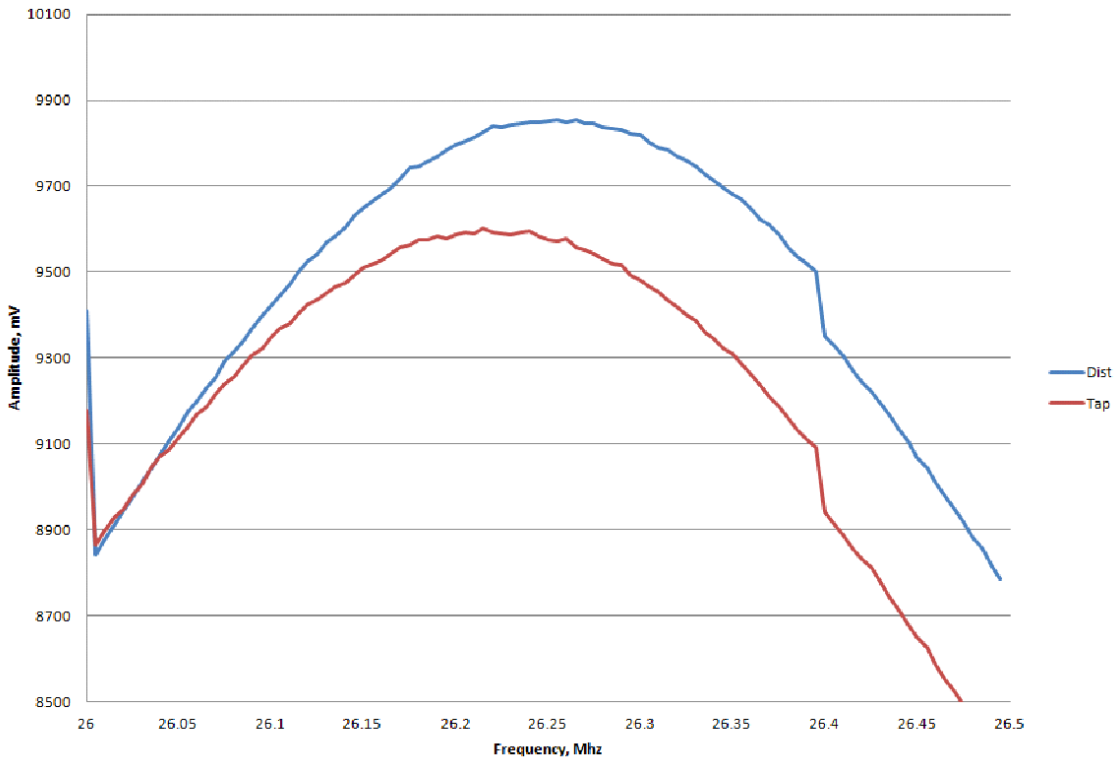

All versions of the tests and measurements demonstrated that the planar sensor has the greatest potential for further application, including in the final product – a capsule for autonomous monitoring of the acidity level of bovine gastric juice.

In addition, the planar sensor provides the most favorable conditions for all adjacent capsule components, partly because, despite its higher sensitivity and measurement accuracy, its overall dimensions are significantly smaller.

Thus, the purpose and objectives of this project stage are to conduct a preliminary comparative verification of all acidity measurement results obtained for synthetic gastric juice, together with a detailed analytical assessment of the following parameters:

- Sensitivity of the test system to changes in the electrical conductivity of gastric juice samples;
- Sensitivity of the test system to changes in the temperature of gastric juice samples;
- Sensitivity of the test system to changes in the chemical composition of gastric juice samples;
- Sensitivity of the test system to changes in the acidity of gastric juice samples when an additional amount of hydrochloric acid is introduced into their chemical composition;
- Sensitivity of the test system to the introduction of particles of organic origin into gastric juice samples;

- Repeatability of measurement results across all test and measurement configurations;
- Comparison of the measurement results in each case with the calibration of the reference instrument and the subsequent results obtained using that reference instrument, which simultaneously monitors:
- The acidity level of the sample;
- The electrical conductivity level of the sample;
- The temperature of the sample;
- The presence and level of the calorimetric content of the sample;
- Determination of the maximum and minimum limiting deviations in the measurement of gastric juice parameters;
- Determination of the permissible maximum and minimum limiting deviations in acidity level when measuring the acidity of gastric juice.

This stage may be implemented in at least two different forms:

The first implementation option involves performing all necessary measurements using a sensor with a planar solenoid on various gastric juice samples containing different fillers and impurities, in accordance with experimental tables comprising 22 variants that form the structure of the final analytical report. This option will be implemented if additional funding is available or obtained.

The second implementation option involves performing all necessary measurements using a sensor with a planar solenoid on gastric juice samples in order to calibrate the measurement parameters and enter the resulting data into the measurement software and model specified in Sections 3 and 4. This option will be implemented if additional funding is available or obtained.

References, Patent, and Licensing Information

Hellmold, J., et al. *Smart Absorbent Article and Components*. United States Patent Application No. 20190167490, Kind Code A1, June 6, 2019.

Hellmold, J., et al. *Smart Absorbent Article, Components, and Process of Making*. United States Patent Application No. 20190167489, Kind Code A1, June 6, 2019.

Ma, M. T. *Methods and System for Managing Intellectual Property Using a Blockchain*. United States Patent Application No. 20180285996, Kind Code A1, October 4, 2018.

Ramamurthy, R., et al. *Process Discovery and Automatic Robotic Scripts Generation for Distributed Computing Resources*. United States Patent Application No. 20200233707, Kind Code A1, July 23, 2020.

Mendes, R. S. *Modular Electronic Vase with Automated, Digital Control and Monitoring System, Used for Aeroponic Growth of Plants in Inner and Outer Environments*. United States Patent Application No. 20190104697, Kind Code A1, April 11, 2019.

Aykroyd, H., et al. *Controllable Power and Lighting System*. United States Patent Application No. 20190090330, Kind Code A1, March 21, 2019.

Adeyoola, T., et al. *Computer Implemented Methods and Systems for Generating Virtual Body Models for Garment Fit Visualisation*. United States Patent Application No. 20160217618, Kind Code A1, July 28, 2016.

Wen, C., et al. *Method and System for Automatic Robot Control Policy Generation via CAD-Based Deep Inverse Reinforcement Learning*. United States Patent Application No. 20190091859, Kind Code A1, March 28, 2019.

Ma, P. *Medicine Dispensing Device for Distributing Medicine Pills Automatically*. United States Patent Application No. 20170312182, Kind Code A1, November 2, 2017.

Wettels, N. *Systems and Methods for Sensing Objects*. United States Patent Application No. 20170165832, Kind Code A1, June 15, 2017.

submitted 21.07.2026;
accepted for publication 04.08.2026;
published 31.08.2026
© Astakhov G. I.
Contact: Gi.Astakhov@yandex.ru

Austrian Journal of Technical
and Natural Sciences, 2026 No 7–8
ISSN 2310-5607

PREMIER Publishing
ppublishing.org

DOI:10.29013/AJT-26-7.8-99-104

PRACTICAL INNOVATIVE SOLUTIONS WITHIN AN ECOSYSTEM FOR ENVIRONMENTAL IMPACT MITIGATION. (Mitigation of Infrastructure-Related Environmental Problems through Practical Innovative Ecosystem-Based Technical Solutions Integrated into Smart Home and Smart Manufacturing Facility Infrastructure Components: The Most Effective Environmental Inventions of Recent Years)

Hryhorii Baranovskyi [1]

[1] Founder & Owner Griznes Auto LLC Miami, Florida, USA

Cite: *Baranovskyi H. (2026). Practical Innovative Solutions Within an Ecosystem for Environmental Impact Mitigation. (Mitigation of Infrastructure-Related Environmental Problems through Practical Innovative Ecosystem-Based Technical Solutions Integrated into Smart Home and Smart Manufacturing Facility Infrastructure Components: The Most Effective Environmental Inventions of Recent Years). Austrian Journal of Technical and Natural Sciences 2026, No 7–8.* https://doi.org/10.29013/AJT-26-7.8-99-104

Abstract

This publication examines contemporary engineering approaches to mitigating environmental problems through the implementation of practical innovative technical solutions integrated into the infrastructure of smart homes and smart manufacturing facilities. Particular emphasis is placed on ecosystem-oriented technologies designed to improve environmental sustainability, reduce the adverse impacts of industrial and urban infrastructure, and enhance the resilience of intelligent technological ecosystems.

The study demonstrates that the successful implementation of modern environmental engineering solutions has become one of the most effective mechanisms for stabilizing both natural and industrial ecosystems. Recent technological innovations and examples of their practical deployment indicate that significant improvements in environmental performance can be achieved while maintaining economically justified implementation costs, thereby supporting the transition toward sustainable intelligent infrastructure.

Particular attention is devoted to current global environmental challenges associated with increasing atmospheric pollution, greenhouse gas emissions, and the growing concentration of carbon dioxide, as well as the influence of these processes on climate change, ecosystem degradation, and public health. The publication also examines examples of localized environmental contamination caused by industrial emissions, including heavy-metal pollution, airborne particulate matter, and atmospheric inversion phenomena that increase human exposure to hazardous pollutants in densely populated urban environments.

The publication further emphasizes that the modernization of infrastructure components

within smart buildings and intelligent manufacturing facilities provides practical opportunities for reducing environmental risks through the introduction of advanced monitoring systems, environmentally responsible engineering technologies, intelligent environmental control systems, energy-efficient manufacturing processes, and innovative ecosystem-based technical solutions capable of minimizing harmful emissions and improving the environmental safety of industrial and urban infrastructure.

Special emphasis is placed on recent technological breakthroughs in the fields of environmental engineering, advanced materials, and energy technologies. Particular consideration is given to innovative developments in high-density energy storage, environmentally sustainable manufacturing technologies, and intelligent engineering systems that create new opportunities for improving energy efficiency, reducing environmental impact, and supporting the long-term sustainability of modern industrial ecosystems.

The study concludes that the integration of practical ecosystem-based engineering solutions into the infrastructure of smart homes and smart manufacturing facilities represents one of the most promising directions for addressing contemporary environmental challenges. The implementation of intelligent environmental monitoring systems, advanced engineering technologies, and innovative infrastructure components provides a practical foundation for improving environmental protection, increasing industrial sustainability, and supporting the development of next-generation intelligent ecological ecosystems.

Keywords: *Ecology; Ecosystem; Environmental Problems; Infrastructure; Infrastructure-Related Environmental Problems; Ecosystem-Level Environmental Problems; Smart Home Infrastructure Components; Smart Manufacturing Facility Components; Practical Opportunities for Stabilizing the Smart Home Ecosystem; Stabilization of Smart Manufacturing Facility Infrastructure; Effective Ecosystem-Based and Infrastructure Protection Technologies*

Introduction

Recent years have clearly demonstrated that addressing global environmental challenges requires not only governmental policies and international climate initiatives but also the practical implementation of innovative engineering solutions capable of reducing anthropogenic impacts on the environment. Among the most promising approaches are decentralized technological innovations that improve energy efficiency, reduce greenhouse gas emissions, and promote the sustainable use of natural resources within everyday infrastructure and industrial systems.

One illustrative example is an engineering solution developed by an independent inventor who modified a conventional internal combustion engine by integrating an onboard water electrolysis system. Following the modification, the vehicle's fuel consumption was reportedly reduced by approximately **35%** while simultaneously decreasing harmful exhaust emissions.

The proposed system employs an electrolysis unit powered by the vehicle's alternator to decompose water molecules into hydrogen and oxygen. The generated hydrogen is subsequently introduced into the combustion process together with conventional fuel, thereby improving combustion efficiency, increasing engine performance, reducing fuel consumption, and significantly decreasing the formation of environmentally harmful exhaust gases. According to the reported experimental results, approximately **1,500 liters of hydrogen** can be produced from one liter of water under appropriate operating conditions.

Although the vehicle continues to operate using a conventional internal combustion engine, hydrogen functions as an auxiliary energy carrier that enhances fuel combustion rather than replacing fossil fuel entirely. Consequently, the system requires less conventional fuel while substantially reducing emissions of incomplete combustion products. The primary objective of this engineering solution is not only to improve fuel economy but also to contribute to the mitigation of environmental pollution associated with road transportation.

The motivation for developing this technology originated from increasing concern regarding global climate change and the growing concentration of atmospheric pollutants. At the same time, the practical reduction in fuel consumption provided an ad-

ditional economic incentive supporting the implementation of the proposed engineering concept. The inventor subsequently proposed the commercialization of hydrogen-assisted conversion systems for conventional vehicles as a practical contribution toward environmentally sustainable transportation technologies.

The growing deterioration of environmental conditions together with the global energy crisis has stimulated intensive research into technologies capable of either preventing environmental pollution or substantially reducing its adverse effects. As a result, numerous innovative engineering developments have emerged during the past decade, several of which are already demonstrating measurable environmental benefits.

One notable example is the development of highly energy-efficient LED lighting technologies. Modern high-efficiency LED lamps consume less than 10 W of electrical power while providing luminous output comparable to that of traditional 60-W incandescent lamps. Long-term durability testing has demonstrated operational lifetimes of approximately 25,000 hours, significantly exceeding the 1,000–2,000-hour service life of conventional incandescent lamps. Consequently, the adoption of advanced LED technologies enables electricity savings of up to 83%, substantially reducing both energy consumption and associated greenhouse gas emissions.

Another significant environmental innovation is the development of biodegradable polymer packaging materials. Researchers have created environmentally friendly polymer films based on methylcellulose and protein complexes that undergo biological decomposition within approximately two weeks under soil conditions, compared with nearly ten years required for conventional polyethylene. Beyond packaging applications, these biodegradable materials have also demonstrated potential for biomedical applications, including biodegradable wound dressings and other medical products.

An additional breakthrough is represented by the development of reusable electronic paper (i2R e-paper). Unlike conventional paper products, this technology permits repeated printing and erasing of information without continuous electrical power during reading. Text is written and erased using thermal printing technology, allowing each sheet to be reused approximately 260 times. This innovation has the potential to substantially reduce paper consumption, decrease deforestation associated with paper manufacturing, minimize industrial waste generation, and support more sustainable information management systems.

These examples demonstrate that practical engineering innovations are increasingly becoming effective instruments for improving environmental sustainability. Their implementation within transportation systems, energy infrastructure, advanced materials engineering, and intelligent information technologies provides realistic opportunities for reducing environmental pollution while simultaneously improving resource efficiency and supporting the long-term transition toward sustainable technological development.

Introduction (continued)

Another remarkable example of environmentally sustainable engineering is the development of Concrete Canvas, an innovative flexible concrete composite created by British engineers. This material consists of a cement-impregnated fabric that remains flexible during transportation and installation but rapidly hardens upon contact with water, forming a thin, durable, waterproof, and fire-resistant concrete structure.

Prior to activation, the material is supplied in compact rolls that can be easily transported and deployed. After shaping the material over an inflatable or structural framework and applying water, the hydration process is initiated. Within approximately 24 hours, the structure becomes fully operational. Two individuals are capable of deploying a complete shelter system within approximately one hour without requiring specialized construction equipment.

Compared with conventional concrete construction, the material occupies approximately 95% less transportation volume, significantly reducing transportation costs, construction time, energy consumption, and associated environmental impacts. Furthermore, the surface of the hardened concrete gradually supports natural vegetation growth, allowing the structure to integrate

more effectively into the surrounding ecosystem while improving both environmental compatibility and architectural aesthetics.

Another noteworthy environmental innovation is the development of high-efficiency environmentally optimized gasoline formulations. One example is the advanced Gold-95 gasoline, developed through collaboration between the fuel industry and leading international manufacturers of fuel additives and lubricant technologies.

The optimized fuel formulation improves combustion efficiency, reduces corrosion within engine components, minimizes carbon deposit formation, and decreases long-term mechanical wear. Experimental evaluations have demonstrated that the use of this fuel reduces fuel consumption by approximately 4% under low-engine-load operating conditions, such as urban traffic congestion and idle operation.

Improved combustion efficiency also results in a reduction of harmful atmospheric emissions. Measurements indicate decreases of approximately 20% in nitrogen oxide (NO_x) emissions, one of the principal contributors to urban photochemical smog, together with reductions of approximately 4% in carbon dioxide (CO_2) emissions due to improved fuel economy. Importantly, these environmental benefits are achieved without increasing the retail cost of the fuel, thereby facilitating its practical implementation on a large commercial scale.

Despite the rapid development of environmentally sustainable technologies, one of the principal barriers to their widespread adoption remains the high cost of technological innovation. Consequently, many countries have initiated comprehensive national programs aimed at supporting the development and commercialization of alternative energy technologies through governmental investment, venture capital financing, and long-term tax incentives.

Such strategic programs seek not only to reduce dependence on fossil fuels but also to establish national leadership in emerging clean-energy industries. Government-supported venture funds, financial assistance for technology demonstration projects, and preferential tax policies encourage private-sector investment and accelerate the commercialization of environmentally sustainable technologies. The growing number of startup companies specializing in alternative energy systems demonstrates the effectiveness of these innovation-driven economic policies.

Alongside organizational and financial mechanisms supporting environmental innovation, significant technological breakthroughs continue to emerge.

One particularly promising development has been achieved by researchers from **Stanford University** and **Yonsei University**, who successfully demonstrated the direct generation of electrical current from living algal cells. During photosynthesis, algae convert solar energy into chemical energy while simultaneously producing electrical charge that can be harvested by specially designed bioelectrochemical systems.

This achievement represents one of the first practical demonstrations of environmentally sustainable bioelectricity generation based on natural biological processes. Unlike conventional fossil-fuel-based electricity production, this technology operates without direct emissions of carbon dioxide and therefore provides a promising foundation for the future development of renewable, carbon-neutral energy systems capable of supporting environmentally sustainable industrial and urban infrastructures.

Introduction (continued)

Another breakthrough in environmentally sustainable energy technologies has been achieved through research on bioelectricity generation from living photosynthetic cells. According to the research team, this represents one of the first successful demonstrations of extracting electrons directly from living plant cells without destroying their biological functionality.

To accomplish this, researchers developed ultra-sharp gold nanoelectrodes specifically designed to penetrate the cellular membrane while maintaining cell viability. The nanoelectrodes are carefully inserted into photosynthetic cells, where they collect high-energy electrons generated during photosynthesis, thereby producing a measurable electric current.

At the current stage of development, the technology remains a proof-of-concept

demonstrating the fundamental feasibility of direct electron harvesting from living biological cells. Initial experiments were performed using individual photosynthetic cells to verify the underlying scientific principles before scaling the technology for practical applications.

Photosynthesis naturally converts solar energy into chemical energy stored in carbohydrates synthesized within chloroplasts. During this process, water molecules are split into oxygen, protons, and electrons. Solar radiation excites these electrons to higher energy states, after which they are transferred through a sequence of protein complexes that ultimately drive carbohydrate synthesis.

The proposed technology intercepts these electrons while they remain at their highest energy level. By positioning gold nanoelectrodes within the chloroplasts of algal cells, researchers successfully extracted electrons directly from the photosynthetic process, thereby generating electrical current without interrupting the fundamental biochemical mechanisms of photosynthesis.

As a result, electrical energy was generated through an environmentally sustainable process that produced no carbon dioxide emissions. The only by-products of the photosynthetic reactions remained oxygen and protons, making the technology one of the cleanest approaches currently under investigation for renewable electricity generation.

Although the present electrical output remains relatively small – approximately one picoampere per individual cell – the study demonstrates the technical feasibility of this fundamentally new approach. The researchers identified two principal limitations affecting current performance: the limited operational lifetime of individual cells following electrode insertion and the relatively small collection area available for electron extraction.

Experimental measurements indicate that the electron-harvesting approach achieves an energy-conversion efficiency of approximately 20%, substantially exceeding the effective utilization of solar energy typically achieved through conventional biofuel production, where only 3–6% of incident solar energy becomes available as usable chemical energy. Unlike biofuel technologies, the proposed approach does not require combustion, thereby avoiding the associated energy losses and atmospheric emissions.

Future research is directed toward the utilization of plant cells possessing larger chloroplasts, the development of improved nanoelectrode architectures, and the extension of cell viability following electrode insertion. These advances are expected to increase electron collection efficiency and facilitate the large-scale implementation of bioelectricity generation systems.

Another significant advancement in sustainable energy storage has been achieved through the application of nanotechnology to the development of ultralight flexible paper-based supercapacitors. Researchers at Stanford University successfully fabricated flexible energy-storage devices by impregnating ordinary paper substrates with conductive nanoparticle-based inks.

The exceptional performance of this technology results from the unique one-dimensional nanostructure of the conductive materials, whose extremely small diameters enable efficient penetration into the fibrous structure of the paper substrate. This architecture significantly improves electrical conductivity while maintaining the mechanical flexibility of the material.

The resulting paper-based supercapacitor is capable of withstanding approximately 40,000 charge-discharge cycles, exceeding the cycle life of conventional lithium-ion batteries by an order of magnitude. The incorporation of nanomaterials substantially enhances electron transport throughout the conductive network, resulting in improved charging and discharging performance. Moreover, the flexible device remains fully operational even after repeated bending or crumpling, demonstrating its potential for next-generation lightweight, flexible, and environmentally sustainable energy-storage systems.

References, Patent, and Intellectual Property Information

United States Patent Application No. 20120029845 A1. *Apparatus and Method for Fluid Monitoring*. Published February 2, 2012.

United States Patent No. 8,694,091. *In Vivo Determination of Acidity Levels*. Issued April 8, 2014.
United States Patent No. 9,316,605. *Determination of Attributes of Liquid Substances*. Issued April 19, 2016.
United States Patent Application No. 20130178721 A1. *In Vivo Determination of Acidity Levels*. Published July 11, 2013.
United States Patent Application No. 20130173180 A1. *Determination of Attributes of Liquid Substances*. Published July 4, 2013.

submitted 11.07.2026;
accepted for publication 25.07.2026;
published 31.08.2026
© Baranovskyi H.
Contact: grisnes.auto.group@gmail.com

Austrian Journal of Technical
and Natural Sciences, 2026 No 7–8
ISSN 2310-5607

PREMIER Publishing
ppublishing.org

DOI:10.29013/AJT-26-7.8-105-111

SMART LIGHTING TECHNOLOGIES. (Possible Applications of the Light Emitting Apparatus Inventions with the Additional Use of Composite Materials and the Integration of Artificial Intelligence and Artificial Neural Network Technologies)

Aleksandra Efimova [1]

[1] A specialist in medical and psychological rehabilitation, dedicated to restoring patients' psycho-emotional well-being through the application of modern psychological intervention methods Self employed, Moscow, Russia

Cite: *Efimova A. (2026). Smart Lighting Technologies. (Possible Applications of the Light Emitting Apparatus Inventions with the Additional Use of Composite Materials and the Integration of Artificial Intelligence and Artificial Neural Network Technologies). Austrian Journal of Technical and Natural Sciences 2026, No 7–8.* https://doi.org/10.29013/AJT-26-7.8-105-111

Abstract

This article examines current trends in the development of intelligent lighting technologies based on Light Emitting Apparatus designs. Particular attention is given to the application of composite materials incorporating synthetic diamonds in combination with advanced light-emitting diode (LED) technologies, as well as to the integration of artificial intelligence (AI) and artificial neural networks (ANNs) into intelligent lighting control systems. The paper presents prospective applications of these innovative engineering solutions aimed at improving energy efficiency, thermal management, operational reliability, and the functional performance of next-generation smart lighting systems. The proposed technological approaches may serve as a foundation for the development of advanced energy-efficient lighting solutions for industrial, transportation, architectural, and smart city infrastructure applications.

Keywords: *Laser; Laser Diode; Light-Emitting Diode (LED); Light-Emitting Apparatus; Composite Ceramics; Artificial Diamonds Embedded in Composite Ceramics; LED Luminaires with Optical Lenses; LED Luminaire Configurations Incorporating Miniature Lenses.*

Introduction

1. Machine Vision

Lasers generate characteristic optical structures resulting from the mutual interference of coherent light waves. These structures, commonly referred to as **speckle patterns**, are random interference patterns formed by the interaction of coherent waves exhibiting random phase shifts and/or random intensity distributions. Such patterns typically consist of bright speckles separated by dark regions, producing non-uniform illumination.

For automated manufacturing processes and industrial machine vision applications, the operational area must be illuminated with highly uniform monochromatic light to

ensure reliable image acquisition, measurement accuracy, and object recognition.

Figure 1. *Laser diode module with a cooling system based on composite materials incorporating synthetic diamonds*

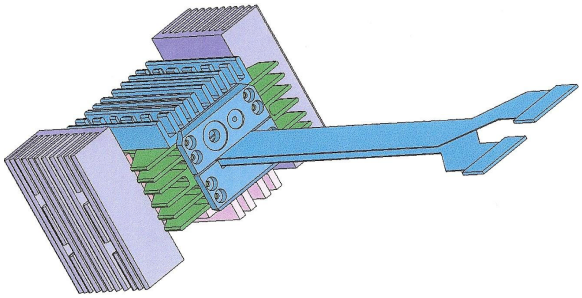

Conventional laser sources are unsuitable for many machine vision applications because the speckle phenomenon introduces undesirable intensity fluctuations and image artifacts. Light-emitting diodes (LEDs) do not generate speckle and therefore eliminate this limitation; however, LEDs generally exhibit lower optical brightness and produce non-uniform radiation distributions in the far field.

The proposed **Light Emitting Apparatus** overcomes these limitations through the implementation of the patented design incorporating a phosphor microdroplet deposited on the end face of an optical fiber. In this configuration, the effective size of the emitting region is determined either by the phosphor droplet diameter, approximately **100–150 μm**, or by the diameter of the **optical fiber core**, typically **30–50 μm**.

This emitting area is approximately three times smaller than that of a conventional LED while simultaneously providing significantly greater spatial uniformity of the emitted light. These characteristics make the proposed technology particularly suitable for high-precision machine vision systems requiring compact, homogeneous, and high-quality illumination.

The cost of commercially available industrial machine vision lighting systems typically ranges from USD2,000–3,000 for standard configurations to USD25,000–50,000 for advanced integrated solutions. According to preliminary engineering estimates, the proposed Light Emitting Apparatus is expected to reduce system cost by approximately 35–50%, depending on the selected configuration and system architecture.

The operational lifetime of the proposed apparatus is primarily determined by the service life of the laser diode. The proposed design incorporates multiple engineering solutions intended to maximize laser diode longevity, including an advanced high-efficiency cooling system, a modified mounting module, intelligent control and regulation electronics operating in the radio-frequency range, optimized material selection, specialized protective coatings, and synthetic diamond-based thin-film technologies for enhanced thermal management. Based on these design features, the expected operational lifetime of the apparatus is estimated to be 10,000 operating hours or more.

Figure 2.

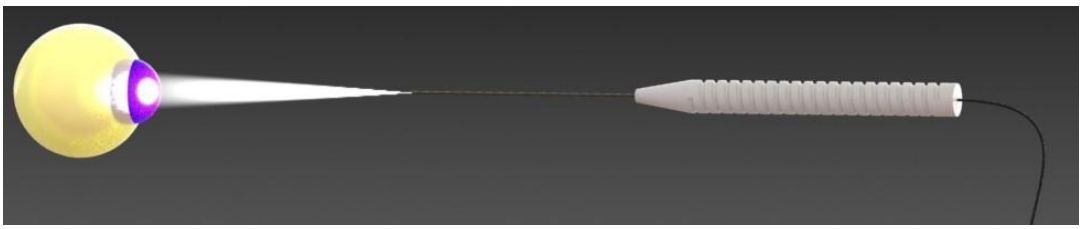

2. Illumination Systems for Microscopes

The monochromatic light generated by the proposed Light Emitting Apparatus provides significant advantages for microscopic imaging. The use of monochromatic illumination substantially reduces chromatic aberration, thereby improving image quality, optical resolution, and measurement accuracy. These characteristics are particularly important for high-resolution optical microscopy and precision analytical applications.

The cost of illumination systems currently employed in various types of micro-

scopes typically ranges from approximately USD2,000 to USD3,000, depending on the microscope configuration and optical performance requirements.

Implementation of the proposed invention is expected to reduce illumination-related energy consumption by approximately 85–95%. Furthermore, the projected manufacturing cost of the proposed illumination system is estimated to be at least 50–60% lower than that of existing commercial solutions while maintaining or improving optical performance.

The application of the proposed Light Emitting Apparatus is expected to significantly improve the overall technical characteristics of modern microscopes, including optical efficiency, illumination uniformity, energy efficiency, and operational reliability. These improvements considerably expand the potential applications of microscopy across scientific research, medicine, industrial inspection, materials science, biotechnology, and advanced manufacturing.

The operational lifetime of the proposed apparatus is primarily determined by the service life of the laser diode. To maximize durability, the proposed design incorporates multiple engineering solutions, including an advanced high-efficiency cooling system, a modified mounting module, intelligent control and regulation electronics operating in the radio-frequency range, optimized material selection, specialized protective coatings, and synthetic diamond-based thin-film technologies for enhanced thermal management. Based on these design features, the expected operational lifetime of the apparatus is estimated to be 10,000 operating hours or more.

Figure 3.

3. Medical Applications of the Proposed Light Emitting Apparatus

One of the most promising medical applications of the proposed Light Emitting Apparatus is endoscopy.

The proposed optical fiber design incorporating a phosphor microdroplet at the fiber tip enables uniform omnidirectional illumination, allowing light to be emitted in all directions around the distal end of the endoscope. Conventional endoscopic illumination systems are generally limited by the divergence angle of the optical fiber, resulting in illumination of only a relatively narrow field of view.

In contrast, the proposed invention provides substantially improved illumination of the surrounding tissue while supporting the generation of multiple wavelengths, including full-spectrum white light. Furthermore, the apparatus enables operation at specific wavelengths required for specialized medical procedures, including photodynamic therapy (PDT) and ultraviolet (UV) irradiation, thereby expanding both the diagnostic and therapeutic capabilities of modern endoscopic systems.

According to preliminary engineering assessments, an endoscopic illumination system based on the proposed invention is expected to reduce manufacturing costs by approximately 35–45% compared with existing technologies. At the same time, the improved optical performance is anticipated to significantly enhance endoscopic visualization, diagnostic accuracy, procedural efficiency, and overall clinical effectiveness.

The operational lifetime of the proposed apparatus is primarily determined by the service life of the laser diode. To maximize durability, the proposed design incorporates multiple engineering solutions, including an advanced high-efficiency cooling system, a modified mounting module, intelligent control and regulation electronics operating in

the radio-frequency range, optimized material selection, specialized protective coatings, and synthetic diamond-based thin-film technologies for enhanced thermal management. Based on these design features, the expected operational lifetime of the apparatus is estimated to be 10,000 operating hours or more.

Figure 4.

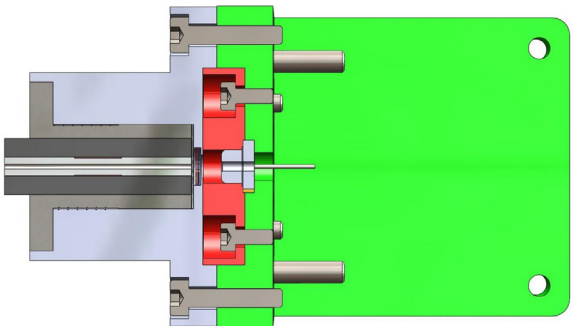

4. Application of the Proposed Light Emitting Apparatus for Surgical Field Illumination

Another important medical application of the proposed **Light Emitting Apparatus** is the illumination of the surgical field during operative procedures.

The optical fiber incorporated in the proposed system can be easily attached to a surgeon's finger or integrated directly into surgical instruments such as scalpels, forceps, or other microsurgical devices, providing localized, highly uniform illumination precisely at the operative site.

This technology is particularly valuable in ophthalmic surgery, where homogeneous illumination of the sclera is essential for achieving optimal visualization and surgical precision. The optical fiber employed for this application has an extremely small diameter of approximately 100 μm, allowing it to be introduced into the eye with minimal tissue trauma while providing uniform omnidirectional illumination of the scleral region. Such illumination is considered an important factor contributing to improved visualization, enhanced surgical accuracy, and successful clinical outcomes.

The estimated cost of the proposed localized surgical illumination system is expected to be approximately USD3,000, depending on the specific configuration and intended clinical application.

The operational lifetime of the proposed apparatus is primarily determined by the service life of the laser diode. To maximize durability, the proposed design incorporates multiple engineering solutions, including an advanced high-efficiency cooling system, a modified mounting module, intelligent control and regulation electronics operating in the radio-frequency range, optimized material selection, specialized protective coatings, and synthetic diamond-based thin-film technologies for enhanced thermal management. Based on these design features, the expected operational lifetime of the apparatus is estimated to be 10,000 operating hours or more.

Figure 5.

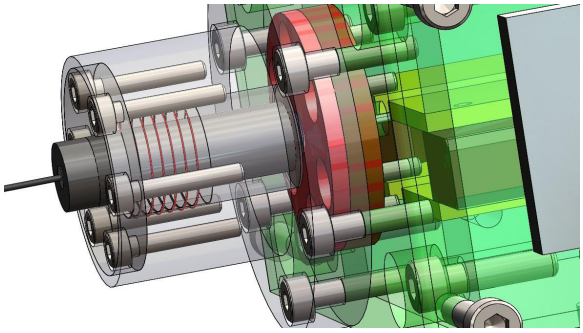

5. Online Inspection System for Nuclear Reactor Containment Structures and Adjacent Nuclear Facility Components

Another potential application of the proposed Light Emitting Apparatus is its integration into online inspection systems for monitoring the condition of nuclear reactor containment structures and critical components located in the vicinity of nuclear reactors.

The proposed technology may be incorporated into advanced optical inspection and monitoring systems designed to support continuous or periodic assessment of reactor infrastructure, enabling high-quality illumination for visual inspection, defect detection, and structural condition monitoring under demanding operating environments.

According to preliminary engineering estimates, the cost of a complete inspection system based on the proposed invention may reach several hundred thousand U.S. dollars, depending on the configuration, level of automation, and integration requirements.

The anticipated market demand includes several hundred systems worldwide for monitoring commercial nuclear power plants.

In addition, several hundred comparable systems may be required for inspection and maintenance of nuclear reactors installed aboard submarines and other platforms equipped with nuclear propulsion systems.

The operational lifetime of the proposed apparatus is primarily determined by the service life of the laser diode. To maximize durability, the proposed design incorporates multiple engineering solutions, including an advanced high-efficiency cooling system, a modified mounting module, intelligent control and regulation electronics operating in the radio-frequency range, optimized material selection, specialized protective coatings, and synthetic diamond-based thin-film technologies for enhanced thermal management. Based on these design features, the expected operational lifetime of the apparatus is estimated to be 10,000 operating hours or more.

Figure 6.

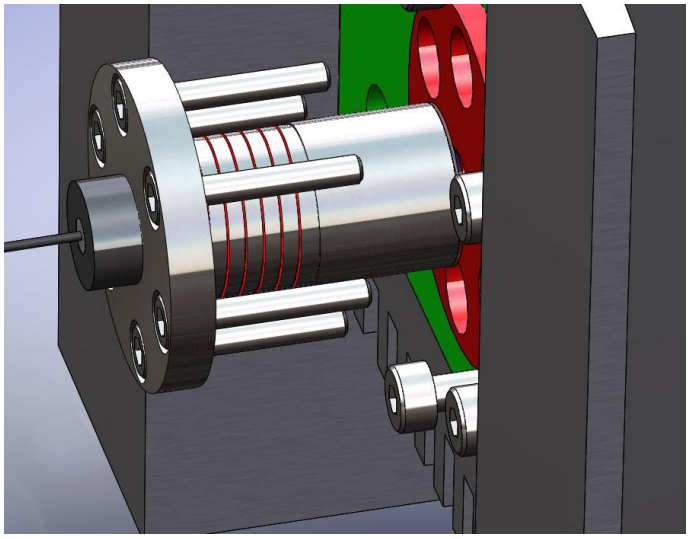

6. Underwater Illumination Systems for Submersibles and Professional Diving Applications

Another promising application of the proposed **Light Emitting Apparatus** is the development of advanced underwater illumination systems for **submersibles, bathyscaphes, remotely operated underwater vehicles (ROVs), autonomous underwater vehicles (AUVs), and professional diving equipment**.

The proposed technology offers the potential to provide high-intensity, energy-efficient, and highly reliable illumination under extreme underwater operating conditions, where optical performance, thermal stability, and long-term operational reliability are of critical importance.

Depending on the system configuration and intended application, the estimated cost of a complete underwater illumination system may reach up to USD100,000.

The overall service life of the proposed apparatus depends on multiple engineering components; however, the operational lifetime of the illumination system itself is primarily determined by the durability of the laser diode. To maximize service life, the proposed design incorporates multiple engineering solutions, including an advanced high-efficiency cooling system, a modified mounting module, intelligent control and regulation electronics operating in the radio-frequency range, optimized material selection, specialized protective coatings, and synthetic diamond-based thin-film technologies for enhanced thermal management. Based on these design features, the expected operational lifetime of the apparatus is estimated to be 10,000 operating hours or more.

Should there be specific commercial or technical interest, the proposed underwater illumination system can be further developed, optimized, and engineered in greater detail to meet the requirements of particular marine, scientific, industrial, or defense applications.

Figure 7.

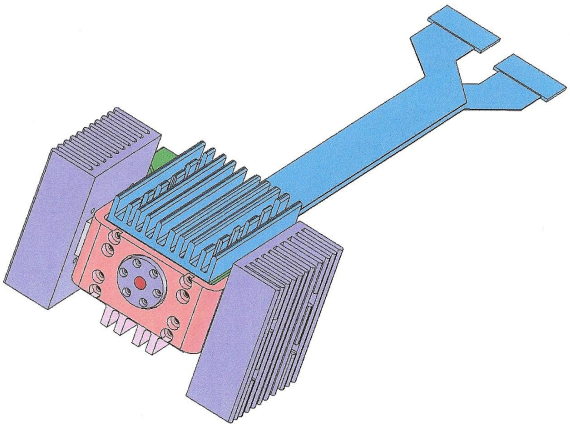

7. Underwater Optical Communication Systems

Another promising application of the proposed **Light Emitting Apparatus** is underwater optical communication between divers, surface vessels, submersibles, and submarines.

The proposed system may utilize green wavelengths for communication in coastal and shallow-water environments, where green light provides superior propagation characteristics, while blue wavelengths are more suitable for deep-ocean applications due to their lower attenuation in seawater.

According to preliminary engineering assessments, the proposed technology may provide reliable communication over distances of up to 100 meters between divers. Communication between a surface vessel and a bathyscaphe or other underwater vehicle may potentially reach distances of up to 10,000 meters, depending on environmental conditions, optical system configuration, and communication protocols.

The estimated cost of a fully integrated underwater optical communication system is expected to be approximately USD1 million, particularly for specialized applications in defense, emergency response, underwater rescue operations, and the management of technological disasters.

The overall operational lifetime of the proposed apparatus depends on multiple engineering components; however, the service life of the optical communication subsystem is primarily determined by the durability of the laser diode. To maximize reliability, the proposed design incorporates advanced thermal management, an enhanced mounting module, intelligent control and regulation electronics operating in the radio-frequency range, optimized material selection, specialized protective coatings, and synthetic diamond-based thin-film technologies for superior heat dissipation. Based on these engineering solutions, the expected operational lifetime of the apparatus is estimated to exceed 10,000 operating hours.

Should specific commercial or governmental interest arise, the proposed underwater optical communication system may be further optimized and engineered to satisfy the requirements of particular industrial, scientific, maritime, or defense applications.

Potential Applications of the Proposed Light Emitting Apparatus

The proposed **Light Emitting Apparatus** represents a next-generation intelligent lighting platform that combines advanced laser-based illumination, phosphor-conversion technology, composite materials incorporating synthetic diamonds, and artificial intelligence-driven control systems.

Unlike conventional LED luminaires employing optical lenses or micro-lenses, the proposed technology provides enhanced optical efficiency, superior illumination uniformity, improved thermal management, and significantly greater flexibility in controlling the spectral and spatial characteristics of the emitted light.

These characteristics enable its application across a broad range of sectors, including:

- intelligent industrial lighting and machine vision systems;
- microscopy and scientific instrumentation;
- medical imaging, endoscopy, and surgical illumination;
- underwater lighting and optical communication systems;
- nuclear facility inspection and monitoring;
- transportation and autonomous systems;
- architectural and urban lighting;
- defense and aerospace technologies;

- smart manufacturing and Industry 4.0 infrastructure;
- Smart City lighting networks integrated with artificial intelligence and sensor technologies.

The integration of artificial intelligence, artificial neural networks, advanced composite materials, and intelligent optical control enables the proposed technology to significantly improve energy efficiency, operational reliability, illumination quality, and functional adaptability compared with conventional LED lighting systems.

References

Burov, A., et al. *Piezoelectric Step Motor*. United States Patent **US 6,242,849 B1**, June 5, 2001.

Uchino, K., et al. *Piezoelectric Motor and Method of Exciting an Ultrasonic Traveling Wave to Drive the Motor*. United States Patent **US 7,095,160 B2**, August 22, 2006.

Moteki, T., et al. *Rotary Drive Device*. United States Patent **US 7,116,037 B2**, October 3, 2006.

Vyshnevskyy, O., et al. *Method for Operating a Piezoelectric Motor, and Piezoelectric Motor Comprising a Stator in the Form of a Hollow-Cylindrical Oscillator*. United States Patent **US 7,218,031 B2**, May 15, 2007.

European Parliament and the Council of the European Union. *Regulation (EU) 2024/1689 of the European Parliament and of the Council of 13 June 2024 Laying Down Harmonised Rules on Artificial Intelligence (Artificial Intelligence Act, AI Act)*. Official Journal of the European Union, 2024.

submitted 10.08.2026;
accepted for publication 24.08.2026;
published 31.08.2026
© Efimova A.
Contact: sedova.alina7810@gmail.com

Austrian Journal of Technical
and Natural Sciences, 2026 No 7–8
ISSN 2310-5607

PREMIER Publishing
ppublishing.org

DOI:10.29013/AJT-26-7.8-112-117

MULTIDISCIPLINARY DIGITAL TECHNOLOGIES WITH ELEMENTS OF ARTIFICIAL INTELLIGENCE. (Modern Multidisciplinary Digital Technologies with Elements of Artificial Intelligence and Artificial Neural Networks, and Aspects of Production and Marketing of Products Created Based on and in the Development of These Technologies in Their Interaction with TRIZ and ARIZ)

Oleksii Hrachov [1]

[1] DevSecOps engineer, Odessa, Ukraine

Cite: *Hrachov O. (2026). Multidisciplinary Digital Technologies with Elements of Artificial Intelligence. (Modern Multidisciplinary Digital Technologies with Elements of Artificial Intelligence and Artificial Neural Networks, and Aspects of Production and Marketing of Products Created Based on and in the Development of These Technologies in Their Interaction with TRIZ and ARIZ). Austrian Journal of Technical and Natural Sciences 2026, No 7–8.* https://doi.org/10.29013/AJT-26-7.8-112-117

Abstract

This article examines the application of modern intelligent multidisciplinary digital technologies incorporating elements of artificial intelligence and artificial neural networks in the development of innovative engineering solutions based on the principles of the Theory of Inventive Problem Solving (TRIZ) and the Algorithm of Inventive Problem Solving (ARIZ). Particular attention is devoted to the analysis of psychological barriers, established engineering stereotypes, and the technological and commercial factors influencing the transformation of inventive concepts into competitive market-oriented products. The article substantiates the necessity of integrating systematic inventive methodologies with intelligent digital technologies in response to the continuous reduction of innovation cycles, increasing complexity of engineering systems, and rising costs of prototype development and experimental validation. The proposed approach emphasizes the identification and implementation of auxiliary non-obvious innovative functions capable of enhancing the commercial value, consumer attractiveness, and technological competitiveness of new products. It is concluded that the comprehensive integration of TRIZ, ARIZ, artificial intelligence, artificial neural networks, and multidisciplinary digital technologies significantly improves the efficiency of engineering innovation, supports informed decision-making, overcomes psychological barriers, and increases the probability of successful commercialization of advanced technical solutions.

Keywords: *Digital Technologies; Modern Multidisciplinary Digital Technologies with Elements of Artificial Intelligence; Inventive Idea; TRIZ ARIZ; Market Demands; Technical Stereotypes; High Level of Commercial Success; Technical Contradictions; Psychological Barriers; Base for Selective Selection; Information Technologies; Non-Obvious Technical Solutions*

New Directions in Element Manufacturing Technology

In composite technical solutions, the methods and technologies for manufacturing parts and components of a product are crucial factors determining the overall feasibility of implementing that product.

For example, consider a nozzle or fuel injector for an internal combustion engine.

This is one of the most mass-produced items, with over a billion such injectors being manufactured worldwide each year.

The product's consumer value is determined by several key factors: the diameter of the outlet holes and ensuring leak-tightness at high fuel pressures (up to 2000 atmospheres).

Traditional drilling technology limits the minimum diameter of the holes. However, since high pressures require holes with diameters measured in microns, the technology for creating these holes must be, for example, laser-based.

In this case, the inventor of a new injector must consider the composite aspect of the invention's novelty, expressed in compliance with the specific requirements of laser drilling equipment.

Constantly changing conditions and consumer demands, combined with local consumption standards, and cultural and national traditions (which form the basis for local consumption standards), create informal but tacitly present conditional consumer standards.

The inventor's goal is to ensure the commercial success of their invention: a fundamental understanding of the current consumer standard criteria, and the technical, operational, and functional characteristics of the new product. This is a crucial part of their commercial strategy.

Even if technological risk is eliminated due to positive test results for the new product, the risk of commercial failure remains if the inventors and their commercialization partners have not considered or understood the essence of the consumer standard for their product.

Availability of Principally New, Non-Obvious Materials

Let's consider, for example, two new structural and technological directions: creating efficient vortex tube sources and creating composite vortex generators based on efficient aerodynamic and hydrodynamic activation mixing systems.

Both mentioned technological directions require structural materials for development, which, due to their properties, will allow obtaining parameters in each of the directions that are impossible to obtain with conventional materials.

The possibility of using new materials is not absolute, and to make it possible to use them, a primary composite and structural solution is required.

Given the rather complex structure of the double vortex generator design, it is necessary to pay attention again to the environmental aspects that take place in a technically complex innovative process.

There are known cases when, for example, an internal combustion engine with an innovative cylinder layout was invented, with an extremely efficient fuel economy system, but the concentration level of nitrogen oxides and soot in its exhaust gases exceeded the permissible level according to the future standard, which should come into force in two years.

This turned out to be enough for the newest engine to be sent for revision, during which its technical solution was changed to the level of a composite one with the inclusion of previous technical solutions.

As can be seen from the diagram, the device receives electricity from a solar mini-battery with a voltage stabilizer, connected to a battery – energy storage.

In turn, the battery – storage is connected to a planar electric generator from which electricity is supplied to all actuators and, first of all, to double vortex generators creating vortex tubes in which the process of accelerated condensation takes place.

Air compression is carried out using an innovative screw compressor.

Thus, the entire supersystem of the shoulder generator for condensing drinking water from atmospheric air is a sequential complex combining several innovative subsystems, both assembled and separately having full compliance with the criteria of non-obviousness.

Figure 1. *The figure shows a schematic diagram of the device, connection, and operation of a shoulder generator for condensing drinking water from the ambient air; The designations of the constituent elements are given in the figure*

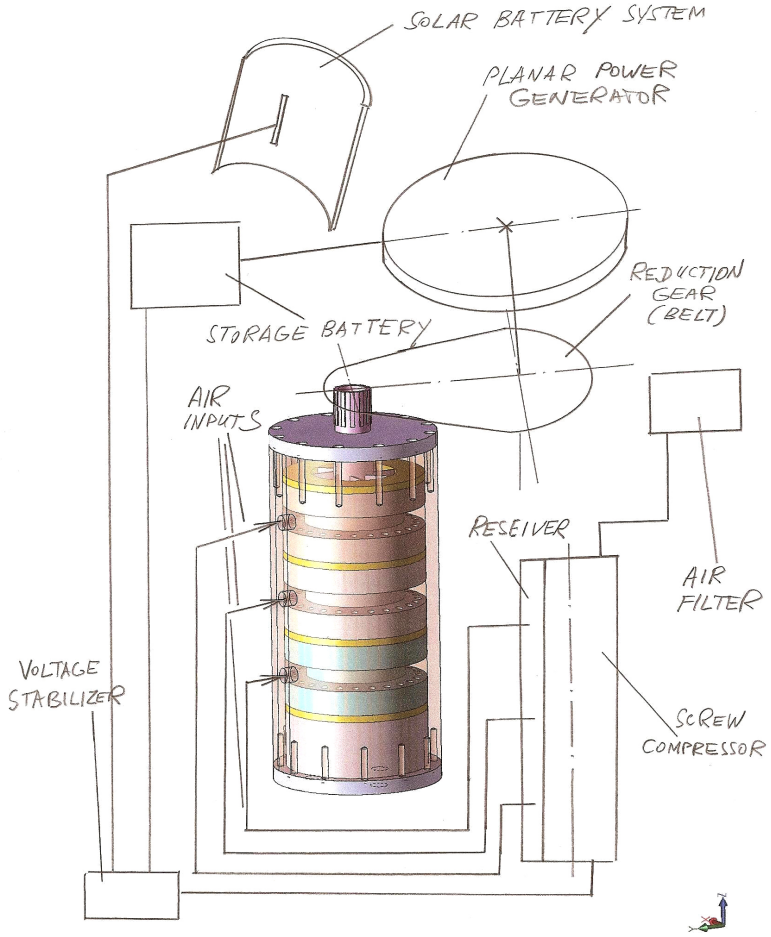

Figure 2. *The figure shows a schematic diagram – a three-dimensional model of the device, connection, and operation of a shoulder generator for condensing drinking water from the ambient air; The designations of the incoming nodes and components are given in the figure*

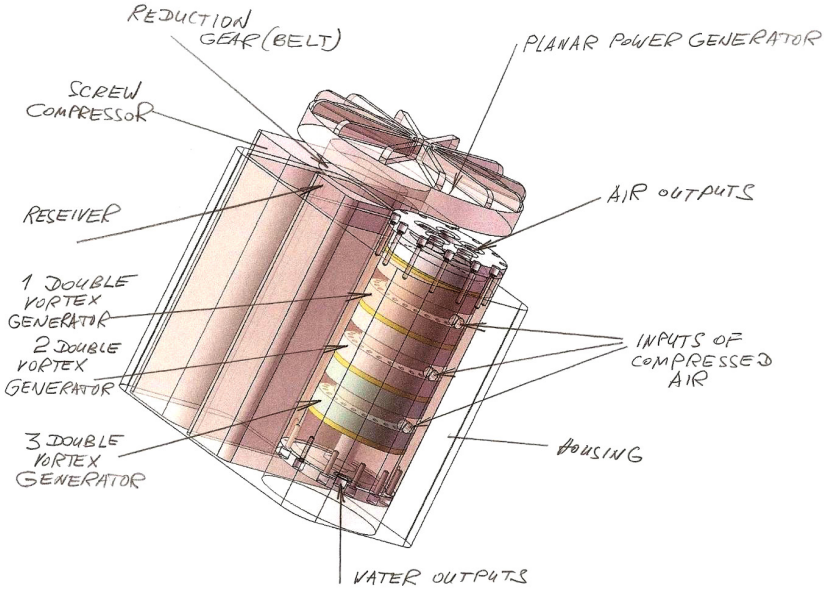

Figure 3. *The figure shows a three-dimensional model of a vortex generator, which is the main actuator of a compact shoulder generator for condensing drinking water from atmospheric air*

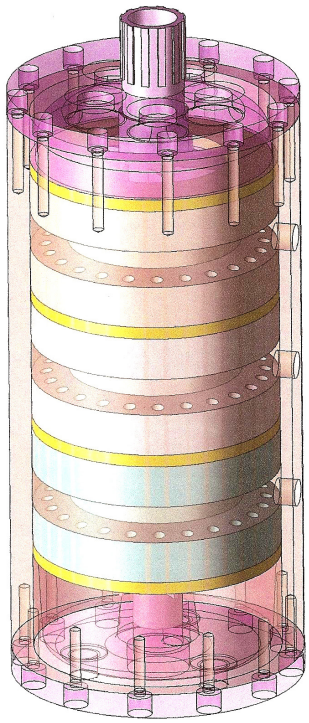

The mechanism of aerodynamic formation of accumulating local vortex tubes of the main vortex tube consists of three double local vortex generators.

Figure 4. *The figure shows a three-dimensional model of an accumulating central vortex generator with the designations of the constituent components*

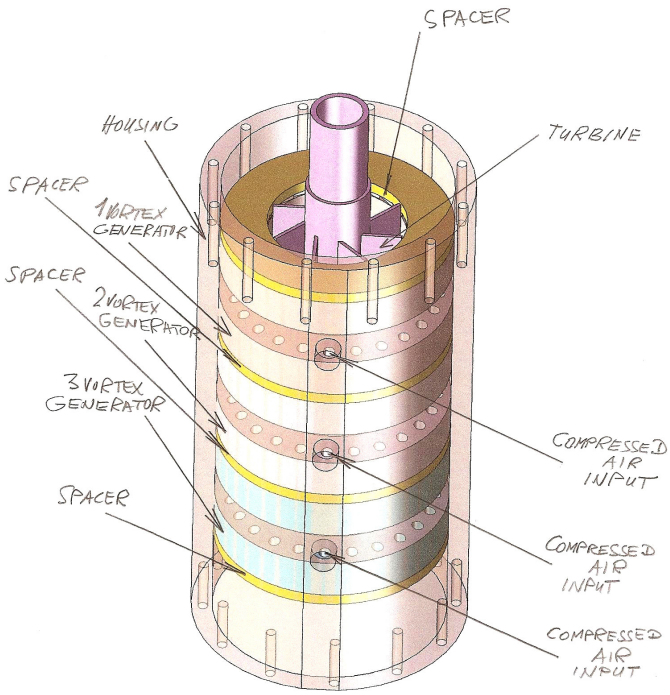

It makes sense to link the description of the design properties and qualities of the generator with the features of the modern development of innovative developments as elements of smart technologies

Availability and Continuous Intensive Development of Software Products

The significant complication of all types of technology, and especially various electronic and microelectronic devices, has fundamentally changed the principles of their protection as objects of non-obvious, complex, multifaceted, and multifunctional intellectual property.

In addition, the recent qualification of technical solutions such as smart technologies, smart devices, and smart materials requires additional arguments for such proof.

For such objects, significant differences concerning purely design features, circuit solutions, and combinations of these solutions do not determine all aspects of the invention, since today very often all the listed features and differences can be realized in a working system or prototype only under certain conditions and manufacturing and control technology capabilities. It is manufacturing in combination with proven non-obviousness of design solutions that determines the main properties of the invention.

The development of processor control systems also determines the viability of a technical solution, which means that an algorithm or algorithms, programs, and feedback between the elements of a design or circuit become or have already confidently become an integral part of the technical solution underlying the claimed invention.

To this argument, it is necessary to add the results of a step-by-step analysis of the state of an innovative object in combination with the possibility of a non-obvious principle of using artificial intelligence and artificial neural networks.

Thus, it is necessary to combine or integrate several different technologies in one description. This combination, the identified possible channels and links of such integration, should be presented in the claims in such a way as not to allow the patent office examiner to doubt the unity of all integrated distinguishing features of the future invention and to divide it into several local technical solutions based on one technological direction.

The possibilities of integrative patenting in information technology affect a huge layer of activity in modern society.

And if quite recently it was possible to very accurately characterize or limit one or another technological sector, then with the advent of high technologies and their offshoot, information technologies, into all spheres of human activity, such classification possibilities and protection mechanisms have significantly changed and transformed into a new system of technical solutions.

New Environmental Standards

As is known, the restrictive requirements of environmental standards are becoming increasingly stringent. When working on the invention of a new product, the use of which in any way affects the limits of permissible parameters regulated by environmental protection standards, it is necessary to ensure full compliance with the requirements and restrictions of the current standards during the operation of the new product.

As a rule, the current standards are constantly being improved, and the requirements will be systematically tightened in a planned manner in a few years.

This is especially important for various power equipment, condensation systems, and internal combustion engines.

Figure 5. *The figure shows a three-dimensional model of air and water flows at the main accumulating vortex generator, which is the main actuator of a compact shoulder generator for condensing drinking water from atmospheric air*

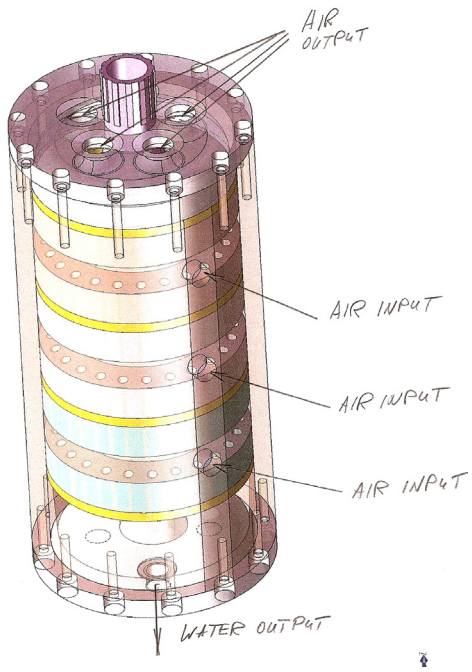

The mechanism of aerodynamic formation of accumulating local vortex tubes of the main vortex tube consists of three double local vortex generators, each operating autonomously

Figure 5.1. *The figure shows a three-dimensional model of the external view of a device for condensing drinking water from atmospheric air*

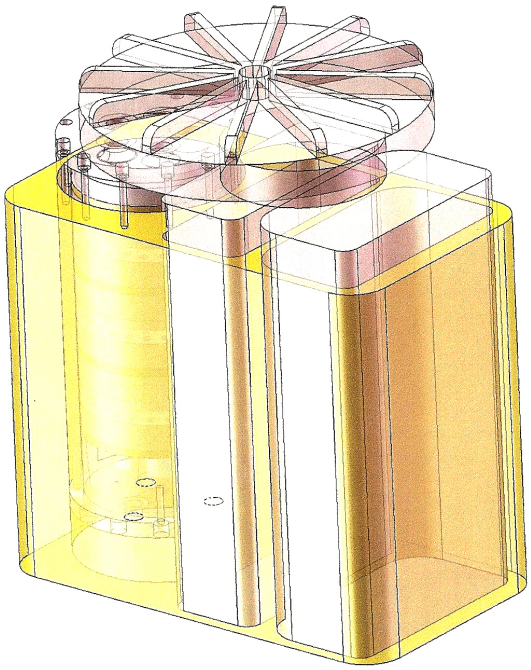

References

Ackerman. *Water Harvester and Purification System*. United States Patent No. 10,071,918, September 11, 2018.

Catherwood, Sr. *Dehydrating Air-Filtering Apparatus*. United States Patent No. 4,594,082, June 10, 1986.

Rolandson. *Exhaust Gas Recirculation Compressor Inlet Thermal Separation System*. United States Patent No. 10,767,659, September 8, 2020.

Hedlund. *Self-Contained Photovoltaic Distillation Apparatus*. United States Patent No. 10,759,677, September 1, 2020.

Kow. *Humid Air Stream Generator*. United States Patent No. 10,731,880, August 4, 2020.

Stuckenberg. *Atmospheric Water Generation Systems and Methods*. United States Patent No. 10,583,389, March 10, 2020.

Panda et al. *Economically Viable Atmospheric Water Generator*. United States Patent No. 10,718,101, July 21, 2020.

Bravo et al. *Modular Apparatus for Water Production*. United States Patent No. 10,422,112, September 24, 2019.

Bravo et al. *Water Production Apparatus for Rigorous Climates*. United States Patent No. 10,385,549, August 20, 2019.

Hering et al. *Advanced Laminar Flow Water Condensation Technology for Ultrafine Particles*. United States Patent No. 9,821,263, November 21, 2017.

submitted 15.06.2026;
accepted for publication 29.06.2026;
published 31.08.2026
© Hrachov O.
Contact: dariabooksclub@gmail.com

Austrian Journal of Technical
and Natural Sciences, 2026 No 7–8
ISSN 2310-5607

PREMIER Publishing
ppublishing.org

DOI:10.29013/AJT-26-7.8-118-123

HIGH-EFFICIENCY ELECTROCHEMICAL PROCESSING TECHNOLOGIES. (Methods and Devices for Non-Contact Resonance Inspection in High-Efficiency Electrochemical Processing, Including High-Speed Metallization Technologies and Atmospheric Water Harvesting)

Sergii Marakshyn [1]

[1] CEO, LLC MYHOME NYC INC. Florida, USA

Cite: *Marakshyn S. (2026). High-Efficiency Electrochemical Processing Technologies. (Methods and Devices for Non-Contact Resonance Inspection in High-Efficiency Electrochemical Processing, Including High-Speed Metallization Technologies and Atmospheric Water Harvesting). Austrian Journal of Technical and Natural Sciences 2026, No 7–8.* https://doi.org/10.29013/AJT-26-7.8-118-123

Abstract

This article examines current approaches to the development of New Smart Manufacturing Technologies based on the integration of digital technologies, advanced composite materials, intelligent control systems, and modern engineering methodologies into contemporary manufacturing processes. Particular attention is given to the application of systems engineering principles for optimizing production processes and achieving the Ideal Final Result (IFR) in accordance with the concepts of the Theory of Inventive Problem Solving (TRIZ) and the Algorithm for Inventive Problem Solving (ARIZ).

The paper discusses the influence of digital transformation, intelligent manufacturing, and innovative engineering solutions on the evolution of industrial production systems. Special emphasis is placed on the development of integrated manufacturing ecosystems capable of improving production efficiency, product quality, resource utilization, process reliability, and operational sustainability. The article presents modern engineering approaches to the integration of intelligent monitoring systems, real-time process control technologies, non-contact inspection methods, artificial intelligence, and advanced manufacturing infrastructure into unified smart production environments. These technologies significantly expand the functional capabilities of manufacturing systems while increasing productivity, precision, automation, and decision-making efficiency.

The proposed concepts may serve as a scientific and engineering foundation for the development of next-generation smart manufacturing systems within the framework of Industry 4.0, digital transformation, and intelligent industrial ecosystems, providing new opportunities for innovation, sustainable industrial development, and continuous improvement of manufacturing technologies.

Keywords: *Electrochemical Processing; Electrochemical Resonance Spectroscopy; Non-Contact Resonance Inspection; High-Speed Metallization Technology; Atmospheric Water*

Harvesting; Advanced Composite Materials; Ideal Final Result (IFR); Theory of Inventive Problem Solving (TRIZ); Algorithm for Inventive Problem Solving (ARIZ); New Smart Manufacturing Technologies; Intelligent Manufacturing Systems; Smart Production Ecosystems; Digital Manufacturing; Real-Time Process Monitoring; Non-Contact Inspection Technologies; Innovative Engineering Solutions; Industrial Digital Transformation; Production Process Optimization; Advanced Manufacturing Infrastructure; Industry 4.0.

1. Introduction

At the present stage of industrial development, manufacturing processes are increasingly characterized by the comprehensive integration of digital technologies, intelligent control systems, and advanced composite materials into conventional production methods. Under these conditions, it is essential to utilize these technological advancements effectively and to fully exploit the engineering advantages they provide in achieving the Ideal Final Result (IFR).

As established by the classical principles of the Theory of Inventive Problem Solving (TRIZ) and its further development through the Algorithm for Inventive Problem Solving (ARIZ), innovative system-oriented approaches to manufacturing provide a comprehensive set of engineering tools that, when applied in combination, enable production systems to approach the Ideal Final Result most appropriate for a particular technology, manufacturing process, or engineering device.

The emergence of new technological components, digital engineering solutions, and advanced manufacturing concepts has made it possible, through appropriate system integration and carefully selected implementation strategies, not only to redefine the concept and evaluation criteria of the Ideal Final Result but also to refine its engineering characteristics in accordance with contemporary manufacturing requirements.

In the context of the globalization of industrial production and the transition of technologically advanced economies toward innovation-driven models of development, it has become necessary to reconsider both the organizational principles governing manufacturing systems and the strategic objectives that define modern production processes.

In several industrialized countries, this new concept of manufacturing – integrating the latest technological achievements across every stage of production and throughout the development of manufacturing equipment – has become known as New Smart Manufacturing Technologies.

Practical experience gained during the design, development, and implementation of smart manufacturing systems demonstrates that these technologies exhibit a continuous tendency toward expanding the application of original engineering solutions to increasingly complex production environments.

This expansion follows a progressive, multidirectional pattern, gradually extending beyond primary manufacturing operations to encompass numerous supporting processes, including monitoring, quality assurance, process optimization, and production control.

A representative example is the widespread adoption of **real-time non-contact inspection** technologies, which constitute one of the key elements of intelligent manufacturing systems. These technologies fundamentally transform conventional inspection methodologies by providing substantially higher measurement accuracy, operational reliability, and process efficiency while eliminating physical interaction with the object under investigation.

The practical implementation of this technology initially began in the agricultural sector, where increasing demands for efficient water management, particularly in large-scale irrigation projects, created the need for advanced non-contact monitoring systems.

Considering the immediate industrial demand, the first practical application focused on non-contact monitoring of pH (acidity) levels in water and aqueous solutions.

2. The principal characteristics of the proposed non-contact resonance-based pH monitoring technology include:

- the measurement range for pH determination in water and aqueous solutions is not limited by the operating

principles of the non-contact resonance inspection method;

- measurement accuracy can be adjusted according to specific application requirements, with a minimum resolution of **0.1 pH units**, consistent with internationally accepted measurement standards;
- measurement accuracy is independent of the concentration of organic compounds present in the liquid and is unaffected by the chemical aggressiveness of the aqueous solution, since all inspection procedures are performed remotely without direct physical contact with the monitored medium.

Since irrigation systems account for the largest consumption of water and typically involve the introduction of fertilizers and other chemical additives, the next stage of technological development focused on **non-contact monitoring of nutrient and fertilizer concentrations** in irrigation solutions.

When the composition of the nutrient solution is known in advance, the integrated sensing system incorporates a corresponding number of **selective resonance sensors**, each individually configured to detect a specific chemical component within the solution.

The proposed system provides a measurement accuracy of approximately **0.5 mg/L** for individual chemical constituents.

Because the electrical conductivity of water and aqueous solutions is one of the principal indicators of water quality, the subsequent expansion of this technology involved the implementation of **non-contact monitoring of electrical conductivity**, thereby further extending the functionality of intelligent electrochemical process control systems.

3. Electrical Conductivity Monitoring of Water and Aqueous Solutions

The methodology for monitoring the electrical conductivity of water and aqueous solutions is based on principles similar to those employed for non-contact pH measurement.

For successful industrial implementation, a measurement accuracy of approximately **1 μS/cm** is considered sufficient for the majority of technological applications.

The logical continuation of this technological development was the introduction of **integrated non-contact quality assessment methods** for water and process liquids.

Integrated Quality Monitoring of Water and Aqueous Solutions

Two principal approaches are proposed for comprehensive quality monitoring.

The first approach utilizes a **single integrated resonance sensor** that provides an overall indication of the general quality characteristics of water or another liquid by generating a composite quality parameter.

The second approach employs a **multi-sensor integrated module** consisting of a number of selective sensors corresponding to the required monitoring parameters. Each sensor is individually configured to monitor a single physicochemical parameter or the concentration of a specific component.

The successful implementation of this stage of technological development established the basis for the subsequent expansion of non-contact resonance monitoring technologies toward the determination of **heavy metal concentrations** in water and aqueous solutions.

4. Monitoring of Heavy Metal Concentrations in Water and Aqueous Solutions

Heavy metal monitoring may be performed using either a **generalized** or a **selective** measurement approach.

In the generalized configuration, the sensor module provides an indication of the overall presence of heavy metals within the monitored liquid.

In the selective configuration, the integrated sensor module incorporates individually tuned resonance sensors, each designed to detect and quantify a specific heavy metal.

The integrated sensing platform may simultaneously incorporate additional sensors for comprehensive monitoring of overall water quality, enabling the simultaneous evaluation of multiple physicochemical parameters within a single measurement system.

Since organic compounds are widely used in numerous industrial process solutions, the next stage in the evolution of non-contact resonance technologies involved the development of methods for monitoring **organic**

compound concentrations in technological aqueous solutions.

5. Monitoring of Organic Compound Concentrations in Water and Aqueous Solutions

Monitoring of organic substances may be performed either as a **total organic concentration measurement**, representing the cumulative concentration of all organic compounds present, or as a **selective analysis** of individual organic components.

For selective measurements, the integrated resonance sensor module incorporates individually calibrated sensors dedicated to each target organic compound.

Because the proposed measurement technique operates without direct contact with the monitored liquid, it eliminates contamination of the sample and minimizes measurement errors associated with conventional contact-based analytical methods.

Although numerous conventional techniques are available for temperature measurement, the proposed non-contact resonance method provides significant advantages for modern industrial production lines by enabling continuous **active temperature monitoring** without requiring the insertion of temperature probes into electrochemical reactors or other complex chemical processing equipment.

6. Temperature Monitoring of Water and Aqueous Solutions

The methodology for non-contact temperature monitoring is based on principles similar to those employed for electrical conductivity measurements.

The proposed technology enables continuous real-time monitoring while eliminating direct interaction between the sensing elements and the monitored medium.

For advanced manufacturing processes, particularly semiconductor fabrication and **photolithography technologies** involving silicon wafers, the **dielectric permittivity** of water and process solutions represents one of the most critical technological parameters affecting process stability and product quality.

Consequently, the next stage of technological development focused on extending non-contact resonance monitoring methods to the determination of the **dielectric permittivity** of water and aqueous solutions.

7. Monitoring of the Dielectric Permittivity of Water and Aqueous Solutions

The monitoring methodology for dielectric permittivity is analogous to that employed for determining the concentration of organic compounds in water and aqueous solutions.

All measurements are performed using selectively configured resonance sensors or integrated sensor arrays mounted externally on the pipeline surface or supplied as a dedicated pipeline section designed for installation within an existing piping system.

During project implementation, specialized software will be developed to identify and process resonance sensor signals, enabling accurate interpretation of monitored physicochemical parameters and determination of their concentrations within water and aqueous solutions.

The project also предусматривает the development of a standardized range of sensor configurations suitable for installation on pipelines with diameters ranging from 10 mm to 120 mm.

In addition, sensor manufacturing technology will be optimized to achieve economically viable production costs for integrated water-quality monitoring systems intended for agricultural and industrial applications.

Further refinement of sensor designs and monitoring methodologies has led to the concept of a specialized non-contact analytical instrument capable of verifying the compliance of drinking water with environmental regulations and public health standards through comprehensive real-time quality assessment.

8. Applications of the Non-Contact Instrument for Verifying Compliance of Drinking Water with Quality Standards

The proposed instrument has two principal configurations. The first configuration is designed for permanent installation directly on the water pipeline immediately upstream of the consumer tap within residential build-

ings. The second configuration is a portable device intended for rapid testing of drinking water samples collected directly from the tap into a dedicated pipeline section equipped with the integrated resonance sensor.

Both versions of the instrument feature a compact, ergonomic, and functional design. The housing is manufactured from engineering-grade polymeric materials, primarily polyvinyl chloride (PVC), providing durability, ease of operation, and suitability for continuous domestic use.

The operating principle of both configurations is based on **comparative resonance analysis**, in which the signal generated by the monitored water sample is continuously compared with a previously established reference resonance signature.

The reference signal is obtained from water that fully complies with applicable drinking water quality standards. The resonance sensor is capable of detecting extremely small deviations from this reference signal.

The estimated detection thresholds are as follows:

- heavy metals: approximately 5×10^{-9} g/L;
- radioactive isotopes: approximately 1×10^{-12} g/L;
- hardness salts and silicates: approximately 1×10^{-6} g/L;
- organic acids, phenolic compounds, surfactants, detergents, and mineral fertilizer residues: approximately 1×10^{-7} g/L.

All concentrations are expressed per one liter of water.

The proposed instrument is not intended to selectively identify every individual contaminant. Instead, owing to its exceptionally high sensitivity, it provides an integrated assessment of water quality and detects contamination levels approaching approximately 50% of the maximum permissible concentrations considered potentially hazardous to human health. Such performance enables continuous domestic monitoring of drinking water quality and allows preventive measures to be taken before contaminant concentrations reach hazardous levels.

Public health authorities in many developed countries recommend continuous monitoring of drinking water quality. However, the widespread implementation of this recommendation has been limited by the absence of reliable, accurate, user-friendly, and economically affordable monitoring instruments suitable for large-scale domestic application.

The proposed instrument configurations are designed to comply with applicable safety requirements governing both construction materials and operational performance.

Both versions are well suited for industrial production and do not require specialized manufacturing technologies. Consequently, they can be manufactured efficiently by small and medium-sized enterprises while maintaining competitive production costs.

This manufacturing approach also enables **regional assembly**, allowing final assembly to be performed close to the target markets. Such decentralization reduces transportation costs, minimizes warehousing requirements, and facilitates rapid product distribution.

Figure 1.

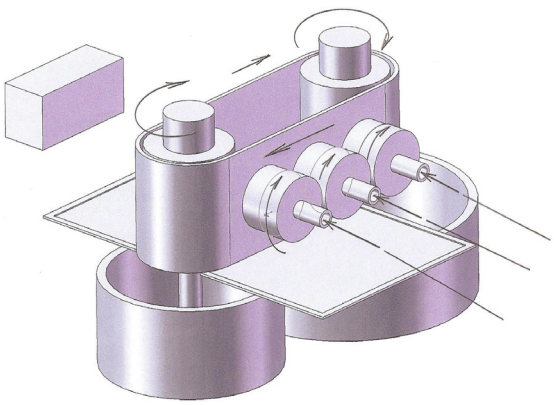

Block Diagram of a Seawater Desalination Module Utilizing High-Speed Electrochemical Salt Deposition onto a Moving Porous Cathode Manufactured from Carbon–Carbon Composite Fabric

As illustrated by the three-dimensional model of the proposed seawater desalination module, seawater is supplied to three rotating anodes, through which it is uniformly distributed onto a moving porous cathode manufactured from carbon–carbon composite fabric.

The module performs a complete cycle of high-speed electrochemical salt deposition,

during which dissolved salts contained in seawater, acting as a natural electrolyte, are continuously deposited onto the moving conveyor-type cathode.

As the cathode conveyor passes around the drive drums, the deposited salt is mechanically separated from the cathode surface and collected in a dedicated salt collection chamber.

This technology addresses one of the principal limitations of conventional reverse osmosis (RO) desalination systems, namely the discharge of highly concentrated brine back into the marine environment after desalination. In the proposed electrochemical process, dissolved salts are recovered directly as a solid product, thereby significantly reducing the environmental impact associated with concentrated brine disposal.

Furthermore, unlike membrane-based reverse osmosis technologies, the proposed approach enables the development of compact, autonomous, and modular desalination units with relatively low production capacities tailored to local requirements. For example, a single module may be designed to produce approximately 50 m³ of desalinated water per hour, providing an efficient solution for decentralized water supply systems, industrial facilities, coastal infrastructure, and remote regions requiring reliable freshwater production.

Figure 2.

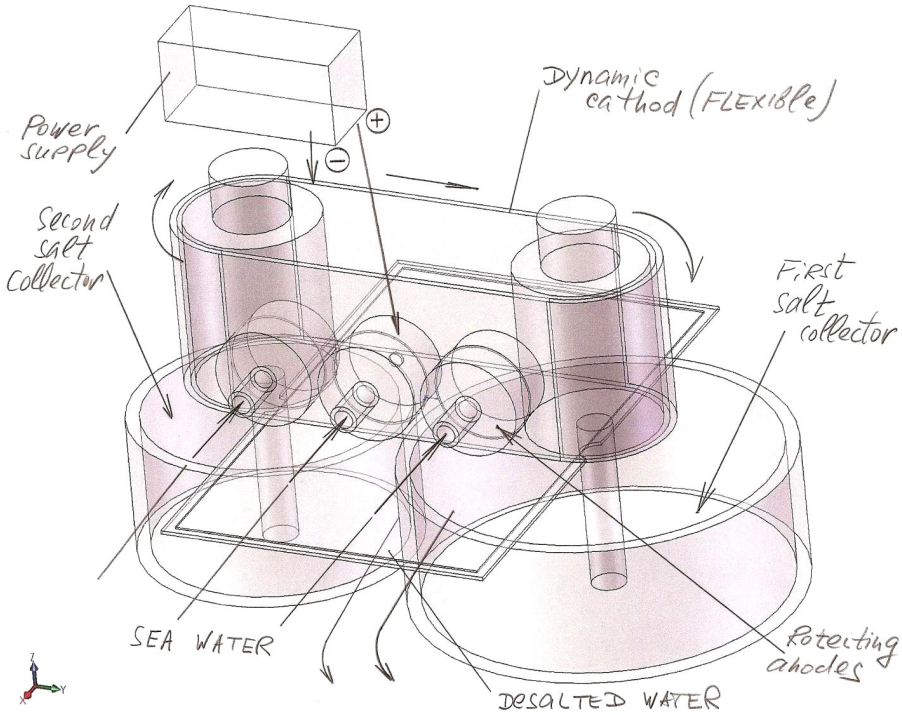

Conceptual Model of a Seawater Desalination Module Based on High-Speed Electrochemical Salt Deposition with Complete Recovery of Salt in Solid Form

Figure 2 illustrates the conceptual design of a seawater desalination module utilizing high-speed electrochemical salt deposition, enabling the complete recovery of dissolved salts from seawater in dry solid form.

As discussed previously, the application of high-speed electrochemical coating technologies, originally developed for automated production lines and flexible manufacturing modules in the microelectronics industry, makes it possible to create an entirely new generation of engineering systems operating at a significantly larger industrial scale. This technological transition demonstrates that innovative manufacturing principles developed for one industrial sector can be successfully adapted to fundamentally different technological applications.

The proposed desalination technology represents a practical example of how engineering concepts originating in precision

manufacturing can be integrated into large-scale water treatment systems through the principles of New Smart Manufacturing Technologies. Such integration facilitates the development of compact, modular, energy-efficient, and environmentally sustainable production systems capable of solving complex engineering problems using intelligent manufacturing approaches.

To further illustrate the progressive expansion of smart manufacturing principles, the following section examines the technological evolution of atmospheric water harvesting systems, demonstrating how innovative engineering concepts can be systematically enhanced by incorporating the characteristic features of New Smart Manufacturing Technologies.

Figure 3.

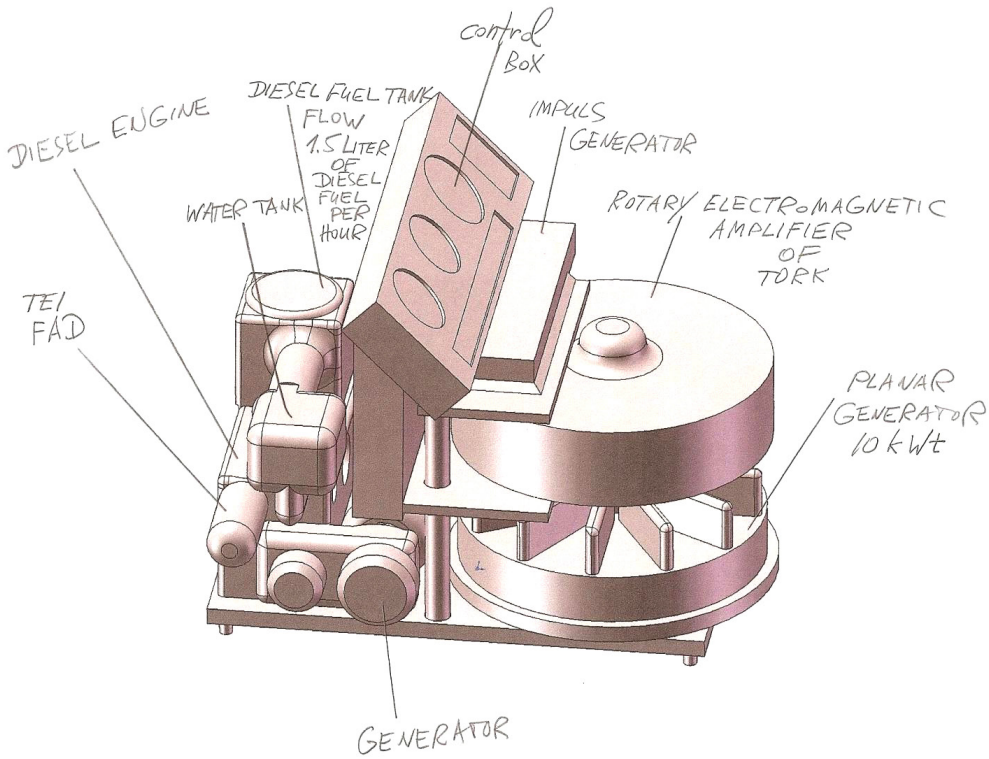

Three-Dimensional Model of an Innovative Diesel Generator Module for Atmospheric Water Harvesting Systems

Figure 3 presents a three-dimensional model of an innovative diesel generator module incorporating several advanced engineering components that establish fundamentally new operating conditions and significantly improve the performance of industrial systems designed for atmospheric water harvesting through condensation.

The proposed diesel generator module is also designed to incorporate an automatic fuel emulsion preparation and control system, together with an online fuel homogenization system. The integration of these technologies provides a number of important engineering and operational advantages, including:

- reduction of nitrogen oxide (NO_x) emissions in the exhaust gases;
- decreased fuel consumption;
- increased engine torque;
- improved vibration stability of the power generation unit;
- reduced aerodynamic noise levels during operation.

The combination of these intelligent engineering solutions contributes to enhanced energy efficiency, improved environmental performance, increased operational reliability, and optimized overall performance of atmospheric water generation systems operating under the principles of New Smart Manufacturing Technologies.

Figure 4.

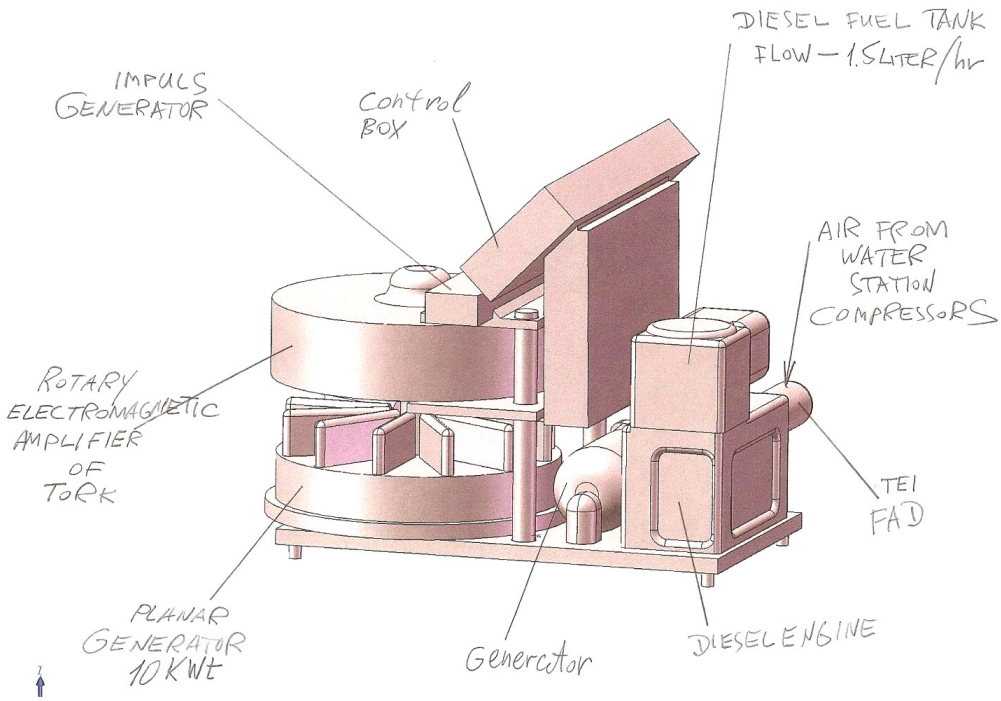

Three-Dimensional Model of an Intelligent Diesel Generator Module Incorporating Advanced Engineering Technologies

Figure 4 presents a three-dimensional model of an advanced diesel generator module integrating several of the innovative engineering technologies described above, including a planar electrical generator and a rotary electromagnetic pulse amplifier.

The diesel engine incorporated into the module is specifically designed to operate using either conventional diesel fuel or a water-fuel emulsion. The emulsion is prepared using water produced by the atmospheric water generation system, while the electrical energy required for the operation of the water production unit is supplied by the diesel generator itself, thereby forming an integrated autonomous energy and water production system.

The novelty of this comprehensive engineering solution lies in several innovative structural, functional, and system-integration aspects.

The intelligent characteristics of the proposed technology result from the synergistic combination of multiple independent engineering innovations. Each patented component provides specific technical advantages, while their integrated application creates a comprehensive package of innovative benefits that significantly exceed the performance of conventional technological solutions.

For example, the application of a rotary torque amplifier operating according to the Otto principle, in combination with a planar electrical generator capable of maintaining high efficiency even at relatively low rotational speeds, enables an increase in power generation of at least 10%.

Furthermore, the use of a water-fuel emulsion in the diesel engine substantially reduces exhaust emissions while simultaneously decreasing fuel consumption by at least 10%.

Further development of this integrated system may include the introduction of additional compressed air into the fuel emulsion preparation process, thereby transforming the conventional incompressible emulsion into a compressible air-fuel-water emulsion. This engineering approach offers additional improvements in combustion efficiency, further reductions in fuel consumption, and a significant decrease in nitrogen oxide (NO_x) emissions, resulting in enhanced environmental performance and overall operational efficiency of the power generation system.

Figure 5.

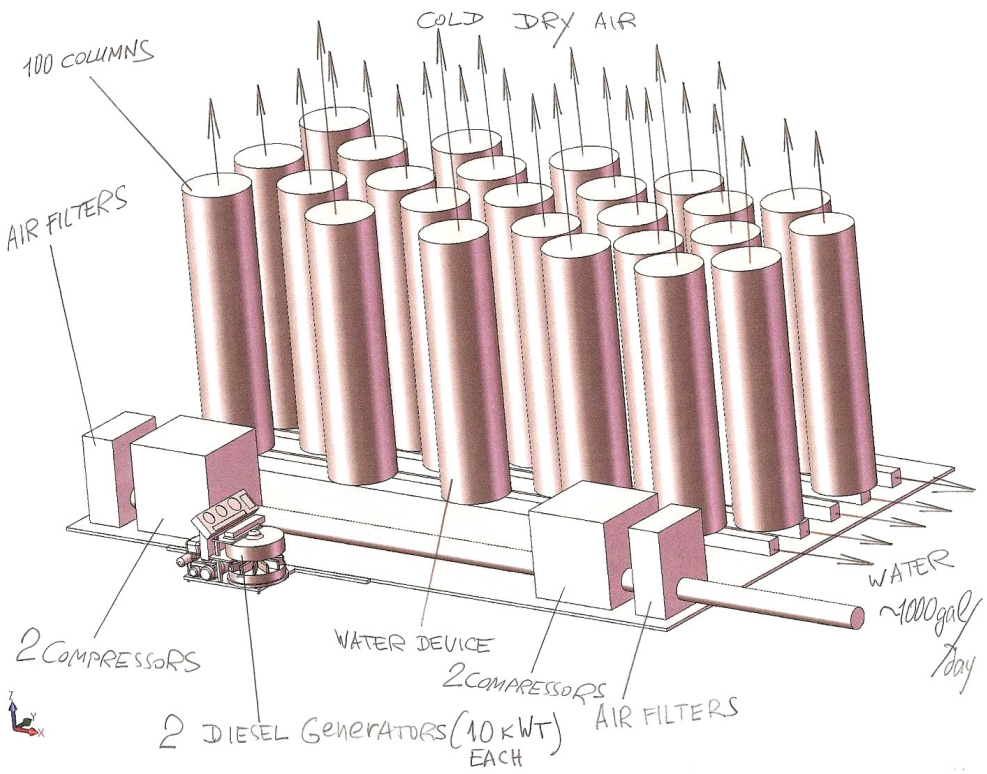

The figure presents a three-dimensional model of an industrial modular installation for water production by the condensation of atmospheric moisture.

Figure 6. *Figure 6 presents an industrial modular atmospheric water generation system based on the condensation of atmospheric moisture, shown in plan view*

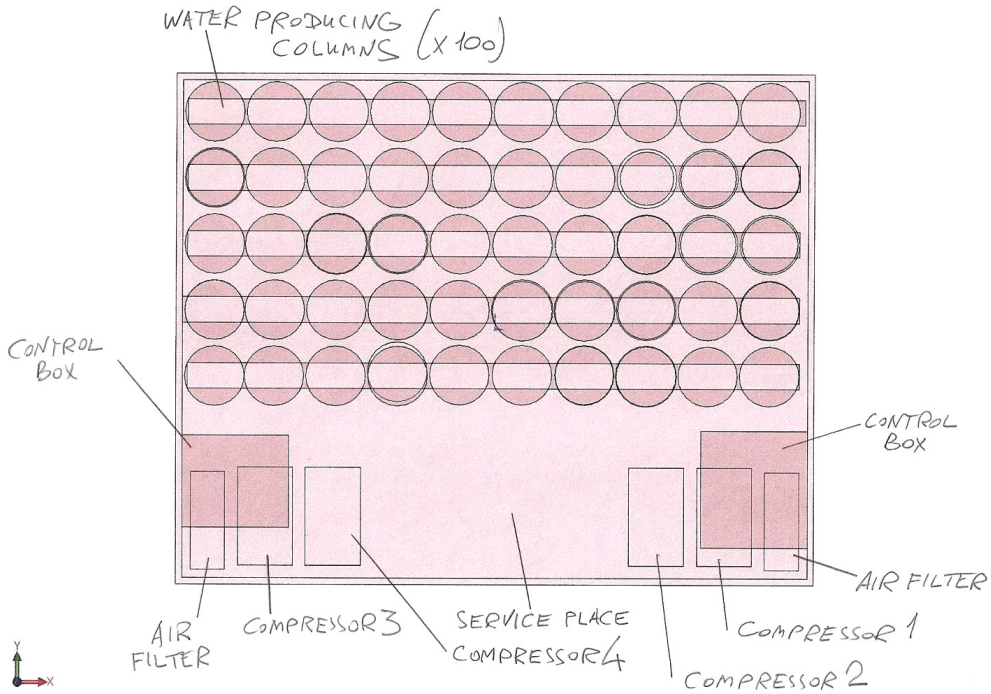

The proposed installation is designed to utilize **universal diesel generator modules**, the operating principles and technical advantages of which have been described in the preceding sections.

Figure 7. *Illustrates a new system layout providing the possibility of vertical aggregation and a substantial reduction in the production floor area required for the installation of the complete equipment incorporated into the water production complex, while providing reserve capacity for supplying surplus electrical energy to external consumers*

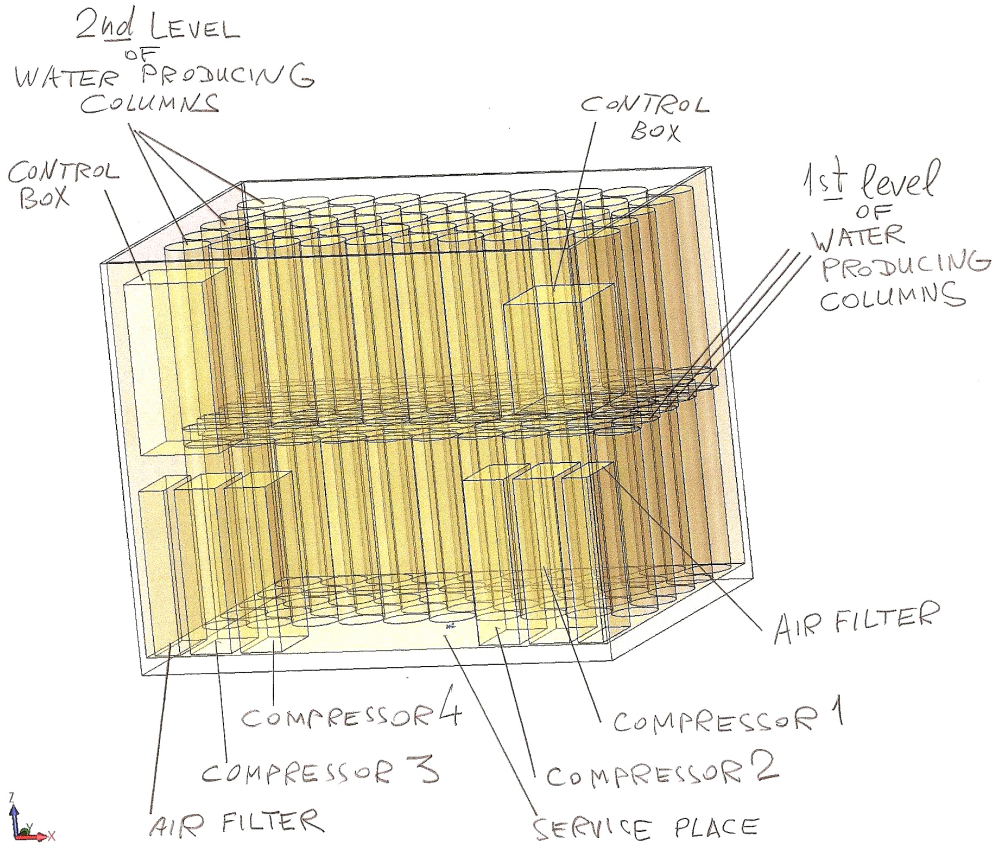

Figure 8. *Illustrates the architecture of a two-level atmospheric water generation system, identifying its principal structural and functional components*

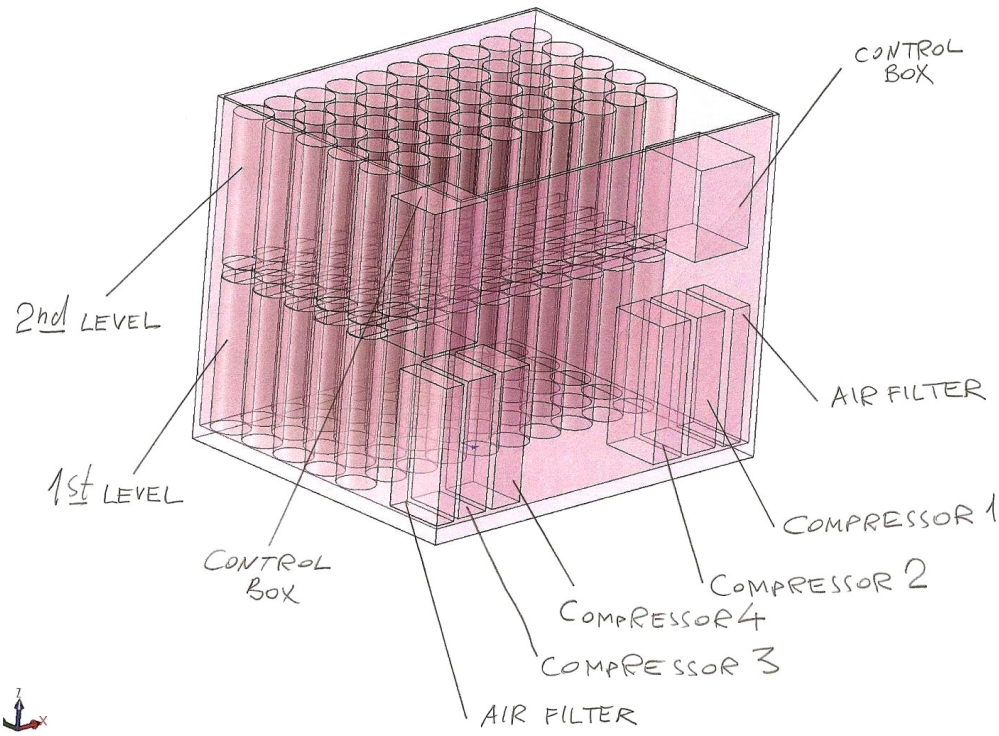

As demonstrated by the system models, the application of **New Smart Manufacturing Technologies** makes it possible to develop industrial atmospheric water generation systems characterized by **minimum specific energy consumption** and **minimal environmental impact**.

Through the application of comprehensive computer-aided modeling, the proposed system can be designed with optimally selected engineering and operational parameters. Furthermore, these parameters may be automatically optimized in accordance with external operating conditions, including atmospheric pressure at the installation site, ambient air humidity, ambient temperature, and other environmental factors that influence system performance.

The range of simulated parameters and engineering configurations may be further expanded to include numerous additional operating variables and technical characteristics of the individual system components.

In addition to optimizing the principal operating parameters, digital modeling enables the development of highly accurate schedules for preventive maintenance, technical servicing, replacement of wear components and mechanical assemblies, as well as quality control procedures for the produced water, thereby improving the overall reliability, operational efficiency, and lifecycle management of the installation.

In conclusion, it should be emphasized that New Smart Manufacturing Technologies have a significant positive impact on the comprehensive development of virtually all manufacturing systems, industrial equipment, and integrated engineering solutions.

The practical implementation of these technologies demonstrates that the integration of intelligent engineering principles, digital manufacturing technologies, advanced composite materials, and automated control systems substantially expands the functional capabilities, operational efficiency, and technological flexibility of modern production facilities.

References

Device and Method for the Extraction of Metals from Liquids. United States Patent Application US 20100224497 A1, September 9, 2010.

Magnet Assembly with Reciprocating Core Member and Associated Method of Operation. United States Patent US 6,188,151 B1, February 13, 2001.

Rotary Valve Internal Combustion Engine. United States Patent US 9,951,685 B2, April 24, 2018.

Rotary Internal Combustion Engine with Exhaust Purge. United States Patent US 9,926,842 B2, March 27, 2018.

Power Transmission Device and Lock-Up Device for Torque Converter. United States Patent US 9,915,329 B2, March 13, 2018.

Naruoka, T., et al. *Rotary Unit of Supercharger for Engine and Balance Adjustment Method Thereof*. United States Patent US 9,945,288 B2, April 17, 2018.

Dedicated Exhaust Gas Recirculation System. United States Patent US 9,932,939 B2, April 3, 2018.

submitted 15.06.2026;
accepted for publication 29.06.2026;
published 31.08.2026
© Marakshyn S.
Contact: 3338830@gmail.com

Austrian Journal of Technical
and Natural Sciences, 2026 No 7–8
ISSN 2310-5607

PREMIER Publishing
ppublishing.org

Section 6. Transport

DOI:10.29013/AJT-26-7.8-129-134

CC BY

THE HIDDEN COST LAYER: DEADHEAD, UTILIZATION THRESHOLDS, AND MARGIN FORMATION IN FREIGHT CARRIER OPERATIONS

Shevchenko Maxim Igorevich [1]

[1] Head of the Transport Analytics Laboratory, Institute of Applied Transportation Management Systems, Kazan

Cite: *Shevchenko M.I. (2026). The Hidden Cost Layer: Deadhead, Utilization Thresholds, and Margin Formation in Freight Carrier Operations. Austrian Journal of Technical and Natural Sciences 2026, No 7–8.* https://doi.org/10.29013/AJT-26-7.8-129-134

Abstract

Carrier operating cost reported as a single per-mile figure conceals a compositional structure that determines profitability. This paper synthesizes econometric, technical, and carrier-economics literatures around one organizing question: how does a reduction in deadhead mileage or an improvement in fleet utilization translate into margin, and does that translation depend on where the affected assets sit relative to a break-even threshold? The analysis applies a cost-decomposition and threshold-translation method built on published literature. It separates operating cost into a visible layer and a submerged layer comprising detention, deadhead, and administrative friction, and it evaluates routing, network, and procurement interventions according to whether they plausibly move a fleet segment across its break-even utilization floor. The synthesis shows that algorithmic routing advances set a ceiling on deadhead reduction; carrier scale, network topology, and procurement structure set a floor beneath which no algorithmic gain can compensate for structural disadvantage.

Keywords: *deadhead reduction; fleet utilization; break-even threshold; submerged cost; carrier margin; vehicle routing; freight carrier economics*

Introduction

Operating cost reported as a single per-mile figure conceals a compositional structure that determines whether a freight carrier is profitable. Treating that figure as a flat ledger obscures exactly the variation that determines margin. A narrow set of cost drivers accounts for most of the variance in carrier margin. The remainder splits between two layers: a visible one that appears directly on profit-and-loss statements, and a submerged one that erodes margin without registering as a discrete line item. Doskach (2026 b) describes this distinction as a cost iceberg: detention time, deadhead repositioning, and administrative friction together account for

a further 14 to 22 percent of effective operating cost once the opportunity cost of idle capital equipment is included. Doskach develops this cost-iceberg framework from direct observation of carrier operations, drawing on the kind of granular detail that rarely surfaces in industry-facing reporting.

Doskach's (2026 a) break-even utilization floor is the minimum weekly loaded-mile threshold below which a given truck generates negative net revenue. Below that floor, submerged cost stops being a marginal drag and starts determining whether the asset is profitable at all. Absorbing a deadhead mile costs a carrier operating comfortably above the floor only reduced profit. The same mile costs a carrier operating near or below it the difference between solvency and loss on that unit of equipment. Crossing the floor changes an asset's profitability status. That threshold structure is the object this paper analyzes.

Econometric, technical, and carrier-economics literatures each address a piece of this problem without connecting them. Econometric studies of empty miles quantify the scale of the deadhead problem and its structural causes, yet stop short of translating a percentage-point reduction into a margin effect that depends on where an affected vehicle sat relative to a profitability threshold. Vehicle-routing research has produced increasingly capable algorithms for reducing deadhead and improving dispatch efficiency. Those algorithms are evaluated almost exclusively against distance or cost objectives, disconnected from the threshold-crossing logic that determines whether an efficiency gain changes a carrier's solvency. Carrier-economics research on scale, procurement, and network structure explains why margin varies across carriers and segments, without incorporating the submerged-cost decomposition that identifies where that variance originates operationally.

Materials and Methods

This paper applies a cost-decomposition and threshold-translation method built on the published literature synthesized below. A submerged-cost taxonomy, introduced above, supplies the decomposition mechanism, separating operating cost into visible line items and a submerged layer comprising detention, deadhead, and administrative friction that behaves differently from the visible layer under threshold-crossing analysis. Doskach's (2026 a) break-even utilization floor supplies the translation mechanism: a claimed efficiency improvement, whether from routing technology, network redesign, or procurement strategy, is evaluated according to whether it plausibly moves the fleet segment it addresses across a profitability threshold, not according to its raw magnitude alone.

This paper draws evidence from four bodies of literature, moving from the scale of the deadhead problem to the mechanisms available for reducing it, the carrier-level structures that determine how much of a reduction actually reaches margin, and the exogenous shocks that test whether that architecture holds under stress. Econometric studies of empty-mile incidence and its structural causes establish the scale of the deadhead problem and the mechanisms generating it (Yang, 2024; Heilmann, 2020; Allen et al., 2024). Technical operations-research literature on vehicle routing establishes the algorithmic solution space available for deadhead reduction and its performance characteristics under realistic demand uncertainty (Nazari et al., 2018; Kool et al., 2019; Ulmer et al., 2020). Carrier-economics literature on scale, network structure, and procurement establishes how margin varies across carrier configurations independent of any single routing intervention (Miller & Muir, 2020; Muir et al., 2019; Acocella & Caplice, 2023; Acocella et al., 2020; Owczarek, 2024; Rodrigue, 2020; Solakivi & Ojala, 2024; Izadi et al., 2019). Regulatory and technology-shock literature establishes how an exogenous change to the operating environment stresses margin architecture and reveals which carriers were operating close to a profitability threshold before the shock (Scott et al., 2021; Miller et al., 2021; Trick et al., 2021; Miller, Muir, et al., 2020).

This design carries limitations that follow directly from its structure, and the most consequential concerns the evidentiary status of the cost-decomposition figures themselves. The percentages attached to the submerged-cost taxonomy applied here originate in a practitioner synthesis (Doskach, 2026 b) and have not been independently replicated against the carrier-level panel data used elsewhere in this

paper. The threshold logic built on this taxonomy treats the figures as illustrative of an order of magnitude documented in industry practice; the argument holds regardless of whether any single percentage is exactly correct.

Results

Fuel, driver wages, equipment depreciation, and insurance dominate visible operating cost, and carriers that manage exclusively against this visible total systematically misallocate improvement effort. Izadi et al. (2019), reviewing cost models used across the road freight literature, found that the majority of published models categorize cost by broad functional type, such as operational, value-of-time, and external cost, without a structural mechanism for identifying which categories respond nonlinearly to utilization change; this gap is precisely what Doskach's (2026 b) submerged-cost taxonomy addresses, separating fixed, variable, and quasi-fixed cost components and showing that the quasi-fixed category generates discontinuous margin cliffs as utilization crosses replacement-cycle thresholds, a step pattern that conventional per-mile accounting cannot represent.

A carrier whose utilization sits just below a quasi-fixed threshold, such as a tire replacement cycle or a maintenance interval, absorbs the full fixed component of that cost over a smaller loaded-mile base than a carrier whose utilization crosses the threshold. The distinction changes which carriers stay solvent. Two carriers with identical average deadhead percentages can face materially different margin outcomes depending on which side of a quasi-fixed threshold their fleets predominantly occupy, a distinction that a single aggregate deadhead statistic cannot reveal and that motivates the threshold-based framework this paper applies throughout.

The practical consequence extends to how carriers allocate improvement budgets. A capital investment in equipment-focused efficiency, such as an aerodynamic retrofit, produces a bounded and well-documented improvement on a cost category that is already visible and already accounted for in most fleet budgets. A comparable investment directed at dispatch-layer coordination targets the submerged category directly, and because that category is measured poorly or not at all in conventional reporting, its baseline is frequently understated and its achievable improvement correspondingly underestimated by managers comparing the two investment options using visible-cost metrics alone. This measurement asymmetry drives the persistent industry pattern of overinvestment in equipment specification relative to dispatch coordination. The underlying economic opportunity in the two categories is the same.

The mechanisms generating empty miles have been isolated with increasing precision at the level of individual carrier decisions. Heilmann (2020), studying how a digital freight brokerage platform introduced an algorithmic load-bundling feature, estimated a 22.6 percent reduction in deadhead miles following adoption, equivalent to an increase in measured truck utilization from 81.6 to 85.8 percent, and attributed the improvement specifically to resolving information frictions that had previously prevented drivers from identifying compatible return loads within their available operating window. Allen et al. (2024), documenting trip-chaining behavior among Colombian truckers, found that drivers frequently construct complex multi-stop sequences instead of executing simple out-and-back trips, avoiding empty repositioning by design, evidence that deadhead avoidance behavior is already a first-order consideration in driver decision-making, and that further gains depend on improving the information available to support that behavior.

Vehicle routing research has approached deadhead reduction primarily as an algorithmic optimization problem. Two methodological shifts over the past decade show how far that toolkit has moved. Nazari et al. (2018) demonstrated that a reinforcement-learning policy trained through policy-gradient methods could match or exceed classical routing heuristics on stochastic capacitated instances without hand-engineered rules specific to a given network structure. Kool et al. (2019) extended this approach with an attention-based encoder-decoder architecture, showing that self-attention mechanisms generalize across routing problem variants more effectively than recurrent alternatives, a property directly relevant to carriers whose lane structure changes as their customer base evolves.

Ulmer et al. (2020) formalized the distinction between static and dynamic routing architectures, which determines which of these algorithmic advances actually reduce deadhead in practice. Policies that incorporate anticipated future demand information systematically outperform reactive dispatch rules under conditions of meaningful demand uncertainty, and the performance gap between the two widens as uncertainty increases. Static planning performs within a narrow margin of dynamic optimization under low volatility, but that gap grows large enough under high volatility to determine whether a fleet segment operates above or below a utilization threshold. This threshold sensitivity connects Ulmer's routing finding directly to the threshold framework applied throughout this paper: an algorithmic improvement that appears modest when measured in average deadhead percentage can be consequential when it disproportionately benefits vehicles operating near the break-even floor.

The value of anticipatory routing varies sharply across a carrier's network, a point the aggregate performance statistics in this literature tend to obscure. Because static planning already approximates the dynamic optimum under low volatility, lanes with stable, predictable demand gain comparatively little from a shift toward forecast-integrated dispatch; the disproportionate gains sit instead on lanes with volatile, thin, or seasonally concentrated demand, precisely where reactive dispatch diverges furthest from an anticipatory policy. A carrier deploying dynamic routing technology uniformly across its network, without segmenting lanes by volatility, captures only a fraction of the available benefit on its most valuable lanes and still pays the full implementation cost across lanes where the technology adds little.

Network topology sets a further ceiling on how much of a routing algorithm's theoretical gain a carrier can actually realize, because it determines whether deadhead is reabsorbed or simply relocated. Point-to-point structures generate deadhead at the destination of every unmatched load, since no return network exists to reabsorb it; Rodrigue (2020) contrasts this with hub-and-spoke topologies, which absorb the same deadhead through network-level backhaul balancing instead of letting it accumulate at the endpoint. Equipment choice interacts with this topology constraint instead of substituting for it: Solakivi and Ojala (2024), comparing high-capacity trucks against standard semitrailers, found that larger vehicles are not uniformly more cost-efficient, since their advantage depends on achieving a higher load factor than the equipment they replace, which confirms that utilization determines realized margin more than equipment specification alone does.

Procurement structure determines how much of a utilization gain survives contact with the market a carrier actually sells into. Acocella and Caplice (2023), reviewing the truckload procurement literature comprehensively, identified a persistent gap between strategic procurement decisions and execution-stage outcomes, with committed capacity frequently going unused or unavailable capacity being sourced at spot-market premiums that erode the margin a routing improvement would otherwise deliver. This execution-stage gap varies across carriers: Acocella et al. (2020) found that carrier behavior in response to shipper tender patterns varies systematically between carriers that behave reciprocally, accepting a stable volume in exchange for stable future tenders, and those that behave opportunistically, which is why the margin benefit of a utilization improvement depends on the shipper relationship structure within which it operates as much as on the improvement itself. Because relationship structure mediates how much of a utilization gain a carrier retains, the pricing mechanism through which that gain converts into revenue matters just as much: Owczarek (2024), modeling less-than-truckload pricing for light commercial vehicles, showed that the intensity of vehicle usage and the number of loading and unloading points jointly determine achievable pricing, confirming at the carrier level that utilization intensity functions as a pricing variable in its own right, beyond its role as a cost input.

These procurement-side findings interact with the threshold framework in a way that is easy to overlook. A carrier whose fleet sits near its break-even floor is also the carrier with the least slack to absorb the spot-market premiums that Acocella and Caplice (2023) identify as a common consequence

of procurement mismatch. The same undercapitalization that pushes a fleet toward its utilization threshold in the first place also limits that fleet's ability to negotiate the kind of reciprocal shipper relationship that Acocella et al. (2020) find reduces opportunistic exposure, so the carriers most exposed to threshold-crossing risk from deadhead are frequently the same carriers least equipped to manage procurement-side margin risk through relationship structure alone.

Discussion

The evidence assembled here supports a layered view of utilization, whose components determine margin through different mechanisms instead of through one performance percentage. Doskach's (2026b) distinction between the visible and submerged cost layers explains why carriers that manage exclusively against reported per-mile cost systematically underinvest in dispatch-layer improvement relative to equipment-focused interventions with smaller theoretical ceilings but greater accounting visibility. This visible/submerged distinction functions as a practical prioritization tool: it identifies which specific lever, dispatch-layer coordination or equipment-focused investment, a given carrier should prioritize given its position relative to the break-even floor, instead of leaving that choice to whichever category happens to be easier to measure.

The routing literature and the carrier-economics literature synthesized in this paper answer different questions that are frequently conflated in practice. Nazari et al. (2018), Kool et al. (2019), and Ulmer et al. (2020) establish that algorithmic dispatch improvement is technically achievable and that its value scales with demand uncertainty, a finding about the ceiling on deadhead reduction; Miller and Muir (2020), Muir et al. (2019), and Rodrigue (2020) show that the same routing improvement produces different margin outcomes depending on carrier scale, specialization, and network topology, which sets the floor beneath which no algorithmic improvement can compensate for structural disadvantage. A carrier evaluating a routing technology investment needs both answers, and treating the algorithmic ceiling as sufficient evidence of margin recovery, without reference to the carrier's position relative to its break-even floor, overstates the return that investment will deliver.

The regulatory and turnover evidence reviewed in this paper indicates that margin architecture is tested most clearly during shocks, when carriers already close to their break-even thresholds are pushed across them by a uniform external change. Scott et al. (2021) and Miller et al. (2021) show that a uniform compliance mandate produces uneven consequences precisely because carriers entered the shock at different positions relative to their break-even thresholds, a pattern consistent with the threshold-crossing logic this paper applies to deadhead reduction.

Conclusion

The threshold-translation method applied throughout this paper changes what an efficiency claim has to answer. A percentage-point reduction in deadhead, or a percentage-point gain in utilization, carries no fixed margin value on its own: its value depends on where the affected fleet segment sat relative to its break-even floor before the intervention. Routing technology sets a ceiling on how much deadhead a carrier can eliminate; carrier scale, network topology, and procurement structure set the floor beneath which no amount of algorithmic improvement closes the remaining gap. Regulatory mandates and driver turnover reveal this floor instead of creating it: they push already-exposed carriers across a line that was there before the shock.

References

Acocella, A., & Caplice, C. (2023). Research on truckload transportation procurement: A review, framework, and future research agenda. Journal of Business Logistics, – 44(2). – P. 228–256. URL: https://doi.org/10.1111/jbl.12333

Acocella, A., Caplice, C., & Sheffi, Y. (2020). Elephants or goldfish? An empirical analysis of carrier reciprocity in dynamic freight markets. Transportation Research Part E: Logis-

tics and Transportation Review, 142, Article 102073. URL: https://doi.org/10.1016/j.tre.2020.102073

Allen, T., Atkin, D., Cantillo Cleves, S., & Hernández, C. E. (2024). The traveling trucker problem. AEA Papers and Proceedings, – 114. – P. 334–339. URL: https://doi.org/10.1257/pandp.20241044

Doskach, H. (2026 a). Building a profitable trucking company in the U.S. LAP LAMBERT Academic Publishing.

Doskach, H. (2026 b). Logistics efficiency and cost reduction strategies. LAP LAMBERT Academic Publishing.

Heilmann, K. (2020). Information frictions, load matching, and route efficiency in the trucking industry (SSRN Working Paper No. 3545019). URL: https://doi.org/10.2139/ssrn.3545019

Izadi, A., Nabipour, M., & Titidezh, O. (2019). Cost models and cost factors of road freight transportation: A literature review and model structure. Fuzzy Information and Engineering, – 11(3). – P. 257–278. URL: https://doi.org/10.1080/16168658.2019.1706960

Kool, W., van Hoof, H., & Welling, M. (2019). Attention, learn to solve routing problems! International Conference on Learning Representations (ICLR 2019).

Miller, J. W., & Muir, W. A. (2020). A new perspective on returns to scale for truckload motor carriers. Journal of Business Logistics, – 41(3). – P. 236–258.

Miller, J. W., Muir, W. A., Bolumole, Y., & Griffis, S. E. (2020). The effect of truckload driver turnover on truckload freight pricing. Journal of Business Logistics, – 41(4). – P. 294–309. URL: https://doi.org/10.1111/jbl.12252

Miller, J. W., Scott, A., & Williams, B. (2021). Pricing dynamics in the truckload sector: The moderating role of the electronic logging device mandate. Journal of Business Logistics, – 42(4). – P. 388–405. URL: https://doi.org/10.1111/jbl.12256

Muir, W. A., Miller, J. W., Griffis, S. E., Bolumole, Y. A., & Schwieterman, M. A. (2019). Strategic purity and efficiency in the motor carrier industry: A multiyear panel investigation. Journal of Business Logistics, – 40(3). – P. 204–228.

Nazari, M., Oroojlooyjadid, A., Snyder, L. V., & Takáč, M. (2018). Reinforcement learning for solving the vehicle routing problem. Advances in Neural Information Processing Systems, – 31. – P. 9839–9849.

Owczarek, P. (2024). Price valuation modeling of less-than-truckload (LTL) shipments for financial continuity assurance. European Research Studies Journal, – 27(3). – P. 209–224.

Rodrigue, J.-P. (2020). The geography of transport systems (5th ed.). Routledge.

Scott, A., Balthrop, A., & Miller, J. W. (2021). Unintended responses to IT-enabled monitoring: The case of the electronic logging device mandate. Journal of Operations Management, – 67(2). – P. 152–181. URL: https://doi.org/10.1002/joom.1110

Solakivi, T., & Ojala, L. (2024). Environmental and economic potential of high-capacity trucks. Case Studies on Transport Policy. URL: https://doi.org/10.1016/j.cstp.2024.101284

Trick, S., Peoples, J., & Ross, A. (2021). Driver turnover in the trucking industry: What's the cost of reducing driver quit rates? Research in Transportation Economics, 89, Article 101129. URL: https://doi.org/10.1016/j.retrec.2021.101129

Ulmer, M. W., Goodson, J. C., Mattfeld, D. C., & Thomas, B. W. (2020). On modeling stochastic dynamic vehicle routing problems. EURO Journal on Transportation and Logistics, 9, Article 100008. URL: https://doi.org/10.1016/j.ejtl.2020.100008

Yang, R. (2024). Geographic imbalance, search frictions, and regulation: Causes of empty miles in freight trucking (World Bank Policy Research Working Paper No. 10775).

submitted 15.06.2026;
accepted for publication 29.06.2026;
published 31.08.2026
© Shevchenko M. I.
Contact: shevchenkomaksig@gmail.com

Austrian Journal of Technical
and Natural Sciences, 2026 No 7–8
ISSN 2310-5607

PREMIER Publishing
ppublishing.org

Section 7. Technical sciences. Applied research

DOI:10.29013/AJT-26-7.8-135-144

CC BY

SYSTEMIC IMPLEMENTATION OF INNOVATION IN THE TEXTILE INDUSTRY (Innovation and Its Systemic Implementation Under Contemporary Conditions in the Light Industry Sector. Methodology for Developing Innovation Motivation According to the Creative Design System of Malyeryk Khrystyna)

Tatiana Chyrka [1]

[1] *Owner of the ZHYVA brand and a manufacturing company specializing in the production of contemporary women's apparel for various fashion brands. Lviv, Ukraine*

Cite: *Chyrka T. (2026). Systemic Implementation of Innovation in the Textile Industry. (Innovation and Its Systemic Implementation Under Contemporary Conditions in the Light Industry Sector. Methodology for Developing Innovation Motivation According to the Creative Design System of Malyeryk Khrystyna). Austrian Journal of Technical and Natural Sciences 2026, No 5–6.* https://doi.org/10.29013/AJT-26-7.8-135-144

Abstract

The article examines the relationship between innovation and its creator, with particular emphasis on the role of professional reputation, knowledge, creativity, and expertise in determining the successful development and practical implementation of innovative solutions. The limitations of existing innovation financing mechanisms and investment models in supporting the sustainable development of innovation-oriented projects are considered. Particular attention is given to the importance of education, continuing professional development, and specialized training in strengthening the innovative and creative potential of specialists. The article substantiates the need for new educational models adapted to advanced manufacturing technologies, digital production systems, and knowledge-driven innovation. The development of innovation competencies and interdisciplinary thinking is considered an essential prerequisite for enhancing specialists' ability to generate, develop, and successfully implement innovative solutions in the modern textile and light industry sectors.

Keywords: *Systemic implementation of innovation; systemic implementation of innovation in the textile industry and the production of innovative textile materials; innovation motivation according to the creative design system of Malyeryk Khrystyna; assessment of the nature and outcomes of implementing an innovation model; systematic organization and management of innovation projects and innovation-oriented initiatives; innovation process management practices; specialized professional development programs and advanced training for emerging professions created by the transition of industrial production toward high technologies and digital manufacturing*

Innovation and Its Systemic Implementation Under Contemporary Conditions; A Methodology for Developing Innovative Design Motivation According to the Malyeryk Khrystyna System

Innovation cannot be separated from its creator.

Behind every innovation stands its author, and very often the personality and talent of the creator determine both the nature of the innovation and the outcome of implementing each innovative idea.

The creative reputation of an author or inventor is the hallmark and public face of an innovative product or technology.

In our opinion, conducting lotteries whose proceeds may help finance innovation processes neither solves nor, in principle, can solve the problem of insufficient funding for the systematic and consistent development of innovation infrastructure.

Likewise, the latest approaches, techniques, and methods of organizing investments provide only limited support for the purposeful and systematic implementation of innovation projects or projects of an innovative nature.

One of the fundamental reasons for this situation is the association of a project with the creative work of a particular inventor. As a rule, investors trust certain inventors, often anticipating each new invention created by them, while paying little attention to the work of others.

As demonstrated by the practice of innovation management, for the statistically average generator of ideas and future inventor, successful promotion of ideas and inventions is largely determined by the fundamental education received, beginning with secondary school, continuing through higher education, and, most importantly, in the opinion of the authors of this publication, through specialized continuing education courses and new professional orientation programs developed in response to the transition of modern industry toward advanced and digital technologies.

Research in this direction is ongoing, and publications reporting the results of such studies continue to appear regularly.

Many researchers first turn to the study of the genetic characteristics of future generators of innovative ideas and founders of innovative start-ups. One such example is presented below.

Scientists have identified hereditary characteristics associated with improved electrical conductivity of signals in the brain and with higher intelligence test scores.

The study involved 472 volunteers from Australia, including 85 pairs of genetically identical (monozygotic) twins, 100 pairs of non-identical twins, as well as their biological brothers and sisters. During the study, the participants completed IQ tests and underwent magnetic resonance imaging (MRI).

The researchers examined the volume of specific brain structures and the characteristics of nerve impulse transmission by neurons. They measured the electrical insulation of individual nerve fibers, with higher insulation corresponding to faster signal transmission by neurons. The obtained results were then compared with the participants' genetic data.

The researchers identified 24 variants of six genes associated with improved electrical conductivity in the brain. These variants represented single-nucleotide polymorphisms (SNPs) – variations in the DNA sequence involving a single nucleotide. In addition to improved electrical conductivity, several of the identified polymorphisms were also associated with intelligence test scores that were several points higher.

According to the analysis, the genes containing these polymorphisms formed a functional network, in which the presence of a favorable variant of one gene enhanced the performance of another. In other words, these "intelligence-associated" polymorphisms exhibited a synergistic effect.

Previously, the same authors published a study identifying genetic characteristics that influence the volume of the hippocampus, a brain structure associated with memory and emotions.

Many leading technology companies invest substantial resources in artificial intelligence research. One widely discussed example involved the development of a large-scale artificial neural network capable of independently recognizing visual objects. According to published reports, researchers trained the system using large collections of unlabeled images extracted from online vid-

eo resources. During the learning process, the neural network successfully developed the ability to recognize images of cats, as well as human faces and bodies, without explicit human supervision.

Although the ability to recognize cats may appear trivial from a human perspective, it represented an important milestone in artificial intelligence research. This result is frequently discussed in the context of Moravec's paradox, which states that tasks humans perform effortlessly, such as visual perception and object recognition, are often significantly more difficult for computers than highly structured intellectual activities such as playing chess or solving mathematical problems.

The researchers themselves emphasized that their artificial neural network remained extremely limited in comparison with the human visual cortex, whose number of neurons and synaptic connections exceeds that of artificial systems by many orders of magnitude. This observation suggests that successful progress in artificial intelligence requires not only computational resources but also scientifically grounded methodologies, interdisciplinary research teams, and systematic engineering approaches.

Regardless of their immediate practical outcomes, such investigations contribute to a deeper understanding of existing scientific and technological challenges. At the same time, there remains a noticeable shortage of effective methodological frameworks capable of systematically overcoming complex engineering problems encountered during innovation processes.

From the perspective of practical invention and engineering design, one of the most comprehensive methodological approaches remains the Theory of Inventive Problem Solving (TRIZ) together with the Algorithm of Inventive Problem Solving (ARIZ). These methodologies provide structured analytical tools for identifying technical contradictions, generating innovative concepts, and guiding the systematic development of engineering solutions across projects of varying complexity.

Successful application of TRIZ and ARIZ requires considerably more than theoretical familiarity with their principles. In addition to comprehensive engineering knowledge and practical design experience, specialists must possess the ability to creatively adapt these methodologies to real industrial conditions while taking into account the specific technological constraints of each innovation project.

Particularly important for innovation projects implemented in the United States is the ability of multidisciplinary specialists to combine expertise in the fundamental sciences with practical knowledge of TRIZ and ARIZ while simultaneously understanding U.S. engineering standards, regulatory requirements, and industrial design practices. Such interdisciplinary competence enables more effective adaptation of innovative concepts to the technical, legal, and commercial requirements of specific projects.

It should also be recognized that the technological environment existing at the time TRIZ and ARIZ were originally developed differed substantially from today's digital engineering landscape. Their successful application therefore requires integration with modern computational technologies, including digital product design, computer simulation, virtual prototyping, and engineering animation. Combining the universal principles of TRIZ and ARIZ with contemporary computer-aided design technologies significantly expands the effectiveness of innovative engineering development.

Numerous attempts have been made to establish educational programs capable of preparing comprehensively trained innovation specialists possessing both deep engineering knowledge and creative problem-solving skills. However, these efforts have frequently encountered substantial methodological and organizational challenges.

A significant step toward addressing this issue was achieved through the development of a structured methodology for cultivating innovation-oriented design motivation. Unlike educational approaches based primarily on spontaneous creativity or intuitive idea generation, this methodology emphasizes a systematic understanding of TRIZ and ARIZ and their close relationship with the fundamental principles of science, particularly classical physics, engineering, and industrial design.

The principal contribution of Malyeryk Khrystyna, the author of this educational methodology, lies in combining

multidisciplinary professional education with extensive practical experience in applying TRIZ and ARIZ to resolve complex technical contradictions. Through academic study, professional training, and research conducted at universities in the United States, she acquired a comprehensive understanding of contemporary approaches to technological innovation and identified effective methods for integrating these practices into educational programs based on TRIZ and ARIZ.

As a result of her academic and professional activities in the United States, she developed more than twenty educational and pedagogical integrative teaching concepts representing pioneering instructional innovations. She subsequently published more than ten scientific articles and methodological guidelines presenting practical recommendations and structured instructional approaches intended for specialists engaged in the development of innovative products and advanced technologies supporting the innovation ecosystems of the United States and other countries.

TRIZ and ARIZ in the Contemporary Innovation Environment

To begin, let us return to the current understanding of the Theory of Inventive Problem Solving (TRIZ) and the Algorithm of Inventive Problem Solving (ARIZ).

Modern TRIZ encompasses several schools of thought that continue to develop the classical methodology while introducing new concepts and disciplines that were not originally included in the classical framework. The technically mature core of classical TRIZ – including the Inventive Principles, ARIZ, and Substance-Field (Su-Field) Analysis – has remained largely unchanged. Consequently, the activities of many contemporary TRIZ schools are directed primarily toward reinterpretation, restructuring, and promotion of the methodology rather than toward expanding its technical foundation. As a result, their work is often considered to have a stronger philosophical and educational orientation than a purely engineering focus. Today, TRIZ is actively applied in areas such as business management, marketing, advertising, education, the arts, and early childhood development, although it was originally created as a systematic methodology for engineering creativity and technological innovation.

Classical TRIZ represents a general engineering methodology. However, effective practical application requires the development of specialized versions adapted to specific technological domains. Such specialized versions differ in the structure and content of their knowledge bases, analytical tools, and engineering information resources. Several major industrial corporations have already adapted selected TRIZ principles to their own technological environments. In our opinion, a specialized version of TRIZ should likewise be developed for startup companies, emphasizing the rapid commercialization of innovative technologies and products.

At present, no specialized versions of TRIZ have been developed specifically to stimulate scientific discoveries in disciplines such as physics, chemistry, biology, or related natural sciences.

As a designer of beachwear collections, Malyeryk Khrystyna approached this issue critically by examining the logical relationships between the fundamental principles of industrial design and innovative engineering concepts, which frequently extend beyond the classical frameworks of exact sciences and traditional engineering disciplines.

One of the principal limitations affecting further development of TRIZ is the absence of a comprehensive methodology for analyzing initial problem situations, diagnosing technological contradictions, and forecasting future engineering challenges that subsequently become the objectives of innovation. Addressing this limitation requires the development of a modern design methodology focused on creating solutions that are compatible with future technological requirements. The educational methodology developed by Malyeryk Khrystyna significantly reduces these limitations by directing students' analytical capabilities and creative potential toward the most promising innovation pathways.

Another important trend in technological development is the growing importance of intellectual property protection. As competition for authorship and ownership of tech-

nological innovations increases, so does the demand for personnel capable of generating patentable engineering solutions. Consequently, innovation activities require increasingly sophisticated methodological support, educational frameworks, and software tools. From this perspective, the theoretical foundations supporting innovation should continue to expand rather than remain restricted to traditional interpretations.

While the successors of Genrich Altshuller have understandably preserved the classical interpretation of TRIZ, contemporary technological realities create opportunities for complementary methodological developments. Such developments do not replace classical TRIZ but instead extend its practical applicability under modern engineering conditions. To avoid unnecessary methodological disputes, newly developed approaches to innovation modeling may appropriately receive independent designations while remaining conceptually compatible with the fundamental principles established by classical TRIZ.

The widespread adoption of computer-aided engineering technologies has fundamentally transformed modern product development. Today it has become increasingly difficult to distinguish between virtual engineering activities and traditional industrial design, as both have become integrated components of a unified development process.

According to Malyeryk Khrystyna, the most effective mechanism for integrating classical engineering principles with modern digital technologies is a systematic educational methodology based on composition-oriented learning. Within this framework, the fundamental laws of classical physics and theoretical mechanics are taught simultaneously with three-dimensional computer-aided design, digital modeling, engineering simulation, and virtual representation of physical processes.

Such an educational methodology enables learners of different educational levels and professional backgrounds to combine classical engineering knowledge with advanced digital technologies in balanced proportions, thereby maximizing both creative efficiency and engineering effectiveness.

The following examples from contemporary high-technology innovation illustrate this integrated methodological approach.

There is little need to emphasize the strategic importance of computer and information security technologies in today's digital society. Instead, the following discussion demonstrates how the combination of classical scientific principles with heuristic innovation methodologies can generate effective technological solutions within this rapidly evolving field.

Innovations in Computer Security Based on Electromagnetic Resonance and Resonance Spectroscopy

Corporate computer networks are frequently vulnerable to increasingly sophisticated cyberattacks despite the implementation of conventional cybersecurity measures.

Numerous examples could be presented; however, one particularly significant case illustrates the scale of this problem.

Beginning in July 2011, the internal computer network of the House of Representatives of the Japanese Parliament was subjected to repeated cyberattacks. According to information published by Japanese media citing anonymous governmental sources, attackers obtained access credentials to parliamentary e-mail accounts through the deployment of malicious software. It was assumed that the primary objective of the attack was to obtain information related to Japan's defense policy and international relations.

Reports further indicated that the initial malware originated from a server registered in China; however, investigators were unable to determine who had originally uploaded the malicious software to that server.

This was by no means the first cyberattack targeting the computer systems of the House of Representatives of the Japanese Parliament. At the same time, no evidence was found indicating that the attackers had altered, deleted, or relocated any information stored within the Parliament's internal network.

Reports of the cyberattack on the Japanese parliamentary network appeared approximately one month after the first publicly documented attack against Japan's defense industry. In that incident, hackers compromised the computer network of Mitsubishi Heavy Industries Ltd. (MHI), a corporation engaged in the manufacture of naval vessels, missile systems, and components for nuclear power plants.

However, the problem is not confined to a single country. Cybersecurity threats continuously migrate across national borders, with technologically advanced countries typically becoming the primary targets.

Threats to users' information are diverse and include self-propagating computer viruses, phishing websites designed to obtain confidential information through deception, and a wide range of malicious software applications.

Modern web browsers incorporate built-in mechanisms designed to protect users from many of these threats by warning them when they attempt to access websites that may compromise the security of their computers. According to analyses published by NSS Labs, one of the highest levels of protection against such threats was provided by the SmartScreen technology integrated into Microsoft Internet Explorer.

Subsequent generations of Internet Explorer further improved SmartScreen technology. At its peak, newer versions of the Microsoft browser reportedly blocked between two and five million attacks against users' computers every day, representing a level of protection several times greater than that demonstrated by competing browsers during the same period.

Initially, the principal function of SmartScreen consisted of evaluating website addresses for suspicious characteristics. The system calculated the reputation of individual web resources using numerous parameters, including the website address itself, traffic frequency, domain characteristics, associated IP addresses, and DNS infrastructure. This comprehensive reputation analysis significantly increased the cost and complexity for cybercriminals attempting to relocate malicious infrastructure after being identified and blacklisted.

Beginning with Internet Explorer 7, Microsoft introduced phishing detection capabilities, enabling the browser to identify fraudulent websites designed to imitate legitimate online resources. Since the introduction of this technology, Microsoft browsers reportedly detected more than 160 million phishing websites. Furthermore, since the release of Internet Explorer 8, approximately 1.5 billion malware-related attacks were reportedly prevented. Overall, Internet Explorer was estimated to mitigate approximately 90% of known web-based security threats.

The remaining threats were addressed through the introduction of an additional SmartScreen protection layer based on application reputation analysis. At the time of its introduction, comparable functionality was not available in competing web browsers.

According to Microsoft, approximately one out of every fourteen downloaded applications contained malicious software. Since most users lack the expertise required to distinguish legitimate software from malicious programs, Internet Explorer utilized application reputation analysis to provide users with security recommendations before software installation.

Application reputation was determined through evaluation of multiple factors. The browser verified digital code-signing certificates issued by software developers, assigning higher confidence to digitally signed applications. Additional factors included the age and historical reputation of the hosting website, with newly created domains receiving lower trust scores than well-established software distribution platforms. In many cases, reputation analysis enabled potentially malicious applications to be identified before conventional antivirus software detected them.

Because the majority of reputable software publishers had already established positive trust profiles, approximately 90% of software downloads proceeded without security warnings. Conversely, when previously unknown applications were encountered, SmartScreen displayed a warning. Microsoft estimated that users who ignored these warnings had a 25% to 70% probability of downloading malicious software. Fortunately, approximately 95% of users followed the browser's recommendations and refrained from executing suspicious applications.

The browser generated high-priority security alerts only when the estimated risk reached particularly elevated levels. According to Microsoft's internal estimates, an average user of the latest Internet Explorer version encountered such warnings only about twice per year.

The practical effectiveness of this security architecture was reflected in Microsoft's projections that the application reputation mechanism alone would prevent more than 20

million malware infections every month, excluding the additional protection provided by conventional SmartScreen website filtering.

The effectiveness of such reputation-based protection systems depends directly upon the volume of accumulated security intelligence. Consequently, the longer SmartScreen remained in operation, the closer its overall detection capability approached comprehensive protection, resulting in a continuously increasing number of successfully protected computer systems.

Nevertheless, in our opinion, the most promising approach to solving the entire spectrum of modern cybersecurity challenges is the application of an innovative integrative methodology for the identification and authentication of optical information storage media based on the physical principles of electromagnetic resonance. This technology was developed and experimentally evaluated in California and utilizes the unique electromagnetic resonance characteristics of optical data storage devices as an additional mechanism for information protection and authentication.

A brief description of the proposed innovative technologies is presented below:

Innovative Products Based on Electromagnetic Resonance Identification Technology

The first proposed innovation is a microresonance sensor designed for integration into the spindle assembly of optical data reading and recording devices.

The product consists of a miniature resonance sensor incorporating numerous possible topological configurations of highly sensitive nanoscale detectors, with considerable flexibility in both detector arrangement and detector quantity. The sensor is installed within the receiving unit of the spindle assembly of an optical storage drive and is integrated with dedicated software responsible for interpreting signals generated by the detectors. Following successful identification, the software authorizes operation of the optical drive; if proper identification cannot be established, access to the drive is automatically blocked. Reliable operation requires precise correspondence between the spatial coordinates of the nanoscale detectors within the sensor and the coordinates of the nanoscale coding implants incorporated into the optical storage medium.

The principal advantages of the proposed technology include:

- exceptionally high measurement accuracy;
- simple and reliable mechanical design;
- long operational lifetime;
- completely non-contact measurement;
- compatibility with existing optical storage architectures as well as future-generation optical memory systems, including terabyte-capacity optical media;
- construction entirely from standard industrial components, resulting in high reliability, low manufacturing costs, and production without specialized fabrication equipment;
- compatibility of detector manufacturing with conventional semiconductor production technologies;
- extremely low power consumption, requiring only a few milliwatts for sensor operation;
- capability of recognizing virtually any nanoscale implant topology;
- capability of identifying ultra-pure materials and distinguishing materials differing at the isotopic level;
- suitability for integration into automated control systems extending beyond optical storage technologies; and
- exceptionally high sensitivity capable of detecting signals generated by ferromagnetic nanopowders even when the total material volume does not exceed approximately **100 cubic nanometers**, while maintaining stable autonomous operation under external electromagnetic interference.

A second proposed innovation is an **optical storage medium incorporating coding information generated by nanoscale magnetic implants**.

The product consists of a conventional optical storage disc in which nanoscale magnetic capsules enclosed within non-magnetic shells are embedded according to a predetermined topological pattern at a specified depth inside the storage medium. Prior to bonding the two halves of the optical disc, microscopic recesses corresponding to the

dimensions of the magnetic nanocapsules are formed within the substrate. The capsules are subsequently positioned inside these recesses before final assembly using conventional optical disc manufacturing technology.

Such optical media remain compatible with standard optical drives whenever information is recorded without employing the resonance coding procedure. However, when data are encoded using the proposed resonance identification technology, the stored information can be accessed only by optical drives equipped with the corresponding micro-resonance sensor, provided that the spatial coordinates of the embedded nanoscale implants exactly correspond to the coordinates of the sensor's nanoscale detectors.

This approach enables large corporate organizations to establish proprietary optical storage infrastructures consisting of customized optical drives installed throughout their computer systems together with uniquely coded optical media containing organization-specific implant topologies. Under these conditions, unauthorized reading of confidential information becomes impossible without possession of the corresponding resonance-identification hardware, thereby providing an additional physical layer of information security against unauthorized access, theft, duplication, or other malicious activities.

The ability to develop this integrated technological solution within a comparatively short period became possible through the continuous professional retraining methodology applied throughout the project. This methodology was developed byMalyeryk Khrystyna and emphasizes systematic innovation education, interdisciplinary engineering training, and practical integration of modern technological approaches.

Legislative Limitations and the Efficiency of the Innovation Process

Recent international competitiveness assessments once again demonstrate the changing balance among the world's leading economies.

While **Hong Kong** retained first place, the **United States**, which had previously shared the leading position, ranked slightly lower, followed by **Switzerland**, which advanced significantly compared with previous years. The world's ten most competitive economies also included **Singapore, Sweden, Canada, Taiwan, Norway, Germany,** and **Qatar**.

According to the **IMD World Competitiveness Center**, despite numerous economic and political challenges, the United States continues to occupy a central position in the global economy because of the exceptional dynamism of its companies and their strong capacity for innovation.

The Center further emphasized that the competitiveness of the United States exerts a substantial influence on virtually every developed and emerging economy, creating a unique global innovation environment that currently has no comparable equivalent elsewhere.

The IMD competitiveness evaluation is based on **329 separate indicators** covering national economic performance, government efficiency, business efficiency, and infrastructure development.

In continuation of these observations, we believe that greater attention devoted to integrative methodologies for retraining innovation specialists, combined with other strategic development factors, may further accelerate the competitiveness of the world's leading economies.

In our opinion, the integrative educational and methodological developments created by Malyeryk Khrystyna can make a meaningful contribution to this process.

Moreover, such educational methodologies may also accelerate progress in fundamental scientific research.

One representative example concerns the first successful experimental confirmation of the **ergodic theorem**, one of the fundamental principles describing the behavior of dynamic systems.

Dynamic systems evolve over time, and in ergodic systems the statistical behavior of individual particles corresponds to that of the entire system. Consequently, repeated measurements of a single particle produce the same statistical characteristics as measurements performed on the complete ensemble.

For many years, direct experimental verification remained impossible because measurements of individual particles required highly diluted suspensions with slow particle

motion, whereas measurements of complete systems required dense particle populations moving at considerably higher velocities.

Researchers eventually overcame these limitations by constructing an experimental system based on nanoporous materials containing channels only a few nanometers in diameter. Fluorescent dye molecules dispersed within an alcohol solution served as experimental particles, allowing individual molecules to be tracked with exceptionally high positional accuracy while simultaneously enabling characterization of the complete molecular ensemble.

The experimental results demonstrated that measurements performed on individual molecules and on the complete system produced statistically identical results, thereby providing direct experimental confirmation of the ergodic theorem.

Because these investigations involve emulsions – and particularly nanoscale emulsions – their results are of considerable technological importance. Reports describing these experiments immediately stimulated the development of new engineering concepts that were subsequently tested in leading research laboratories.

Since the authors of the present publication participated directly in these developments, we believe there are substantial grounds to conclude that the methodological framework developed by Malyeryk Khrystyna enabled an immediate technological response to significant advances in fundamental scientific research, thereby facilitating rapid transformation of scientific discoveries into practical engineering innovations.

Integrating the Algorithm of Inventive Problem Solving (ARIZ) with Contemporary Commercialization Theories

The Theory of Inventive Problem Solving (TRIZ) and all subsequently developed versions of the Algorithm of Inventive Problem Solving (ARIZ) were created during a historical period and within an economic environment in which the commercialization of innovative technologies received relatively little attention. Indeed, during the formative years of TRIZ and ARIZ, commercialization issues were deliberately subordinated to the development of purely technological solutions, largely isolated from the realities of market economics and, in many cases, from the practical demands of society.

As a consequence of this historically limited approach to innovation management, many inventors educated within the classical TRIZ and ARIZ framework became exceptionally skilled at generating technical solutions while remaining insufficiently prepared for the competitive realities of modern market economies. They possess outstanding engineering creativity and enthusiasm for invention, yet frequently lack the entrepreneurial knowledge and commercialization strategies necessary to obtain appropriate financial returns for their intellectual achievements.

Consequently, one of the most important stages of any innovation process is the preliminary evaluation of whether commercialization should be initiated at all, together with a systematic assessment of the alternative development scenarios that may arise during subsequent market implementation.

To facilitate such decision-making, we propose the application of a structured evaluation methodology based on an Innovation Assessment Scorecard comprising 44 evaluation criteria. This assessment framework enables a comprehensive examination of the commercial, technological, organizational, and strategic characteristics of an emerging innovative concept.

The complete assessment form is presented in Appendix IV. Individual scores may be calculated manually or implemented in spreadsheet software such as Microsoft Excel, where automatic formulas can be used to determine the overall innovation potential. Each evaluation criterion is assigned a numerical score reflecting its contribution to the overall commercialization prospects of the project.

Innovation Assessment Criteria

1. Urgent unmet market need
2. Clearly explainable uniqueness
3. Sustainable differentiation
4. Readiness for immediate demonstration
5. Favorable competitive environment
6. Unfavorable competitive environment
7. Attractive pricing strategy
8. Customers willing to purchase a product before its market launch

9. Strength of evidence supporting market demand
10. Ability to stay ahead of the market
11. Ambush strategy
12. Presence within a "hot" market
13. Confidence and willingness to accept risk
14. Commitment to fulfilling obligations
15. Business resilience
16. Passion and motivation
17. Management competence
18. Integrity and reliability
19. Ethical foundation for long-term success
20. Attractiveness to strategic advocates and lobbyists
21. Availability of immediate cash flow
22. Revenue exceeding operating costs
23. Competitive advantages of the delivery system
24. Availability of required resources
25. Market leadership and competitive dominance
26. Market penetration strategy
27. Crossing-the-chasm strategy
28. Intellectual property protection
29. Partnership potential
30. Appropriate selection of business location
31. Quality of the contingency plan
32. Unearned strategic advantages
33. Capital requirement management
34. Availability of initial operating capital
35. Visible investment capital
36. High potential enterprise value
37. Predictability of expected results
38. Critical taboos and unacceptable risks
39. Project "show-stoppers"
40. Ostrich syndrome (avoidance of critical problems)
41. Access to highly influential professional networks
42. A compelling and persuasive innovation narrative
43. Relationships with governmental and regulatory institutions
44. Path of least resistance ("low-hanging fruit")

We believe that the continued development of the educational and methodological framework proposed by Malyeryk Khrystyna, together with its systematic integration into contemporary versions of TRIZ and ARIZ, has the potential to produce a substantial increase in the effectiveness of innovation management and technology commercialization.

Such integration would extend the traditional engineering capabilities of classical TRIZ beyond technical problem solving by incorporating strategic business planning, commercialization methodology, innovation economics, intellectual property management, and entrepreneurial decision-making. As a result, future innovation specialists would be equipped not only to create technologically advanced inventions but also to transform those inventions into commercially successful products capable of generating sustainable economic value.

References and Patent Information

Johnson, L. E., et al. (2018). Smart glasses having interfering light filtering (United States Patent Application No. US 20180031836 A1). U.S. Patent and Trademark Office.

Kawamura, T. (2017). Head mounted apparatus and gripping apparatus (United States Patent Application No. US 20170307787 A1). U.S. Patent and Trademark Office.

Kuehne, M., et al. (2015). Method for operating virtual reality glasses and system with virtual reality glasses (United States Patent Application No. US 20150378155 A1). U.S. Patent and Trademark Office.

Joo, G.-H. (2016). Wearable glasses and method of providing content using the same (United States Patent Application No. US 20160034042 A1). U.S. Patent and Trademark Office.

Park, J., et al. (2018). Glasses-type mobile terminal and method of operating the same (United States Patent Application No. US 20180005421 A1). U.S. Patent and Trademark Office.

submitted 15.06.2026;
accepted for publication 29.06.2026;
published 31.08.2026
© Chyrka T.
Contact: Bbparts36@gmail.com

Contents

Section 1. Chemistry

Abdisattorov Javokhir[1], Taniyev Okhunjon, Berdimurodov Elyor, Akbarov Khamdam

SYNTHESIS OF IONIC LIQUIDS BASED ON ORTHO-PHENYLENEDIAMINE AND PHOSPHORIC ACID 3

Nadirbek Sabirov, Mansur Ashirov, Norbek Palvanov

DEVELOPMENT OF A FUNCTIONAL MATERIAL BASED ON TIRON-IMMOBILIZED FILTER PAPER FOR THE DETERMINATION OF SILVER(I) IONS AND ITS SPECTROSCOPIC CHARACTERIZATION 8

Bakhtiyor Berdikulov, Gulnora Ikhtiyarova

RECOVERY OF RHENIUM AND MOLYBDENUM FROM INDUSTRIAL WASTEWATER USING THE KAOLIN-CHITOSAN COMPOSITE BIOSORBENT: SORPTION KINETICS AND ELEMENTAL ANALYSIS 18

Gulnoza Zayniddin qizi Khomitova, Matluba Mukhtarovna Amonova

INVESTIGATION OF THE SORPTION PROPERTIES OF SAPROPEL IN INDUSTRIAL WASTEWATER TREATMENT AND PROSPECTS FOR ENSURING ENVIRONMENTAL SAFETY. 25

Shakhnoza Shukhrat qizi Rashitovaa

INTERPHASE PARTITIONING OF IRON AND ALUMINUM DURING ALKALINE PROCESSING OF ARAL SEA SAPROPEL 30

Rustamov Sardor Rustam og'li, Mamarakhmonov Mukhamatdin Khomidovich, Kodirov Abdulakhad Abduraimovich, Khamrayeva K. B., Tokhirova Maryam

MODERN QUANTUM–CHEMICAL STUDY OF THE ELECTRONIC STRUCTURE AND REACTIVITY OF THIOPHENE 37

Mukhtarjan Mukhamediev, Muslimbek Murtozaqulov, Davronbek Bekchanov, Yusufjon Fayzullayev, Farangizkhon Murtozaqulova

SORPTION OF FORMIC ACID FROM AQUEOUS SOLUTIONS ON THE AN-31 ANION EXCHANGE RESIN 41

Jahongir Mustaqim o'g'li Sharopov

3-AMINO-1,2,4-TRIAZOLE AT THE CHITOSAN–COLLAGEN INTERFACE: A MECHANISTIC FRAMEWORK FOR BRIDGING, CAPPING AND LATTICE INCLUSION. 46

Husan Yakhshinorov, Davron Kuronboev, Nodira Eshmamatova, Elyor Berdimurodov, Khamdam Akbarov

GRAVIMETRIC METHOD OF CORROSION PROTECTION FOR STEEL N20 IN AN ACIDIC ENVIRONMENT 53

Section 2. Computer science

Daniil Nuzhdin

TEST AUTOMATION IN IOS DEVELOPMENT: IMPLEMENTATION PRACTICES AND THEIR IMPACT ON PRODUCTION RELEASE STABILITY 58

Section 3. Food processing industry

Akhmedov Azimjon Normuminovich, Normurodova Ugiloy Uroz kizi

IMPROVEMENT OF SOYBEAN OIL HYDRATION PROCESS 67

Karim K. Sattarov, Gulnoza K. Tukhtamishova, Khilola Sh. Zhuraeva

ASSESSMENT AND IMPROVEMENT OF OILSEED STORAGE TECHNOLOGY UNDER THE CONDITIONS OF THE SYRDARYA REGION 71

Section 4. Materials science

Amonov Mukhtor Rahmatovich, Jumayeva Matluba Sultonovna

AMINATION AND DYEING PROPERTIES AND OPERATIONAL PERFORMANCE OF CELLULOSE FIBER FABRICS 80

Section 5. Technical sciences in general

Kirill Andreevich Melnikov

OPTIMIZING EDGE TOPOLOGIES: A REVIEW OF PREDICTIVE NETWORK ROUTING ALGORITHMS 86

G. I. Astakhov

INNOVATIVE DESIGN OF EQUIPMENT WITH ARTIFICIAL INTELLIGENCE ELEMENTS 92

Hryhorii Baranovskyi

PRACTICAL INNOVATIVE SOLUTIONS WITHIN AN ECOSYSTEM FOR ENVIRONMENTAL IMPACT MITIGATION. 99

Aleksandra Efimova

SMART LIGHTING TECHNOLOGIES 105

Oleksii Hrachov

MULTIDISCIPLINARY DIGITAL TECHNOLOGIES WITH ELEMENTS OF ARTIFICIAL INTELLIGENCE. 112

Sergii Marakshyn

HIGH-EFFICIENCY ELECTROCHEMICAL PROCESSING TECHNOLOGIES. 118

Section 6. Transport

Shevchenko Maxim Igorevich

THE HIDDEN COST LAYER: DEADHEAD, UTILIZATION THRESHOLDS, AND MARGIN FORMATION IN FREIGHT CARRIER OPERATIONS 129

Section 7. Technical sciences. Applied research

Tatiana Chyrka

SYSTEMIC IMPLEMENTATION OF INNOVATION IN THE TEXTILE INDUSTRY 135